

Numerical approximations of population balance equations in particulate systems

Dissertation

zur Erlangung des akademischen Grades

doctor rerum naturalium
(Dr. rer. nat.)

von **M.Sc. Jitendra Kumar**
geb. am 01.04.1978 in Bijnor, India

genehmigt durch die Fakultät für Mathematik
der Otto-von-Guericke-Universität Magdeburg

Gutachter:

Prof. Dr. rer. nat. habil. Gerald Warnecke
Jun.-Prof. Dr.-Ing. Stefan Heinrich

Eingereicht am: 29.08.2006
Verteidigung am: 04.10.2006

Acknowledgements

The life of a PhD student has never been easy but I have certainly relished this experience. During this period I derived my inspiration from several sources and now I want to express my deepest gratitude to all those sources.

Foremost, I owe special thanks to my supervisor Prof. Dr. Gerald Warnecke who has not only encouraged me but has given his remarkable suggestions and invaluable supervision throughout my thesis. His advices and constructive criticism have always been the driving force towards the successful completion of my thesis.

I also deeply appreciate the help of all members of the Institute for Analysis and Numerics. Now I would like to thank Mr. Narni Nageswara Rao for his assistance with numerous aspects of the preparation of this thesis and Dr. Mathias Kunik for his valuable advice and discussion.

I must thank the financial support I received from the DFG-Graduiertenkolleg-828, "Micro-Macro-Interactions in Structured Media and Particle Systems", Otto-von-Guericke-Universität Magdeburg for this PhD program.

At the Institute of Process Equipment and Environmental Technology, I am indebted to Prof. Dr.-Ing. Lothar Mörl and Jun.-Prof. Dr.-Ing. Stefan Heinrich for their willingness to involve me in this project. During past three years they have given me lot of financial support and provided me with the facilities to write this thesis.

I am very grateful to Dr.-Ing. Mirko Peglow, who spared lot of his precious time in advising and helping me throughout the research work. This work would be unthinkable without his guidance and persistent help.

At the University of Sheffield U.K., I would like to express my special thank to Prof. Mike Hounslow for his hospitality treatment during my two weeks visit to Sheffield. His valuable remarks and suggestions enabled me to complete this thesis efficiently.

I am overwhelmingly grateful to all my friends and colleagues for their cooperation and guidance. I want to express my deepest gratitude to my very special friends Mr. Ayan Kumar Bandopadhyaya and Mr. Amit Kumar Tyagi who have ever been encouraging and optimistic.

Now I would like to express my deep obligation to my parents and relatives back home in India. Their consistent mental supports have always been the strong push for me during this period.

Finally, an especially profound acknowledgement is due to my wife Chetna whose forbearance and supports have been invaluable.

Contents

Nomenclature	iii
1 General Introduction	1
1.1 Overview	1
1.2 Problem and Motivation	9
1.3 New Results	10
1.4 Outline of Contents	13
2 Population Balances	14
2.1 Introduction	14
2.2 Aggregation	15
2.2.1 Population Balance Equation	15
2.2.2 Existing Numerical Methods	15
2.3 Breakage	22
2.3.1 Population Balance Equation	22
2.3.2 Existing Numerical Methods	23
2.4 Growth	25
2.4.1 Population Balance Equation	25
2.4.2 Existing Numerical Methods	25
2.5 Combined Processes	33
3 New Numerical Methods: One-Dimensional	35
3.1 Introduction	35
3.2 The Cell Average Technique	36
3.2.1 Pure Breakage	44
3.2.2 Pure Aggregation	61
3.2.3 Pure Growth	93
3.2.4 Simultaneous Aggregation and Breakage	103
3.2.5 Simultaneous Aggregation and Nucleation	106
3.2.6 Simultaneous Growth and Aggregation	113
3.2.7 Simultaneous Growth and Nucleation	118
3.2.8 Choice of Representative Sizes	119
3.3 Mathematical Analysis	120
3.3.1 The Fixed Pivot Technique	123
3.3.2 Direct Approach	130
3.3.3 The Cell Average Technique	132

CONTENTS

3.4	The Finite Volume Scheme	140
3.4.1	Pure Breakage	140
3.4.2	Simultaneous Aggregation and Breakage	152
4	New Numerical Methods: Multi-Dimensional	158
4.1	Introduction	158
4.2	Reduced Model	162
4.2.1	Mathematical Modeling	162
4.2.2	Numerical Methods	166
4.2.3	Test Cases	181
4.3	Complete Model	187
4.3.1	Numerical Methods	188
4.3.2	Test Cases	196
5	Conclusions	205
	Appendices	208
A	Analytical Solutions	208
A.1	Pure breakage	208
A.2	Pure aggregation	208
A.3	Pure growth	211
A.4	Simultaneous aggregation and breakage	213
A.5	Simultaneous aggregation and nucleation	215
A.6	Simultaneous growth and aggregation	216
A.7	Simultaneous growth and nucleation	217
A.8	Analytical solutions of a two component PBE	217
A.9	Analytical solutions of tracer weighted mean particle volume	218
B	Mathematical Derivations	219
B.1	Birth and death rates for aggregation in the fixed pivot technique	219
B.2	A different form of the fixed pivot technique	221
B.3	Comparison of accuracy of local moments	222
B.4	Discrete birth and death rates for breakage	223
B.5	Second moment of the Gaussian-like distribution	223
B.6	Discrete birth rate for aggregation	224
B.7	Stability condition for the combined problem	226
B.8	Mass conservation of modified DTPBE	227
B.9	Discrete birth and death terms of TPBE	228
B.10	Two-dimensional discrete PBE	230
B.11	Consistency with the first cross moment	231
	Bibliography	232
	Curriculum Vitae	241

Nomenclature

Latin Symbol

a_1, a_2, a_3, a_4	Fraction of particles	—
b	Breakage function	m^{-3}
B	Birth rate	$m^{-6} \cdot s^{-1}$
\tilde{B}	Binary breakage function	$m^{-3} \cdot s^{-1}$
c	Tracer volume	m^3
C	Constant	—
D	Death rate	$m^{-6} \cdot s^{-1}$
E	Error	—
f	Multi-dimensional number density function	$m^{-3} \cdot \left(\prod_j [i_j]\right)^{-1}$
F	Mass flux	s^{-1}
g	Volume density function	—
G_j	Growth rate along internal coordinate j	$[i_j]/s$
h	Enthalpy	J
H	Heaviside function	—
I	Total number of cells	—
I_{agg}	Degree of aggregation	—
J	Numerical mass flux	$1/s$
K	Constant	—
l	Mass of liquid	kg
m	Tracer volume density function	m^{-3}
M	Tracer volume	—
n	Number density function	m^{-6}
N	Number	m^{-3}
N_0	Initial number of particles	m^{-3}
p_k^i	Limit of integral defined by the function (3.27)	m^3
q	Discretization parameter	—
Q	Flow rate	$m^3 \cdot s^{-1}$
r	Ratio x_{i+1}/x_i	—
S	Selection function	s^{-1}

NOMENCLATURE

t	Time	s
T_a	Dimensionless time for aggregation	—
T_g	Dimensionless time for growth	—
T_s	Dimensionless time for simultaneous processes	—
T_z	Dimensionless time for 2-D aggregation	—
u, v, x	Volume of particles	m^3
\bar{v}	Average volume	m^3
v_0, x_0	Initial mean volume	m^3
V	Rate of change of volume	s^{-1}
\tilde{V}	System volume	m^3
\mathbf{V}	Velocity	$([\mathbf{i}]/s, [\mathbf{e}]/s)$
\mathbf{x}	Phase space	$([\mathbf{i}], [\mathbf{e}])$
\mathbf{x}_e	Vector of external coordinates	$[\mathbf{e}]$
\mathbf{x}_e^j	Component j of external coordinates	$[\mathbf{e}_j]$
\mathbf{x}_i	Vector of internal coordinates	$[\mathbf{i}]$
\mathbf{x}_i^j	Component j of internal coordinates	$[\mathbf{i}_j]$

Greek Symbols

α	Integer	—
β	One-dimensional aggregation kernel	$m^3 s^{-1}$
$\hat{\beta}$	Multidimensional dimensional aggregation kernel	$m^3 s^{-1}$
$\delta(x)$	Dirac-delta distribution	—
δ_i	A function defined by the equation (2.65)	—
δ_{ij}	Kronecker delta	—
Δx	Size of a cell	—
ϵ	Global truncation error	—
η	Particle distribution function	—
θ	A function defined by the equation (2.51)	—
λ	Fractions	—
Λ	Discretized domain	—
μ_r	The r th moment	$m^{3r} \cdot m^{-3}$
$\tilde{\mu}$	Logarithmic norm	—
ν	Parameter in Gaussian-like distribution	—
σ	Spatial truncation error	—
τ	Age of particles	s
ϕ	Limiter function	—
ω	Constant	—

Subscripts

agg	Aggregation
break	Breakage
i, j	Index

<i>in</i>	Inlet
<i>nuc</i>	Nucleation
<i>out</i>	Outlet
<i>p</i>	Particle
<i>T</i>	Tracer
<i>w</i>	Water

Superscripts

\sim	Constant values
$-$	Mean or average values
\wedge	Numerical approximations
<i>ana</i>	Analytical
<i>gel</i>	Gelation
<i>mod</i>	Modified
<i>num</i>	Numerical

Acronyms

CA	Cell Average
CST	Continuous Stirred Tank
DPBE	Discretized Population Balance Equation
DTPBE	Discretized Tracer Population Balance Equation
EOC	Experimental Order of Convergence
FP	Fixed Pivot
GA	Generalized Approximation
GSD	Granule Size Distribution
MOL	Method of Line
MSMPR	Mixed-Suspension-Mixed-Product-Removal
ODE	Ordinary Differential Equation
PBE	Population Balance Equation
PPD	Particle Property Distribution
PSD	Particle Size Distribution

Chapter 1

General Introduction

In this chapter a general overview of population balances is provided. The problems with existing numerical techniques for solving population balances are discussed. The requirements needed for a numerical solutions are pointed out and it is found that none of the existing methods fulfill these requirements. Then, a short summary of the new findings followed by an outline of the thesis is given.

1.1 Overview

This thesis is concerned with the mathematical modeling of particulate systems and numerical tools for solving the resulting models. Particulate processes are well known in various branches of engineering including crystallization, comminution, precipitation, polymerization, aerosol and emulsion processes. These processes are characterized by the presence of a continuous phase and a dispersed phase composed of particles with a distribution of properties. The particles might be crystals, grains, drops or bubbles and may have several properties like size, composition, porosity and enthalpy etc. In many applications, the size of a particle is considered as the only relevant particle property. It is comparatively easy to measure and therefore commonly used to characterize a particle. It may be determined in various forms such as a typical length, area or the volume respectively mass. It might be diameter in case of a sphere, side-length for a cube, surface area or volume for more complicated particles.

Since particles may have different sizes and properties, a mathematical description of their distribution or the so called particle property distribution is needed to characterize them. The shape of particles from grinding or crystallization processes is often uniform enough that a characteristic shape factor can be defined and the particles can be described using the one-dimensional distribution function. However, more distributed properties are often needed to characterize the particles in process engineering like fluidized bed agglomeration as well as in pharmaceutical processes. Thus, a multidimensional distribution function is required.

The particles may change their properties in a system due to several mechanisms. However, the most common mechanisms which we have considered in this work are aggregation, breakage, nucleation and growth. A short description of these mechanisms is given below.

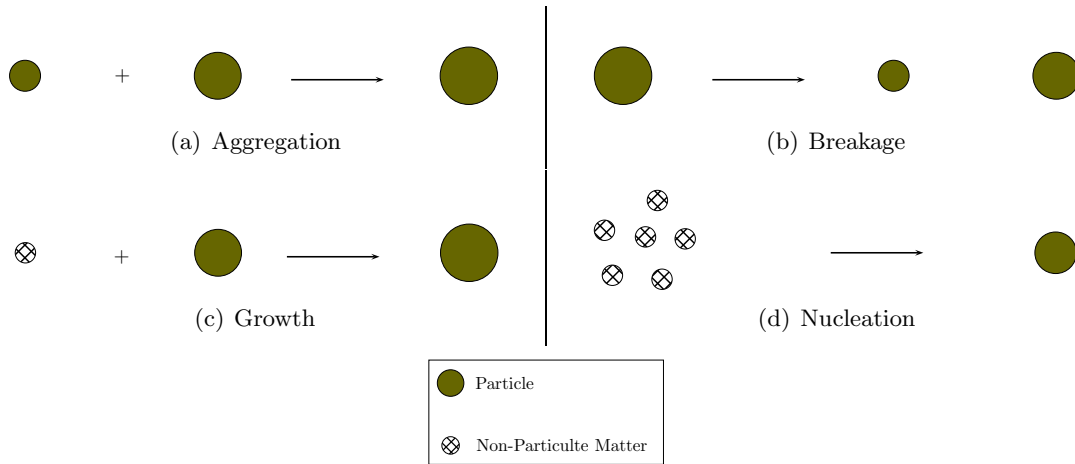


Figure 1.1: Different particle formation mechanisms.

Aggregation: Aggregation or agglomeration is a process where two or more particles combine together to form a large particle. The total number of particles reduces in a aggregation process while mass remains conserved. This process is most common in powder processing industries. Agglomeration of small particles reduces dust formation and therefore improves their handling properties. One other advantage of the agglomerated powder is a higher dissolution rate by reducing lump formation or flotation of the powder. A diagrammatic representation of aggregation is given in Figure 1.1(a).

Agglomeration in the fluidized bed takes place, if, after the drying of liquid bridges, solid bridges arise. This is accomplished through the deliberate addition of a soluble binder. The liquid binds the particles together by a combination of capillary and viscous forces until more permanent bonds are formed by subsequent drying or sintering. There are a large number of theoretical models available in the literature for predicting whether or not two colliding particles will stick together. These models involve a wide range of different assumptions about the mechanical properties of the particles and the system characteristics.

The aggregation of liquid droplets is called coagulation. Whereas in solid particles agglomeration the original particles stay intact, in coagulation the original droplets become an indistinguishable part of the newly formed droplets, see Gerstlaur [25].

Breakage: In a breakage process, particles break into two or many fragments. Breakage has a significant effect on the number of particles. The total number of particles in a breakage process increases while the total mass remains constant. A graphical representation of breakage is shown in Figure 1.1(b). In granule breakage, there are two separate phenomena to consider:

1. Breakage of wet granules in the granulator; and
2. Attrition or fracture of dried granules in the granulator, drier or in subsequent handling.

For a detailed description, readers are referred to Iveson et al. [41]. Breakage of wet granules will influence and may control the final granule size distribution, especially in high shear granulators.

In some circumstances, breakage can be used to limit the maximum granule size or to help distribute a viscous binder. On the other hand, attrition of dry granules leads to the generation of dusty fines. As the aim of most granulation processes is to remove fines, this is generally a disastrous situation to be avoided.

Growth: The particles grow when a non-particulate matter adds to the surface of a particle. Growth has no effect on the number of particles but the total volume of particles increases. The size of a particle increases continuously in this process. A graphical representation of growth is provided in Figure 1.1(c).

In a fluidized bed, a liquid (suspension, solution or melt) is sprayed onto the solid particles by an injection nozzle in the form of drops. A part of the drops is deposited on the particles and is distributed through spreading. The intensive heat and mass transfer, due to the surrounding gas stream, results in a rapid increase of hardness of the fluid film through drying, if the initial product is a solution or molten mass, or through cooling, if the sprayed upon product is melted. The solvent evaporates in the hot, unsaturated fluidization gas, and the remaining solid particles grow bigger through multiple spraying, spreading and hardening, having an onion-like effect on the particle surface, see for example Heinrich et al. [29]. This phenomenon is known as growth, layering or coating.

Nucleation: The formation of a new particle by condensation of non-particulate matter is called nucleation. The nuclei are usually treated as the smallest possible particles in the system. A graphical representation of nucleation is given in Figure 1.1(d). Nucleation has also a significant effect on the total number of particles but less effect on the total volume of particles.

In the literature, nucleation is often considered as the appearance of particles in the smallest size cell. This consideration is motivated by problems in particle size measurement. Especially in crystallization, it is not possible to distinguish between nuclei of different sizes due to insufficient resolutions of measuring devices in this range of small particle sizes. A further problem is the formation of nuclei in a range that is smaller than the smallest measurable range. By growth and agglomeration these particles become visible. This process is also often called as nucleation, see Peglow [82]. In fluidized bed agglomeration where particles are formed in a range from 50 μm up to 2000 μm , nucleation is reported in a wide range of particle sizes.

As a result of the mechanisms mentioned above particles change their properties and therefore a mathematical model named *population balance* is required to describe the change of particle property distribution. Population balances describe the dynamic evolution of the distribution of one or more properties. Since we are dealing mainly with aggregation or breakage problems, it is convenient to consider the volume as a measure of size. On the other hand for pure growth processes a linear based measure i.e. length or diameter is more preferable. Until mentioned otherwise, we have assumed that the solid density of particles is constant and the mass of a particle can be replaced by the volume of the particle.

The first task is to identify a method of representation for processes in which discrete particles are present and each particle can have a variety of properties. The method we adopt is to describe the distribution of particle properties by a population density function. So if particle

CHAPTER 1. GENERAL INTRODUCTION

size x is the distributed property then the distribution of particle sizes would be given by $n(t, x)$. It follows that the number of particles per unit volume (or some other basis) in the size range $[x_{i-1/2}, x_{i+1/2}]$ is given as

$$N_i = \int_{x_{i-1/2}}^{x_{i+1/2}} n(t, \epsilon) d\epsilon. \quad (1.1)$$

As Hulburt and Katz [36] have shown, this method may readily be extended to situations where the particles have multiple properties - termed by them, multiple internal coordinates. So, for example, each particle might be characterized by its size and its moisture content. The choice of how many internal coordinates are considered is essentially a practical one. If a system can be described by one coordinate only, then there is no need to add further coordinates. If, however, the drying behavior is a complex function of material properties and particles states, then a longer list of coordinates might be desirable. In this case practical computational limits usually mean that two or at most three coordinates are considered.

It is also possible that the distribution of properties will vary in space. In this way the population density will be a function of spatial - or in Hulburt and Katz's language external-coordinates. If these are given by a vector \mathbf{x}_e , and the internal coordinates by a vector \mathbf{x}_i , the total coordinate space, also called *phase space*, is given by $\mathbf{x} = (\mathbf{x}_i, \mathbf{x}_e)$.

The next step in the descriptions being developed here is to recognize that it is possible to write a conservation statement - or Population Balance Equation (PBE) - that describes how the number density varies with time and in space. Various derivations of such an equation can be found, most famously by Hulburt and Katz [36], Randolph and Larson [95] and Ramkrishna [94]. In essence, for a small volume in space (a space comprised of internal and external coordinates), the rate of change of the number density must be matched by the divergence in the flux of particles as well as source and sink terms (called birth and death terms, B and D). The flux is, of course, the local product of velocity \mathbf{V} and number density, where

$$\mathbf{V} = \frac{d\mathbf{x}}{dt}. \quad (1.2)$$

So the velocity components related to the external coordinates give the conventional speeds, while those related to the internal coordinates give a description of, for example, the rate of change of size, or moisture content. The population balance equation is then

$$\frac{\partial f}{\partial t} + \nabla \cdot (\mathbf{V}f) = B(t, \mathbf{x}) - D(t, \mathbf{x}). \quad (1.3)$$

Here f describes a multidimensional distribution function. In order to use the PBE it is necessary that the velocities are known as functions of position in space and that rate laws can be found for the birth and death terms. The birth and death terms in this equation are the rates at which particles are born and die at a location in phase space, per unit volume of phase space. These terms appear in the PBE due to certain discrete events which can occur at arbitrary locations in phase space and that add or remove particles. Examples of these birth and death terms include breakage, which results in one death and two or more birth events; aggregation which results in one birth and two or more deaths; and nucleation which results in a single birth event. The birth and the death terms usually include integrals which make the solution of the population balance

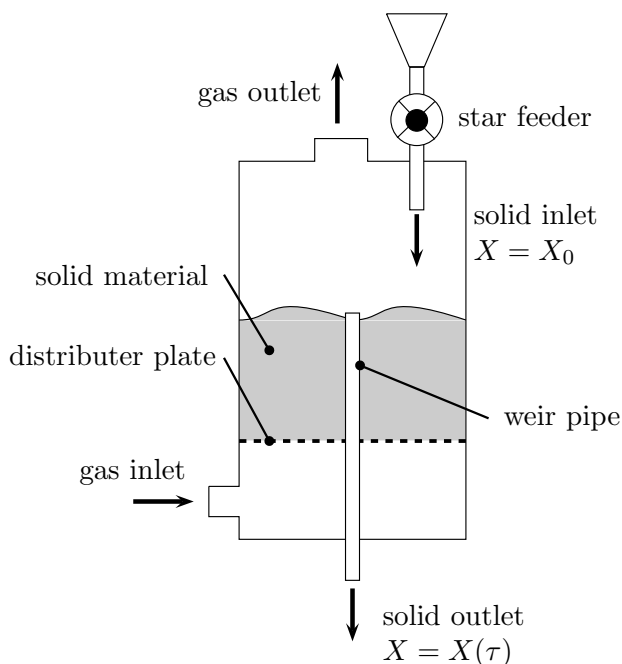


Figure 1.2: Schematic diagram of a continuous fluidized bed dryer.

equation more complicated. Finally, numerical techniques are almost inevitably required for their solutions. That topic is the main subject for this thesis.

Many commercial processes in drying technology are concerned with discrete or particulate materials. In these processes individual particles will vary in properties and as a consequence frequently vary in drying behavior. The most obvious example is that the particles may vary in size and, as a consequence, dry at different rates. One of the aims of this work is to explain how problems of this type can be posed and then how they can be solved.

Before we proceed to explain problems with previously existing numerical schemes, we first give an impression of the significance of the population balances in real applications. Here we consider two applications in drying where the population balances can be used. The population balances provide a better understanding of drying processes. The first application concerns the drying of particles in a continuous fluidized bed dryer, while the second application involves the process of simultaneous particle size enlargement and drying.

Application 1: The first application for applying population balances is a continuous fluidized bed dryer. The wet solid material can be conveyed into the dryer by an adequate equipment such as a star feeder. At the same time the dried product is discharged so that the total mass of solid in the apparatus remains constant. This process is shown schematically in Figure 1.2.

A traditional approach for modeling this process considers the disperse solids as the only phase with average properties like particle size, moisture content and enthalpy. Certainly such kind of models always predict a uniform moisture content for the solids in the dryer. However, Kettner et al. [44] demonstrated that uniform properties do not appear in practice. They have measured

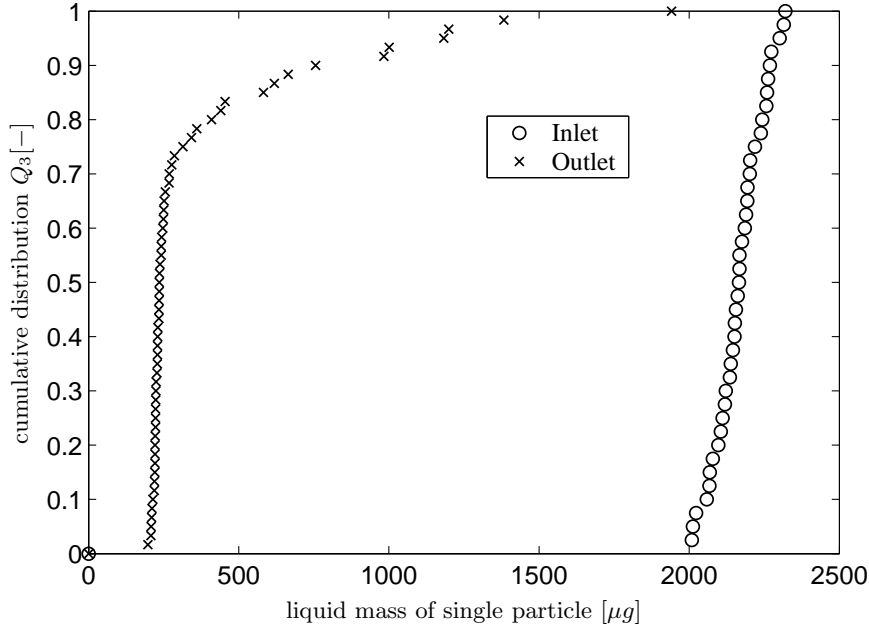


Figure 1.3: Measured moisture distribution of single particle at the solid inlet and outlet of a continuous fluidized bed dryer.

the moisture content of single particles in a lab scale dryer using a combination of NMR and coulometric measurement techniques. Some typical results of these measurements are presented in Figure 1.3.

It can be seen from the figure that the moisture of dried solids is not uniform but widely distributed. Kettner et al. [44] claimed that different residence times or in other words the age of the particles causes such broad distributions. One might also argue that spatial distributions may be the reason for the distributed product properties. This is certainly the case for large scale horizontal fluidized bed dryers, where the product is transported in horizontal direction from the inlet to the outlet. This is not the case for lab scale apparatus. By tracer experiments Burgschweiger and Tsotsas [14] proved that such small scale fluidized bed dryers can be treated as a well mixed system where spatial distributions of the solid phase can be neglected. Thus, we concentrate on the residence time or respectively the age of particles as the only additional particle property.

As soon as the age of the particle is introduced as a new property of solids the moisture and enthalpy need to be considered as distributed properties, because they depend directly on the age of particles. Thus, a number of internal coordinates of the solid phase have been identified which are required to be incorporated in a more precise drying model. They are the moisture of solids l , the enthalpy h and the age of particles τ .

The population balance approach allows now to combine the distributed properties of the solid phase into one equation. For a well mixed system the temporal change of the number density

distribution of the solid phase can be derived as

$$\frac{\partial f}{\partial t} + \frac{\partial G_\tau \cdot f(\tau, l, h)}{\partial \tau} + \frac{\partial G_l \cdot f(\tau, l, h)}{\partial l} + \frac{\partial G_h \cdot f(\tau, l, h)}{\partial h} = \dot{f}_{in} - \dot{f}_{out}. \quad (1.4)$$

In this equation the parameter f indicates the number density distribution of particles. The second term on the left hand side of this equation represents the aging of particles with $G_\tau = 1$, the third term describes the drying of particles, where the variable G_l indicates the drying rate of particles in kg/s . The fourth term corresponds to the change of enthalpy due to heat and mass transfer, wherein G_h denotes the rate of change of enthalpy. The last two terms indicate a source and a sink for particles being conveyed and discharged, respectively. The accuracy of a drying model incorporating population balances is significantly improved. Burgschweiger and Tsotsas [14] have shown that an extended model based on population balances predicts the performance of a fluid bed dryer more precisely than traditional models.

Application 2: The second application concerns the process of particle formation in fluidized beds. Generally there are three main mechanisms, namely growth, agglomeration and breakage, that influence the size of particles. For simplicity only the mechanism of agglomeration will be considered in this example. The particle size enlargement by agglomeration transforms fine sized primary particles into an easily soluble, free-flowing and dust-less product. The fluidized bed technology offers the possibility to combine agglomeration and drying in a single apparatus. In the literature, many attempts have been made to describe the process of particle formation in fluidized bed in terms of population balances. But they all consider the particle size or particle volume as the only significant property. The influence of operating conditions on the evolution of particle size has been investigated by various authors, e.g. Adetayo et al. [2], Watano et al. [119] and Schaafsma et al. [101]. Watano et al. [119] pointed out that the moisture content in solids is one of the most important particle properties to control the agglomeration process. It is obvious that such a significant particle property needs to be incorporated in a more complex model of the solid phase.

Figure 1.4 depicts schematically, how the mechanisms of agglomeration, drying and wetting are coupled. Let us consider two primary particles with a dry solid volume u and $v - u$. Both particles contain a certain amount of liquid denoted by γ and $l - \gamma$ respectively. It is clear, that the solid volume and the amount of liquid of a newborn particle are given by v and l respectively. Thus, the agglomeration influences not only the particle size but also the moisture distribution. During the agglomeration process the particles get wetted with a liquid binder solution. Thus, the moisture content in the particles increases. In addition to that the particles are dried due to contact with the hot fluidization gas. Therefore the amount of liquid in a particle is influenced by drying and wetting but not by the particle size.

It should be noted, that the drying and wetting rates may also depend on the size of particles. This is due to the fact that the mass transfer coefficient depends on the particle size. The consequence of a size dependent drying rate is a non-uniform distribution of moisture within the disperse phase. Analogously, the enthalpy of particle can be described. Similarly to the moisture content, the enthalpy does not only change by the agglomeration of particles but also by the size dependent heat and enthalpy transfer rates. Then, the population balance approach

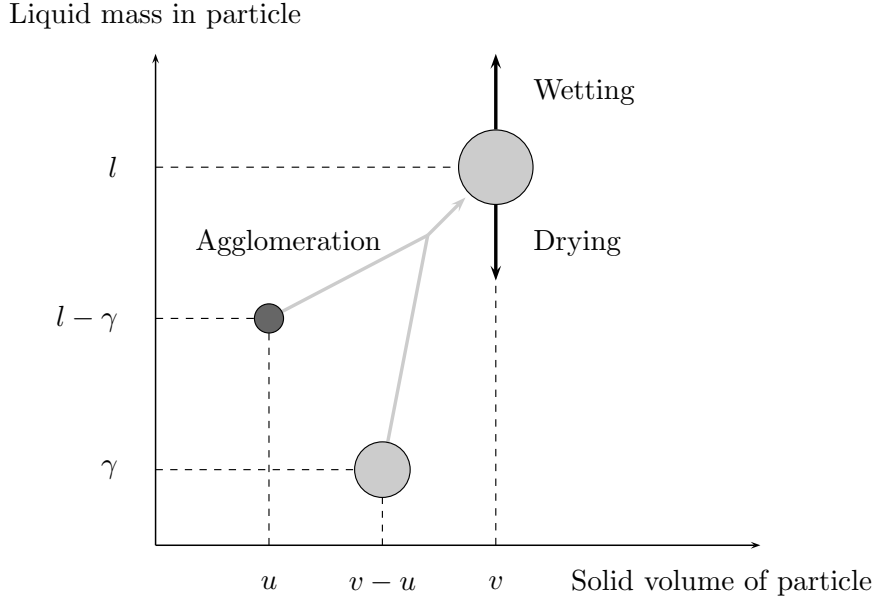


Figure 1.4: Coupled mechanisms of agglomeration, drying and wetting.

can be used to model the combined processes of agglomeration and drying as

$$\frac{\partial f(t, v, l, h)}{\partial t} + \frac{\partial G_l \cdot f(t, v, l, h)}{\partial l} + \frac{\partial G_h \cdot f(t, v, l, h)}{\partial h} = \tag{1.5}$$

$$\begin{aligned} & \frac{1}{2} \int_0^v \int_0^l \int_0^h \hat{\beta} \cdot f(t, v-u, l-\gamma, h-\epsilon) \cdot f(t, u, \gamma, \epsilon) \, d\epsilon \, d\gamma \, du \\ & - \int_0^\infty \int_0^\infty \int_0^\infty \hat{\beta} \cdot f(t, v, l, h) \cdot f(t, u, \gamma, \epsilon) \, d\epsilon \, d\gamma \, du. \end{aligned} \tag{1.6}$$

Again, f denotes the number density distribution. The advection terms on the left hand side of this equation represent the change of mass of liquid and change of enthalpy respectively. The parameter G_l indicates the rate of change of liquid mass. Positive and negative values of G_l describe the wetting and drying of particles respectively. The expression on the right hand side of this equation represents the birth and death of particles due to agglomeration. The triple integral shows that three independent particle properties are considered. The above equation provides the possibility to incorporate additional particle properties in the agglomeration kinetics $\hat{\beta}$. Thus, the function $\hat{\beta}$ may not only depend on particle size but also on moisture content and enthalpy, which is certainly the case in practice.

From the examples explained above it can be concluded that the population balance approach is a very powerful tool to gain a better description of drying and to establish a better understanding of the process. Several other applications of population balances in fluidized bed granulation can be found in J. Kumar et al. [53] and Peglow et al. [83, 85].

1.2 Problem and Motivation

In particle technologies population balance equations are widely used, e.g. in processes such as crystallization, comminution and fluidized bed granulation. They appear also in mathematical biology as well as in aerosol science. These are partial integro-differential equations of hyperbolic or parabolic type. Included are conservation laws with integral fluxes. Independent variables are particle properties, especially particle size, over which a particle number distribution is considered for which the population balance is formulated. Analytical solutions are available only for a limited number of simplified problems and therefore numerical solutions are frequently needed to solve a population balance system.

Several numerical techniques including the method of successive approximations [94], the method of moments [5, 71, 75], the finite elements methods [72, 78, 97], the finite volume scheme [8, 11, 15, 21, 77, 117] and Monte Carlo simulation methods [52, 63, 68, 104] can be found in the literature for solving population balance equations. Besides the approximation of the particle property distribution, a correct prediction of some selected properties such as the total number of particles and total mass etc. is mainly required in many particulate systems. These requirements lead to the choice of sectional methods. The sectional methods approximate the continuous size distribution by a finite number of size sections (intervals, cells). A system of ordinary differential equations describing the change of the number of particles in each cell is usually obtained and then using any higher order time integrator is solved. The accuracy of the method certainly depends on the number of cells. Such methods rely on predicting some selected properties of the distribution exactly rather than capturing all details of the distribution. Moreover, simplicity and low computational cost of these methods make them highly practical in process engineering.

There are several sectional methods in the literature which predict the particle property distribution accurately while using a linear grid, see for example Sutugin and Fuchs [108], Tolpfo [111], Kim and Seinfeld [46], Gelbard et al. [24], Sastry and Gaschignard [99] as well as Marchal et al. [74]. Linear grid discretization has a great advantage especially in aggregation problems since each aggregate finds a new position for its allocation. This discretization does however have one problem of extremely high computational cost due to the requirement of excessively many cells to cover the property domain. Instead, a geometric type discretization is commonly used to reduce the computational cost. The difficulty that arises in a non-uniform grid is, where to allocate newborn particles which do not have exactly the size of the grid point. Several authors proposed different methods which can be used using geometric, Gillette [26], Batterham et al. [7], Marchal et al. [74], Hounslow et al. [34], or arbitrary grid, Kim and Seinfeld [46], Gelbard et al. [24], Sastry and Gaschignard [99], Marchal et al. [74], Kumar and Ramkrishna [57]. Batterham et al. [7] produced numerical results for aggregation that correctly predicted conservation of total particles volume but failed to predict the correct evolution of total numbers. On the other hand, Gelbard et al. [24] predicted the rate of change of total particle number correctly but lost total particle volume. Nonetheless, Hounslow et al. [34] have been the first in the literature to produce a population balance scheme that correctly predicts the total number and total volume of particles. They have considered a geometric discretization with a factor of 2 progression in size. This has the drawback that one cannot refine the grid. Afterwards, Litster et al. [69] have extended the technique for adjustable geometric discretizations with a progression factor of $2^{1/q}$, where q is an integer greater than or equal to 1. It has been investigated by Wynn [120] that the extended formulation is valid only for $q < 4$. Since then, Wynn has corrected

the formulation. The complex structure of the formulation and its restriction to specified grids are the major disadvantages of this method. Wynn [121] has also presented a more simplified form of Hounslow's discretization to improve some computational aspects. An evaluation of the various sectional methods can be found in [6, 48, 49, 79].

The first general formulation consistent with the first two moments has been proposed as the so called *fixed pivot technique* by Kumar and Ramkrishna [57]. The formulation takes the form of Hounslow's formulation when applied on the geometric grid with a factor of 2 progression in size. It uses point masses at a representative location in each section (cell). Despite the fact that the numerically calculated moments are fairly accurate, the fixed pivot technique consistently over-predicts the results. The technique focuses on an accurate calculation of some selected moments instead of calculation of the whole particle property distribution. However, the fixed pivot technique can only be applied for aggregation and breakage problems. The authors have proposed a completely different concept for combined processes of aggregation or breakage where additionally growth and nucleation are present.

Filbet and Laurençot [21] proposed a different approach of using a finite volume scheme for solving aggregation PBEs. Finite volume schemes are frequently used for solving conservation laws. In the case of the aggregation PBE, it has been applied by transforming the number density PBE to a mass conservation law. A second order accuracy has been obtained by the finite volume scheme. Though the scheme predicts the numerical results for particle size distribution accurately, it is consistent with respect to the first moment only. The prediction of the zeroth moment of the number density by the proposed scheme becomes very poor.

Some of the existing methods overestimate the numerical results while others are inconsistent with moments. Moreover, of the existing sectional methods none can be implemented for solving combined processes effectively. We wish to have a general, accurate, ease to use, computationally less expensive and simple scheme. By these standards, none of the previous schemes we know of are completely satisfactory, although some are much better than others. Furthermore, there is a lack of numerical schemes which can be extended or applied for solving higher dimensional problems. This leads to a clear motivation for the development of the new scheme. Thereby the objective of this work is to develop a general and simple scheme which preserves all advantages of the existing schemes and can be used to solve all processes simultaneously. Additionally, the aim is to extend the scheme to multi-dimensional problems.

1.3 New Results

It is of interest to have a numerical discretization that is suitable for the differential as well as integral parts of the partial integro-differential equations. Main challenges are the non-local character of convolution integrals describing particle agglomeration and a large variation in scale of the independent and dependent variables. During last decade, an intensive work on this subject has produced many different numerical schemes. One of those, namely the fixed pivot technique, has been by far the most widely used. In this method, all particles within a cell, which by some researchers is called a class, section or interval, are supposed to be of the same size. Indeed, the fixed pivot technique belongs to the class of sectional methods which are well known for their simplicity and conservation properties. However, these methods converge slowly

towards the exact solution and over-predicts the numerical results for particle size distribution and higher moments. Furthermore, numerical methods that can be used to solve growth, nucleation aggregation and breakage processes simultaneously are rarely available.

This work presents a new numerical scheme, *the cell average technique*, for solving a general population balance equation which assigns particles within the cells more precisely. The technique follows a two step strategy: one is to calculate the average size of the newborn particles in a cell and the other to assign them to neighboring nodes such that the properties of interest are exactly preserved. The new technique preserves all the advantages of conventional discretized methods and provides a significant improvement in predicting the particle size distribution and higher moments. The technique allows the convenience of using non-homogeneous, geometric- or equal-size cells. The effectiveness of the technique is illustrated by application to several analytically solvable problems. The numerical results show the ability of the new technique to predict very well the time evolution of the second moment as well as the complete particle size distribution. Also, the computation time taken by the cell average technique is comparable to the fixed pivot technique. More interestingly, for several aggregation problems the cell average technique takes even less computation time than the fixed pivot technique.

Moreover, the cell average technique enjoys the major advantage of simplicity for solving combined problems over other existing schemes. This is done by a special coupling of the different processes that treats all processes in a similar fashion as it handles the individual process. It is demonstrated that the new coupling makes the technique more useful by being not only more accurate but also computationally less expensive. Furthermore, a new idea that considers the growth process as aggregation of existing particle with new small nuclei is presented. In that way the resulting discretization of the growth process becomes very simple and consistent with first two moments. Additionally, it becomes easy to combine the growth discretization with other processes. Furthermore, all discretizations including the growth have been made consistent with the first two moments. The new discretization of growth is a little diffusive but it predicts the first two moments exactly without any computational difficulties like appearance of negative values or instability etc. The numerical scheme proposed in this work is consistent only with the first two moments but it can easily be extended to the consistency with any two or more than two moments.

In order to fully understand what the important features of a given scheme are and how to derive schemes with desired properties, it is essential to perform a thorough mathematical analysis of a scheme, investigating in particular its stability and convergence towards the exact solution. Moreover it provides a necessary basis for further improvements of a scheme. This work provides a mathematical analysis of the cell average method and some other schemes discussed in this work. All investigations are carried out for pure breakage problems since they are easy to deal with due to their linearity. At first, some basic properties of the schemes are investigated. Then the consistency, stability and convergence are proved and they are also confirmed numerically. It is found that the fixed pivot technique is a first order scheme while the cell average technique provides a second order accuracy for most breakage problems. On the other hand, due to the non-linear behavior of aggregation problems, it becomes difficult to analyze them mathematically. Therefore, the schemes for aggregation problems are studied numerically only. It is clearly observed that the convergence of the cell average technique is much faster than that of the fixed pivot technique.

CHAPTER 1. GENERAL INTRODUCTION

The approach of Filbet and Laurençot [21] for solving aggregation PBEs is extended to solving breakage PBEs. A mass conservation law corresponding to the breakage PBE is described and then a fully discrete form of the finite volume scheme is formulated. A stability condition on time step that ensures the positivity and some other properties of the solution is derived. Further, a semi-discrete form of the scheme is introduced. It is also verified by a stability and convergence analysis. The second order convergence is confirmed, both analytically and numerically. The proposed scheme is then coupled with the existing finite volume scheme for solving combined aggregation and breakage problems. Again, a stability condition with a restriction on time step is derived in this case. Several comparisons between the numerical results obtained by the cell average and finite volume schemes are made for pure breakage as well as for coupled problems.

Furthermore, the discretized tracer population balance equations of Hounslow et al. [33] for aggregation problems are discussed and modified. It is shown that the original version was not entirely consistent with the associated discretized population balance equation. These inconsistencies are remedied in a new formulation that retains the advantages of the original discretized tracer population balance equation, such as conservation of total tracer mass, prediction of tracer-weighted mean particle volume, and so on. Furthermore, the discretized tracer population balance equation has been extended to an adjustable discretization. Numerous comparisons are made to demonstrate the validity of the extended and modified formulation.

Additionally, a new discretization for tracer population balance equations is developed. It is compared to the modified discretized tracer population balance equation of Peglow et al. [86]. The new formulation provides excellent prediction of the tracer mass distribution in all test cases. Furthermore, the new formulation is more efficient from a computational point of view. It takes less computational effort and is able to give a very good prediction on a coarser grid. Again, it is independent of the type of grid chosen for computation, i.e. the scheme can be implemented using any type of grid. For finer grids, both formulations tend to produce the same results. The performance of the new formulation is illustrated by the comparison with various analytically tractable problems. Moreover, the new formulation preserves all the advantages of the modified discretized tracer population balance equation and provides a significant improvement in predicting tracer mass distribution and tracer-weighted mean particle volume during an aggregation process.

Finally, the new discretization is extended to solving a two-dimensional population balance equation. Similar to the one-dimensional case, the scheme is based on an exact prediction of certain moments of the population. The formulation is quite simple to implement, computationally less expensive than previous approaches and highly accurate. Numerical diffusion is a common problem with many numerical methods while applied on coarse grids. The presented technique nearly eliminates numerical diffusion and predicts three moments of the population at high accuracy. The technique may be implemented on any type of grid. The accuracy of the scheme has been analyzed by comparing analytical and numerical solutions of some test problems. The numerical results are in excellent agreement with the analytical results and show the ability to predict higher moments very precisely. Additionally, an extension of the proposed technique to higher dimensional problems is discussed.

1.4 Outline of Contents

We start in Chapter 2 with a brief overview of sectional methods for solving population balance equations. In particular we focus in Section 2.2 on the mathematical model and the existing schemes for solving aggregation population balance equations. Hounslow's discretization, the first consistent method with the first two moments for aggregation problems is addressed. Next we present the fixed pivot technique which we use as the building block for our new scheme. Furthermore, the idea of applying a finite volume scheme to the aggregation problems is also discussed. At this point it is shown how the number density based population balance equation can be transformed to a mass conservation law. Section 2.3 presents the population balance equation for breakage and some numerical schemes related to this work. Numerical treatments for growth and nucleation problems have been summarized in Section 2.4. It has been shown there that consistent sectional numerical schemes are oscillatory and inaccurate while finite volume schemes are more diffusive and inconsistent with respect to certain moments.

We then proceed to construct our new scheme in Chapter 3. We are primarily concerned with the general formulation of the scheme for one-dimensional problems followed by a detailed discussion about some advantages of the new scheme over the existing ones. Then the mathematical formulation of the proposed scheme is derived for each case in different sections. We conclude each section by presenting several numerical examples where analytical results are easily available. Finally, some mathematical analysis of the cell average and the fixed pivot techniques is provided. In Section 3.4 the finite volume scheme for breakage population balance equation is introduced. The mass conservation law for breakage is formulated in order to apply the finite volume scheme.

In Chapter 4, the cell average technique is extended to multidimensional aggregation problems. First the scheme is applied to a reduced problem. Then it is formulated for the complete two-dimensional aggregation problem. We begin this chapter with the mathematical modeling of the reduced system. Then, a short overview of Hounslow's discretization for solving the reduced system is given. It is shown with the help of a numerical example that the existing discretization is not able to predict some properties of the distribution. These problems are then overcome by modifying the existing formulation. Then the cell average technique is formulated for solving the reduced system. It is shown there that the new scheme retains all the advantages of the previously existing methods. Further, it has been found there that the two-dimensional formulation is simply an extension of the one-dimensional formulation and therefore it has been shown that the formulation can easily be extended to more than two-dimensional problems. Detailed comparisons of numerical results obtained by the cell average and the extended fixed pivot technique with analytical results for some simple problems are illustrated.

Chapter 5 presents some general conclusions regarding the improvements of the cell average technique over the existing techniques. Finally, some future developments for improving the technique are pointed out.

At the end of the thesis we put two Appendixes. Appendix A summarizes all analytical solutions for pure and coupled processes used in this work. Some more technical mathematical derivations are presented in Appendix B.

Chapter 2

Population Balances

This chapter provides the mathematical models for different particulate processes and a short overview of numerical techniques relating to this work. In particular, we consider aggregation, breakage, growth and nucleation processes. In addition to the sectional methods, the existing finite volume schemes to solve such models will be explored. In this survey we try to describe all methods that appear to be practical and are more or less related to our work.

2.1 Introduction

Equation (1.3) is an micro-distributed form of the population balance equation because it refers to a microscopic region in space. In many cases this form of the PBE is unnecessarily detailed. Therefore it is safe to assume that particles are well mixed throughout the external coordinate region and so the population balance may be integrated over all points in space. A general one-dimensional PBE for a well mixed system then becomes [32, 87]

$$\begin{aligned} \frac{\partial n(t, x)}{\partial t} = & \frac{Q_{\text{in}}}{\tilde{V}} n_{\text{in}}(x) - \frac{Q_{\text{out}}}{\tilde{V}} n_{\text{out}}(x) - \frac{\partial [G(t, x)n(t, x)]}{\partial x} + B_{\text{nuc}}(t, x) \\ & + B_{\text{agg}}(t, x) - D_{\text{agg}}(t, x) + B_{\text{break}}(t, x) - D_{\text{break}}(t, x). \end{aligned} \quad (2.1)$$

This equation must be supplemented with the appropriate initial and boundary conditions. The parameter x represents the size of a particle. The first two terms on the right hand side represent the flow into and out of a *continuous process*. The symbols Q_{in} and Q_{out} denote the inlet and outlet flow rates from the system. The nucleation and growth rates are given by $B_{\text{nuc}}(t, x)$ and $G(t, x)$ respectively. The terms nuc, agg, break have been abbreviated for nucleation, aggregation and breakage respectively. The system volume is represented by \tilde{V} . A *batch process* has no net inflow or outflow of particles. Therefore the first two terms on the right hand side of equation (2.1) can be removed for a batch process. We will be concerned mainly with batch processes in this work.

It is convenient to define moments of the particle size distribution at this time. The j th moment of the particle size distribution n is defined as

$$\mu_j = \int_0^{\infty} x^j n(t, x) dx. \quad (2.2)$$

The first two moments represent some important properties of the distribution. The zeroth ($j = 0$) and first ($j = 1$) moments are proportional to the total number and the total mass of particles respectively. In addition to the first two moments, the second moment of the distribution will be used to compare the numerical results. The second moment is proportional to the light scattered by particles in the Rayleigh limit [57].

2.2 Aggregation

2.2.1 Population Balance Equation

In this section we discuss some numerical techniques for solving aggregation population balance equations. The phenomenon of aggregation appears in a wide range of applications, e.g. in physics (aggregation of colloidal particles), meteorology (merging of drops in atmospheric clouds, aerosol transport, minerals), chemistry (reacting polymers, soot formation, pharmaceutical industries, fertilizers). The temporal change of particle number density in a spatially homogeneous physical system is described by the following well known population balance equation developed by Hulburt and Katz [36]

$$\frac{\partial n(t, x)}{\partial t} = \frac{1}{2} \int_0^x \beta(t, x - \epsilon, \epsilon) n(t, x - \epsilon) n(t, \epsilon) d\epsilon - n(t, x) \int_0^\infty \beta(t, x, \epsilon) n(t, \epsilon) d\epsilon, \quad (2.3)$$

where $t \geq 0$. The first term represents the birth of the particles of size x as a result of the coagulation of particles of sizes $(x - \epsilon)$ and ϵ . Here we shall refer to size as the particle volume. The second term describes the merging of particles of size x with any other particles. The second term is called the death term. The nature of the process is governed by the coagulation kernel β representing properties of the physical medium. It is non-negative and satisfies the symmetry condition $\beta(t, \epsilon, x) = \beta(t, x, \epsilon)$. Analytical solutions of the preceding PBE can be found only in some simplified cases and therefore we need numerical techniques to solve it. Note though, that the known analytical solutions are very useful to assess the accuracy of numerical schemes.

2.2.2 Existing Numerical Methods

Among various numerical techniques: the method of successive approximations, the method of Laplace transforms, the method of moments, weighted residuals, sectional methods, the finite volume methods and Monte Carlo simulation methods, we discuss here only the sectional methods and the finite volume scheme. The sectional methods are well known in process engineering because they are simple to implement and produce exact numerical results of some selected properties. On the other hand the finite volume schemes are well suited for solving conservation laws. The number density based PBE (2.3) can easily be transformed to a conservation law of mass. Then the finite volume schemes can be implemented efficiently.

Hounslow's technique

Hounslow et al. [34] proposed a relatively simple technique using a geometric discretization where the width of i th cell is directly proportional to the width of $(i - 1)$ th. It is convenient to assume that smallest size (volume) in the i th cell is 2^i and the largest size is 2^{i+1} . There are 5 binary interaction mechanisms which are responsible for the changes of particles in the i th

CHAPTER 2. POPULATION BALANCES

cell. The detailed descriptions of the mechanisms can be found in Hounslow et al. [34]. Here we present them briefly.

- Mechanism 1: Aggregates are formed by collisions between particles in the $(i - 1)$ th cells with the particles from the first to the $(i - 1)$ th cells. Some interactions give particles in the i th cell and some interactions give particles smaller than the i th cell. The total birth rate in the i th cell results to the following expression (after including volume correction factor discussed in Hounslow et al. [34])

$$B_i^{[1]} = \sum_{j=1}^{i-2} 2^{j-i+1} \beta_{i-1,j} N_{i-1} N_j. \quad (2.4)$$

- Mechanism 2: The second mechanism is a birth in the cell i by the coalescence of two particles of the cell $i - 1$. Any aggregate formed by two particles coming from cell the $i - 1$ will result in a birth in the cell i . Total birth due to this mechanism is given by

$$B_i^{[2]} = \frac{1}{2} \beta_{i-1,i-1} N_{i-1} N_{i-1}. \quad (2.5)$$

- Mechanism 3: This mechanism represents death in the i th cell due to the coalescence of a particle from size the cell i with a particle sufficiently large enough for the resultant granule to be larger than the upper size limit of the i th cell. The resulting expression (including volume correction factor) for this mechanism results in

$$D_i^{[3]} = N_i \sum_{j=1}^{i-1} 2^{j-i} \beta_{i,j} N_j. \quad (2.6)$$

- Mechanism 4: The fourth mechanism is death in the i th cell due to coalescence of a particle in the i th cell and a particle of that or a higher size cell. All interactions remove particles from the i th cell.

$$D_i^{[4]} = N_i \sum_{j=i}^I \beta_{i,j} N_j. \quad (2.7)$$

- Mechanism 5: Some interactions between the particles of i th cell with the particles from first to the i th cell produce the particles that are still in the i th cell. This mechanism is also a birth mechanism regarding mass and other higher moments but it has no effect on number of particles. This mechanism is different from the others. Hounslow et al. [34] did not consider this mechanism for the formulation of rate of change of the particles in the cell i as the rate of change of particles due to this mechanism is zero. Particles are getting larger within the cell due to this mechanism. This means that mass is increasing in the cell while the number of particles is constant. Hounslow et al. [34] introduced a volume correction factor to compensate for this and probably other effects. It may play a significant role for example when formulating an expression for the mass distribution during aggregation.

Combining all mechanisms stated above, the net rate of change of particles in the cell i is given by

$$\frac{dN_i}{dt} = \sum_{j=1}^{i-2} 2^{j-i+1} \beta_{i-1,j} N_{i-1} N_j + \frac{1}{2} \beta_{i-1,i-1} N_{i-1}^2 - N_i \sum_{j=1}^{i-1} 2^{j-i} \beta_{i,j} N_j - N_i \sum_{j=i}^I \beta_{i,j} N_j \quad i = 1, 2, \dots, I. \quad (2.8)$$

Here I denotes the total number of cells. Litster et al. [69] has generalized this technique to an adjustable geometric size discretization of the form $x_{i+1/2} = 2^{1/q} x_{i-1/2}$, where q is an integer greater than or equal to one. The final discretized set of equations for q is given by

$$\begin{aligned} \frac{dN_i}{dt} = & \sum_{j=1}^{i-S(q)-1} \beta_{i-1,j} N_{i-1} N_j \frac{2^{(j-i+1)/q}}{2^{1/q} - 1} + \frac{1}{2} \beta_{i-q,i-q} N_{i-q}^2 + \sum_{k=2}^q \sum_{j=i-S(q-k+1)-k+1}^{i-S(q-k+1)-k} \\ & \beta_{i-k,j} N_{i-k} N_j \frac{2^{(j-i+1)/q} - 1 + 2^{-(k-1)/q}}{2^{1/q} - 1} + \sum_{k=2}^q \sum_{j=i-S(q-k+1)-k+2}^{i-S(q-k+1)-k+1} \\ & \beta_{i-k+1,j} N_{i-k+1} N_j \frac{-2^{(j-i)/q} + 2^{1/q} - 2^{-(k-1)/q}}{2^{1/q} - 1} \\ & - \sum_{j=1}^{i-S(q)} \beta_{i,j} N_i N_j \frac{2^{(j-i)/q}}{2^{1/q} - 1} - \sum_{j=i-S(q)+1}^I \beta_{i,j} N_i N_j, \end{aligned} \quad (2.9)$$

where $S(q) = \sum_{p=1}^q p$. Higher order moments of particle size distribution can be predicted correctly for sufficiently large values of q . A large value of q implies that a large number of cells are needed to cover the same size domain. Consequently more computational time is required to solve the PBE for larger values of q .

Thereafter, Wynn [120] showed that the above adjustable discretization is not valid for all values of q . For $q > 4$, the formulation (2.9) is not correct. The correct formulation according to Wynn [120] is given as

$$\begin{aligned} \frac{dN_i}{dt} = & \sum_{j=1}^{i-S_1} \frac{2^{(j-i+1)/q}}{2^{1/q} - 1} \beta_{i-1,j} N_{i-1} N_j + \sum_{p=2}^q \sum_{j=i-S_p-1}^{i-S_p} \frac{2^{(j-i+1)/q} - 1 + 2^{-(p-1)/q}}{2^{1/q} - 1} \beta_{i-p,j} N_{i-p} N_j \\ & + \frac{1}{2} \beta_{i-q,i-q} N_{i-q}^2 + \sum_{p=1}^{q-1} \sum_{j=i+1-S_p}^{i+1-S_{p+1}} \frac{2^{1/q} - 2^{(j-i)/q} - 2^{-p/q}}{2^{1/q} - 1} \beta_{i-p,j} N_{i-p} N_j \\ & - \sum_{j=1}^{i-S_1+1} \frac{2^{(j-i)/q}}{2^{1/q} - 1} \beta_{i,j} N_i N_j - \sum_{j=i-S_1+2}^I \beta_{i,j} N_i N_j, \end{aligned} \quad (2.10)$$

where $S_p = \text{Int} \left[1 - \frac{q \ln(1-2^{-p/q})}{\ln 2} \right]$ with $\text{Int}[x]$ being the integer part of x . Wynn et al. [120] introduced this parameter to correct the limits of the sums which were wrong in the original work of Litster et al. [69].

The fixed pivot technique

The discretization discussed above has the disadvantage that it can only be applied on a specified grid. Kumar and Ramkrishna [57] developed the fixed pivot technique. This technique does not only preserve the number and mass of the particles, but it can also be generalized for the preservation of any two desired properties of the population. This technique divides the entire size range into small cells. The size of a cell can be chosen arbitrarily. The size range contained between two sizes $x_{i-1/2}$ and $x_{i+1/2}$ is called the i th cell. The particle population in this size range is represented by a size x_i , called grid point, such that $x_{i-1/2} < x_i < x_{i+1/2}$. A new particle of size x in the size range $[x_i, x_{i+1}]$, formed either due to breakup or aggregation, can be represented by assigning fractions $a_1(x, x_i)$ and $a_2(x, x_{i+1})$ to the populations at x_i and x_{i+1} respectively. For the consistency with two general properties $f_1(x)$ and $f_2(x)$, these fractions must satisfy the following equations

$$a_1(x, x_i)f_1(x_i) + a_2(x, x_{i+1})f_1(x_{i+1}) = f_1(x) \quad (2.11)$$

$$a_1(x, x_i)f_2(x_i) + a_2(x, x_{i+1})f_2(x_{i+1}) = f_2(x). \quad (2.12)$$

Furthermore, these equations can be generalized for the consistency with more than two properties by assigning the particle size x to more than two grid points. The population at representative volume x_i gets a fractional particle for every particle that is born in size range $[x_i, x_{i+1}]$ or $[x_{i-1}, x_i]$. Integrating the continuous equation (2.3) over a cell i , we obtain

$$\begin{aligned} \frac{dN_i(t)}{dt} &= \frac{1}{2} \int_{x_{i-1/2}}^{x_{i+1/2}} \int_0^x \beta(t, x - \epsilon, \epsilon)n(t, x - \epsilon)n(t, \epsilon) d\epsilon dx \\ &\quad - \int_{x_{i-1/2}}^{x_{i+1/2}} n(t, x) \int_0^\infty \beta(t, x, \epsilon)n(t, \epsilon) d\epsilon dx. \end{aligned} \quad (2.13)$$

Let us denote the first and second terms on the right hand side by B_i and D_i respectively. We now consider the birth term which has been modified according to Kumar and Ramkrishna [57] as

$$\begin{aligned} B_i^{\text{FP}} &= \frac{1}{2} \int_{x_i}^{x_{i+1}} a_1(x, x_i) \int_0^x \beta(t, x - \epsilon, \epsilon)n(t, x - \epsilon)n(t, \epsilon) d\epsilon dx \\ &\quad + \frac{1}{2} \int_{x_{i-1}}^{x_i} a_2(x, x_i) \int_0^x \beta(t, x - \epsilon, \epsilon)n(t, x - \epsilon)n(t, \epsilon) d\epsilon dx. \end{aligned} \quad (2.14)$$

Kumar and Ramkrishna have considered that particles with number concentrations $N_i, i = 1, 2, \dots, I$ are sitting at sizes $x_i, i = 1, 2, \dots, I$ respectively. Mathematically the number density function $n(t, x)$ can be represented in terms of Dirac-delta distribution as

$$n(t, x) \approx \sum_{i=1}^I N_i \delta(x - x_i). \quad (2.15)$$

Substituting the number density from (2.15) into the equation (2.14), the discrete birth term can be obtained. For the consistency with numbers and mass, the discrete birth rate for aggregation

is given by

$$B_i^{\text{FP}} = \sum_{\substack{j \geq k \\ j, k \\ x_{i-1} \leq x < x_{i+1}}} \left(1 - \frac{1}{2} \delta_{j,k}\right) \eta(x) \beta_{j,k} N_j N_k, \quad (2.16)$$

with η taken to be

$$\eta(x) = \begin{cases} \frac{x_{i+1} - x}{x_{i+1} - x_i}, & x_i \leq x < x_{i+1} \\ \frac{x - x_{i-1}}{x_i - x_{i-1}}, & x_{i-1} \leq x < x_i, \end{cases} \quad (2.17)$$

where $x = x_j + x_k$ and $\beta_{j,k} = \beta(t, x_j, x_k)$. Similarly the death rate can be obtained by substituting the number density from equation (2.15) into the death term D_i . A complete derivation of the birth and death terms is provided in Appendix B.1. The final set of discrete equation is given as

$$\frac{dN_i}{dt} = \sum_{\substack{j \geq k \\ j, k \\ x_{i-1} \leq x < x_{i+1}}} \left(1 - \frac{1}{2} \delta_{j,k}\right) \eta(x) \beta_{j,k} N_j N_k - N_i \sum_{k=1}^I \beta_{i,k} N_k, \quad i = 1, 2, \dots, I. \quad (2.18)$$

A different form of the formulation (2.18) is presented in Appendix B.2. Although the technique possesses many features of flexibility, the authors have shown that the proposed technique has the disadvantage of over-prediction of the number density in the large size range when applied on coarse grids. Consequently, it highly overestimates the higher moments of the particle size distribution. Kumar and Ramkrishna have also developed a moving pivot technique [58] to overcome the over-prediction. The latter technique is more complex and gives difficulties to solve the resulting set of ordinary differential equations (ODEs). The moving pivot approach of discretizing the PBE results in a system of stiff differential equations.

It is also of interest to simplify the fixed pivot formulation for geometric grids of the type $x_{i+1} = 2x_i$. The formulation (2.18) for the grids $x_{i+1} = 2x_i$ takes the following form in this case

$$\frac{dN_i}{dt} = \sum_{j=1}^{i-2} 2^{j-i-1} \beta_{i-1,j} N_{i-1} N_j + \frac{1}{2} \beta_{i-1,i-1} N_{i-1}^2 + N_i \sum_{j=1}^{i-1} (1 - 2^{j-i}) \beta_{i-1,j} N_j - N_i \sum_{j=1}^I \beta_{i,j} N_j. \quad (2.19)$$

The preceding equation can be simplified further to get

$$\frac{dN_i}{dt} = \sum_{j=1}^{i-2} 2^{j-i-1} \beta_{i-1,j} N_{i-1} N_j + \frac{1}{2} \beta_{i-1,i-1} N_{i-1}^2 + N_i \sum_{j=1}^{i-1} 2^{j-i} \beta_{i-1,j} N_j - N_i \sum_{j=i}^I \beta_{i,j} N_j. \quad (2.20)$$

This equation is exactly the same as Hounslow's discretized population balance equation (2.8). Note that the birth and death terms have different expressions in both discretizations but the final form of both schemes is the same. In Hounslow's discretization, the birth and death terms compute the net birth and death rates while in the fixed pivot technique the total birth and death rates are computed.

The finite volume scheme

Now we present a completely different approach, the finite volume scheme, for solving aggregation population balance equation. The finite volume schemes are frequently used for solving conservation laws. Filbet and Laurençot [21] applied the finite volume approach to the aggregation population balance equation by modeling the aggregation process as mass conservation law, see also Makino et al. [73]. First we present the mass conservation law for aggregation process and then the finite volume discretization to solve the model.

Mass conservation law for aggregation: Aggregation process may be described as the mass flow along the mass coordinate. Thus, the evolution of the mass distribution can be expressed by the following mass conservation laws as

$$\frac{\partial xn(x)}{\partial t} + \frac{\partial F(x)}{\partial x} = 0, \tag{2.21}$$

where $n(x)$ is the number density and $F(x)$ is the mass flux across mass x . For the case of binary aggregation, the outcomes of the aggregation events are trivial, i.e. two particles of masses x_1 and x_2 will form a new particle of mass $x_1 + x_2$. In the case of fragmentation it depends on the mass distribution of fragments created by an impact. The aggregation frequency between particles with masses x_1 and particles with masses x_2 by

$$\beta_{x_1,x_2}n(x_1)n(x_2), \tag{2.22}$$

where $\beta_{x_1,x_2} = \beta_{x_2,x_1}$ is the aggregation rate of a particle with mass x_1 against particles with mass x_2 .

Consider a particle of mass x_1 with $0 < x_1 < x$ which collides with a particle of mass x_2 satisfying $x - x_1 < x_2 < \infty$. As a result of this aggregation event, there is a mass flow across x which is given by considering the following two cases.

- First, consider collision between particles of masses x_1 for $0 < x_1 < x$ and x_2 for $x \leq x_2 < \infty$. In this case, it is readily seen that mass flux through x is x_1 .
- The remaining collisions where particles of masses x_1 for $0 < x_1 < x$ collide with particles of masses x_2 with $x - x_1 < x_2 < x$, the flux across x is simply $x_1 + x_2$.

Now summing all pairs of particles which gives mass flow across x , we obtain the total mass flux across x as

$$F(x) = \frac{1}{2} \int_0^x \int_{x-x_1}^x (x_1 + x_2)\beta_{x_1,x_2}n(x_1)n(x_2) dx_2 dx_1 + \int_0^x \int_x^\infty x_1\beta_{x_1,x_2}n(x_1)n(x_2) dx_2 dx_1. \tag{2.23}$$

The factor $1/2$ appears due to double counting of collisions in that range. The first term can further be simplified as follows

$$\begin{aligned} \text{I} &= \frac{1}{2} \int_0^x \int_{x-x_1}^x (x_1 + x_2)\beta_{x_1,x_2}n(x_1)n(x_2) dx_2 dx_1 \\ &= \frac{1}{2} \int_0^x \int_{x-x_1}^x x_1\beta_{x_1,x_2}n(x_1)n(x_2) dx_2 dx_1 + \frac{1}{2} \int_0^x \int_{x-x_1}^x x_2\beta_{x_1,x_2}n(x_1)n(x_2) dx_2 dx_1. \end{aligned} \tag{2.24}$$

Changing the order of integration of the second term and then interchanging the integration variables x_1 and x_2 , the first term (I) takes the following simplified form

$$\begin{aligned} \text{I} &= \frac{1}{2} \int_0^x \int_{x-x_1}^x x_1 \beta_{x_1, x_2} n(x_1) n(x_2) dx_2 dx_1 + \frac{1}{2} \int_0^x \int_{x-x_1}^x x_1 \beta_{x_1, x_2} n(x_1) n(x_2) dx_2 dx_1 \\ &= \int_0^x \int_{x-x_1}^x x_1 \beta_{x_1, x_2} n(x_1) n(x_2) dx_2 dx_1. \end{aligned} \quad (2.25)$$

Using this the flux function reduces simply to

$$F(x) = \int_0^x \int_{x-x_1}^{\infty} x_1 \beta_{x_1, x_2} n(x_1) n(x_2) dx_2 dx_1. \quad (2.26)$$

Substituting the flux function $F(x)$ into equation (2.21), we get

$$\frac{\partial x n(x)}{\partial t} + \frac{\partial}{\partial x} \left(\int_0^x \int_{x-x_1}^{\infty} x_1 \beta_{x_1, x_2} n(x_1) n(x_2) dx_2 dx_1 \right) = 0. \quad (2.27)$$

Now we show that the above mass conservation law (2.27) can easily be transformed to the standard continuous population balance equation. By making use of the Leibnitz integration rule, we obtain

$$\frac{\partial x n(x)}{\partial t} + \int_0^x \frac{\partial}{\partial x} \int_{x-x_1}^{\infty} x_1 \beta_{x_1, x_2} n(x_1) n(x_2) dx_2 dx_1 + \int_0^{\infty} x \beta_{x, x_2} n(x) n(x_2) dx_2 = 0. \quad (2.28)$$

Further applying Leibnitz integration rule in the first term, this equation takes the following form

$$\frac{\partial x n(x)}{\partial t} = \int_0^x x_1 \beta_{x_1, x-x_1} n(x_1) n(x-x_1) dx_1 - \int_0^{\infty} x \beta_{x, x_2} n(x) n(x_2) dx_2. \quad (2.29)$$

The first term on the right hand side can be split into two parts

$$\begin{aligned} \frac{\partial x n(x)}{\partial t} &= \int_0^x \left(\frac{x}{2} + x_1 - \frac{x}{2} \right) \beta_{x_1, x-x_1} n(x_1) n(x-x_1) dx_1 - \int_0^{\infty} x \beta_{x, x_2} n(x) n(x_2) dx_2 \\ &= \frac{x}{2} \int_0^x \beta_{x_1, x-x_1} n(x_1) n(x-x_1) dx_1 - \int_0^{\infty} x \beta_{x, x_2} n(x) n(x_2) dx_2 \\ &\quad + \int_0^x \frac{x_1}{2} \beta_{x_1, x-x_1} n(x_1) n(x-x_1) dx_1 - \int_0^x \frac{(x-x_1)}{2} \beta_{x_1, x-x_1} n(x_1) n(x-x_1) dx_1 \\ &= \frac{x}{2} \int_0^x \beta_{x_1, x-x_1} n(x_1) n(x-x_1) dx_1 - \int_0^{\infty} x \beta_{x, x_2} n(x) n(x_2) dx_2 \\ &\quad + \frac{1}{2} \int_0^x x_1 \beta_{x_1, x-x_1} n(x_1) n(x-x_1) dx_1 - \frac{1}{2} \int_0^x x_1 \beta_{x_1, x-x_1} n(x_1) n(x-x_1) dx_1 \\ &= \frac{x}{2} \int_0^x \beta_{x_1, x-x_1} n(x_1) n(x-x_1) dx_1 - x \int_0^{\infty} \beta_{x, x_2} n(x) n(x_2) dx_2. \end{aligned} \quad (2.30)$$

Thus, dividing out x the equation (2.30) turns into the classical aggregation equation (2.3).

CHAPTER 2. POPULATION BALANCES

Numerical discretization: Let us consider a finite domain $[0, x_I]$ for the computation. We consider finite volume scheme for the discretization of equation (2.21). We discretize time in discrete level t_m , $m = 1, 2, \dots$, and the space into I cells $\Lambda_i = [x_{i-1/2}, x_{i+1/2}[$, $i = 1, 2, \dots, I$. Integrating the conservation law on a cell in space-time $\Lambda_i \times [t_m, t_{m+1}]$ we obtain

$$\int_{x_{i-1/2}}^{x_{i+1/2}} xn(t_{m+1}, x) dx = \int_{x_{i-1/2}}^{x_{i+1/2}} xn(t_m, x) dx - \int_{t_m}^{t_{m+1}} (F(t, x_{i+1/2}) - F(t, x_{i-1/2})) dt. \quad (2.31)$$

We can rewrite the above equation as

$$g_i^{m+1} = g_i^m - \frac{\Delta t}{\Delta x_i} (J_{i+1/2}^m - J_{i-1/2}^m), \quad i = 1, 2, \dots, I, \quad (2.32)$$

where g_i^m denotes an approximation of the cell average of $g(t^m, x) = xn(t^m, x)$ on cell i at time t_m , and $J_{i+1/2}^m$ approximates the flux on the boundary of the cell. It is the so called numerical flux. According to Filbet and Laurençot [21], the numerical flux has been approximated as follows

$$J_{i+1/2}^m = \sum_{k=1}^i \Delta x_k g_k^m \left[\sum_{j=\alpha_{i,k}}^I \int_{\Lambda_j} \frac{\beta(u, x_k)}{u} du g_j^m + \int_{x_{i+1/2}-x_k}^{x_{\alpha_{i,k}-1/2}} \frac{\beta(u, x_k)}{u} du g_{\alpha_{i,k}-1}^m \right]. \quad (2.33)$$

The integer $\alpha_{i,k}$ corresponds to the index of the cell such that $x_{i+1/2} - x_k \in \Lambda_{\alpha_{i,k}-1}$. The authors pointed out that the formulation (2.32) provides a second order accuracy. It is important to emphasize that unlike the fixed pivot technique the formulation (2.32) is consistent only with the first moment.

2.3 Breakage

2.3.1 Population Balance Equation

Population balances for breakage are widely known in high shear granulation, crystallization, atmospheric science and many other particle related engineering problems. The general form of population balance equation for breakage is given as [124]

$$\frac{\partial n(t, x)}{\partial t} = \int_x^\infty b(x, \epsilon) S(\epsilon) n(t, \epsilon) d\epsilon - S(x) n(t, x). \quad (2.34)$$

The breakage function $b(x, \epsilon)$ is the probability density function for the formation of particles of size x from particle of size ϵ . The selection function $S(\epsilon)$ describes the rate at which particles are selected to break. The breakage function has the following properties

$$\int_0^x b(\epsilon, x) d\epsilon = \bar{N}(x), \quad (2.35)$$

and

$$\int_0^x \epsilon b(\epsilon, x) d\epsilon = x. \quad (2.36)$$

The function $\bar{N}(x)$ represents the number of fragments obtained from the breakage of particle of size x .

In the literature, it is common to write the above population balance equation for binary breakage as, see Ziff and McGrady [125],

$$\frac{\partial n(t, x)}{\partial t} = 2 \int_x^\infty \tilde{B}(x, \epsilon - x) n(t, \epsilon) d\epsilon - n(t, x) \int_0^x \tilde{B}(\epsilon, x - \epsilon) d\epsilon, \quad (2.37)$$

where $\tilde{B}(x, y) = \tilde{B}(y, x)$, gives the rate that an $(x + y)$ -mer breaks into an x -mer and a y -mer. The relationships between b , S and B can be found from equation (2.34) and equation (2.37),

$$S(x) = \int_0^x \tilde{B}(\epsilon, x - \epsilon) d\epsilon, \quad \text{and} \quad b(x, \epsilon) = 2\tilde{B}(x, \epsilon - x)/S(\epsilon). \quad (2.38)$$

The above PBE (2.34) can only be solved analytically for very simple forms of the breakage and selection functions, see [13, 124, 125]. This certainly leads to a discussion of numerical methods for solving PBE. Numerical methods fall into several categories: stochastic methods, [64, 76], finite element methods, Everson et al. [20], sectional methods, Kumar and Ramkrishna [57, 58], and moment methods [50, 51].

The stochastic methods (Monte-Carlo) are very efficient for solving multi-dimensional population balance equations, since other numerical techniques become computationally very expensive in such cases. A wide varieties of finite element methods, weighted residuals, the method of orthogonal collocation and Galerkin's method are also used for solving breakage population balance equations. In these methods, the solution is approximated as linear combinations of basis functions over a finite number of sub-domain. In recent times, the sectional methods have become computationally very attractive. A detailed review of sectional methods has been recently given by Vanni [116]. In the moment method, the fragmentation equation is transformed into a system of ODEs describing the evolution of the moments of the particle size distribution.

2.3.2 Existing Numerical Methods

Sectional methods are the most important alternatives for solving PBEs since they are simple to implement and predict particle properties accurately. Several sectional methods for breakage PBE have been recently proposed by Hill and Ng [30], Kumar and Ramkrishna [57, 58], as well as Vanni [115]. We briefly discuss them here.

Hounslow et al. [34] proposed a numerical method for solving aggregation problems which emerged to be the first discretized method that preserves the first two moments. Following this Hill and Ng [30] developed a discretized method for general breakage population balance equation. They used two correction factors in the discretized equation to preserve the first two moments. In order to calculate the correction factors they imposed two conditions: the correct evaluation of total mass (the first moment) and the correct evaluation of the total number (the zeroth moment). Since the calculation of the correction factors was not possible for the general case, they considered three different forms of the breakage function and a special form of the selection function $S(x) = S_0 x^\alpha$. Afterwards, Vanni [115] modified the discretized method of Hill and Ng [30] to make it more general. Keeping the entire formulation the same, Vanni changed

CHAPTER 2. POPULATION BALANCES

the second condition to calculate the correction factor. He considered the correct evaluation of the death term while Hill and Ng [30] imposed the correct prediction of the total number of particles. The method becomes more general but finally it leads to less accurate solutions.

Hounslow et al. [33] introduced a new discretization for breakage PBE. They calculated the selection and the breakage functions by imposing the condition of correct evaluation of the total number and the movement of granule volume from one interval to another. The formulation predicts the total number and the total mass correctly, but the selection and the breakage functions require the computation of many single and double integrals. Later, Tan et al. [109], used this discretization in his work on fluidized bed melt granulation.

Kumar and Ramkrishna [57] applied the fixed pivot technique to the breakage population balance equation. It is found that the fixed pivot technique is more general than previously existing techniques. A Similar procedure like we have in the formulation of the discretized equations for aggregation can be followed to get the discretized equations for the breakage. Their final set of discretized equations for the exact preservation of number and mass in this case take the following form

$$\begin{aligned} \frac{dN_i(t)}{dt} &= \sum_{k=i}^I \eta_{i,k} S_k N_k(t) - S_i N_i(t), \quad i = 1, 2, \dots, I, \\ &=: B_i^{\text{FP}} - D_i^{\text{FP}}, \quad i = 1, 2, \dots, I. \end{aligned} \quad (2.39)$$

Here, S_k is $S(x_k)$ and the function η is described by

$$\eta_{i,k} = \int_{x_i}^{x_{i+1}} a_1(x, x_i) b(x, x_k) dx + \int_{x_{i-1}}^{x_i} a_2(x, x_i) b(x, x_k) dx, \quad (2.40)$$

where

$$a_1(x, x_i) = \frac{x_{i+1} - x}{x_{i+1} - x_i}, \quad a_2(x, x_i) = \frac{x - x_{i-1}}{x_i - x_{i-1}}. \quad (2.41)$$

Note that the following local conservation properties hold

$$a_1(x, x_i) + a_2(x, x_{i+1}) = 1, \quad (2.42)$$

and

$$x_i a_1(x, x_i) + x_{i+1} a_2(x, x_{i+1}) = x. \quad (2.43)$$

The fundamental concept behind the fixed pivot technique can be summarized as follows. Suppose a new particle of a size which is not a representative of any cell appears due to breakage of larger particles. The particle has to be divided to neighboring representatives in such a way that number and mass are conserved. In this process numerical diffusion is of course possible due to the assignment of particles to the representatives to whom they do not really belong. Nevertheless, quite satisfactory results can be obtained by this technique. However, it will be shown later that the fixed pivot technique over-predicts the results. Since in breakage process particles flow towards the smaller particles, the fixed pivot technique overestimates the number density of smaller particles. Moreover, we will see in Section 3.3 that the fixed pivot technique is a first order method for breakage problems.

2.4 Growth

2.4.1 Population Balance Equation

A growth process is common in a wide range of particulate process including crystallization and granulation. The population balance equation for pure growth is given as

$$\frac{\partial n(t, x)}{\partial t} + \frac{\partial [G(x)n(t, x)]}{\partial x} = 0. \quad (2.44)$$

This is a hyperbolic type equation due to growth term. It suffers from many computational difficulties. A detailed review of some simple numerical schemes used for solving such equations will be presented here. A more complex methods can be found in Hundsdorfer and Verwer [37] as well as in LeVeque [66] and references therein.

2.4.2 Existing Numerical Methods

Finite volume schemes are known to be a good approach to solve such equations, since they automatically incorporate conservation of number in a growth process. We first briefly discuss the finite volume schemes. Then numerical problems with these methods will be mentioned. Our interest here is in formulating a semi-discretized form of the above equation so that the method of lines (MOL) approach can easily be applied. The reason for the MOL approach here is the easy coupling of various process like aggregation, breakage etc. and of course easily available ODE integrators. We discretize the domain into equal spatial cells $\Omega_i = [x_{i-1/2}, x_{i+1/2}]$ and define as nodes $x_i = (x_{i-1/2} + x_{i+1/2})/2$ the centers of the cells. Direct integration of equation (2.44) over each cell gives the semi-discrete formulation

$$\frac{dN_i(t)}{dt} = G(x_{i-1/2})n(t, x_{i-1/2}) - G(x_{i+1/2})n(t, x_{i+1/2}), \quad i = 1, 2, \dots, I. \quad (2.45)$$

Various methods for the numerical solutions of equation (2.44) can be obtained from different choices of the approximation of $n(t, x_{i-1/2})$ and $n(t, x_{i+1/2})$ in terms of $N_i(t)$. The easiest approximation $n(t, x_{i+1/2}) \approx N_i(t)/\Delta x$ gives the first order upwind difference discretization

$$\frac{dN_i(t)}{dt} = \frac{1}{\Delta x} [G(x_{i-1/2})N_{i-1} - G(x_{i+1/2})N_i]. \quad (2.46)$$

The choice

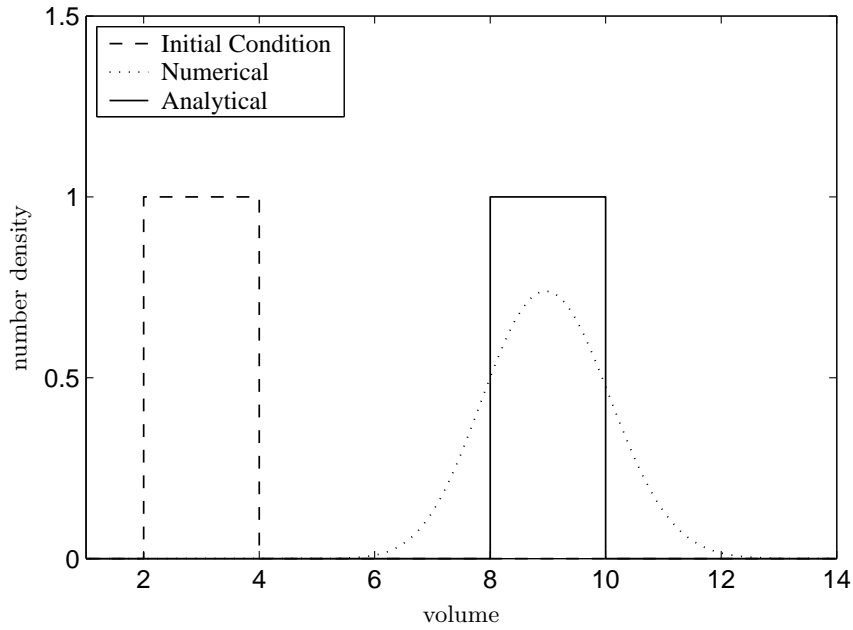
$$n(t, x_{i+1/2}) \approx \frac{1}{2\Delta x} [N_i(t) + N_{i+1}(t)]$$

gives the second order central discretization

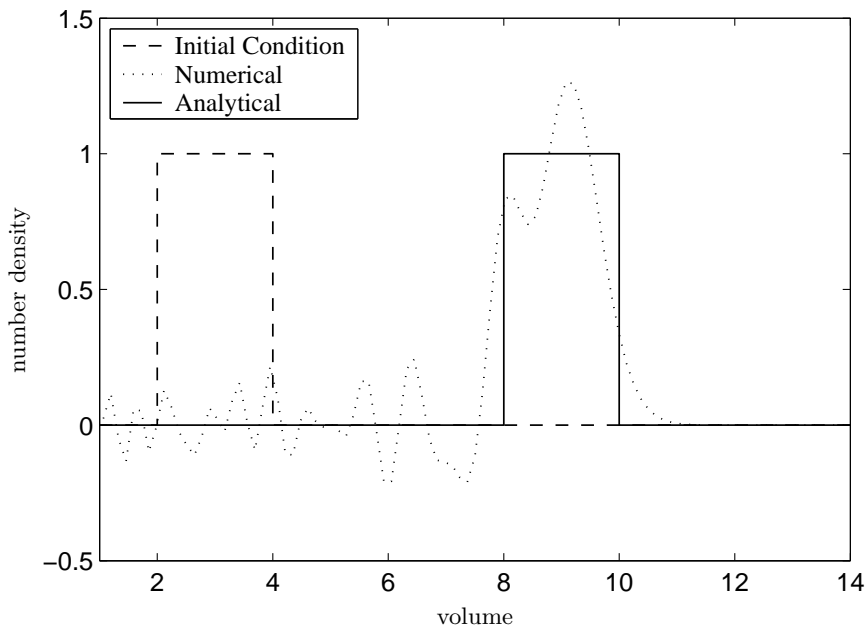
$$\frac{dN_i(t)}{dt} = \frac{1}{2\Delta x} [G(x_{i-1/2})\{N_{i-1}(t) + N_i(t)\} - G(x_{i+1/2})\{N_i(t) + N_{i+1}(t)\}]. \quad (2.47)$$

The PBE (2.44) is solved using the first order upwind discretization and the second order central discretization for $G(v) = 1$ and

$$n(0, x) = \begin{cases} 1, & 2 \leq x \leq 4, \\ 0, & \text{otherwise.} \end{cases} \quad (2.48)$$



(a) First order upwind scheme.



(b) Second order central scheme.

Figure 2.1: Particle size distributions for pure growth with constant growth rate at $t = 6$ obtained on 100 uniform fixed grid points.

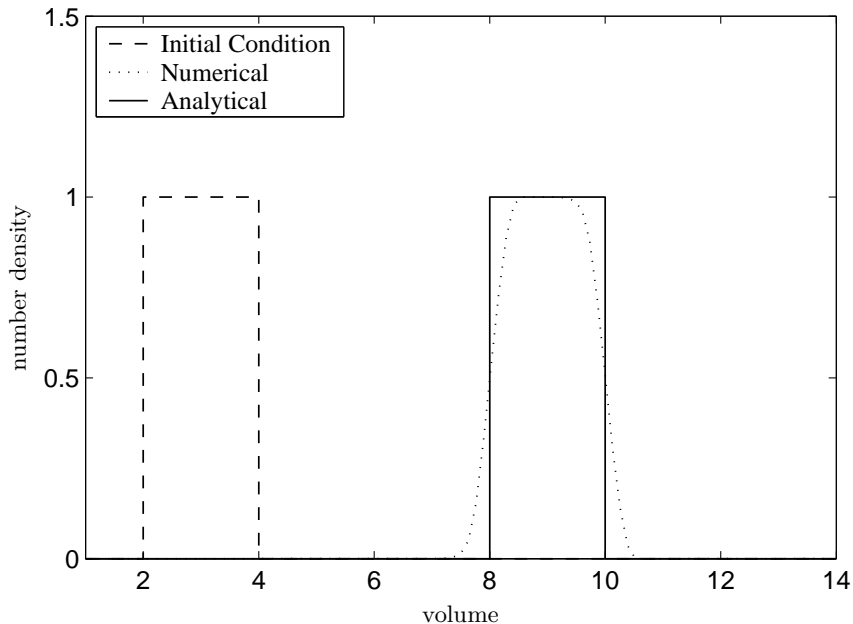


Figure 2.2: Particle size distributions for pure growth with constant growth rate at $t = 6$ obtained on 100 uniform fixed grid using flux limiter method.

The computation is carried out on 100 uniform fixed cells at $t = 6$. For the integration of both the discrete formulations, MATLAB ODE45 solver has been used. It is a one step solver based on an explicit Runge-Kutta (4,5) formula. The results have been plotted in Figure 2.1. The first order upwind scheme smeared and therefore is not accurate. The second order scheme produces oscillations and seems to be unstable. The second order scheme is expected to be more accurate than the first order scheme. This is only true for very smooth solutions. Unfortunately most of the higher order schemes suffer from oscillations and produce negative values that are unrealistic. The first order upwind scheme is an alternative for non-oscillatory simple scheme but that is very diffusive and inaccurate. Therefore the first order upwind scheme in real application is not usually recommended.

A class of more sophisticated discretization methods that preserve positivity and attain more accuracy than the first order upwind are the so called *flux limiting methods*. These methods, also known as *high resolution schemes*, are obtained by modifying the fluxes of a higher order discretization. The idea behind high resolution schemes is to apply a high order flux in smooth regions and a low order flux near discontinuities. This is achieved by measuring the smoothness of the data. Many high resolution methods can be found in Koren [47], LeVeque [65], Hundsdorfer and Verwer [37] as well as Kurganov and Tadmor [60]. Here we present one example of a flux limiting method which was introduced by Koren [47]. In this method the number density at the boundary is approximated by

$$n(t, x_{i+1/2}) \approx \frac{1}{\Delta x} \left[N_i(t) + \frac{1}{2} \phi(\theta_{i+1/2}) \{ N_i(t) - N_{i-1}(t) \} \right]. \quad (2.49)$$

CHAPTER 2. POPULATION BALANCES

Here ϕ is the limiter function defined as

$$\phi(\theta) = \max \left[0, \min \left\{ 2\theta, \min \left(\frac{1}{3} + \frac{2}{3}\theta, 2 \right) \right\} \right], \quad (2.50)$$

where the parameter θ is defined as

$$\theta_{i+1/2} = \frac{N_{i+1} - N_i + \epsilon}{N_i - N_{i-1} + \epsilon}, \quad (2.51)$$

with a very small constant ϵ to avoid division by zero. Using this method we computed the solution of equation (2.44) on the test problem under the same conditions as before. The numerical results have been shown in Figure 2.2. Clearly this scheme gives a better accuracy than the first order upwind without producing negative values. The application of some other high resolution schemes for growth PBE can be found in Lim et al. [67] and Gunawan et al. [27]. It is known that some of the finite volume methods for hyperbolic problems are more efficient on a direct space-time discretization approach. Since we are interested in the MOL approach, our choice of finite volume schemes is restricted to some extent. Also note that we used only homogeneous grids in our computation. As we have seen for breakage and aggregation problems non-homogeneous grids are preferred and therefore we wish to have the same here. It is of course possible to extend these methods to non-homogeneous grids. But the extension of finite volume scheme to non-uniform grids is not a trivial task, see Hundsdorfer and Verwer [37].

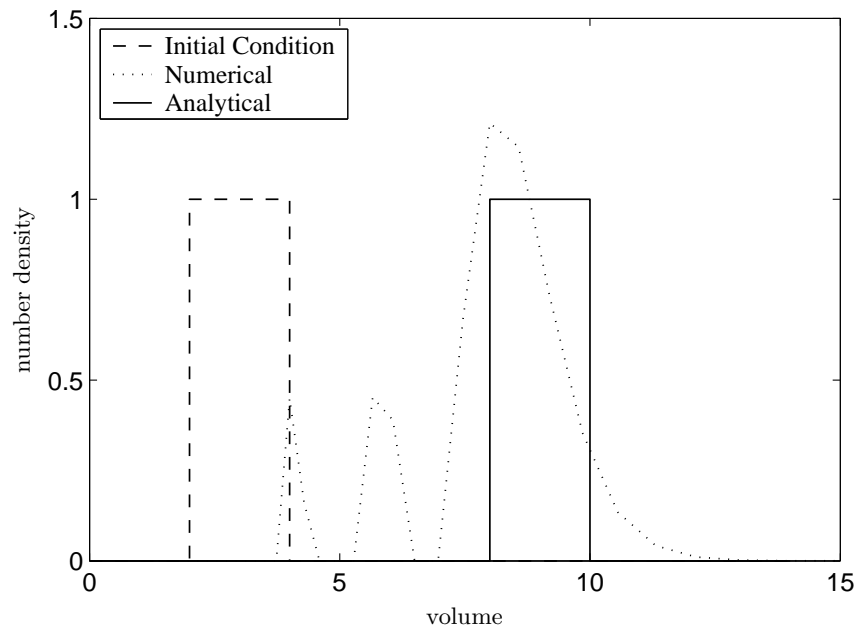
Complexity of the finite volume scheme on non-homogeneous grids and the restricted class of methods where one can apply MOL approach motivate us to discuss a different class of discretized methods. We will discuss some methods that rely on correct prediction of some selected moments. Hounslow et al. [34] seem to have been the first in the literature to propose a method which is consistent with the first three moments with respect to particle length. Their discrete formulation for the equation (2.44) considering volume as an internal coordinate can be obtained by the following expression, see Park and Rogak [80],

$$\frac{dN_i}{dt} = \frac{\check{a}G_{i-1}N_{i-1}}{x_{i-1}} + \frac{\check{b}G_iN_i}{x_i} + \frac{\check{c}G_{i+1}N_{i+1}}{x_{i+1}}, \quad (2.52)$$

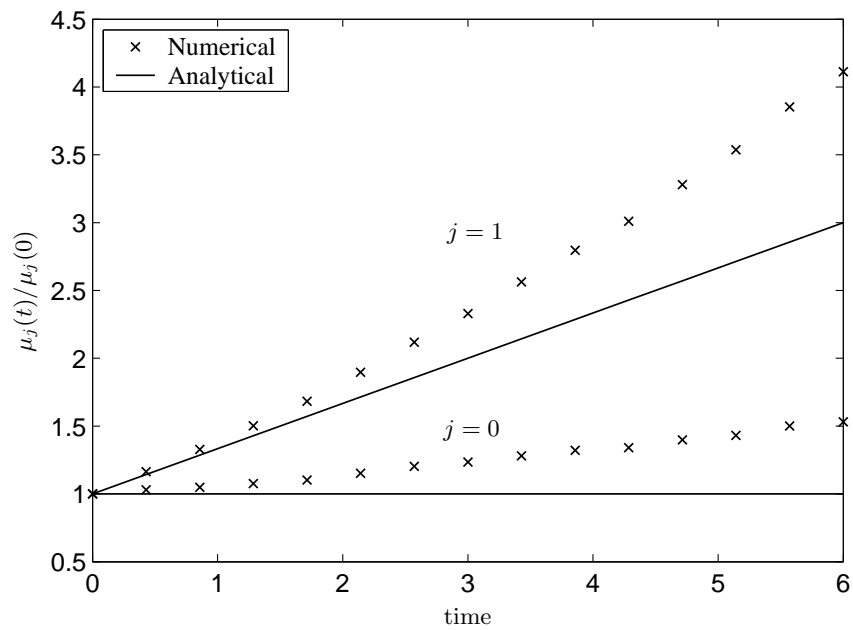
where \check{a} , \check{b} and \check{c} are constants. They have been chosen so that the discretization predicts correctly the first three moments. Their final set of equations is

$$\frac{dN_i}{dt} = \frac{1}{x_i} \left(\frac{r}{r^2 - 1} G_{i-1} N_{i-1} + G_i N_i - \frac{r}{r^2 - 1} G_{i+1} N_{i+1} \right), \quad (2.53)$$

where $r = x_{i+1}/x_i$ and $G_i = G(x_i)$. We have tested this discretization on our model problem (2.48) under the same conditions as in Figures 2.1 and 2.2. As suggested by the authors, we suppressed the negative values to zero that cause an increase of total number and mass. An unstable behavior of the model and inaccurate particle size distribution can be seen in Figure 2.3(a). The temporal over-prediction of total number and volume due to setting of negative values to zeros has been plotted in Figure 2.3(b).



(a) Particle size distribution.



(b) Moments.

Figure 2.3: Numerical results for pure growth with constant growth rate at $t = 6$ obtained on 40 non-uniform logarithmic fixed grid points using Hounslow et al. [34].

CHAPTER 2. POPULATION BALANCES

Following Hounslow et al. [34], an effort to overcome these difficulties has been made recently by Park and Rogak [80]. They also started with the same formulation like (2.52) assigning different constants in each cell. They consider the following formulation

$$\frac{dN_i}{dt} = \frac{\check{a}_{i-1}G_{i-1}N_{i-1}}{x_{i-1}} + \frac{\check{b}_iG_iN_i}{x_i} + \frac{\check{c}_{i+1}G_{i+1}N_{i+1}}{x_{i+1}}, \quad (2.54)$$

where $G_i = G(x_i)$ and the coefficients \check{a}_i , \check{b}_i and \check{c}_i have been calculated by imposing the conditions of correct prediction of the first two moments and the slope of the size distribution as

$$\check{b}_i = \begin{cases} -\frac{r}{r-1} \operatorname{erf}\left(\frac{1}{4} \frac{d \ln N_i}{d \ln x_i}\right), & \frac{d \ln N_i}{d \ln x_i} \leq 0, \\ -\frac{1}{r-1} \operatorname{erf}\left(\frac{1}{4} \frac{d \ln N_i}{d \ln x_i}\right), & \frac{d \ln N_i}{d \ln x_i} > 0, \end{cases} \quad (2.55)$$

$$\check{a}_i = \frac{r - \check{b}_i(r-1)}{r^2 - 1}, \quad (2.56)$$

and

$$\check{c}_i = -(\check{a}_i + \check{b}_i). \quad (2.57)$$

The term $d \ln N_i / d \ln x_i$ in \check{b}_i has been calculated using the second order central scheme. The formulation (2.54) can also be rewritten in conservative form as

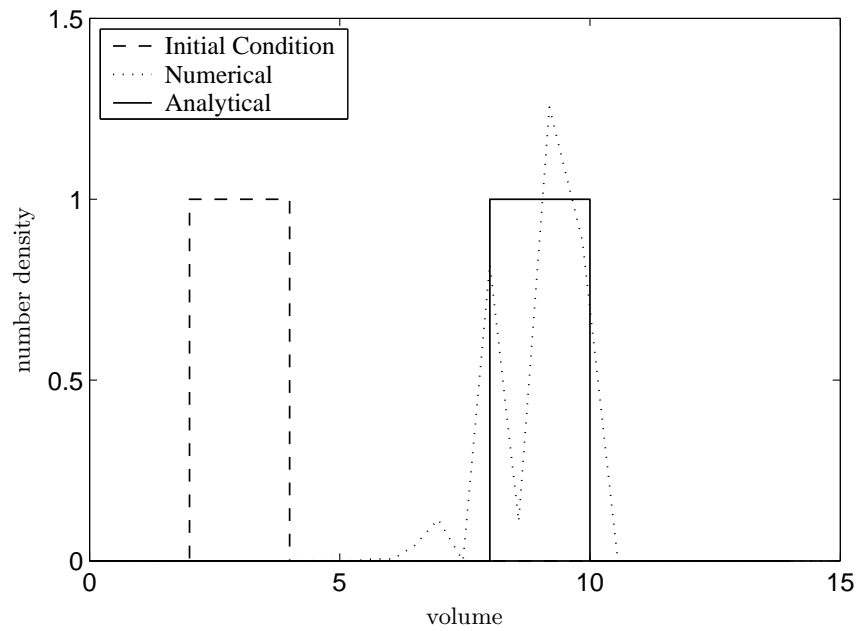
$$\frac{dN_i}{dt} = \frac{\check{a}_{i-1}G_{i-1}N_{i-1} - \check{c}_iG_iN_i/r}{x_{i-1}} - \frac{\check{a}_iG_iN_i - \check{c}_{i+1}G_{i+1}N_{i+1}/r}{x_i}. \quad (2.58)$$

We have implemented also this model on our test problem. The numerical results for the PSDs and the moments have been plotted in Figure 2.4. Similar to the results obtained by the technique of Hounslow et al., the prediction of particle size distribution (PSD) in Figure 2.4(a) shows oscillations. Moreover some higher overshoot in PSD is observed in this case. Nevertheless this model improves the prediction of moments over Hounslow et al. (2.53) as shown in Figure 2.4(b).

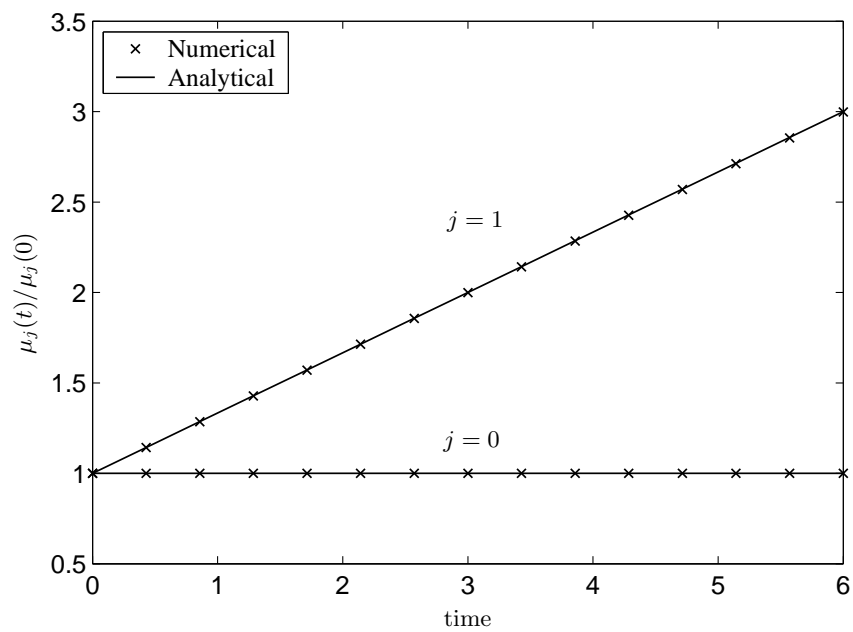
Due to several serious difficulties like inaccuracy, diffusive nature, instability, restriction to special grids etc., it is very difficult to recommend a best method for a general growth problem. There are of course more sophisticated methods available in the literature but they are complicated to implement and difficult to couple with other processes. However the flux limiter method (2.49) while applied on uniform grids seems a good choice. On the other hand, as mentioned before, for aggregation and breakage problems geometric grids are more preferable than uniform grids.

All the difficulties in numerical solutions stated above can be overcome by the *moving sectional methods* proposed by Gelbard and Seinfeld [23] as well as Kim and Seinfeld [45]. They can be classified as Lagrangian type methods. In the moving sectional method all particles initially within a section remain there during computation, i.e.

$$\frac{dN_i(t)}{dt} = 0, \quad (2.59)$$



(a) Particle size distribution.



(b) Moments.

Figure 2.4: Numerical results for pure growth with constant growth rate at $t = 6$ obtained on 40 non-uniform logarithmic fixed grid points using Park and Rogak [80].

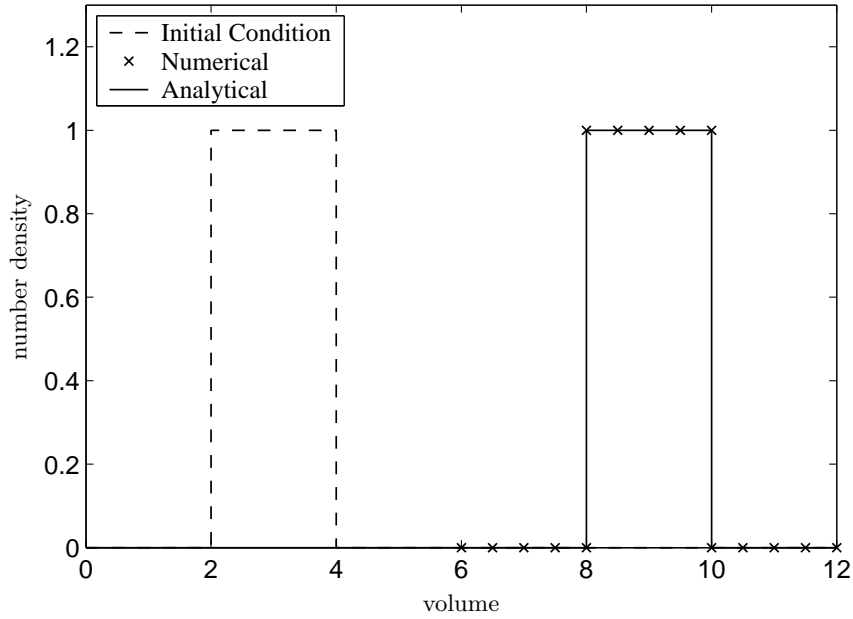


Figure 2.5: Particle size distributions for pure growth with constant growth rate at $t = 6$ obtained on 15 uniform moving grid points.

and the section boundaries move as particles grow. Therefore we have the following governing equations for the boundaries

$$\frac{dx_{i\pm 1/2}(t)}{dt} = G(x_{i\pm 1/2}). \quad (2.60)$$

In order to have a consistent formulation with moments, the section representative has to move as

$$\frac{dx_i(t)}{dt} = G(x_i). \quad (2.61)$$

It must be noted that for simple growth functions like $G(x) = x$ or $G(x) = G_0$ the representative (cell center) can be calculated using $x_{i\pm 1/2}$ without setting the differential equation (2.61) as

$$x_i(t) = \frac{x_{i-1/2} + x_{i+1/2}}{2}. \quad (2.62)$$

This technique is free of diffusion and instability problems independent of the type of grids chosen for computation. The prediction of numerical results is extremely accurate and no significant difference can be observed between numerical and analytical results. Our test problem with a constant growth rate is a trivial case for moving sectional methods and therefore the numerical results look the same as the analytical solution, see Figure 2.5. Only 15 uniform cells have been used for the computation. For a detailed description of the scheme and its application to more models and practical problems, readers are referred to Gelbard and Seinfeld[23], Kim and Seinfeld [45], Kumar and Ramkrishna [59], Spicer et al. [106], Tsantilis et al. [113] as well as Tsantilis and Pratsinis [114]. The moving sectional method is the easiest approach to solve pure

growth problems. However when combined with the other processes of nucleation, aggregation and breakage, implementation of a moving sectional method becomes complex. We will discuss this issue in detail in next sections.

A slightly different idea of hybrid grids was formulated by Jacobson [42] as well as Jacobson and Turko [43]. They fixed the boundaries of the sections and moved their representative sizes. By fixing boundaries other processes like nucleation, aggregation etc. can easily be treated. If the representative crosses the upper boundary than all the particles in the section are moved and averaged with the particles of the next section. The numerical diffusion can significantly be reduced and quite satisfactory results can be obtained. However there might be many difficulties with the implementation of this approach. Consider a cell whose particles are moved to the next cell and become empty at a particular time. In this case fluctuations in PSD are possible at that time. To overcome this difficulty one may delete this cell by extending neighboring cells but certainly this adds more complexity in the implementation.

Next we shall explore some difficulties with the previously existing schemes for solving combined problems. Most of the techniques discussed above can be used for solving combined problems just by adding their individual discretizations corresponding to different processes. However, all the difficulties discussed above remain the same.

2.5 Combined Processes

Among all methods discussed above we conclude that the fixed pivot technique conserves the two moments and allows a quite arbitrary grid in a very simple and straightforward way. The fixed pivot technique, however, cannot be used to solve the growth processes. Kumar and Ramkrishna [59] used a Lagrangian approach for the solution of growth and the fixed pivot technique for aggregation and breakage processes. They obtained quite satisfactory results for this combination of schemes. The problem appears when combining growth and nucleation processes. Due to the Lagrangian treatment of growth, smallest representative size together with its boundaries move and there may not be a cell to place subsequently placed nuclei. This leads to several numerical difficulties. An effort in this direction was also made by Kumar and Ramkrishna [59]. Their formulation was inconsistent with the mass of the particles due to nucleation. It was later improved by Spicer et al. [106] by considering the effect of the mass of new formed nuclei on the movement of cell representatives. Their final set of equations for the consistency of the first two moments is given as

$$\frac{dN_i}{dt} = B^{\text{nuc}} \delta_i, \quad (2.63)$$

and

$$\frac{dx_i}{dt} = G(x_i) + \frac{1}{N_i} (x_{\text{nuc}} - x_i) B^{\text{nuc}} \delta_i. \quad (2.64)$$

where

$$\delta_i = \begin{cases} 1, & x_{\text{nuc}} \in [x_{i-1/2}, x_{i+1/2}] \\ 0, & \text{elsewhere.} \end{cases} \quad (2.65)$$

CHAPTER 2. POPULATION BALANCES

Here x_{nuc} is the size of the nuclei. The system of differential equations (2.63) and (2.64) can be solved to simulate a simultaneous process of growth and nucleation. The grid regeneration principles are explained in Kumar and Ramkrishna [59].

We conclude this chapter with the observation that the existing schemes have several disadvantages: many of them are designed for a specified grid type, others do not have uniform treatment for all processes or they are very complicated to implement. The fixed pivot technique seems good for aggregation and breakage problems but that can not be applied for growth and nucleation problems. Moreover, it will be shown later that the fixed pivot technique over-predicts the number density and gives a very poor prediction of the second moment. As mentioned, the objective is to develop a method which provides a uniform treatment to all processes and predicts the number density as well as higher moments with better accuracy.

Chapter 3

New Numerical Methods: One-Dimensional

In this chapter two different types of numerical methods for solving one-dimensional population balances are developed. The first method approximates the number density in terms of Dirac point masses and is based on an exact prediction of some selected moments. Furthermore, a new perspective of treating growth of particles as an aggregation process has been presented and then the proposed method is applied to combined aggregation and growth processes. The second method treats aggregation and breakage as mass conservation laws and makes use of the finite volume type scheme to solve the population balance equation. It is shown that for a number of test problems both the schemes produce results in excellent agreement with the analytical solutions. In assessing the effectiveness of various methods we will be concerned with the following attributes: generality, accuracy when applied on a coarse grid, computational time, ease of use and simplicity.

3.1 Introduction

The main objective of this chapter is to overcome the numerical problems in current discretized population balances discussed in previous chapter. It has been identified in the last chapter that the fixed pivot technique proposed by Kumar and Ramkrishna [57] results in a consistent over-prediction of number density for the large particles. Moreover, a diverging behavior of higher moments, which is of course caused by the over-prediction of the number density, is also a serious problem. Therefore, the aim is to propose a similar scheme which preserves all the advantages of the fixed pivot technique and improves the accuracy of the numerical results.

As mentioned in the previous chapter, Filbet and Laureçot [21] introduced an application of the finite volume approach to solve a one-dimensional aggregation problems. Finally it has been observed that the finite volume scheme is a good alternative to solve the population balance equations due to its automatic mass conservation property. Since they have considered only aggregation problems, the aim here is to develop a finite volume scheme to solve the breakage population balance equation. Following their idea we shall derive a new form of breakage population balance equation in order to apply the finite volume scheme effectively.

This chapter is organized as follows. First we present the new discretized method, *the cell*

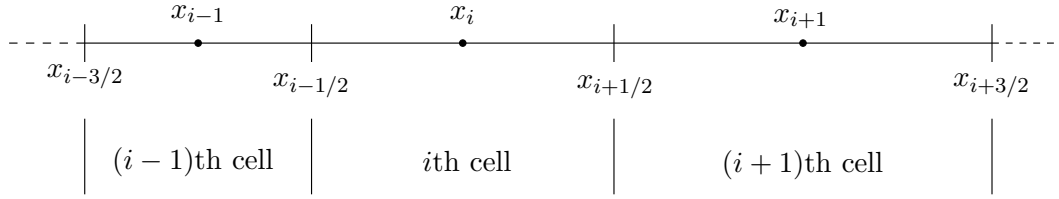


Figure 3.1: A discretized size domain.

average technique, in Section 3.2. Beginning with the fundamental concept of the scheme, it is formulated for several particular cases. The technique is tested by various comparisons of numerical and analytical results in each case. Then the convergence studies of the cell average and fixed pivot techniques are performed in Section 3.3. In Section 3.4, the finite volume is successfully applied to a newly derived form of pure breakage population balance equation. It also includes the combined formulation of simultaneous aggregation and breakage along with different comparisons with the cell average technique. A rigorous mathematical analysis is presented for pure and combined processes.

3.2 The Cell Average Technique

First we present a general idea of the cell average technique. The entire size domain is divided into a finite number I of small cells. The lower and upper boundaries of the i th cell are denoted by $x_{i-1/2}$ and $x_{i+1/2}$ respectively. All particles belonging to a cell are identified by a representative size of the cell, also called grid point. The representative size of a cell can be chosen at any position between the lower and upper boundaries of the cell. In this work the center of the cell, the arithmetic mean of the cell boundaries, is defined as the representative size. The average mean volume of the particles or the geometric mean could be other alternative choice for the representative. A typical discretized size domain is shown in Figure 3.1. The representative of the i th cell is represented by $x_i = (x_{i+1/2} + x_{i-1/2})/2$. The width of the i th cell is denoted by $\Delta x_i = x_{i+1/2} - x_{i-1/2}$. The size of a cell can be fixed arbitrarily depending upon the process of application. In most of the application, however, geometric type grids are preferred.

We wish to transform the general continuous population balance equation into a set of I ODEs that can be solved using any standard ODE solver. Denoting the total number in the i th cell by N_i , we seek a set of ODEs of the following form

$$\frac{dN_i}{dt} = \underbrace{B_i^{\text{CA}}}_{\text{birth due to particulate events}} - \underbrace{D_i^{\text{CA}}}_{\text{death due to particulate events}}, \quad i = 1, 2, \dots, I. \quad (3.1)$$

The particulate events that may change the number concentration of particles include breakage, aggregation, growth and nucleation. The abbreviation CA stands for cell average. Note that this general formulation is not similar to the traditional sectional formulation where birth terms corresponding to the each process are summed up to contribute the total birth. Here all particulate events will be considered in a similar fashion as we treat individual processes. The concept of combining the processes will be further elaborated in next sections.

3.2. THE CELL AVERAGE TECHNIQUE

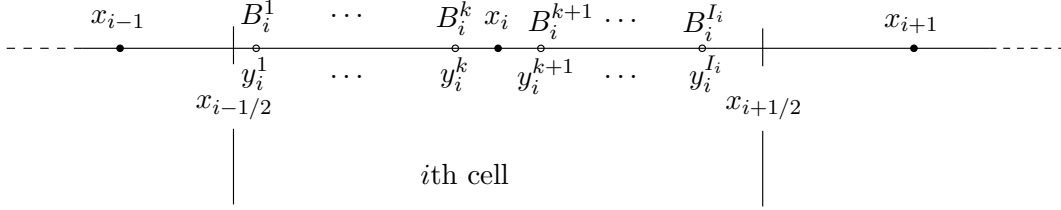


Figure 3.2: Appearance of particles in a cell.

The first step is to compute particle birth and death in each cell. Consideration of all possible events that lead to the formation of new particles in a cell provides the birth term. Similarly all possible events that lead to the loss of a particle from a cell give the death rate of particles. The new particles in the cell may either appear at some discrete positions or they may be distributed continuously in accordance with the distribution function. For example, in a binary aggregation process particles appear at discrete points in the cell whereas in breakage process they are often distributed everywhere according to a continuous breakage function. Due to non-uniform grids, it is then possible that the size of a newborn particle in a cell does not match exactly with the representative size of that cell. The newborn particles whose sizes do not match with any of the representative sizes cause an inconsistency of moments in the formulation. Therefore the aim is to remedy the inconsistency in an efficient manner. Suppose that we just substitute the total birth and death of particles, for example, in the equation (3.1). Then the prediction of the zeroth moment by the formulation will be predicted correctly but the formulation will become inconsistent with respect to the first moment. In this work we propose the cell average technique consistent with the first two moments. But the same idea can be generalized to conserve any two moments.

Let us demonstrate the common concepts of the cell average technique by the following example shown in Figure 3.2. Particle births $B_i^1, B_i^2, \dots, B_i^{I_i}$ take place at positions $y_i^1, y_i^2, \dots, y_i^{I_i}$ respectively due to some particulate processes like aggregation, breakage, birth etc. in the cell i . Here we considered the purely discrete case but analogous steps can be performed for continuous appearance of the particles in the cell. First we compute the total birth of particles in the i th cell as

$$B_i = \sum_{j=1}^{I_i} B_i^j. \quad (3.2)$$

Since we know the positions of the newborn particles inside the cell, it is easy to calculate the average volume of newborn particles, \bar{v}_i . It is given by the following formula

$$\bar{v}_i = \frac{\sum_{j=1}^{I_i} y_i^j B_i^j}{B_i}. \quad (3.3)$$

Now we may assume that B_i particles are sitting at the position $\bar{v}_i \in [x_{i-1/2}, x_{i+1/2}]$. It should be noted that the averaging process still maintains consistency with the first two moments. If the average volume \bar{v}_i matches with the representative size x_i then the total birth B_i can be assigned to the node x_i . But this is rarely possible and hence the total particle birth B_i has to be reassigned to the neighboring nodes such that the total number and mass remain conserved.

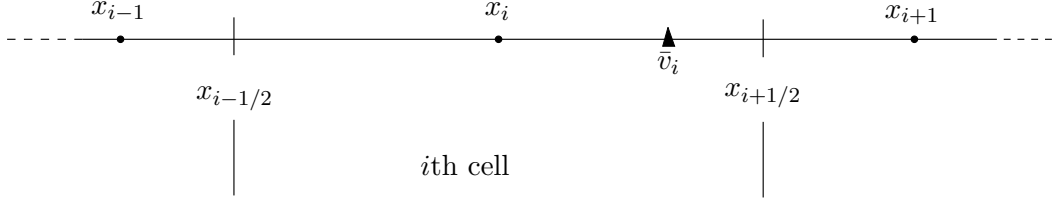


Figure 3.3: Average volume of all newborn particles.

Considering that the average volume $\bar{v}_i > x_i$ as shown in Figure 3.3, the assignment of particles must be performed by the following equations

$$a_1(\bar{v}_i, x_i) + a_2(\bar{v}_i, x_{i+1}) = B_i, \quad (3.4)$$

and

$$x_i a_1(\bar{v}_i, x_i) + x_{i+1} a_2(\bar{v}_i, x_{i+1}) = B_i \bar{v}_i. \quad (3.5)$$

Here $a_1(\bar{v}_i, x_i)$ and $a_2(\bar{v}_i, x_{i+1})$ are the fractions of the birth B_i to be assigned at x_i and x_{i+1} respectively. Solving the above equations we obtain

$$a_1(\bar{v}_i, x_i) = B_i \frac{\bar{v}_i - x_{i+1}}{x_i - x_{i+1}}, \quad (3.6)$$

and

$$a_2(\bar{v}_i, x_{i+1}) = B_i \frac{\bar{v}_i - x_i}{x_{i+1} - x_i}. \quad (3.7)$$

It is convenient for further simplifications to define a function λ as

$$\lambda_i^\pm(x) = \frac{x - x_{i\pm 1}}{x_i - x_{i\pm 1}}. \quad (3.8)$$

The fractions can be expressed in terms of λ as

$$a_1(\bar{v}_i, x_i) = B_i \lambda_i^+(\bar{v}_i), \quad (3.9)$$

and

$$a_2(\bar{v}_i, x_{i+1}) = B_i \lambda_{i+1}^-(\bar{v}_i). \quad (3.10)$$

There are 4 possible birth fractions that may add a birth contribution at the node x_i : Two from the neighboring cells and two from the i th cell. All possible birth contributions have been shown in Figure 3.4. Collecting all the birth contributions, the birth term for the cell average technique is given by

$$\begin{aligned} B_i^{\text{CA}} = & B_{i-1} \lambda_i^-(\bar{v}_{i-1}) H(\bar{v}_{i-1} - x_{i-1}) + B_i \lambda_i^-(\bar{v}_i) H(x_i - \bar{v}_i) \\ & + B_i \lambda_i^+(\bar{v}_i) H(\bar{v}_i - x_i) + B_{i+1} \lambda_i^+(\bar{v}_{i+1}) H(x_{i+1} - \bar{v}_{i+1}). \end{aligned} \quad (3.11)$$

3.2. THE CELL AVERAGE TECHNIQUE

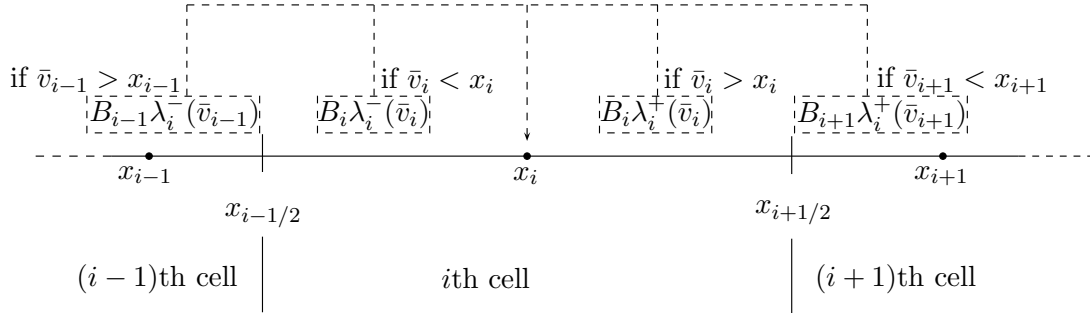


Figure 3.4: Assignment of particles at x_i from all possible cells.

The *Heaviside step function* is a discontinuous function also known as *unit step function* and is here defined by

$$H(x) = \begin{cases} 1, & x > 0 \\ \frac{1}{2}, & x = 0 \\ 0, & x < 0. \end{cases} \quad (3.12)$$

Before we summarize the cell average technique it should be mentioned here that the continuous number density function $n(t, x)$ can be represented, similarly to the fixed pivot technique, in terms of Dirac-delta distributions as given by the equation (2.15). It is due to the fact that all particles in a cell are assumed to be concentrated at the representative size of the cell. This representation of the number density is useful to calculate the discrete birth and death rates in a cell. We now summarize the main steps of the cell average technique discussed above as follows:

1. *Computation of birth and death rates:* The discrete birth and death rates can be obtained by substituting a Dirac-delta representation (2.15) of the density into the continuous form of total birth and death rates in a cell. Thereby computations of B_i and D_i are performed in the first step.
2. *Computation of the volume averages:* The second step is to calculate the average volume of the particles in each cell, i.e. \bar{v}_i . This is a central step of the cell average technique and can easily be obtained after step 1.
3. *Birth modification:* The birth modification, crucial point for the sectional methods, is done according to the equation (3.11). This modified birth rate B_i^{CA} is consistent with the first two moments. Note that there is no need to modify the death term since particles are just removed from the grid points and therefore the formulation remains consistent with all moments due to discrete death. As a result the death term in the cell average formulation D_i^{CA} is equal to D_i .
4. *Solution of the set of ODEs:* Substituting the values of B_i^{CA} and D_i^{CA} into the equation (3.1) we obtain a set of ordinary differential equation. It will be then solved by any higher order ODE solver. An appropriate solver to solve such equations will be recommended at the end of this section.

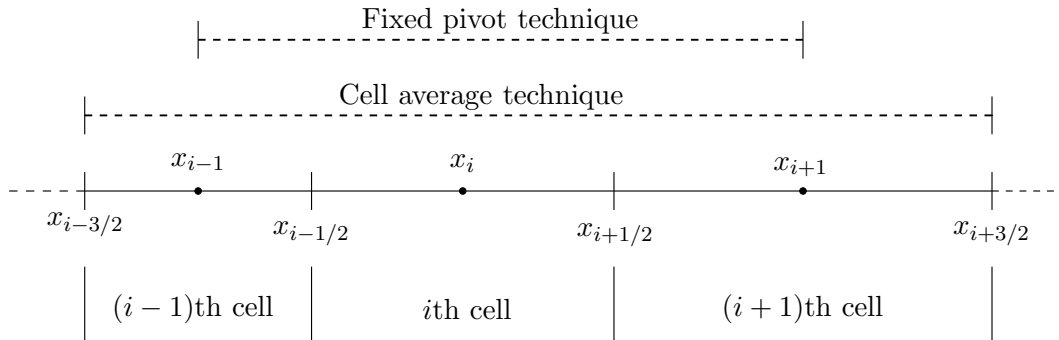


Figure 3.5: Particle domain which may contribute a birth at the node x_i .

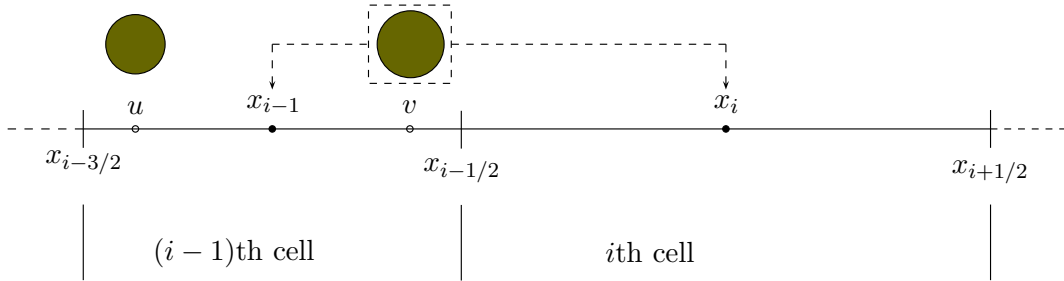
A general procedure of the cell average technique has been explained above. Further details and implementation of the cell average technique for particular and combined processes will be presented later.

At this point it is important to comment on the conceptual difference between the fixed pivot and the cell average techniques. The basic difference between the two techniques is the averaging of the volume. The cell average technique first collects the total birth of particles in a cell and then distributes it once to the neighboring nodes depending upon the position of the volume average in the cell according to the strategy discussed above. On the other hand each birth which takes place in a cell is assigned immediately to the neighboring nodes with the same strategy by the fixed pivot technique. The another substantial difference as a consequence of the averaging arises from the domain of particles which contributes to birth at a node. The particle domain which may contribute a birth at the node x_i is shown in Figure 3.5 for both techniques. The cell average covers the two adjacent cells completely while the fixed pivot technique takes the two adjacent cells only partly into consideration.

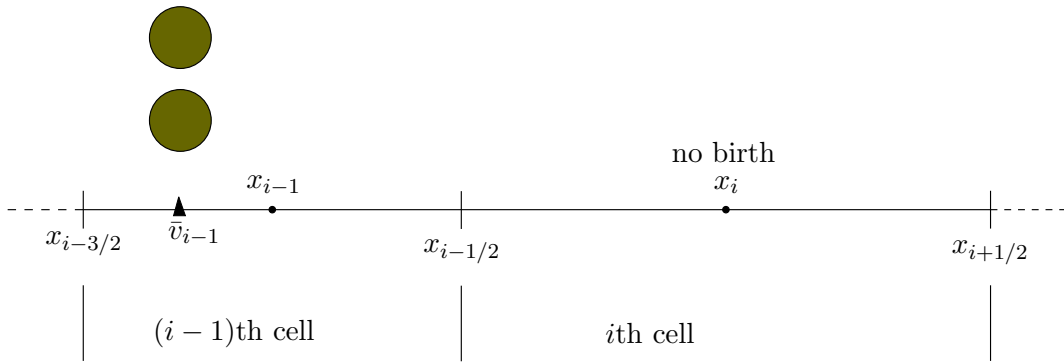
Let us consider a simple example to clarify the difference between the two techniques more apparently. We shall observe, as an example, the contribution of birth in the i th node due to the particle birth in $(i-1)$ th cell. Let us assume that the two particles of sizes u ($x_{i-3/2} < u < x_{i-1}$) and v ($x_{i-1} < v < x_{i-1/2}$) are formed in the $(i-1)$ th cell as a result of some particulate processes. The particle of size v gives a contribution in birth at x_i by the fixed pivot technique, shown in Figure 3.6(a). On the other hand, there are two possibilities with the cell average technique. First, if the volume average $\bar{v}_{i-1} = (u + v)/2$, lies between $x_{i-3/2}$ and x_{i-1} , there will be no birth at x_i due to these newborn particles. This has been depicted in Figure 3.6(b). The second possibility is that the volume average \bar{v}_{i-1} falls between x_{i-1} and $x_{i-1/2}$. It gives a birth contribution at x_i from both particles. The assignment of particles has been shown in Figure 3.6(c). Although the cell average technique considers two neighboring cells for the birth contribution but as we have seen in this example that it may not get any contribution from the neighboring cells if the volume average stands far beyond the representatives of the neighboring cells. This is one of the reasons, that will be explored later, why the cell average technique performs better by handling the variation of number density in a size range by averaging and thus reduces the error due to the discretization.

Up to now we have presented the foundation of the cell average technique and illustrated the difference between the two techniques. We shall now deliberate about the advantages of the

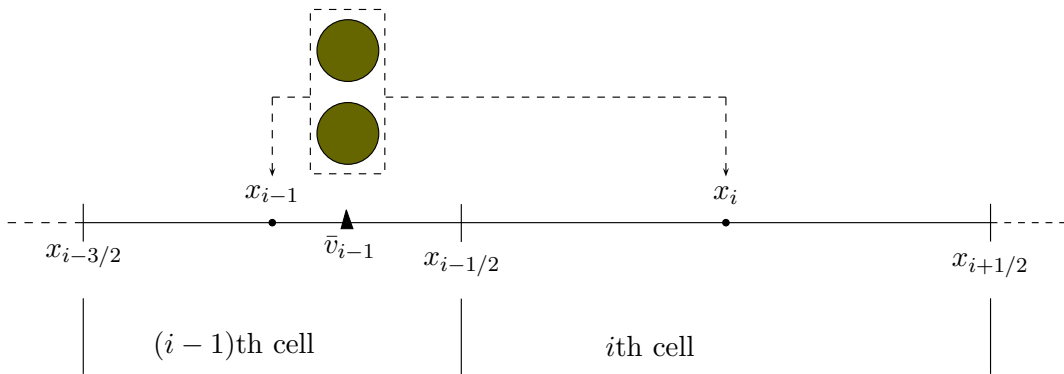
3.2. THE CELL AVERAGE TECHNIQUE



(a) The fixed pivot technique.



(b) The cell average technique, $\bar{v}_{i-1} < x_{i-1}$.



(c) The cell average technique, $\bar{v}_{i-1} > x_{i-1}$.

Figure 3.6: Assignment of particles at the node x_i from the newborn particles in $(i - 1)$ th cell.

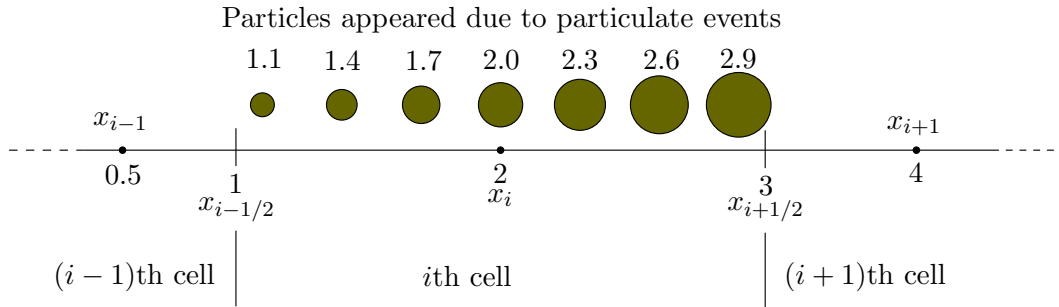


Figure 3.7: Example showing the superiority of the cell average technique.

cell average technique over the fixed pivot technique. In order to demonstrate the idea of the cell average and its improvements over the fixed pivot technique let us first consider a simple example followed by a more general example. Consider the situation shown in the Figure 3.7. Particles appear in the i th cell as a result of aggregation, breakage or any other particulate events. We also assume here that no particle appeared in the neighboring cells. We now want to calculate the change of the zeroth and first moment due to newborn particles in the i th cell using both the techniques. Clearly the exact changes in the zeroth and the first moments are

$$\Delta\mu_0 = 1 + 1 + 1 + 1 + 1 + 1 + 1 = 7, \quad (3.13)$$

and

$$\Delta\mu_1 = 1.1 + 1.4 + 1.7 + 2.0 + 2.3 + 2.6 + 2.9 = 14. \quad (3.14)$$

According to the cell average technique, we first calculate the total number of birth, i.e. 7, in this case and then the volume average of all newborn particles which is given by

$$\bar{v}_i = \frac{1.1 + 1.4 + 1.7 + 2.0 + 2.3 + 2.6 + 2.9}{7} = 2. \quad (3.15)$$

Since the volume average of the newborn particles is exactly matching the representative size of the cell, all the newborn particles will be assigned to the node x_i . Thus, the changes in the first two moments at x_i are the same as the exact values.

We shall now compute the assigned birth at x_i according to the fixed pivot technique. Each birth will be assigned to the neighboring nodes such that particle number and mass remain conserved. For example, the fraction of the first particle of size 1.1 assigned at x_i is given by

$$a_1 = \frac{1.1 - 0.5}{2.0 - 0.5} = 0.4. \quad (3.16)$$

Similarly the other fractions assigned at x_i can be calculated. The sum of all fractions assigned at x_i , i.e. the change of the zeroth moment according to the fixed pivot (FP) technique is given by

$$\Delta\mu_0^{\text{FP}} = 0.4 + 0.6 + 0.8 + 1 + 0.85 + 0.70 + 0.55 = 4.9. \quad (3.17)$$

3.2. THE CELL AVERAGE TECHNIQUE

Consequently the change in the first moment is computed as

$$\Delta\mu_1^{\text{FP}} = 4.9 \times 2 = 9.8. \quad (3.18)$$

The changes in both moments by the fixed pivot technique are completely different. This is due to the fact that the fixed pivot technique distributes the particles by simple interpolation between the representative nodes without taking the cells into account. On the other hand the cell average technique first takes the volume average and if necessary, or in other words if the volume average differs from the representative size, then only it distributes the total number of particles to the neighboring nodes while making the formulation consistent with respect to the first two moments. Nevertheless the situation considered in the example is hardly possible in a real problem but we will see in our next example that the strategy of the cell average technique works better in a more general problem too.

We now take a general situation as shown in the Figure 3.2. As a result of aggregation, breakage or any other event, particle births $B_i^1, B_i^2, \dots, B_i^{I_i}$ take place at the positions $y_i^1, y_i^2, \dots, y_i^{I_i}$ respectively in the cell i . As shown in the figure, let us assume that $y_i^k < x_i$ and $y_i^{k+1} > x_i$. In order to assign them at the nodes x_{i-1} , x_i and x_{i+1} in such a way that particle number and mass remain conserved, we use the fixed pivot and the cell average strategies. The particle number assigned at x_i by the fixed pivot mechanism is given as

$$N_i^{\text{FP}} = \sum_{j=1}^k \left(\frac{y_i^j - x_{i-1}}{x_i - x_{i-1}} \right) B_i^j + \sum_{j=k+1}^{I_i} \left(\frac{x_{i+1} - y_i^j}{x_{i+1} - x_i} \right) B_i^j. \quad (3.19)$$

According to the cell average mechanism the total number of particles assigned to x_i is calculated by either

$$N_i^{\text{CA}} = \left(\frac{\bar{v}_i - x_{i-1}}{x_i - x_{i-1}} \right) \sum_{j=1}^{I_i} B_i^j, \quad \text{if } \bar{v}_i \leq x_i, \quad (3.20)$$

or

$$N_i^{\text{CA}} = \left(\frac{x_{i+1} - \bar{v}_i}{x_{i+1} - x_i} \right) \sum_{j=1}^{I_i} B_i^j, \quad \text{if } \bar{v}_i \geq x_i, \quad (3.21)$$

depending upon the position of \bar{v}_i in the cell which is defined as

$$\bar{v}_i = \frac{\sum_{j=1}^{I_i} y_i^j B_i^j}{\sum_{j=1}^{I_i} B_i^j}. \quad (3.22)$$

It is easy to verify that $N_i^{\text{CA}} \geq N_i^{\text{FP}}$, see Appendix B.3. Equality holds if all particles appear at the same side of the representative x_i , i.e. $B_i^j = 0$ for all $j \geq k + 1$ or $B_i^j = 0$ for all $j \leq k$. Thus, the number of particles from the i th cell assigned at x_i by the cell average technique is larger than that of the fixed pivot technique.

From the preceding discussion it is now evident that the cell average technique retains more information of the cell, i.e. original particles that belong to the cell, during the assignment process. The fixed pivot technique tends to spread particles, i.e. has more numerical dissipation.

In a special case when the average of the particles is equal to the representative size no distribution to neighboring cells takes place by the cell average technique. Assignment of particles to neighboring cells for the consistency with moments causes numerical diffusion. Since the cell average technique maintains consistency with less particle distribution to neighboring cells, we expect the technique to be more accurate and less diffusive.

We shall now turn our attention to a suitable ODE solver to solve the resulting set of ODEs. When integrating the resultant system (3.1) using a standard ODE routine, for example ODE45, ODE15S solvers in MATLAB, this may lead to negative values for the number density at large sizes. These negative values may lead in the sequel to instabilities of the whole system. Therefore, one should take care of the positivity of the solution by the numerical integration routine. We force the positivity in our numerical results using an adaptive time step Runge-Kutta method. The step-size adjustment algorithm is based on embedded Runge-Kutta formulas, originally invented by Fehlberg. It uses a fifth-order method with six functions evaluation where another combination of the six functions gives a fourth order method. The difference between the two estimates is used as an estimate of the truncation error to adjust the step size. A more detailed description of the method and information about implementation can be found in [91].

Next we present the derivation of the discrete equations of the cell average technique for several individual and combined processes. Numerical results will be obtained for many analytically solvable problems using the cell average technique and comparisons will be made with numerical results obtained by the fixed pivot technique.

3.2.1 Pure Breakage

Now we derive the cell average formulation for the pure breakage. The continuous form (2.34) of the pure breakage equation has already been presented in the previous chapter. The total birth and death rates of particles in the i th cell is calculated by integrating the birth and death rates from $x_{i-1/2}$ to $x_{i+1/2}$ as

$$B_{\text{break},i} = \int_{x_{i-1/2}}^{x_{i+1/2}} \int_x^{\infty} b(x, \epsilon) S(\epsilon) n(t, \epsilon) d\epsilon dx, \quad (3.23)$$

and

$$D_{\text{break},i} = \int_{x_{i-1/2}}^{x_{i+1/2}} S(x) n(t, x) dx. \quad (3.24)$$

Substituting the Dirac-delta mass representation (2.15) of the continuous number density $n(t, x)$ into the above birth and death rates, we obtain

$$B_{\text{break},i} = \sum_{k \geq i} N_k(t) S_k \int_{x_{i-1/2}}^{p_k^i} b(x, x_k) dx, \quad (3.25)$$

and

$$D_{\text{break},i} = S_i N_i(t). \quad (3.26)$$

3.2. THE CELL AVERAGE TECHNIQUE

Here the limit p_k^i is defined as

$$p_k^i = \begin{cases} x_i, & \text{if } k = i \\ x_{i+1/2}, & \text{otherwise.} \end{cases} \quad (3.27)$$

The derivation of the discrete birth and death rates is given in Appendix B.4. The total volume flux as a result of breakage into the cell i is given by

$$V_{\text{break},i} = \int_{x_{i-1/2}}^{x_{i+1/2}} \int_x^\infty xb(x, \epsilon) S(\epsilon) n(t, \epsilon) d\epsilon dx. \quad (3.28)$$

Similar to the discrete birth rate we obtain the discrete volume flux as

$$V_{\text{break},i} = \sum_{k \geq i} N_k(t) S_k \int_{x_{i-1/2}}^{p_k^i} xb(x, x_k) dx. \quad (3.29)$$

We now compute the volume average of all newborn particles. Dividing the total volume birth $V_{\text{break},i}$ by the total number birth $B_{\text{break},i}$, we obtain the volume average $\bar{v}_{\text{break},i}$ in the i th cell as

$$\bar{v}_{\text{break},i} = \frac{V_{\text{break},i}}{B_{\text{break},i}}. \quad (3.30)$$

Now the birth rate for the cell average technique can easily be obtained by substituting the discrete birth rate (3.25) and the volume average (3.30) into the equation (3.11). Finally, the resultant set of ODEs takes the following form

$$\begin{aligned} \frac{dN_i}{dt} = & B_{\text{break},i-1} \lambda_i^- (\bar{v}_{\text{break},i-1}) H(\bar{v}_{\text{break},i-1} - x_{i-1}) \\ & + B_{\text{break},i} \lambda_i^- (\bar{v}_{\text{break},i}) H(x_i - \bar{v}_{\text{break},i}) + B_{\text{break},i} \lambda_i^+ (\bar{v}_{\text{break},i}) H(\bar{v}_{\text{break},i} - x_i) \\ & + B_{\text{break},i+1} \lambda_i^+ (\bar{v}_{\text{break},i+1}) H(x_{i+1} - \bar{v}_{\text{break},i+1}) - S_i N_i(t). \end{aligned} \quad (3.31)$$

The set of equations (3.31) is a discrete formulation for solving a general breakage problem. The form of breakage and selection function, also the type of grids can be chosen arbitrarily.

For the case of a uniform breakage function $b(x, y) = 2/y$, a binary breakage, this formulation can be further simplified. Let us consider the following expression for $b(x, y) = 2/y$ as

$$\begin{aligned} x_i - \bar{v}_{\text{break},i} &= \frac{x_i \sum_{k \geq i} N_k(t) S_k \frac{2}{x_k} (p_k^i - x_{i-1/2}) - \sum_{k \geq i} N_k(t) S_k \frac{2}{x_k} (p_k^i - x_{i-1/2}) \frac{(p_k^i + x_{i-1/2})}{2}}{\sum_{k \geq i} N_k(t) S_k \frac{2}{x_k} (p_k^i - x_{i-1/2})} \\ &= \frac{x_i N_i(t) S_i \frac{2}{x_i} (x_i - x_{i-1/2}) - N_i(t) S_i \frac{2}{x_i} (x_i - x_{i-1/2}) \frac{(x_i + x_{i-1/2})}{2}}{\sum_{k \geq i} N_k(t) S_k \frac{2}{x_k} (p_k^i - x_{i-1/2})} \\ &= \frac{N_i(t) S_i \frac{2}{x_i} (x_i - x_{i-1/2}) \left(x_i - \frac{(x_i + x_{i-1/2})}{2} \right)}{\sum_{k \geq i} N_k(t) S_k \frac{2}{x_k} (p_k^i - x_{i-1/2})} \\ &= \frac{N_i(t) S_i (x_i - x_{i-1/2})^2}{x_i \sum_{k \geq i} N_k(t) S_k \frac{2}{x_k} (p_k^i - x_{i-1/2})}. \end{aligned} \quad (3.32)$$

CHAPTER 3. NEW NUMERICAL METHODS: ONE-DIMENSIONAL

Substituting $x_i = (x_{i+1/2} + x_{i-1/2})/2$ we get

$$\begin{aligned} x_i - \bar{v}_{\text{break},i} &= \frac{N_i(t)S_i(x_{i+1/2} - x_{i-1/2})^2}{4x_i \sum_{k \geq i} N_k(t)S_k \frac{2}{x_k} (p_k^i - x_{i-1/2})} \\ &= \frac{N_i(t)S_i \Delta x^2}{4x_i \sum_{k \geq i} N_k(t)S_k \frac{2}{x_k} (p_k^i - x_{i-1/2})} \geq 0. \end{aligned} \quad (3.33)$$

This gives $x_i \geq \bar{v}_{\text{break},i}$.

We now consider the case of ternary breakage. In this case we get the same relation as above. The ternary breakage function is given by

$$b(x, y) = \frac{6}{y} \left(1 - \frac{x}{y} \right). \quad (3.34)$$

The objective is to show that $x_i \geq \bar{v}_{\text{break},i}, \forall i$. Therefore we consider the following expression

$$\begin{aligned} x_i - \bar{v}_{\text{break},i} &= x_i - \frac{\sum_{k \geq i} S_k N_k \int_{x_{i-1/2}}^{p_k^i} x b(x, x_k) dx}{\sum_{k \geq i} S_k N_k \int_{x_{i-1/2}}^{p_k^i} b(x, x_k) dx} \\ &= \frac{x_i \sum_{k \geq i} S_k N_k \int_{x_{i-1/2}}^{p_k^i} b(x, x_k) dx - \sum_{k \geq i} S_k N_k \int_{x_{i-1/2}}^{p_k^i} x b(x, x_k) dx}{\sum_{k \geq i} S_k N_k \int_{x_{i-1/2}}^{p_k^i} b(x, x_k) dx}. \end{aligned} \quad (3.35)$$

For simplicity let us now consider the numerator (I) on the right hand side and substitute the breakage function (3.34). Thus, we obtain

$$\begin{aligned} I &= x_i \sum_{k \geq i} S_k N_k \int_{x_{i-1/2}}^{p_k^i} \frac{6}{x_k} \left(1 - \frac{x}{x_k} \right) dx - \sum_{k \geq i} S_k N_k \int_{x_{i-1/2}}^{p_k^i} \frac{6x}{x_k} \left(1 - \frac{x}{x_k} \right) dx \\ &= x_i S_i N_i \int_{x_{i-1/2}}^{x_i} \frac{6}{x_i} \left(1 - \frac{x}{x_i} \right) dx - S_i N_i \int_{x_{i-1/2}}^{x_i} \frac{6x}{x_i} \left(1 - \frac{x}{x_i} \right) dx \\ &\quad + x_i \sum_{k > i} S_k N_k \int_{x_{i-1/2}}^{x_{i+1/2}} \frac{6}{x_k} \left(1 - \frac{x}{x_k} \right) dx - \sum_{k > i} S_k N_k \int_{x_{i-1/2}}^{x_{i+1/2}} \frac{6x}{x_k} \left(1 - \frac{x}{x_k} \right) dx. \end{aligned}$$

The exact calculation of the integrals give

$$\begin{aligned} I &= x_i S_i N_i \frac{6}{x_i} \left[x_i - x_{i-1/2} - \frac{x_i}{2} + \frac{x_{i-1/2}^2}{2x_i} \right] - S_i N_i \frac{6}{x_i} \left[\frac{x_i^2}{2} - \frac{x_{i-1/2}^2}{2} - \frac{x_i^3}{3x_i} + \frac{x_{i-1/2}^3}{3x_i} \right] \\ &\quad + x_i \sum_{k > i} S_k N_k \frac{6}{x_k} \left[x_{i+1/2} - x_{i-1/2} - \frac{x_{i+1/2}^2}{2x_k} + \frac{x_{i-1/2}^2}{2x_k} \right] \\ &\quad - \sum_{k > i} S_k N_k \frac{6}{x_k} \left[\frac{x_{i+1/2}^2}{2} - \frac{x_{i-1/2}^2}{2} - \frac{x_{i+1/2}^3}{3x_k} + \frac{x_{i-1/2}^3}{3x_k} \right]. \end{aligned}$$

3.2. THE CELL AVERAGE TECHNIQUE

It can be simplified by making use of $(x_{i+1/2} + x_{i-1/2})/2 = x_i$ as

$$I = \frac{6S_i N_i}{x_i} \left[-x_i x_{i-1/2} + x_{i-1/2}^2 + \frac{x_i^2}{3} - \frac{x_{i-1/2}^3}{3x_i} \right] + \sum_{k>i} \frac{6S_k N_k}{x_k} (x_{i+1/2} - x_{i-1/2}) \left[x_i - \frac{x_i^2}{x_k} - x_i + \frac{x_{i+1/2}^2}{3x_k} + \frac{x_{i-1/2}^2}{3x_k} + \frac{x_{i-1/2} x_{i+1/2}}{3x_k} \right].$$

The above equation can be rewritten as

$$I = \frac{6S_i N_i}{x_i} (x_i - x_{i-1/2}) \left[-x_{i-1/2} + \frac{x_i^2}{3x_i} + \frac{x_{i-1/2}^2}{3x_i} + \frac{x_i x_{i-1/2}}{3x_i} \right] + \sum_{k>i} \frac{6S_k N_k}{x_k} (x_{i+1/2} - x_{i-1/2}) \left[-\frac{x_i^2}{x_k} + \frac{x_{i+1/2}^2}{3x_k} + \frac{x_{i-1/2}^2}{3x_k} + \frac{x_{i-1/2} x_{i+1/2}}{3x_k} \right]. \quad (3.36)$$

This can be further simplified as

$$I = \frac{2S_i N_i}{x_i^2} (x_i - x_{i-1/2}) \left[-3x_i x_{i-1/2} + x_i^2 + x_{i-1/2}^2 + x_i x_{i-1/2} \right] + \sum_{k>i} \frac{2S_k N_k}{x_k^2} (x_{i+1/2} - x_{i-1/2}) \left[-3x_i^2 + x_{i+1/2}^2 + x_{i-1/2}^2 + x_{i-1/2} x_{i+1/2} \right] \\ = \frac{2S_i N_i}{x_i^2} (x_i - x_{i-1/2})^3 + \sum_{k>i} \frac{2S_k N_k}{x_k^2} (x_{i+1/2} - x_{i-1/2}) \frac{1}{4} \left[x_{i+1/2}^2 + x_{i-1/2}^2 - 2x_{i-1/2} x_{i+1/2} \right] \\ = \frac{2S_i N_i}{x_i^2} (x_i - x_{i-1/2})^3 + \sum_{k>i} \frac{S_k N_k}{2x_k^2} (x_{i+1/2} - x_{i-1/2})^3. \quad (3.37)$$

Substituting $x_i = (x_{i+1/2} + x_{i-1/2})/2$ in the first term on the right hand side, we get

$$I = \frac{S_i N_i}{4x_i^2} (x_{i+1/2} - x_{i-1/2})^3 + \sum_{k>i} \frac{S_k N_k}{2x_k^2} (x_{i+1/2} - x_{i-1/2})^3 \\ = \frac{S_i N_i}{4x_i^2} \Delta x_i^3 + \sum_{k>i} \frac{S_k N_k}{2x_k^2} \Delta x_i^3 \geq 0. \quad (3.38)$$

This implies that $I \geq 0$ and hence the equation (3.35) leads to

$$x_i - \bar{v}_{\text{break},i} \geq 0, \quad \text{or} \quad x_i \geq \bar{v}_{\text{break},i}. \quad (3.39)$$

Thus, for the breakage functions discussed above we obtain $x_i \geq \bar{v}_{\text{break},i}$. Consequently the equation (3.31) for these breakage functions reduces to

$$\frac{dN_i}{dt} = B_{\text{break},i} \lambda_i^- (\bar{v}_{\text{break},i}) + B_{\text{break},i+1} \lambda_i^+ (\bar{v}_{\text{break},i+1}) - S_i N_i(t). \quad (3.40)$$

The set of equations (3.31), or in the special case (3.40) together with an initial condition can be solved with any higher order ODE solver to obtain the number of particles in a cell N_i .

CHAPTER 3. NEW NUMERICAL METHODS: ONE-DIMENSIONAL

Next section will be concerned with the numerical results. Before we present them it is worthwhile to give, for this particular case, an impression of some advantages of the cell average technique over the fixed pivot technique by a simple example. We consider a problem using the uniform binary breakage function taking as initial condition mono-disperse particles of size unity $n(0, x) = \delta(x - 1)$. The choice of the selection function is arbitrary. Now we compute the rate of change of particles in a cell $i < I$ at time $t = 0$ using the fixed pivot (FP) technique and the cell average (CA) technique calculating all the integrals appearing in the schemes exactly. Note that I is the total number of cells and $x_I = 1$. It is clear that the death rate of particles in i th cell by both schemes is zero since there is no particle present in the cell at time, $t = 0$. So the rate of change of particles in the i th cell according to the fixed pivot technique is given as

$$\left(\frac{dN_i}{dt}\right)_{\text{FP}} = \eta_{i,I} S_I N_I, \quad (3.41)$$

where

$$\eta_{i,I} = \int_{x_i}^{x_{i+1}} \frac{x_{i+1} - x}{x_{i+1} - x_i} \frac{2}{x_I} dx + \int_{x_{i-1}}^{x_i} \frac{x - x_{i-1}}{x_i - x_{i-1}} \frac{2}{x_I} dx. \quad (3.42)$$

This can be evaluated to give

$$\eta_{i,I} = x_{i+1} - x_{i-1}. \quad (3.43)$$

Finally, we obtain

$$\left(\frac{dN_i}{dt}\right)_{\text{FP}} = N_I S_I (x_{i+1} - x_{i-1}). \quad (3.44)$$

Now we calculate the rate of change using the cell average technique. First we compute the discrete birth as

$$V_{\text{break},i} = 2N_i S_i (x_{i+1/2} - x_{i-1/2}). \quad (3.45)$$

Similarly, the volume birth rate can be computed as

$$\begin{aligned} V_{\text{break},i} &= 2N_i S_i \frac{(x_{i+1/2}^2 - x_{i-1/2}^2)}{2} \\ &= 2x_i N_i S_i (x_{i+1/2} - x_{i-1/2}). \end{aligned} \quad (3.46)$$

The volume average is given by

$$\bar{v}_{\text{break},i} = \frac{V_{\text{break},i}}{B_{\text{break},i}} = x_i. \quad (3.47)$$

This is due to the fact that the volume averages lie exactly at the center in this case, i.e. $\bar{v}_{\text{break},j} = x_j$ for $j = 1, 2, \dots, I - 1$. There is no need to distribute the birth to neighboring cells and therefore the cell average technique in this case gives

$$\left(\frac{dN_i}{dt}\right)_{\text{CA}} = 2N_I S_I (x_{i+1/2} - x_{i-1/2}). \quad (3.48)$$

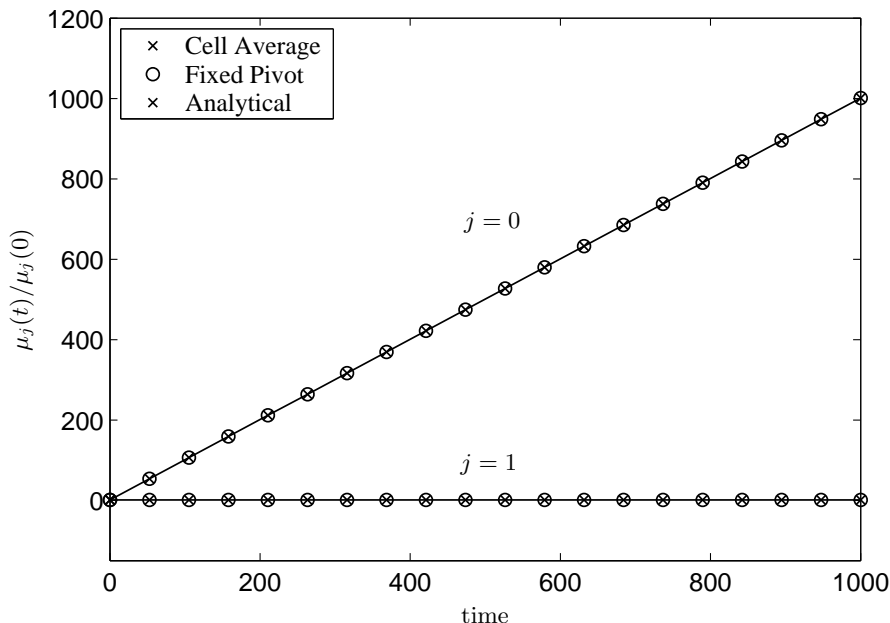


Figure 3.8: Temporal change of the zeroth and first moments for mono-disperse initial condition and $S(x) = x$ and $b(x, y) = 2/y$, grid points 30.

It is interesting in this case to calculate the analytical birth rate at $t = 0$, that is

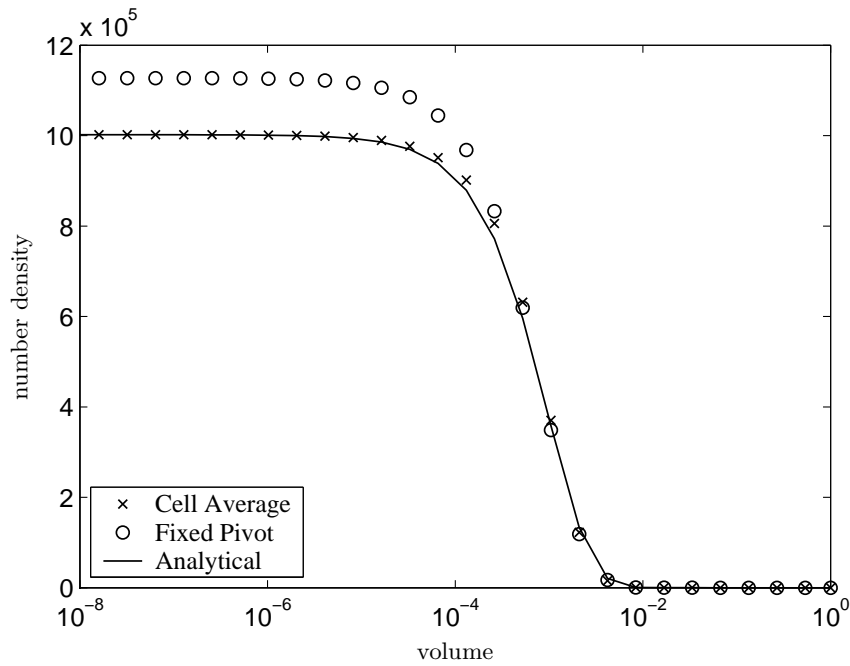
$$\left(\frac{dN_i}{dt}\right)_{\text{Ana}} = 2N_I S_I (x_{i+1/2} - x_{i-1/2}). \quad (3.49)$$

It is not surprising that both the analytical solution and the numerical solution by the cell average technique are, in this case, the same. This is because of the cell averages which lie exactly on the pivots in this case and therefore no division is necessary in order to make the formulation consistent with the first two moments. Though it seems logical not to divide the particles that are already concentrated at the representative size of a cell, the fixed pivot technique always distributes particles to the neighboring cells independently of available local information.

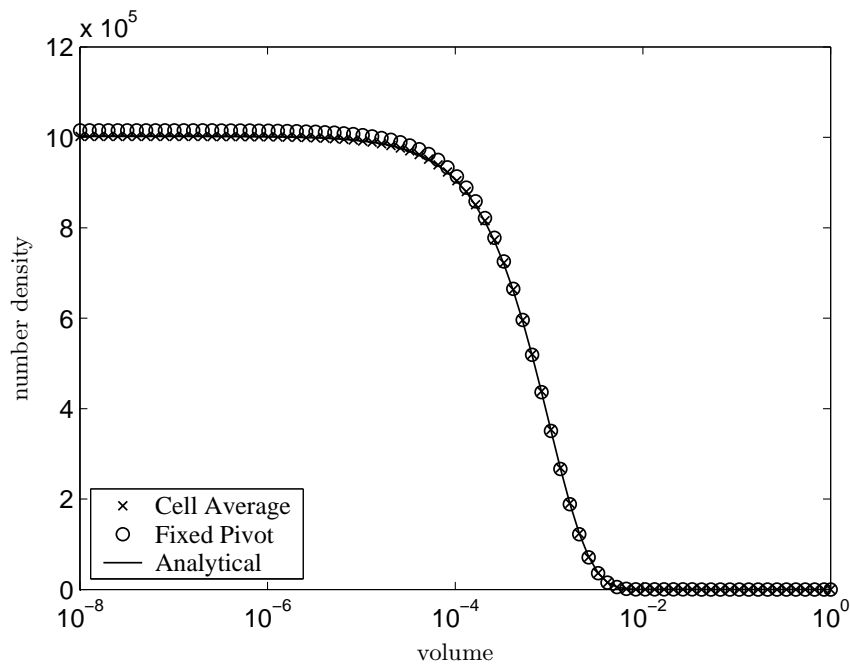
Numerical results

In this section, the performance of the cell average technique is evaluated by a direct comparison of the PSD and its moments calculated by the fixed pivot technique. Four test cases that can be solved analytically have been considered in our comparisons. The analytical solutions for different initial conditions and other parameters have been provided by Ziff and McRedy [125]. Two different types of initial condition, mono-disperse and exponentially distributed particles, have been taken in this work. The analytical solutions corresponding to these initial conditions are given in Appendix A.1.

The comparison between numerical and analytical results is carried out by means of average number density. Since the total number of particles in each cell is obtained from the numerical techniques, it is fair to compare the average number density. It can be calculated in the following



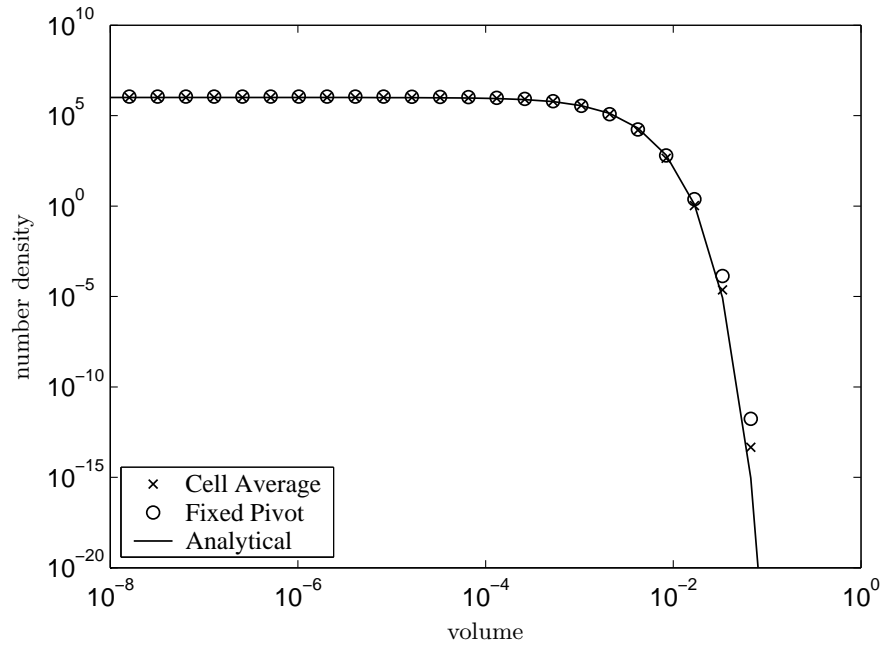
(a) $q = 1$, grid points, 30.



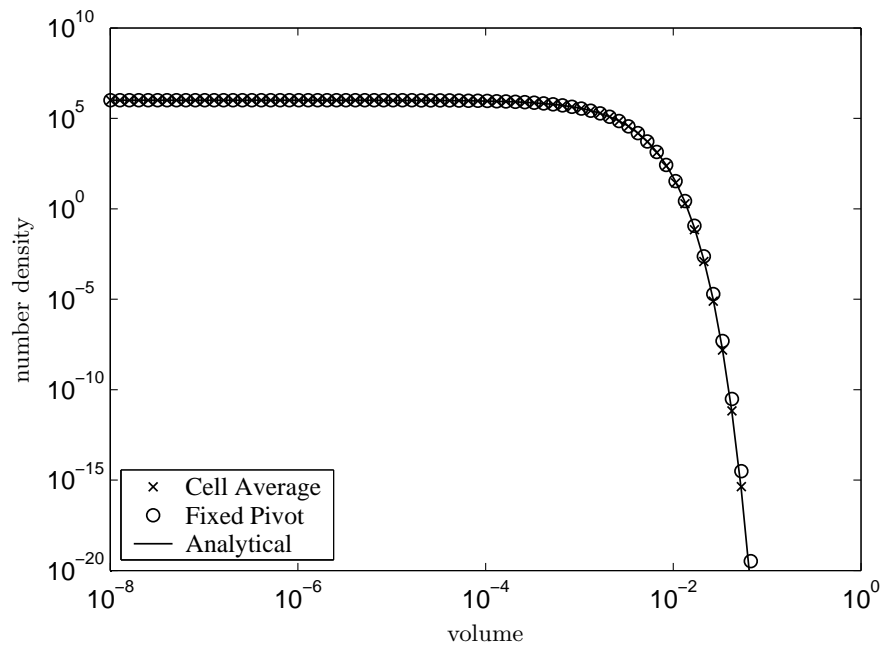
(b) $q = 3$, grid points, 90.

Figure 3.9: A comparison of particle size distributions on semi-log scale for mono-disperse initial condition and $S(x) = x$ and $b(x, y) = 2/y$.

3.2. THE CELL AVERAGE TECHNIQUE

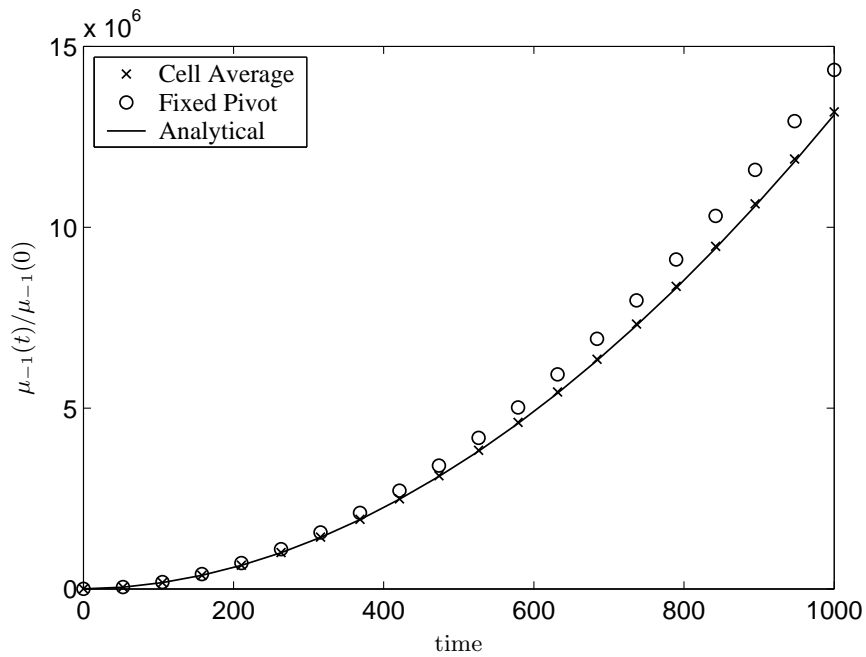


(a) $q = 1$, grid points, 30.

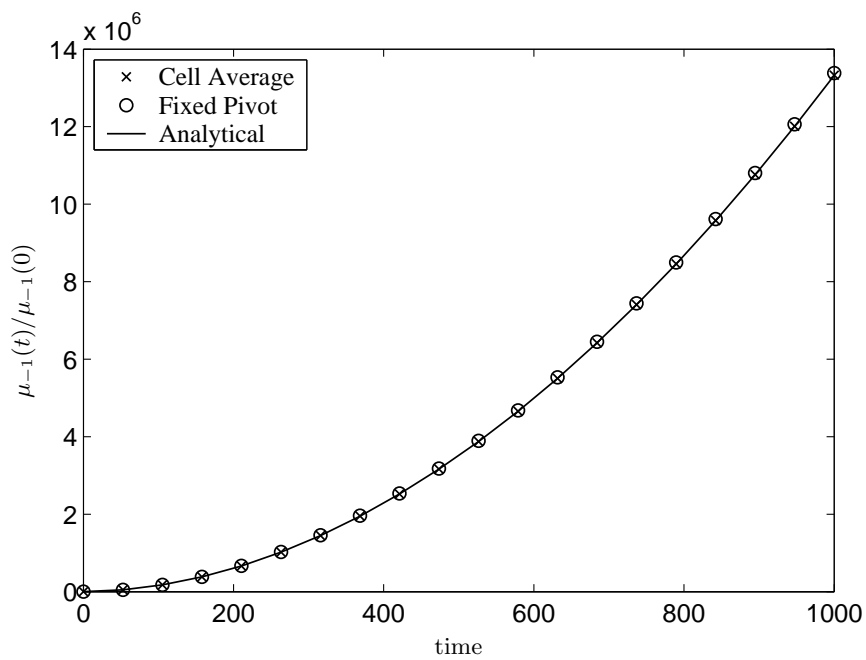


(b) $q = 3$, grid points, 90.

Figure 3.10: A comparison of particle size distributions on log-log scale for mono-disperse initial condition and $S(x) = x$ and $b(x, y) = 2/y$.



(a) $q = 1$, grid points, 30.



(b) $q = 3$, grid points, 90.

Figure 3.11: Temporal change of test moment for mono-disperse initial condition and $S(x) = x$ and $b(x, y) = 2/y$.

3.2. THE CELL AVERAGE TECHNIQUE

way

$$n_i^{\text{num}} = \frac{N_i}{\Delta x_i}, \quad (3.50)$$

where $\Delta x_i = x_{i+1/2} - x_{i-1/2}$. Similarly, from the analytical results we get

$$n_i^{\text{ana}} = \frac{1}{\Delta x_i} \int_{x_{i-1/2}}^{x_{i+1/2}} n(t, x) dx. \quad (3.51)$$

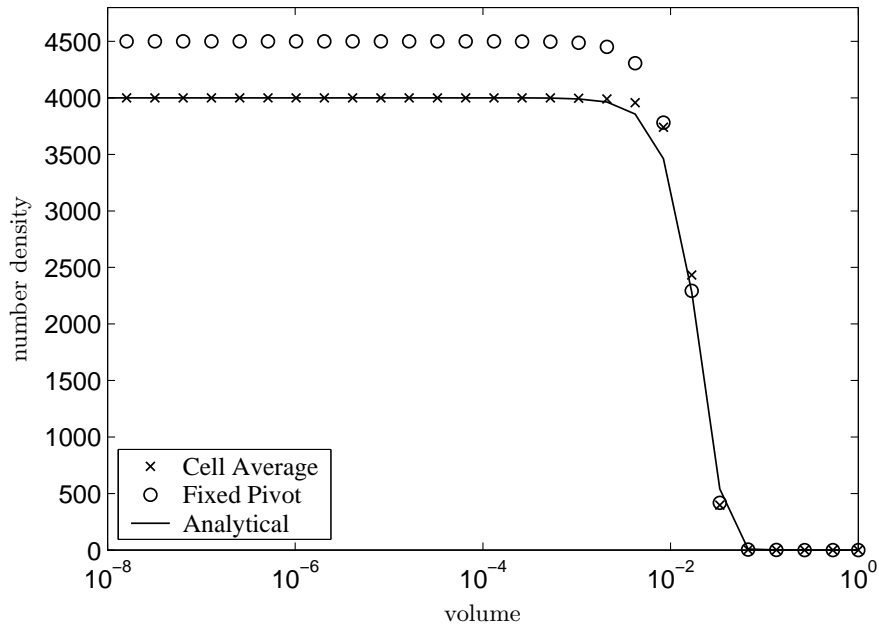
These densities have been plotted at grid points. This criterion of comparison is used in the entire work. The integration appearing in the analytical average density is computed either analytically if possible otherwise numerically by a low order integration routine. A geometrical grid of the type $x_{i-1/2} = 2^{1/q} x_{i-1/2}$ is used in our computations. All four test cases with simulation parameters including computation time, minimum and maximum particle size are given in Table 3.1.

Let us first assess the accuracy of the scheme for the first test case. In Figure 3.8, the analytical solution of the first two moments is compared with the numerical one obtained by the cell average and the fixed pivot technique using 30 geometrical grid points with $q = 1$. Mono-disperse particles of size unity are taken as initial condition. The volume domain is extended from 10^{-9} to 1. As expected, due to their formulations both techniques predict the first two moments exactly. Figure 3.9 compares the average number densities obtained by the two methods with the analytical one. The figures have been plotted on a semi-log scale, log in x axis and linear in y axis, to show the performance of the cell average technique predicting the particle distribution at small size range. Since particles flow towards the lower size range in the breakage process, it is important to check the performance of the scheme to predict these small particles. In Figures 3.9(a) and 3.9(b) the number of geometric grid points are taken to be 30 and 90 respectively. As can be seen, the PSD obtained by the cell average technique is in excellent agreement with the analytical solution even for a very coarse grid. On the other hand the fixed pivot technique over-predicts the numerical results. The Figure 3.9(b) shows the convergence of both the numerical results towards the analytical results as we refine the grid. It must be noted that the performance of the cell average technique using 30 grid points seems better than the fixed pivot technique using 90 grid points. A similar comparison on log-log scale has been performed in Figure 3.10. In these plots the difference between the two numerical solutions is not apparent. Nevertheless, a small over-prediction by the fixed pivot technique can be seen which decreases gradually by refinement of the grid.

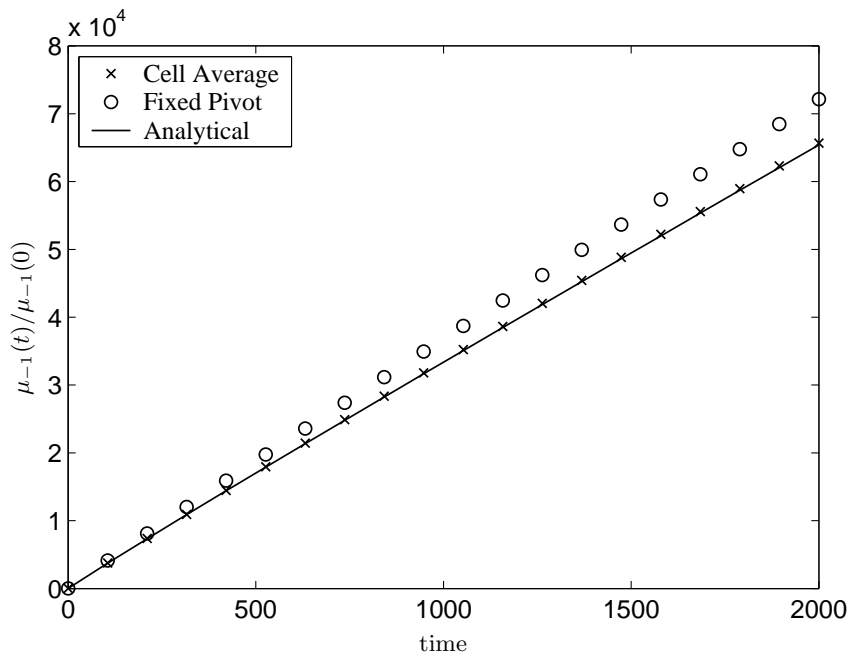
Now the idea is to compare an appropriate quantity which summed up the over-prediction of the PSD. The over-prediction of the number density at small size range of particle can be viewed by a sum of number of particles weighted by the inverse of the size. Thus, we define a *test moment* as

$$\mu_{-1}^{\text{num}}(t) = \sum_{i=1}^I \frac{n_i^{\text{num}} \Delta x_i}{x_i}. \quad (3.52)$$

Similarly $\mu_{-1}^{\text{ana}}(t)$ has been obtained by replacing n_i^{num} to n_i^{ana} in the above equation. Figure 3.11 includes the progress of $\mu_{-1}(t)/\mu_{-1}(0)$ with time for the same problem considered before.



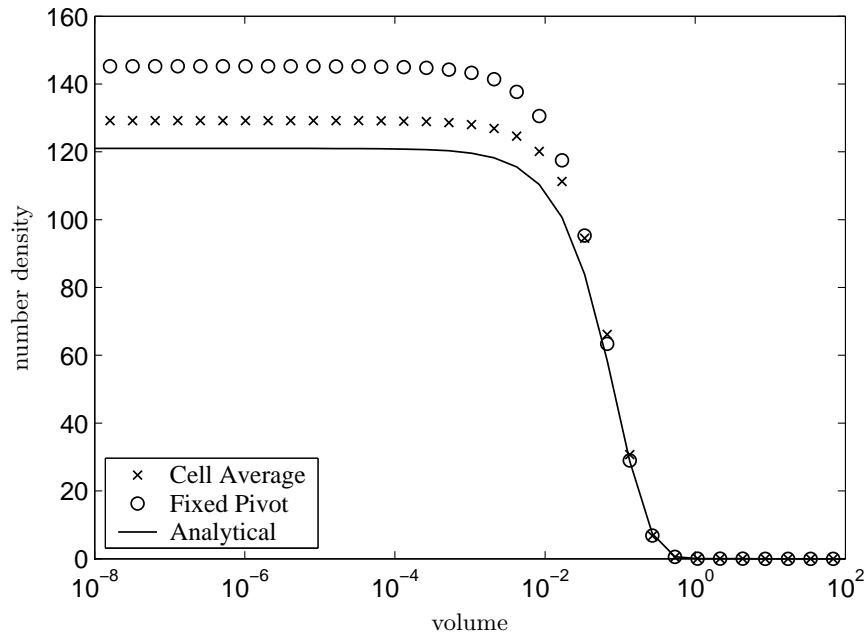
(a) Particle size distribution.



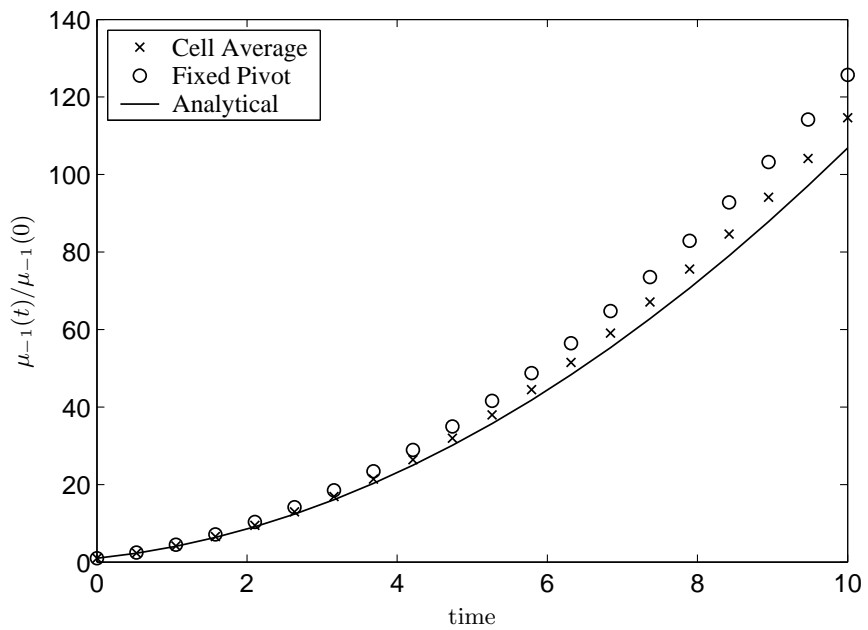
(b) Test moment.

Figure 3.12: A comparison of numerical results for mono-disperse initial condition and $S(x) = x^2$ and $b(x, y) = 2/y$, grid points 30.

3.2. THE CELL AVERAGE TECHNIQUE

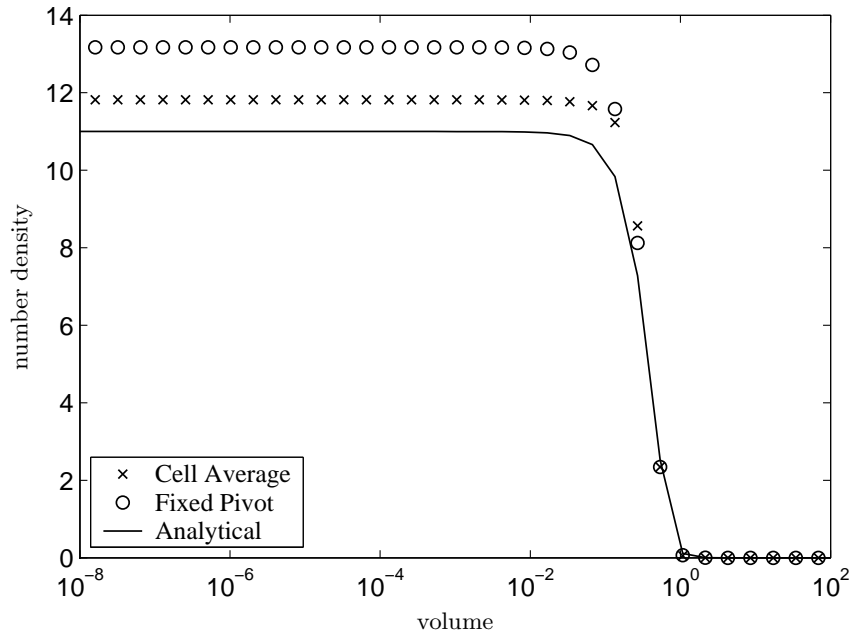


(a) Particle size distribution.

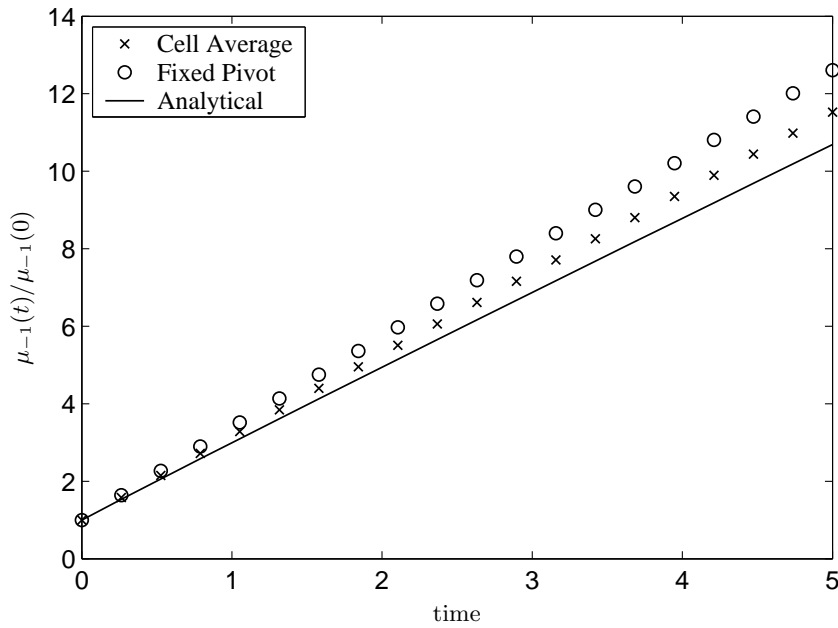


(b) Test moment.

Figure 3.13: A comparison of numerical results for exponential initial condition and $S(x) = x$ and $b(x, y) = 2/y$, grid points 30.



(a) Particle size distribution.



(b) Test moment.

Figure 3.14: A comparison of numerical results for exponential initial condition and $S(x) = x^2$ and $b(x, y) = 2/y$, grid points 30.

3.2. THE CELL AVERAGE TECHNIQUE

Table 3.1: List of test cases for the numerical solution of breakage PBE

<i>Case</i>	$n(0, x)$	$S(x)$	$b(x, y)$	Time	x_{\min}	x_{\max}
1	$\delta(x - L)$	x	$2/y$	1000	10^{-9}	1
2	$\delta(x - L)$	x^2	$2/y$	2000	10^{-9}	1
3	$\exp(-x)$	x	$2/y$	10	10^{-9}	125
4	$\exp(-x)$	x^2	$2/y$	5	10^{-9}	125

Table 3.2: Computation time in seconds for both techniques with mono-disperse initial condition and $b(x, y) = 2/y$

Case	$S(x)$	Grid points	FP technique, t_1	CA technique, t_2	Ratio, t_2/t_1
1	x	30	50	90	1.80
		60	90	160	1.78
		90	158	268	1.70
2	x^2	30	103	175	1.70
		60	205	336	1.64
		90	312	423	1.36

Once again the Figure 3.11(a) and 3.11(b) correspond to the grid points 30 and 90 respectively. For a coarse grid, it is apparent that the overall agreement of the numerical results by the fixed pivot technique with the analytical solutions is not as good as that obtained by the cell average technique. For a finer grid, however, both techniques predict the same results, see Figure 3.11(b).

Let us first conclude the observations from this test case. The numerical results for the first two moments by both techniques are the same. Furthermore, for a finer grid the numerical results obtained by both techniques become close to each others and no significant difference between them can be observed. A significant difference between the two techniques can only be seen in Figures 3.9(a) and 3.11(a). Therefore we compare only a semi-log scale PSD and the special moment μ_{-1} using a coarse grid in our subsequent test cases.

For the second test case of a mono-disperse initial condition with quadratic selection function, the calculated PSDs by the fixed pivot and cell average techniques together with their moments μ_{-1} are directly compared with the analytical solutions in Figure 3.12. The particle size distribution is shown in Figure 3.12(a). A small over-prediction at the steep part of the PSD is obtained by the cell average technique while the fixed pivot technique over-predicts the results of the small size particles. Again, more accurate results can be obtained by increasing the value of the geometric discretization parameter q . In Figure 3.12(b), the analytically and numerically calculated moments μ_{-1} are plotted at different times. The fixed pivot technique consistently overestimates the results at large times. On the other hand, the cell average technique produces very accurate results even at large times.

In Figure 3.13, the analytically and numerically calculated results for the third case are plotted.

Table 3.3: EOC in binary breakage and $S(x) = x, t = 1000$

(a) The cell average technique			(b) The fixed pivot technique		
Grid points, I	Error, L_1	EOC	Grid points, I	Error, L_1	EOC
61	32.8591	-	61	173.4532	-
122	11.6129	1.50	122	89.7167	0.95
244	3.4487	1.75	244	45.2410	0.99
488	0.9378	1.88	488	22.6329	0.99

The level of difficulty has been increased in this case by taking an exponentially decreasing particle size distribution as initial condition. The computation is made for a very short time. As can be seen from the Figure 3.13(a), both techniques give over-prediction of the number density at smaller volumes. In this case the over-prediction is more pronounced due to the integration error in the initial condition and the truncation error on the both sides of the size domain. In contrast to the previous cases, the cell average technique overestimates the numerical results of μ_{-1} , see Figure 3.13(b). However, the extent of over-prediction by the cell average technique is fairly less compare to the fixed pivot technique. A similar observation is obtained for the test case 4. The numerical results for this case are plotted in Figure 3.14.

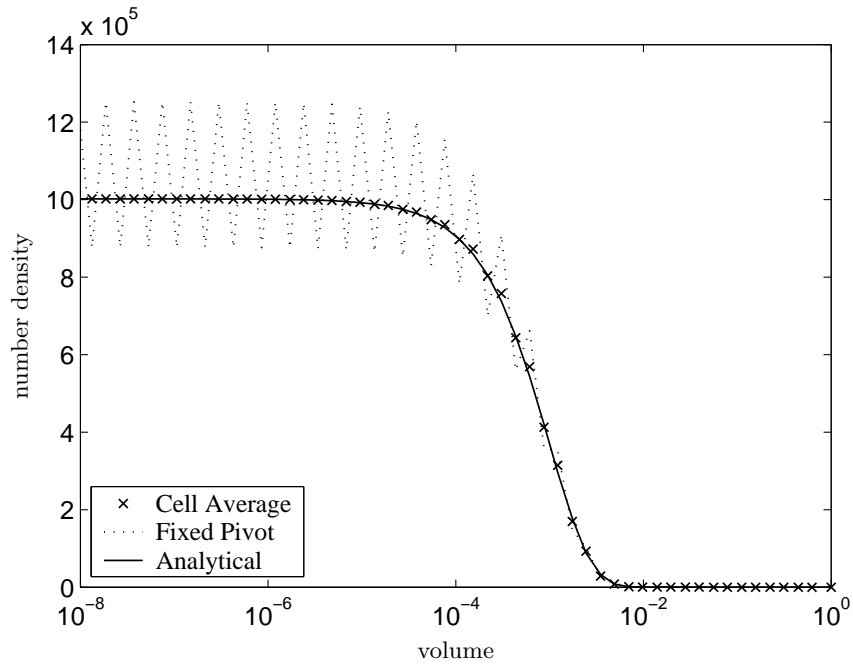
It is of interest to examine the difference of computational time taken by the two techniques. In Table 3.2, the computing times between the fixed pivot technique and the cell average technique along with their ratio are reported for the first two test cases. The cell average technique requires slightly more computing time than the fixed pivot technique for the same number of cells, but less computing time than the fixed pivot technique with twice the number of cells. Additionally, it has been observed that the ratio of computing times between the cell average and fixed pivot techniques is decreasing with increasing number of cells.

Finally, to check the efficiency of the schemes we calculate the experimental order of convergence (EOC). It measures the numerical order of convergence by comparing computations on two meshes. For two meshes where one has cells that are half the size of the other, the EOC is defined by:

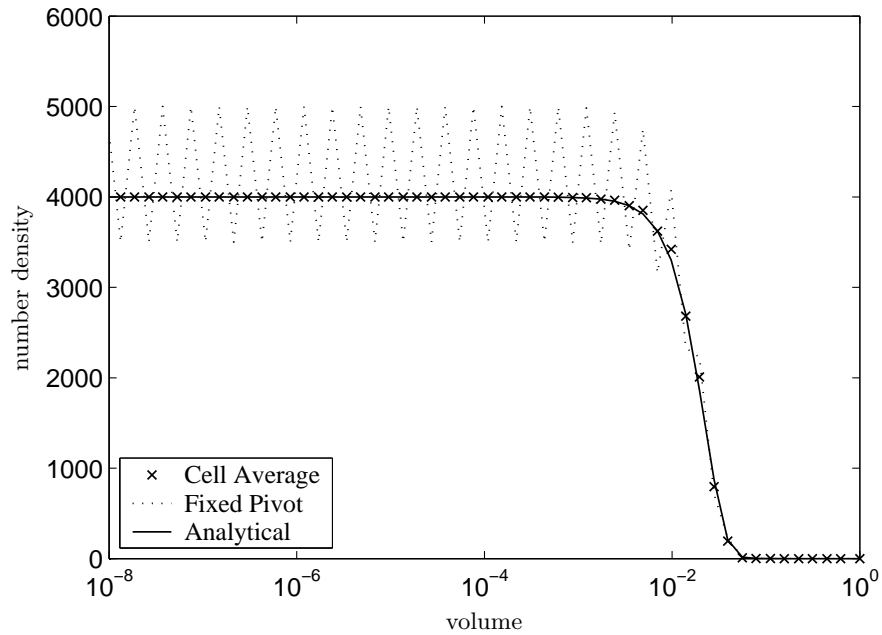
$$\text{EOC} = \ln(E_{r_I}/E_{r_{2I}})/\ln(2), \tag{3.53}$$

where E_{r_I} and $E_{r_{2I}}$ are the errors defined by the L_1 norm $|N^{\text{ana}} - N^{\text{num}}|$. The symbols I and $2I$ correspond to the degrees of freedom. For the case $2I$, each cell of case I was divided into two equal parts. This doubles the number of degrees of freedom. The variable N describes the number distribution of particles. Tables 3.3(a) and 3.3(b) contain EOC tests by both the schemes for the first problem. The EOC for the second problem has been summarized in Tables 3.4(a) and 3.4(b) by the cell average and the fixed pivot technique respectively. Clearly this shows that the cell average technique is of second order while the fixed pivot technique is only first order accurate. In Section 3.3 we will present the mathematical details for the order of convergence of these schemes.

3.2. THE CELL AVERAGE TECHNIQUE



(a) $S(x) = x$ and $b(x, y) = 2/y$.



(b) $S(x) = x^2$ and $b(x, y) = 2/y$.

Figure 3.15: A comparison of particle size distributions for mono-disperse initial condition, grid points 60.

Table 3.4: EOC in binary breakage with $S(x) = x^2$, $t = 2000$

(a) The cell average technique			(b) The fixed pivot technique		
Grid points, I	Error, L_1	EOC	Grid points, I	Error, L_1	EOC
61	2.5326	-	61	13.8570	-
122	0.7733	1.71	122	7.0647	0.97
244	0.2226	1.80	244	3.5574	0.98
488	0.05954	1.90	488	1.7826	0.99

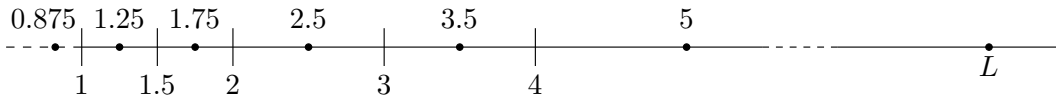


Figure 3.16: A type of discretization to demonstrate the reasons of oscillations in the numerical solutions obtained by the fixed pivot technique.

Computation on special grids: Another important aspect of the schemes is to check flexibility with the discretization of the volume domain. We have tested the first two problems on a special grids. First we have divided the volume domain into the geometric type grids $x_{i+1/2} = 2x_{i-1/2}$ and then each cell is divided into two equal parts. All other computational parameters are the same as before. In Figures 3.15(a) and 3.15(b), the PSDs calculated using the fixed pivot and cell average techniques are compared with the analytical results. As can be seen in the figures, the cell average technique is fairly accurate and predicts the PSD with very high accuracy. On the other hand, the fixed pivot technique produces results with small oscillations at small sizes. It is interesting to note that these oscillations do not destroy the consistency of the fixed pivot scheme with the first two moments.

The reason for such fluctuations by the fixed pivot technique in a breakage problem can be illustrated by the following simple example. We consider N_0 mono-disperse particles of size L_0 as initial condition together with $S(x) = x$ and $b(x, y) = 2/y$. A simple discretized domain which produces fluctuations by the fixed pivot technique is shown in the Figure 3.16. The initial rate of change of particle birth in some cells computed by the fixed pivot and cell average techniques along with the analytical results is presented in Table 3.5. The first two and last two

Table 3.5: Birth rates computed by the two techniques

Number	Cell's range	Analytical	CA technique	FP technique
1	[1, 1.5]	N_0	N_0	$0.875N_0$
2	[1.5, 2]	N_0	N_0	$1.25N_0$
3	[2, 3]	$2N_0$	$2N_0$	$1.75N_0$
4	[3, 4]	$2N_0$	$2N_0$	$2.50N_0$

cells shown in the table have the same size and due to the constant breakage function they get equal number of particles as a result of breakage. Since the volume average of newborn particles due to breakage lies exactly at the grid point, thereby all particles are assigned to the same cell they belong and no redistribution of particles takes place. Consequently the particle birth rate by the cell average technique is the same as the analytical one. On the other hand, this birth rate using the fixed pivot technique depends on the position of neighboring grid points. The two equal size cells have different sizes of the domain from where they get the particles and as a consequence the left cell from the two equal size cells gets a lower birth rate than the right cell.

Based on the above results, one can conclude that the numerically calculated PSDs by the two methods deviate from each other significantly. The numerical results calculated from the cell average technique on a coarse geometric grid are very accurate. On the other hand, an over-prediction in the PSD at lower volumes has been observed in the fixed pivot technique. The computation time taken by the cell average technique is slightly more than for the fixed pivot technique. Interestingly, it has been found that the fixed pivot technique produces small oscillation at smaller volumes. It is due to the fact that the fixed pivot technique assigns the particles to the grids depending upon the position of the neighboring grids. On the other hand, the cell average technique first concentrates all the newborn particles at their average volumes and then reassigns them if necessary to the neighboring nodes according to the position of the average in the cell.

3.2.2 Pure Aggregation

In this section we derive the cell average technique for pure aggregation problems. The PBE for aggregation is the most difficult among the PBEs of all other processes to deal with numerically because of its nonlinear behavior. The PBE for pure aggregation is a nonlinear integro-partial differential equation. The cell average technique is compared to the fixed pivot technique proposed by Kumar and Ramkrishna [57]. The numerical results for aggregation problems by discretized population balances are consistently overpredicting and diverge before the gelling point in the case of a gelling kernel. The cell average technique assigns the particles within the intervals more precisely. This is achieved by taking first the average of the newborn particles within the interval and then assigning them to the neighboring nodes such that pre-chosen properties are exactly preserved. The cell average technique preserves all the advantages of the conventional discretized methods and provides a significant improvement in predicting the particle size distribution. In addition, it is found that the technique is a powerful tool for the computation of gelling problems. The effectiveness of the technique is illustrated by application to several aggregation problems for suitably selected aggregation kernels.

As stated in the previous chapter, Kumar and Ramkrishna [57] proposed a very efficient technique to solve population balance equations. The technique has been formulated such that the prediction of the desired quantities is very accurate. The technique has the advantage of allowing a general grid, but has the disadvantage of not being able to predict the PSDs accurately in the large size range when applied on a coarse geometric grid for solving PBEs with aggregation. The size distributions are consistently over-predicted in the size range where number densities decrease steeply. In this section we first briefly look into the technique and the reasons for over-prediction in the method proposed by Kumar and Ramkrishna. Then we formulate the cell average technique to improve the accuracy of the numerical results.

The finite time breakdown of mass conservation in aggregation systems is known as gelation. Besides the new discretized scheme, the gelation phenomenon will be discussed briefly. It plays an important role in the solution of some PBEs. We shall explore the moment form of the PBE which is convenient for the study of gelation. The gelation point will be calculated for a special case of product kernel and for different initial size distributions. Before we discuss the fixed pivot and the cell average technique in detail, let us first introduce the gelation phenomenon and some useful analytical results concerning gelation.

The gelation point

Let us consider a kernel where the frequency of aggregation increases with the particle size. In this case new forming particles aggregate at a greater frequency than their parents. As aggregation proceeds, the size of the aggregates, and therefore their corresponding frequencies, increase rapidly. According to Ernst et al. [19], a phase transition occurs at the so called *gelation point* where mass is lost from particles of finite size and appears in particles of infinite size. From a macroscopic point of view the gelation effect is represented by a loss of mass in the solution. In the direct simulation process gelation corresponds to the formation of a large particle, comparable in size to the size of the whole system, in finite time. Mathematically, the gelation point can be described in terms of the first moment which is proportional to mass as, see Eibeck and Wagner [18],

$$t^{\text{gel}} = \inf [t \geq 0 : \mu_1(t) < \mu_1(0)], \quad (3.54)$$

and also in terms of second moment as

$$t^{\text{gel}} = \sup [t \geq 0 : \mu_2(t) < \infty]. \quad (3.55)$$

In applications, this phenomenon can be found for the aggregation of cross-linked polymers by Stockmayer [107], colloids by Spanhel and Anderson [105] and food-derived proteins by Fuke et al. [22]. In many applications, such as crystallization, granulation, palletization and aerosol coalescence, the gelation phenomenon is not common, see Smit et al. [103].

Moment form of the population balance

The moment form of population balances reduces to a set of ordinary differential equations which is easy to solve. Moreover, in many applications we are only interested to get moments of the population. In many situations where a full solution of the population balance is not possible, the first three moments provide relevant facts of the solution. The j th moment of the PSD, defined by the equation (2.2), can easily be obtained analytically by multiplying both sides of the aggregation PBE (2.3) by x^j and integrating with respect to x . This yields

$$\frac{d\mu_j}{dt} = \int_0^\infty x^j \left[\frac{1}{2} \int_0^x \beta(t, u, x-u) n(t, u) n(t, x-u) du - n(t, x) \int_0^\infty \beta(t, u, x) n(t, u) du \right] dx.$$

3.2. THE CELL AVERAGE TECHNIQUE

Table 3.6: Moments of the population balance for the batch mode of operation

$\mu_j(t)$	$\beta = \beta_0$	$\beta = \beta_0(u + v)$	$\beta = \beta_0(u \cdot v)$
$j = 0$	$\frac{2\mu_0(0)}{2 + \beta_0\mu_0(0)t}$, for all t	$\mu_0(0) \exp(-\beta_0\mu_1 t)$, for all t	$\mu_0(0) - \frac{1}{2}\beta_0\mu_1^2 t$, $0 \leq t < t^{\text{gel}}$
$j = 1$	$\mu_1(0)$, for all t	$\mu_1(0)$, for all t	$\mu_1(0)$, $0 \leq t < t^{\text{gel}}$
$j = 2$	$\mu_2(0) + \beta_0\mu_1^2 t$, for all t	$\mu_2(0) \exp(2\beta_0\mu_1 t)$, for all t	$\frac{\mu_2(0)}{1 - \beta_0\mu_2(0)t}$, $0 \leq t < t^{\text{gel}}$

Reversing the order of integration, we obtain

$$\begin{aligned} \frac{d\mu_j}{dt} &= \frac{1}{2} \int_0^\infty \int_u^\infty x^j \beta(t, u, x-u) n(t, u) n(t, x-u) dx du - \int_0^\infty \int_0^\infty x^j \beta(t, u, x) n(t, x) n(t, u) dx du \\ &= \frac{1}{2} \int_0^\infty \int_0^\infty (x+u)^j \beta(t, u, x) n(t, u) n(t, x) dx du - \int_0^\infty \int_0^\infty x^j \beta(t, u, x) n(t, x) n(t, u) dx du. \end{aligned}$$

Finally, we get the following form of the PBE

$$\frac{d\mu_j}{dt} = \int_0^\infty \int_0^\infty \left(\frac{(x+u)^j}{2} - x^j \right) \beta(u, x) n(x) n(u) dx du. \quad (3.56)$$

Further simplification of equation (3.56) is not possible without some special forms of the coalescence kernel. We can solve the preceding ordinary differential equation for the cases of size-independent, sum and product kernel analytically. The solution for these cases has been summarized in Table 3.6.

Identification of gelation point

The prediction of mathematical gelation has been investigated by Smit et al. [103] for both the continuous stirred tank (CST) and the batch mode of operation. The population balance equation for CST operation is given by Randolph and Larson [96] as

$$\frac{n(x) - n_{\text{in}}(x)}{\tau} = \frac{1}{2} \int_0^x \beta(t, x-\epsilon, \epsilon) n(t, x-\epsilon) n(t, \epsilon) d\epsilon - n(t, x) \int_0^\infty \beta(t, x, \epsilon) n(t, \epsilon) d\epsilon. \quad (3.57)$$

Here, $n_{\text{in}}(x)$ and $n(x)$ are the number density functions of the feed and exit streams respectively, τ is the mean residence time. For batch operation the form of the population balance equation is given by the equation (2.3).

According to Smit et al. [103], the size-independent kernel is a non-gelling kernel for both modes of operation, while the sum kernel is a gelling kernel for CST operation but a non-gelling kernel

CHAPTER 3. NEW NUMERICAL METHODS: ONE-DIMENSIONAL

for batch operation. Further, the product kernel is a gelling kernel for both batch and CST mode of operation. In this section we discuss the product kernel in detail for the batch mode of operation. The definition of gelation point and the expression of second moment in Table 3.6 give the gelation time t^{gel} as

$$1 - \beta_0 \mu_2(0) t^{\text{gel}} = 0,$$

or,

$$t^{\text{gel}} = \frac{1}{\beta_0 \mu_2(0)}. \quad (3.58)$$

The degree of aggregation at t^{gel} , denoted by $I_{\text{agg}}^{\text{gel}}$, can be evaluated using Table 3.6 as follows

$$\begin{aligned} I_{\text{agg}}^{\text{gel}} &= 1 - \frac{\mu_0(t^{\text{gel}})}{\mu_0(0)} \\ &= \frac{1}{2} \frac{\beta_0 t^{\text{gel}} \mu_1^2}{\mu_0(0)} \\ &= \frac{1}{2} \frac{\mu_1^2}{\mu_0(0) \mu_2(0)}. \end{aligned} \quad (3.59)$$

We consider three types of initial conditions for which $I_{\text{agg}}^{\text{gel}}$ can easily be calculated analytically.

Mono-disperse distribution: Let us assume that initially there are N_0 particles of volume x_0 . In this case, the first three moments at $t = 0$ are easily found to be

$$\begin{aligned} \mu_0(0) &= N_0, \\ \mu_1(0) &= N_0 x_0, \\ \mu_2(0) &= N_0 x_0^2. \end{aligned}$$

When these moments are used in the equation (3.59), the degree of aggregation $I_{\text{agg}}^{\text{gel}}$ can be evaluated as

$$I_{\text{agg}}^{\text{gel}} = 0.5.$$

Bi-disperse distribution: We consider a bi-disperse distribution in order to increase the level of difficulty in the computation. Let us consider that $\check{a}N_0$ particles have size x_1 and $\check{b}N_0$ particles are of size Jx_1 , an integer multiple of x_1 , such that $\check{a} + \check{b} = 1$. Initially, first three moments are

$$\begin{aligned} \mu_0(0) &= N_0, \\ \mu_1(0) &= N_0 x_1 (\check{a} + \check{b}J), \\ \mu_2(0) &= N_0 x_1^2 (\check{a} + \check{b}J^2). \end{aligned}$$

The degree of aggregation in this case is given as

$$I_{\text{agg}}^{\text{gel}} = \frac{1}{2} \frac{(\check{a} + \check{b}J)^2}{\check{a} + \check{b}J^2}.$$

Gaussian-like distribution: Let us consider the following Gaussian-like distribution as the initial condition

$$n(0, x) = \frac{N_0 \check{a}^{\nu+1}}{x_2 \Gamma(\nu + 1)} \left(\frac{x}{x_2} \right)^\nu \exp(-\check{a}x/x_2), \quad (3.60)$$

where N_0 and $x_0 = x_2(\nu + 1)/\check{a}$, are the initial number of particles and initial mean volume respectively. The first three moments are given by

$$\begin{aligned} \mu_0(0) &= N_0, \\ \mu_1(0) &= N_0 x_0, \\ \mu_2(0) &= \frac{\nu + 2}{\nu + 1} N_0 x_0^2. \end{aligned}$$

The calculation for the second moment at $t = 0$ has been carried out in Appendix B.5. The degree of aggregation, in this case, becomes

$$I_{\text{agg}}^{\text{gel}} = \frac{1}{2} \frac{\nu + 1}{\nu + 2}.$$

In numerical calculations, we consider two special cases, $\nu = 0$ and $\nu = 1$. For $\nu = 0$ the Gaussian-like distribution simply becomes the exponential distribution. In these cases, the degree of aggregations are

$$I_{\text{agg}}^{\text{gel}} = \begin{cases} \frac{1}{4}, & \nu = 0 \\ \frac{1}{3}, & \nu = 1. \end{cases}$$

We shall consider these values as the limit values for the extent of aggregation in our numerical calculations. Many discretized numerical methods fail to give a good approximation of moments as well as size distribution close to the gelation point. It will be shown in the section on numerical results that the new method gives quite satisfactory results near gelation while the discretized method of Kumar and Ramkrishna [57] diverges.

The new formulation

As stated earlier, Hounslow's formulation as well as the Kumar and Ramkrishna fixed pivot technique have problems with over-prediction of number density. Kumar and Ramkrishna [58] discussed the reasons for this over-prediction. We will first briefly point out the source of error that causes the over-prediction in numerical solutions and then propose a new strategy to overcome this problem. In many cases, the particle number density can be treated as a combination of steeply decreasing and increasing functions of size. For instance, let us consider a Gaussian distribution as shown in the Figure 3.17(a) as a number density distribution of particles. It has increasing behavior in the small size ranges and decreasing behavior in the large size ranges. Moreover, some part of the distribution can be treated as nearly uniform, in the middle and near to the end points. In order to explain over-prediction, let us approximate the Gaussian distribution by the combination of exponentially increasing, nearly uniform and exponentially decreasing functions.

CHAPTER 3. NEW NUMERICAL METHODS: ONE-DIMENSIONAL

Similar to Kumar and Ramkrishna [57], we begin with the example of aggregation where particles in a volume size range $[x_{i-1/2}, 2x_{i-1/2}[$ colloid with each other. They considered the number density of particles in this size range as $n(x) = 1/x_0 \exp(-x/x_0)$, where x_0 is a parameter. For $x_0 \gg x_{i-1/2}$, the number density can be considered as nearly uniform and for $x_{i-1/2}$ of order x_0 it decreases exponentially. We additionally take $n(x) = 1/x_0 \exp(x/x_0)$, for the increasing part of the distribution, which was not considered by Kumar and Ramkrishna [57]. For a constant aggregation kernel, the number density of new particles in the size range $[2x_{i-1/2}, 4x_{i-1/2}[$ can be calculated analytically. It has been plotted in Figures 3.17(b, c) and (d) for each case.

If we consider the discretized version of the same event, the aggregation of N_i particles of size x_i , the representative size for size range $[x_{i-1/2}, 2x_{i-1/2}[$, forms $N_i/2$ particles of size $x_{i+1}(= 2x_i)$, the representative size for size range $[2x_{i-1/2}, 4x_{i-1/2}[$. As apparent from Figure 3.17(c), the discrete version predicts well in the case of a uniform density. For an exponential density, as shown in Figures 3.17(b) and 3.17(d), almost all particles lie either near the lower boundary or near the upper boundary depending upon the initial distribution. For an exponentially decreasing density, most particles lie near the lower boundary causing an over-prediction. Since the problems involving pure aggregation always have an exponentially decreasing tail even if the initial distribution does not contain it, we frequently observe over-prediction in such problems.

Furthermore, if we have an exponentially increasing part in the distribution, it is also possible to get an under-prediction of the evaluation with these discretized methods, since most particles lie near the upper boundary in this case. Kumar and Ramkrishna [57] observed under-prediction of number density for moderate size particles with the sum and the product kernel. This is evident from the preceding discussion, since the authors considered a Gaussian-like initial distribution which has an increasing density in small size range causing the under-prediction. The under-prediction observed by the authors was not considerably significant because of fine grids in small size ranges. This under-prediction may become significant in a new situation where we have coarse grids in an increasing part of the distribution.

The cell average technique is based on the averaging of particles volume within the cells. The volume averaging controls the non-uniformity in the number density in the cell. Here we will formulate discrete equations which are consistent with number and mass but the idea can easily be generalized for any two other moments of the distribution. For the consistency of two moments, the net birth in i th cell is calculated using the volume average of all newborn particles due to aggregation within three cells, $(i-1)$ th, i th and $(i+1)$ th. The particles should be assigned to the nearby representative sizes depending upon the position of the average value. If the volume average of $(i-1)$ th cell lies between x_{i-1} and $x_{i-1/2}$, then only a part of birth will appear in i th cell. The same arguments can be made for the i th and $(i+1)$ th cells. Similar to Kumar and Ramkrishna [57], the total birth in a cell is given by

$$B_{\text{agg},i} = \frac{1}{2} \int_{x_{i-1/2}}^{x_{i+1/2}} \int_0^x \beta(t, x-u, u)n(t, x-u)n(t, u) du dx. \quad (3.61)$$

Unlike the formulation of the fixed pivot technique by Kumar and Ramkrishna [57], we first discretize the birth to compute the total birth rate in each cell and then redistribute the total birth to neighboring nodes to get the consistency with moments. Since the particles are assumed

3.2. THE CELL AVERAGE TECHNIQUE

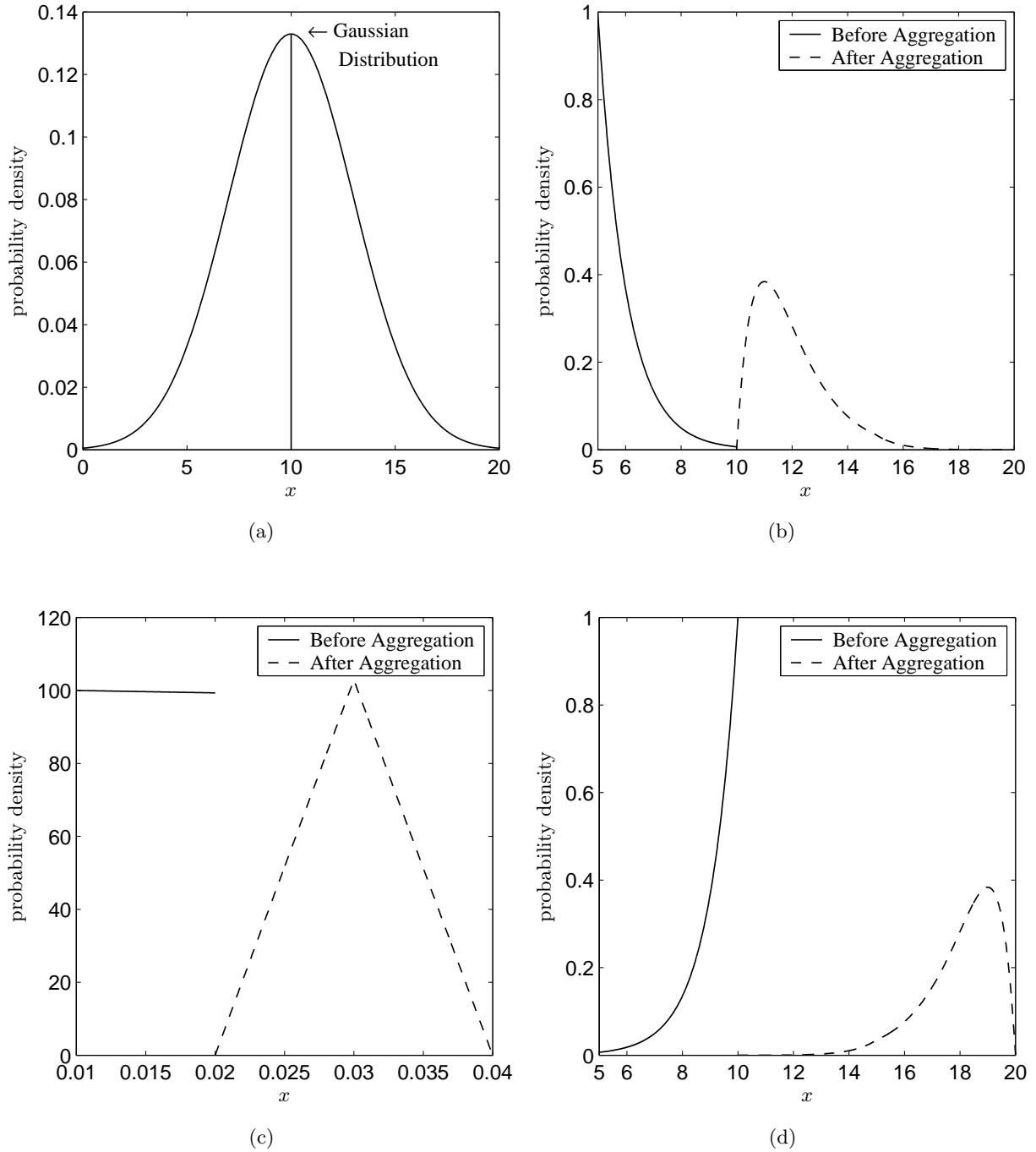


Figure 3.17: Particles initially are distributed (a) Gaussian-like, (b) exponentially decreasing, (c) uniformly, (d) exponentially increasing.

CHAPTER 3. NEW NUMERICAL METHODS: ONE-DIMENSIONAL

to be concentrated at representative sizes x_i , the number density n can be replaced by its Dirac-delta representation (2.15). Substituting the Dirac-delta representation of $n(t, x)$ in equation (3.61), see Appendix B.6, we obtain

$$B_{\text{agg},i} = \sum_{\substack{j \geq k \\ x_{i-1/2} \leq (x_j + x_k) < x_{i+1/2}}} \left(1 - \frac{1}{2} \delta_{j,k}\right) \beta_{j,k} N_j N_k. \quad (3.62)$$

Thus, B_i is the net rate of addition of particles to cell i by coagulation of particles in lower cells. The net flux of volume V_i into cell i as a result of these coagulations is therefore given by

$$V_{\text{agg},i} = \sum_{\substack{j \geq k \\ x_{i-1/2} \leq (x_j + x_k) < x_{i+1/2}}} \left(1 - \frac{1}{2} \delta_{j,k}\right) \beta_{j,k} N_j N_k (x_j + x_k). \quad (3.63)$$

Consequently, the average volume of all newborn particles in the i th cell \bar{v}_i can be evaluated as

$$\bar{v}_i = \frac{V_{\text{agg},i}}{B_{\text{agg},i}}. \quad (3.64)$$

Now we assume that the newborn particles B_i are assigned temporarily at \bar{v}_i . These particles have to be divided depending upon the value of \bar{v}_i to neighboring nodes in such a way that the formulation is consistent with the total number and mass. The birth according to the cell average technique followed by the equation (3.11) is given as

$$B_{\text{agg},i}^{\text{CA}} = B_{\text{agg},i-1} \lambda_i^- (\bar{v}_{i-1}) H(\bar{v}_{i-1} - x_{i-1}) + B_{\text{agg},i} \lambda_i^- (\bar{v}_i) H(x_i - \bar{v}_i) \\ + B_{\text{agg},i} \lambda_i^+ (\bar{v}_i) H(\bar{v}_i - x_i) + B_{\text{agg},i+1} \lambda_i^+ (\bar{v}_{i+1}) H(x_{i+1} - \bar{v}_{i+1}). \quad (3.65)$$

The death term is the same as it was in Kumar and Ramkrishna [57] and is given as (see Appendix B.1)

$$D_{\text{agg},i} = N_i \sum_{k=1}^I \beta_{i,k} N_k. \quad (3.66)$$

Now the final set of discrete equations can be written as

$$\frac{dN_i}{dt} = B_{\text{agg},i-1} \lambda_i^- (\bar{v}_{i-1}) H(\bar{v}_{i-1} - x_{i-1}) + B_{\text{agg},i} \lambda_i^- (\bar{v}_i) H(x_i - \bar{v}_i) \\ + B_{\text{agg},i} \lambda_i^+ (\bar{v}_i) H(\bar{v}_i - x_i) + B_{\text{agg},i+1} \lambda_i^+ (\bar{v}_{i+1}) H(x_{i+1} - \bar{v}_{i+1}) - N_i \sum_{k=1}^I \beta_{i,k} N_k. \quad (3.67)$$

For linear grids $x_j + x_k = x_i$, the equation (3.64) gives the volume average within the cells as $\bar{a}_i = x_i$ and thus the equation (3.67) reduces to the same formula that Kumar and Ramkrishna's fixed pivot technique gives for linear grids. The reduced equation for linear grids $x_j + x_k = x_i$ is also known as discrete aggregation population balance equation.

This new formulation seems, however, computationally a little more expensive, but it balances the particles within the cell more appropriately. Furthermore, we shall later compare the computational time of both schemes for many problems and will observe that the computational

time is comparable. Surprisingly, the cell average technique takes even less computational time for many problems, especially for the gelling-kernel problems. Nevertheless, the cell average technique retains all the advantages of the fixed pivot technique in that it predicts correctly any two moments of the population and can be applied to general grids.

To summarize, the cell average technique concentrates the newborn particles temporarily at the average mean volume and then distributes them to neighboring nodes. For the consistency with two moments, particles have been assigned to two neighboring nodes. It should be evident that the choice of two moments is arbitrary and the formulation can easily be extended for the consistency with any two moments. We now proceed to compare the cell average technique with the fixed pivot technique for certain aggregation problems.

Numerical results

In order to illustrate the improvements over the fixed pivot technique provided by the cell average technique, we compared our numerical results with the known analytical solutions and some physical relevant problems where analytical solutions are not available. In particular, some physically relevant kernels have been considered and results are compared with the generalized approximation (GA) method by Piskunov and Golubev [88]. Piskunov et al. [89] compared several methods and concluded that the GA method is more accurate. Many of the results from this section have already been published in J. Kumar et al. [55].

All computations are carried out in the programming software MATLAB on a Pentium-4 machine with 1.5 GHz and 512 MB RAM. The set of ordinary differential equations resulting from the discretized techniques is solved using a Runge-Kutta fourth and fifth order method with adaptive step-size control based on the embedded Runge-Kutta formulas. It has been observed that the computation with MATLAB standard ODEs solvers produces the negative values at the tail of number density at a certain time. Furthermore, due to negative values the integration becomes unstable and yields large oscillations. In order to avoid such instabilities in our computations we force in our code the non-negativity of the solution by continuing the time integration with a smaller step size.

In order to know the extent of aggregation in numerical computations, it is convenient to express the zeroth moment in dimensionless form. According to Hounslow [31] the index of aggregation, the dimensionless form of the zeroth moment, is defined as

$$I_{\text{agg}} = \begin{cases} 1 - \frac{\mu_0(t)}{\mu_{0,\text{in}}(t)} & \text{for continuous systems} \\ 1 - \frac{\mu_0(t)}{\mu_0(0)} & \text{for batch systems,} \end{cases} \quad (3.68)$$

where $\mu_0(t)$ is the total number of particles at time t (zeroth moment) and μ_0^{in} is the zeroth moment of the feed. The value of aggregation mentioned in this work is reached at final time.

Analytically tractable problems

In this section we compare the cell average technique with the fixed pivot technique for the test problems where analytical results are known. We consider three types of kernels: size-independent, sum and product kernels. The analytical results can be found for various initial

conditions and different kernels in Aldous [3] and Scott [102]. Moreover, all analytical results used in our comparisons have been summarized in Appendix A.2. Most of numerical results reported in this work are obtained for very coarse geometric grids of the type $x_{i+1/2} = 2x_{i-1/2}$ since both schemes produce less distinct results for finer grids.

Computationally, as pointed out by Eibeck and Wagner [17], it is more difficult to handle the gelling problems. We consider both gelling and non-gelling problems to show the effectiveness of the cell average technique developed here. In the gelling case, we will emphasize more the moments to show that the cell average technique is able to predict results very near to the gelling point. For the non-gelling case, the complete evaluation of the number density along with its moments will be analyzed. It can be perceived that the formulation of the fixed pivot as well as the cell average technique leads to the correct total number of particles and conservation of mass. In order to compare the accuracy of the numerical techniques, the second moment and the complete particle size distribution are of interest. As pointed out earlier, for the gelling kernel the first moment is not conserved and the second moment diverges in a finite time. It will be of interest to see how the numerical schemes perform near to the gelation point. A comparison of results by the numerical schemes with analytical results for the first and second moments have been depicted in the case of a gelling kernel.

Size-independent kernel: In order to demonstrate the accuracy of the cell average technique, two different types of initial distribution have been considered. First we take the initial particle size distribution as mono-disperse with dimensionless size unity. The computation has been performed using 14 grid points corresponding to the discretized parameter $q = 1$. In Figure 3.18, the complete size distribution and the corresponding second moment are shown for the size-independent kernel. The prediction of the particle size distribution as well as the second moment is excellent by the cell average technique. At very short times the predictions of the second moment, shown in Figure 3.18(a), by the fixed pivot technique as well as by the cell average technique are the same, but at later times prediction by the cell average technique is considerably better than that predicted by the fixed pivot technique. The cell average technique still predicts extremely accurate results. Figure 3.18(b) shows the improvement of the over-prediction in PSD at large particle sizes by the cell average technique over the fixed pivot technique.

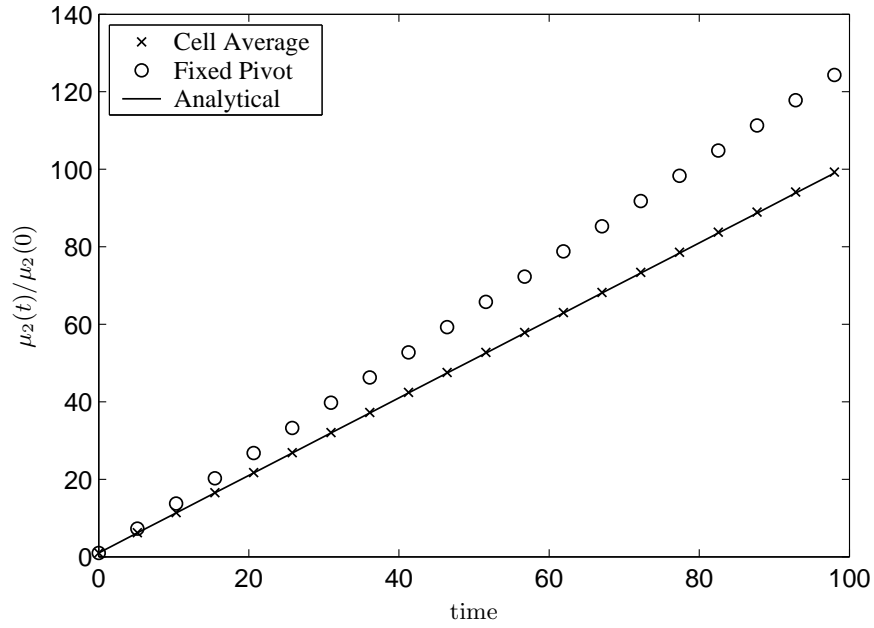
A similar comparison using 52 grid points corresponding to $q = 4$ has been performed for the same problem to illustrate the fact that both techniques produce nearly the same results using fine grids. The results have been plotted in Figure 3.19. As can be seen from the figure that the numerical results obtained by both the techniques are close to each other and converge to the analytical results. All further comparisons are done using coarse grid corresponding to $q = 1$.

We now consider the following exponential initial condition

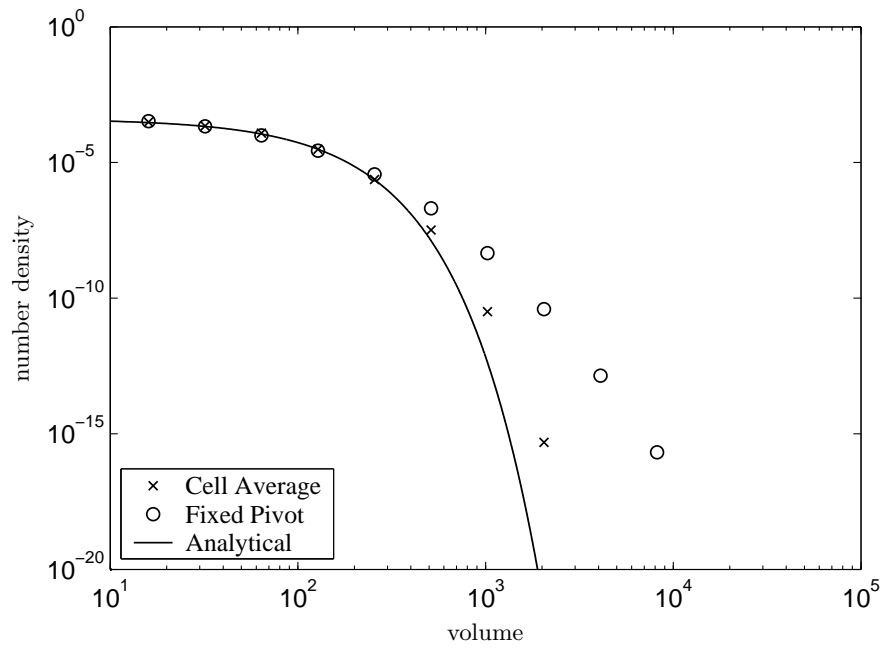
$$n(0, x) = \frac{N_0}{x_0} \exp(-x/x_0). \quad (3.69)$$

The values N_0 and x_0 are the initial number of particles per unit volume and initial mean volume of the particles. The volume of the smallest particle is considered to be 10^{-6} . All the numerical results have been obtained for a geometric grid $x_{i+1/2} = 2x_{i-1/2}$. Figure 3.20(a)

3.2. THE CELL AVERAGE TECHNIQUE

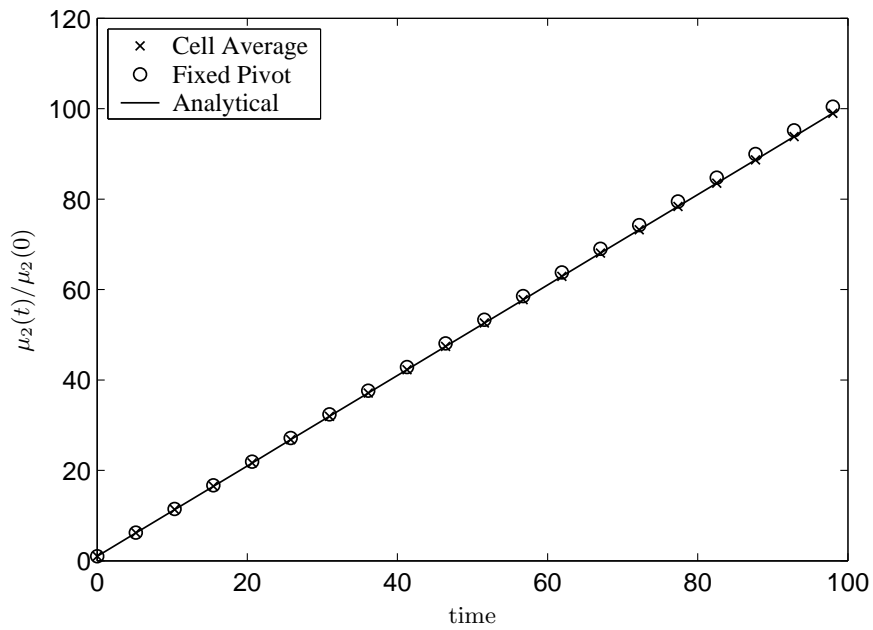


(a) Second moment.

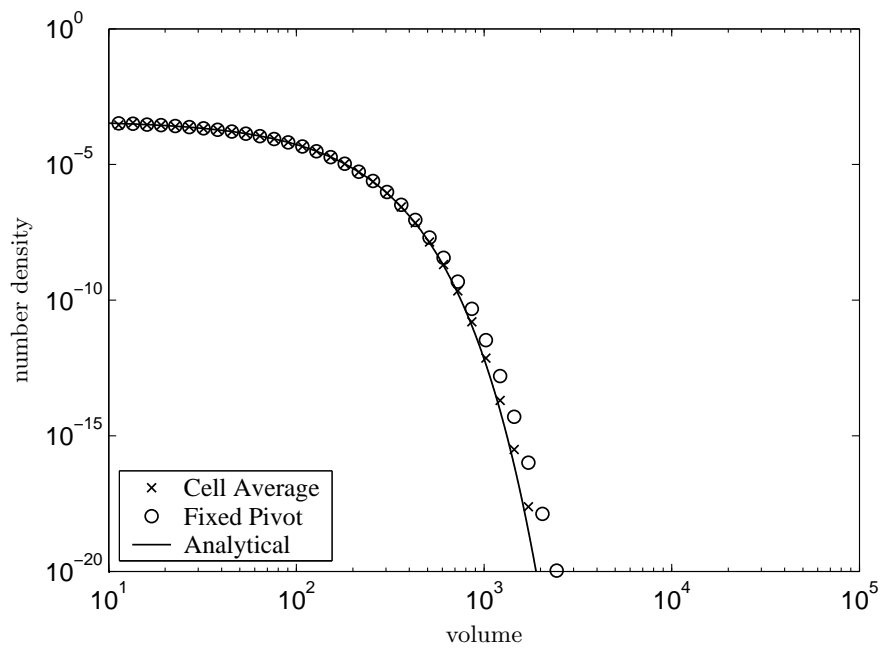


(b) Particle size distribution.

Figure 3.18: A comparison of numerical with analytical results for mono-disperse initial condition and constant kernel, $q = 1$ and $I_{\text{agg}} = 0.98$.



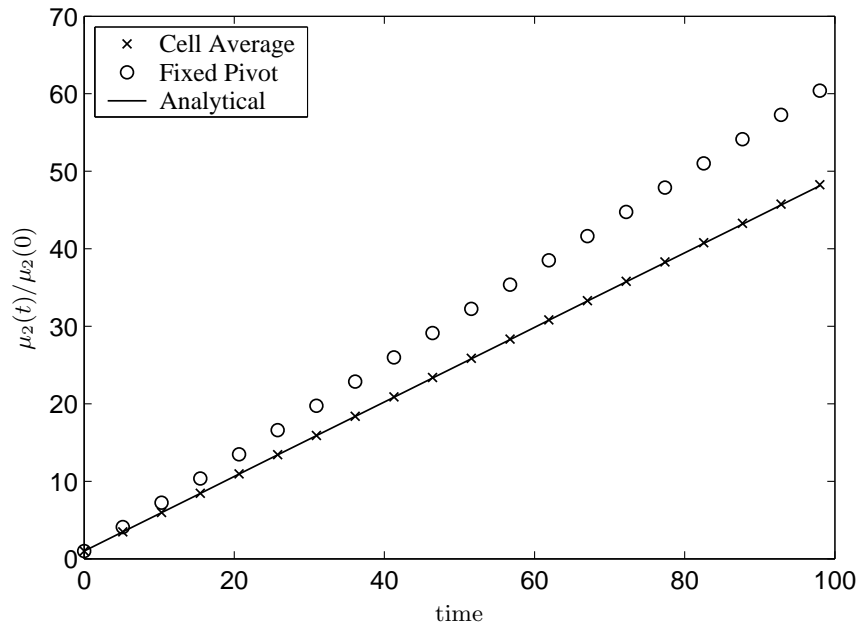
(a) Second moment.



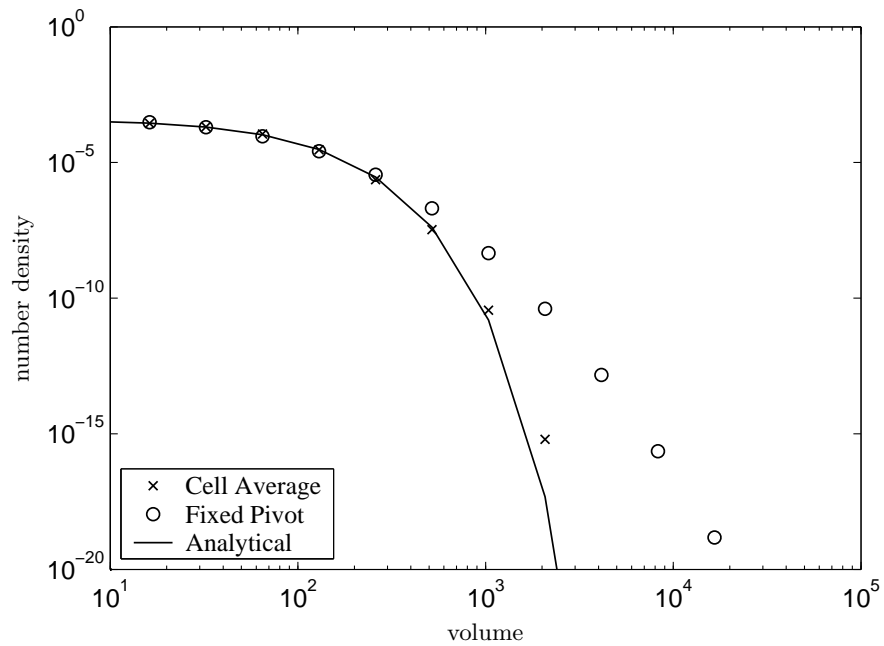
(b) Particle size distribution.

Figure 3.19: A comparison of numerical with analytical results for mono-disperse initial condition and constant kernel, $q = 4$ and $I_{\text{agg}} = 0.98$.

3.2. THE CELL AVERAGE TECHNIQUE



(a) Second moment.



(b) Particle size distribution.

Figure 3.20: A comparison of numerical with analytical results for exponential initial condition and constant kernel, $q = 1$ and $I_{\text{agg}} = 0.98$.

shows the comparison of numerical and the analytical solutions for the variation of second moment. The corresponding predictions for size distribution are shown in Figure 3.20(b). Like the previous case, once again excellent prediction of numerical results can be seen by the cell average technique. The computation has been carried out in both the cases for a very large value of $I_{\text{agg}} \sim (0.98)$.

Sum kernel: The analytical and numerical results for the mono-disperse initial condition with the sum kernel have been shown in Figure 3.21. The computation in this case is performed at 0.80 degree of aggregation. The numerical results for the mono-disperse and the exponential initial conditions reflect the identical behavior. Figure 3.21(a) includes a comparison of the analytical and numerical solutions for the variation of the second moments for the size dependent sum kernel. Once again, the agreement is very good by the cell average technique and the same diverging behavior is observed by the fixed pivot technique. Comparison of size distribution is made in Figure 3.21(b). As for the case of size-independent aggregation, the prediction is poor at large particle sizes by the fixed pivot technique. Once more the degree of fit is very high in the case of the cell average technique.

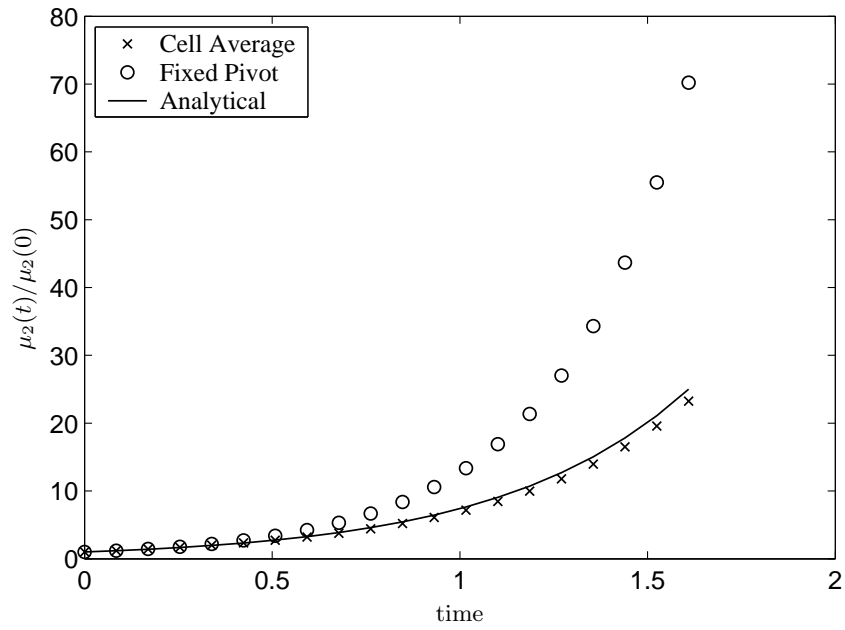
In Figure 3.22, the analytically and numerically calculated particle size distribution and its second moment for the exponential initial condition (3.69) with the sum kernel have been plotted. Figure 3.22(a) includes a comparison of the analytical and numerical solutions for the variation of the second moments. Once more, the agreement is very good by the cell average technique and the same diverging behavior is observed by the fixed pivot technique. Comparison of size distribution is made in Figure 3.22(b). As for the case of size-independent aggregation, the prediction is poor at large particle sizes by the fixed pivot technique and the prediction by the cell average technique is in good agreement with the analytical solutions. The degree of aggregation in this case is taken to be 0.85.

The effectiveness of the cell average scheme for the case when the PSD has an increasing behavior has been demonstrated by considering a Gaussian-like initial distribution. Let us consider the aggregation problem of the initial condition given by the equation 3.60 with $\nu = 1$ and the sum kernel $\beta(t, u, v) = \beta_0(u + v)$. As mentioned earlier, the numerical results by the fixed pivot technique are under-predicted for this problem.

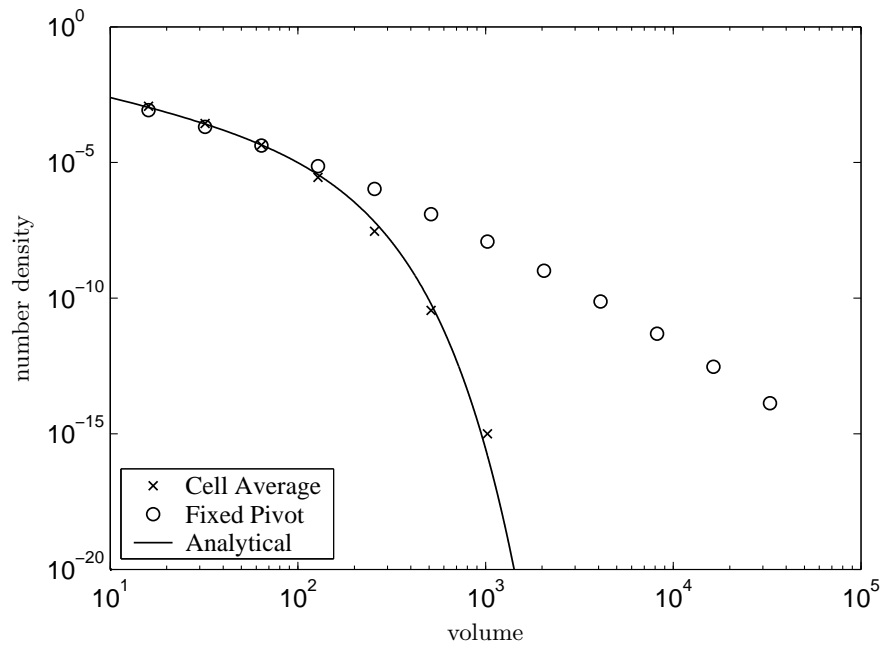
In the numerical computation, the initial mean volume is taken to be 1 and the smallest particle is of volume 10^{-6} . The computation is carried out for a large degree of aggregation, $I_{\text{agg}} = 0.96$. The numerical results along with the analytical results for the number density have been plotted in Figure 3.23. The numerical results by the fixed pivot technique for the moderate size range are under-predicted. The figure clearly shows that with the cell average technique the number density even in this range is predicted very well. The under-prediction is not significant due to the use of fine grids in the small size range. The fixed pivot technique may underestimate results in some situations where an increasing part of the distribution is being discretized using coarse grid.

The results presented so far can be summarized as follows. The numerical results for each case indicate that taking the average within the cells leads to a powerful technique which predicts results with great accuracy. The cell average technique assigns the particles within the cells

3.2. THE CELL AVERAGE TECHNIQUE

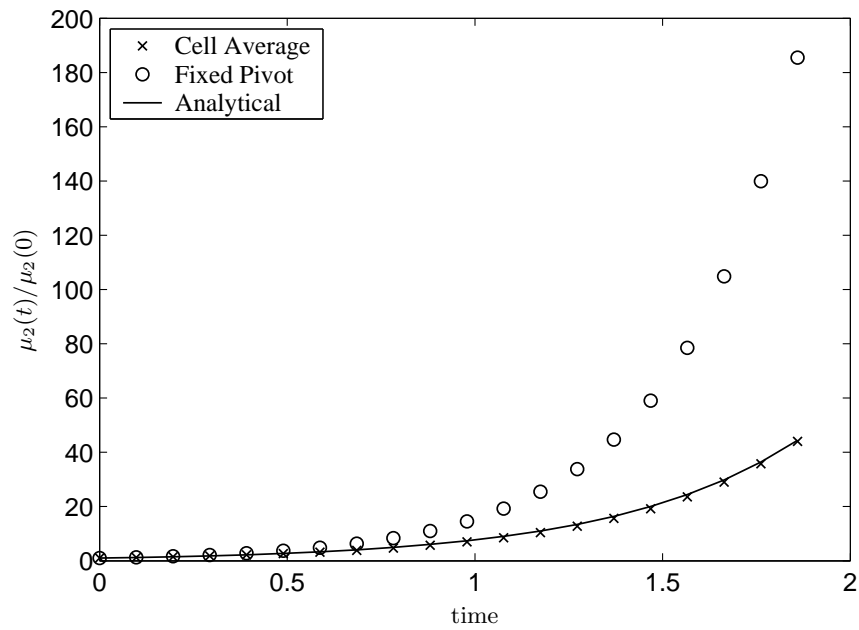


(a) Second moment.

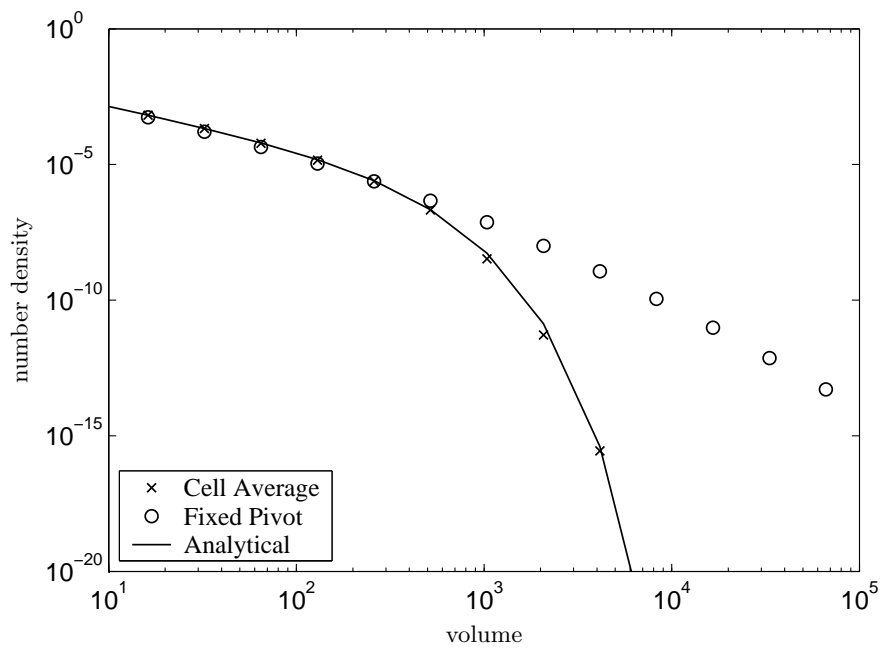


(b) Particle size distribution.

Figure 3.21: A comparison of numerical with analytical results for mono-disperse initial condition and sum kernel, $q = 1$ and $I_{\text{agg}} = 0.80$.



(a) Second moment.



(b) Particle size distribution.

Figure 3.22: A comparison of numerical with analytical results for exponential initial condition and sum kernel, $q = 1$ and $I_{\text{agg}} = 0.85$.

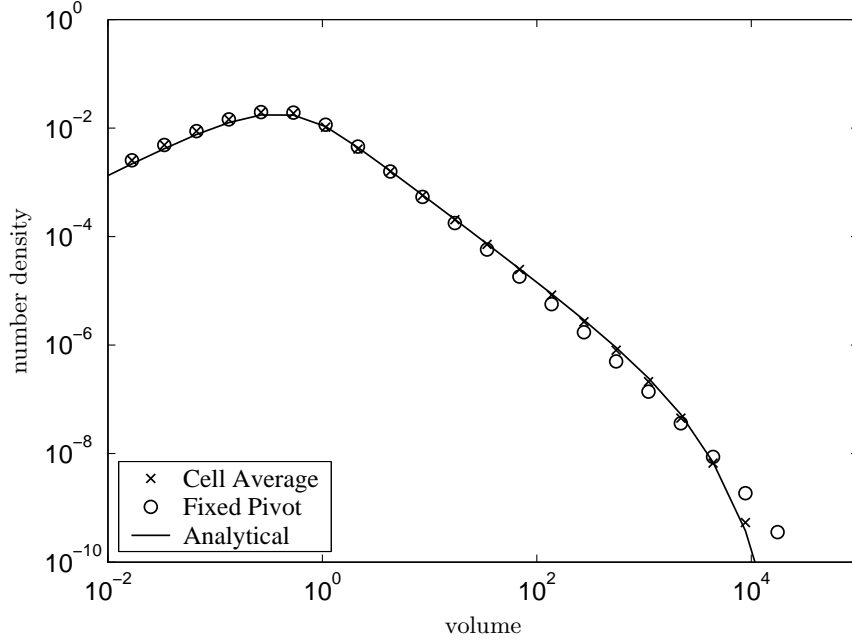


Figure 3.23: A comparison of numerically and analytically calculated particle size distribution, showing the recovery of under-prediction, $q = 1$.

more accurately without increasing the complexity in numerics. This can be observed by the accurate prediction of PSD as well as of the second moment in each case.

Product kernel: The product kernel is a gelling kernel for any arbitrary charge PSD, see Smit et al. [103], however, $I_{\text{agg}}^{\text{gel}}$ depends on the shape of the charge PSD. The gelling time has been provided in the preceding section for three different types of initial distribution: Mono-disperse, bi-disperse and Gaussian-like particle size distribution.

In Figure 3.24, the numerical solution for first and second moments computed with both the schemes is compared with the analytical solution for a mono-disperse initial distribution. Since the degree of aggregation is more important in order to analyze the gelling behavior, moments have been plotted with respect to the degree of aggregation instead of time. For a product kernel, the relationship between time and degree of aggregation is linear. It is related by the following relationship

$$I_{\text{agg}} = \check{C}t,$$

where \check{C} is a constant related to the total initial number and the mass of the system. It is easy to get the value of \check{C} as

$$\check{C} = \frac{\beta_0 \mu_1^2}{2\mu_0(0)}.$$

The degree of aggregation at the gelation point $I_{\text{agg}}^{\text{gel}}$ is 0.5 in this case. Figure 3.24(a) shows that after a certain degree of aggregation the fixed pivot technique starts losing mass while the cell average technique conserves mass up to $I_{\text{agg}} = 0.49$, very close to the gelling point. The comparison of the second moments has been plotted in Figure 3.24(b) up to the degree of

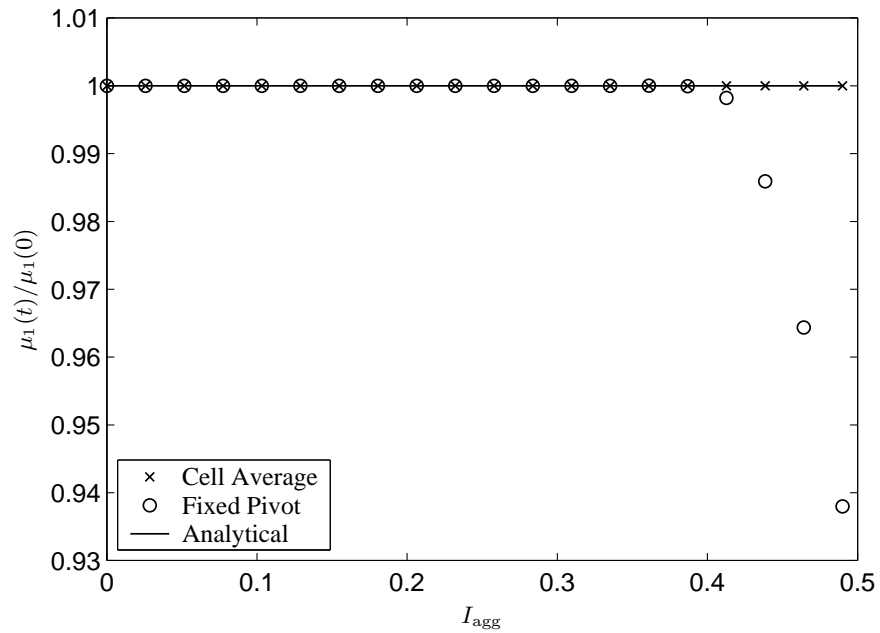
aggregation of 0.3. The computation runs up to $I_{\text{agg}} = 0.30$, because after this point the fixed pivot technique begins to lose mass. Moreover, the results are not comparable after this point since the value of the moment diverges in the fixed pivot technique. The figure shows that the numerical results predicted by the cell average technique are in excellent agreement with the analytical results in the entire range.

Figure 3.25 shows a similar comparison for an exponential initial distribution. The volume of the smallest particle considered in the calculation is 10^{-6} . The initial mean volume in both cases is taken to be 1. Once again, more or less the same features can be seen. In Figure 3.25(a) is shown again the comparison of numerical and analytical results of first moments up to $I_{\text{agg}} = 0.24$. The first moment decays by the fixed pivot technique before the point of gelation. The value of degree of aggregation at the gelation point in this case is 0.25. The variation of second moment of the size distribution is compared in Figure 3.25(b). Like the previous cases, the second moment diverges after $I_{\text{agg}} = 0.14$ for the fixed pivot technique, while the results by the cell average technique are slightly under-predicted. The deviation from the analytical results by the cell average technique is more pronounced at large times. It can obviously be improved by further refinement of the grid at a higher computational cost. A similar observation, shown in Figure 3.26, has been found for the case of Gaussian-like initial condition.

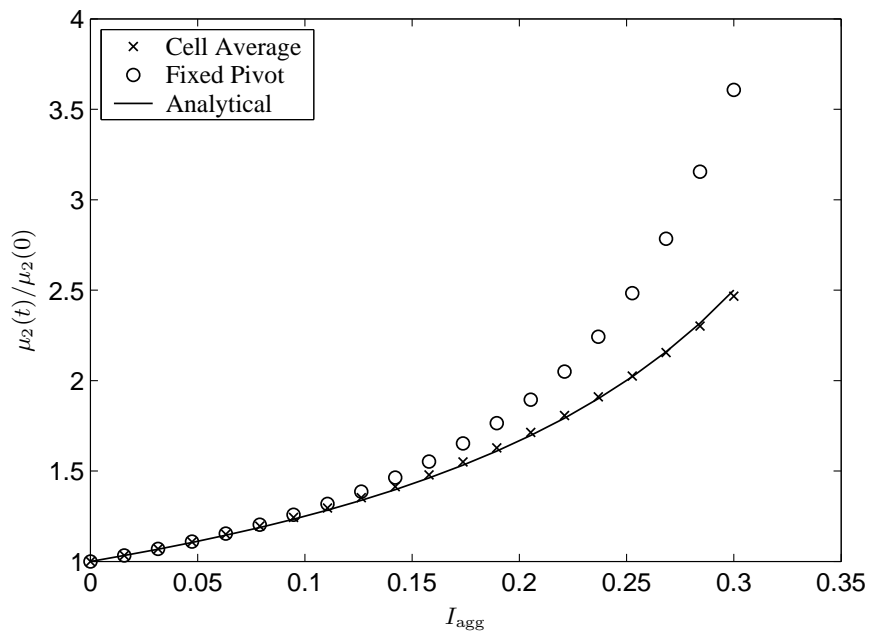
Additionally, we have plotted the prediction of PSD with the product kernel and two different initial conditions: the exponential and the mono-disperse distribution. The results are presented at the same extent of aggregation as above. In Figure 3.27(b), the number density versus volume for the mono-disperse initial distribution is depicted. The situation is different here from that in the previous cases; the deviation of the numerical results from the analytical results is more pronounced. This is expected because of the stronger dependence of the kernel on its argument giving a larger extent of over-prediction. The prediction by the cell average technique is reasonably close to the analytical distribution even for large sizes. On the other hand, the prediction of the PSD at large size ranges using the fixed pivot technique is very poor. It can be observed that a rather much finer discretization is required for good agreement in comparison with the case of a non-gelling kernel.

A similar exercise has been carried out for a bi-disperse particle size distribution. Initially, one half fraction of the particles is fixed in the first class $x_1 = 1$ and the rest is assigned to the second class $x_2 = 2$. As determined earlier, the degree of aggregation at gelation, in this case, is 0.45. The computation of first moments is carried out up to $I_{\text{agg}} = 0.44$. Note that the first moment in Figure 3.28(a) by the cell average technique is conserved even very near to the gelation point while the conservation breaks down at $I_{\text{agg}} = 0.30$ for the fixed pivot technique. Figure 3.28(b) shows the comparison of the second moments up to $I_{\text{agg}} = 0.30$. At small times or analogously at small degree of aggregation, the second moment is predicted reasonably well by the fixed pivot technique. However, as time progresses, the predictions of the moments deviate significantly from the analytical results. At large times, after $I_{\text{agg}} = 0.30$, it is unable to predict the second moment. On the other hand, the prediction agrees very well with the cell average technique even for large degree of aggregation. It should be noted in this case that due to the geometric type grid it is more difficult to predict the complete distribution. It will be shown later that the PSD becomes oscillatory at small particle size range in this case. Nevertheless, the prediction of moments is in very good agreement by the cell average technique.

3.2. THE CELL AVERAGE TECHNIQUE

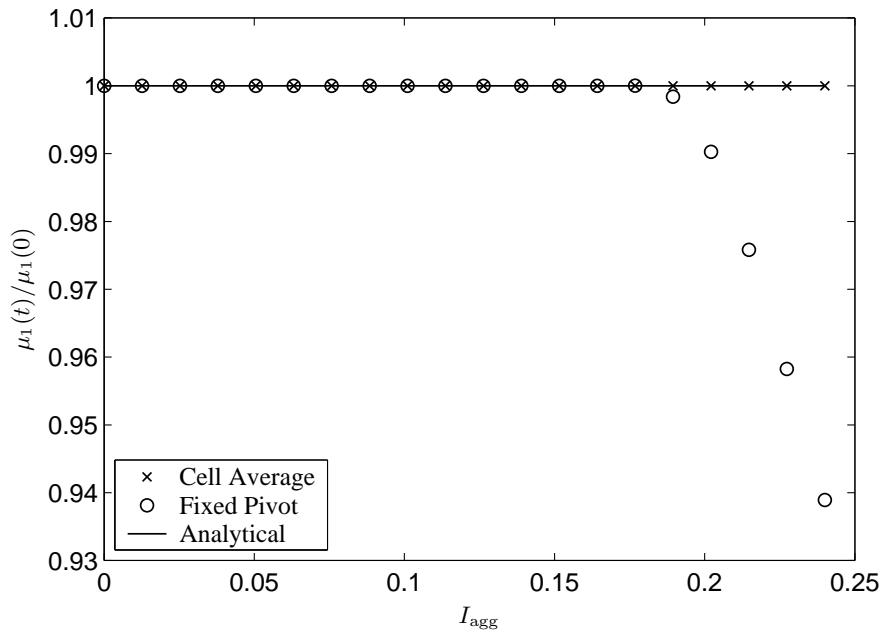


(a) Variation of the first moment, final $I_{agg} = 0.49$.

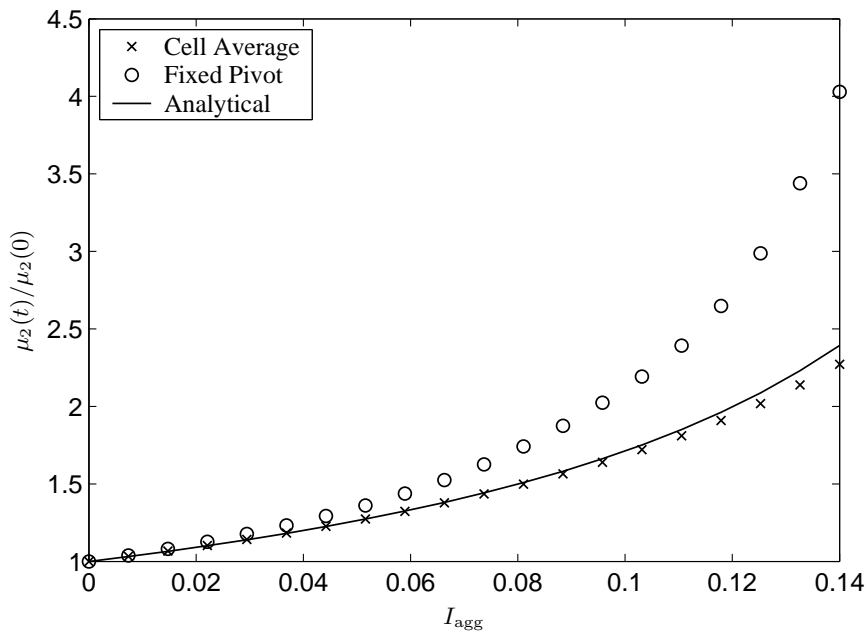


(b) Variation of the second moment, final $I_{agg} = 0.30$.

Figure 3.24: A comparison of numerical with analytical results for product kernel and mono-disperse initial condition, $q = 1$ and $I_{agg}^{gel} = 0.5$.

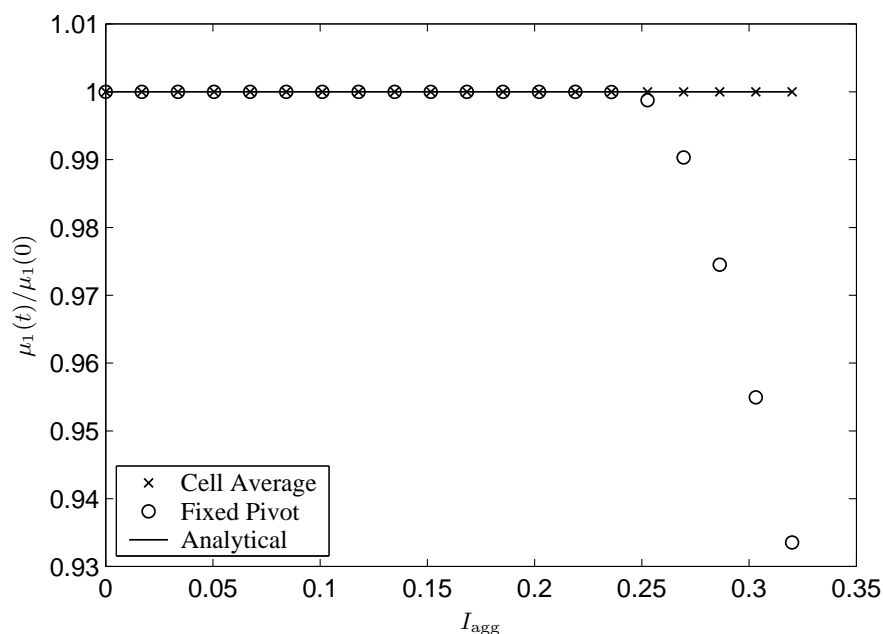


(a) Variation of the first moment, final $I_{agg} = 0.24$.

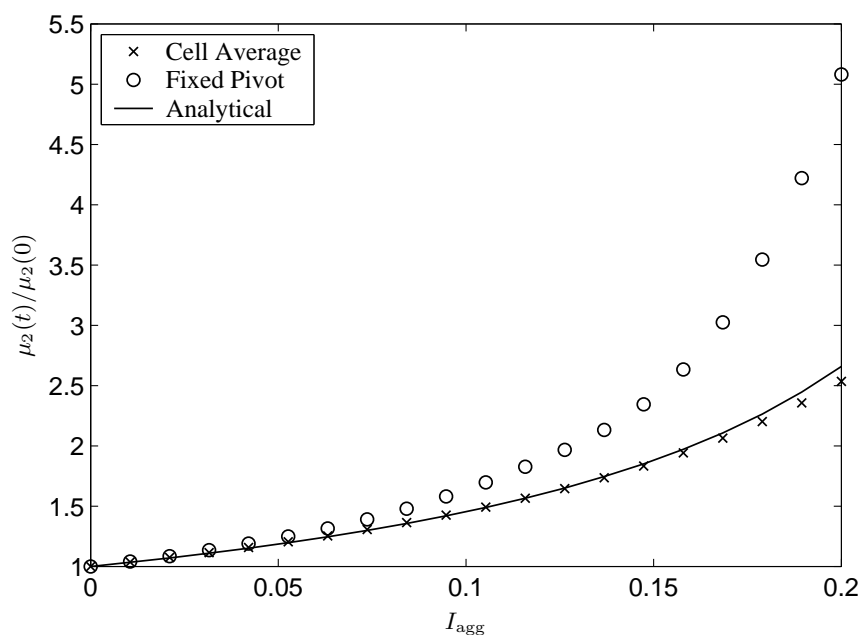


(b) Variation of the second moment, final $I_{agg} = 0.14$.

Figure 3.25: A comparison of numerical with analytical results for product kernel and exponential initial condition, $q = 1$ and $I_{agg}^{gel} = 0.25$.

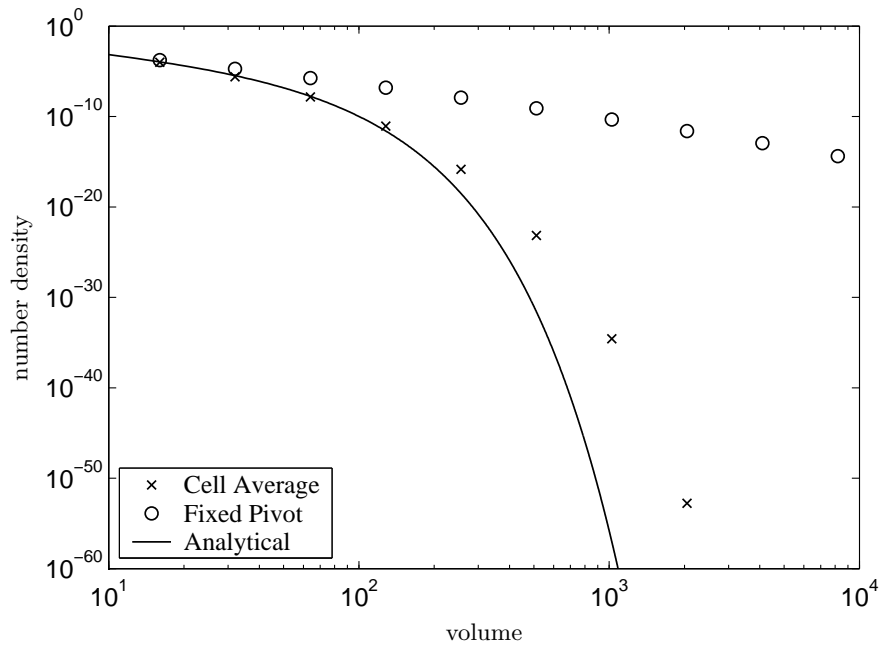


(a) Variation of the first moment, final $I_{agg} = 0.32$.

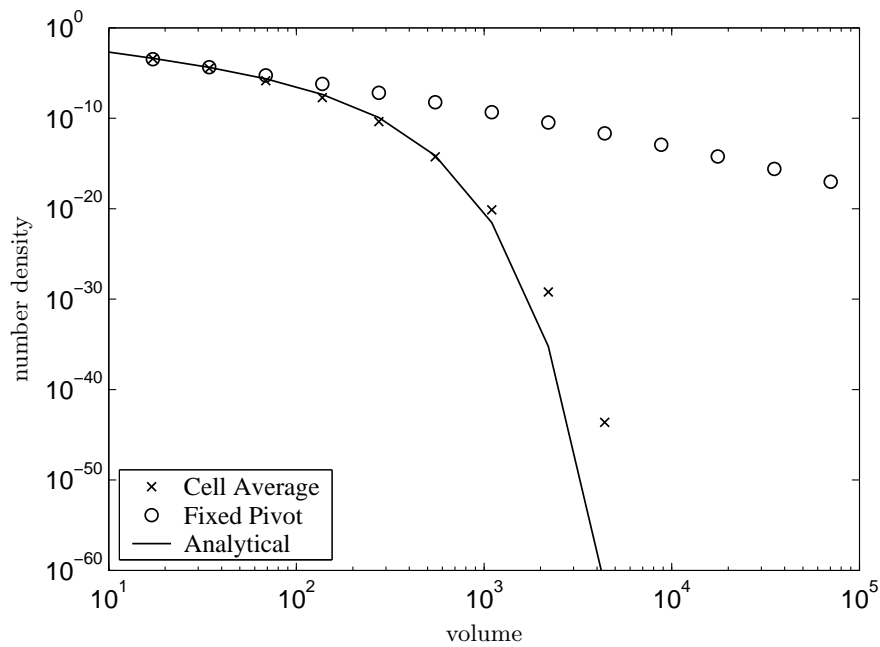


(b) Variation of the second moment, final $I_{agg} = 0.20$.

Figure 3.26: A comparison of numerical with analytical results for product kernel and Gaussian-like initial condition, $q = 1$ and $I_{agg}^{gel} = 0.33$.

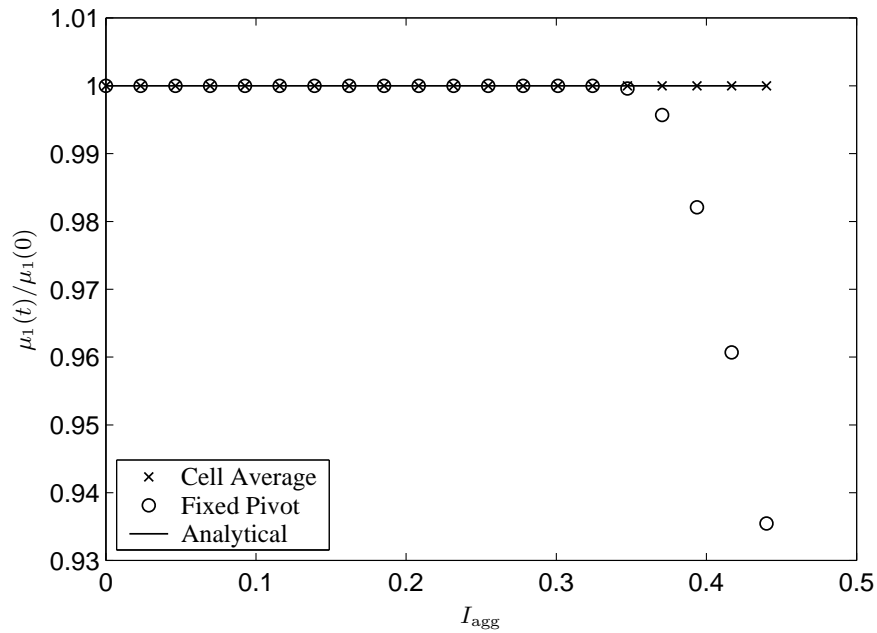


(a) Mono-disperse initial condition, final $I_{\text{agg}} = 0.30$.

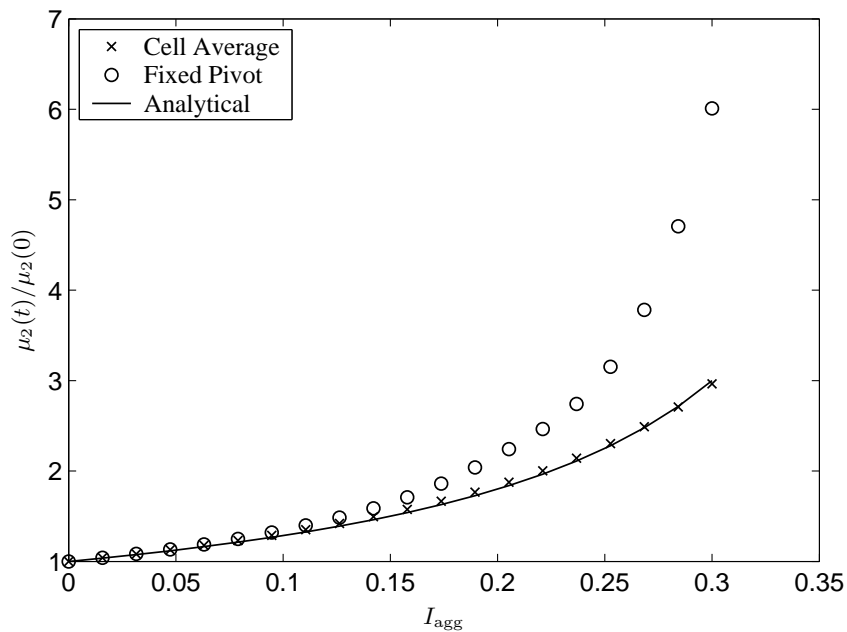


(b) Exponential initial condition, final $I_{\text{agg}} = 0.14$.

Figure 3.27: A comparison of PSDs with analytical results for product kernel, $q = 1$.



(a) Variation of the first moment, final $I_{agg} = 0.44$.



(b) Variation of the second moment, final $I_{agg} = 0.30$.

Figure 3.28: A comparison of numerical with analytical results for product kernel and bi-disperse initial condition, $q = 1$ and $I_{agg}^{gel} = 0.45$.

CHAPTER 3. NEW NUMERICAL METHODS: ONE-DIMENSIONAL

In summary, the cell average technique, in either case, provides an excellent prediction of the second moment as well as conservation of the first moment. The results are obtained with a coarse grid. A finer grid can obviously be used to improve the accuracy of the numerical results to any desired accuracy. Later we will show that the technique presented in this work is adequate to compute moments and PSD very near to the gelation point at a low computational cost.

Physically relevant problems

Now the remaining comparisons are analogous to Piskunov et al. [89]. They considered the following initial condition

$$n(0, x) = \frac{N_0}{\sqrt{2\pi x\sigma}} \exp\left(-\frac{\ln^2(x/x_0)}{2\sigma^2}\right), \quad (3.70)$$

with $N_0 = 1$, $x_0 = \sqrt{3}/2$ and $\sigma = \sqrt{\ln(4/3)}$. The volume domain has been discretized uniformly on a logarithmic scale. It should be mentioned here that Piskunov et al. [89] calculated second moments by varying a set of parameters. We have chosen their best values of second moment for the comparison.

Table 3.7: Comparison of second moments between FP, CA, and GA methods for kernel β_B

t	$I = 68$		$I = 277$		$I = 346$		GA
	FP	CA	FP	CA	FP	CA	
0	1.35	1.35	1.33	1.33	1.33	1.33	1.33
10	43.82	42.96	42.83	42.75	42.80	42.75	42.7
50	213.96	209.57	209.02	208.61	208.85	208.61	209
100	426.64	417.83	416.75	415.93	416.43	415.93	416

Brownian coagulation kernel: We consider the following coagulation kernel for Brownian motion due to Smoluchowski [118]

$$\beta_B(u, v) = (u^{1/3} + v^{1/3})(u^{-1/3} + v^{-1/3}). \quad (3.71)$$

We compare numerical results obtained using fixed pivot technique, cell average technique and generalized approximation method. Table 3.7 gives the second moment obtained by three methods at different dimensionless times and for different class numbers. As can be seen from the table, the cell average technique converges very fast and the values of the second moments are close to the values obtained by the GA method. Moreover, we can observe that on coarse grids the differences between the fixed pivot and cell average techniques are considerably larger at large times. As expected both the fixed pivot and cell average techniques produce the same results on very fine grids.

Coagulation kernel β_+ : We now consider the following frequently used kernel

$$\beta_+(u, v) = u^{2/3} + v^{2/3}. \quad (3.72)$$

3.2. THE CELL AVERAGE TECHNIQUE

Table 3.8: Comparison of second moments between FP, CA, and GA methods for kernel β_+

t	$I = 85$		$I = 306$		$I = 337$		GA
	FP	CA	FP	CA	FP	CA	
0	1.36	1.36	1.34	1.34	1.33	1.33	1.33
10	398.72	370.26	369.30	366.92	368.86	366.86	367
50	3.33E+4	3.06E+4	3.05E+4	3.03E+4	3.05E+4	3.03E+4	3.02E+4
100	2.51E+5	2.32E+5	2.30E+5	2.29E+5	2.30E+5	2.29E+5	2.29E+5

Table 3.9: Comparison of second moments between FP, CA, and GA methods for kernel β_G

t	$I = 104$		$I = 519$		$I = 628$		GA
	FP	CA	FP	CA	FP	CA	
0	1.36	1.36	1.33	1.33	1.33	1.33	1.33
10	159.43	117.20	112.68	110.52	112.05	110.51	104
50	2.89E+5	1.78E+5	1.41E+5	1.35E+5	1.39E+5	1.34E+5	1.19E+5
100	11.8E+6	7.93E+6	6.0E+6	5.7E+6	5.90E+6	5.68E+6	4.93E+6

This kernel is computationally more expensive than the Brownian kernel. The final distribution in this case is much wider than that for Brownian kernel as can be seen from the values of second moment. The numerical results for the second moment have been summarized in Table 3.8. Once again more or less the same observations as before have been found in this case. The values of second moments using the cell average technique are quite close to that obtained by GA method. Table 3.8 clearly shows the over-prediction of the fixed pivot technique.

Gravitational coagulation kernel: The gravitational kernel takes the following form

$$\beta_G(u, v) = (u^{1/3} + v^{1/3})^2 |u^{1/6} - v^{1/6}|. \quad (3.73)$$

Piskunov et al. [89] mentioned that the equations become very stiff and difficult to solve, computation becomes very expensive in this case. Moreover, they could not obtain results for some sets of parameters at large times. Table 3.9 shows that the results using both fixed pivot and cell average techniques are over-predicting at large times even for fine grids. However, the cell average values are more accurate than the fixed pivot ones.

A kernel leading to critical phenomena: Here we consider the following coagulation kernel

$$\beta_C(u, v) = (u^{1/3} + v^{1/3})^2 |u^{2/3} - v^{2/3}|. \quad (3.74)$$

Like the product kernel, certain moments of the distribution diverge at a finite time t^{gel} for this kernel. The value of critical time depends on the initial distribution. Similar to Piskunov et al. [89], we consider two types of initial conditions here. First we take the same initial condition (3.70) as before. Table 3.10 gives the values of second moment obtained using fixed pivot and cell average techniques for different grids. The values have been compared with the values obtained by GA method. The results are comparable only up to $t = 0.4$. At later times the

CHAPTER 3. NEW NUMERICAL METHODS: ONE-DIMENSIONAL

Table 3.10: Comparison of second moments between FP, CA, and GA methods for kernel β_C

t	$I = 231$		$I = 461$		$I = 576$		GA
	FP	CA	FP	CA	FP	CA	
0	1.34	1.34	1.33	1.33	1.33	1.33	1.33
0.1	1.65	1.65	1.64	1.64	1.64	1.64	1.62
0.2	2.20	2.18	2.18	2.18	2.18	2.18	2.12
0.3	3.33	3.25	3.26	3.24	3.26	3.24	3.10
0.4	34.31	6.64	6.21	5.82	6.01	5.80	5.41
0.5	51948.44	4113.97	2275.64	521.81	1392.88	455.67	12.6

Table 3.11: Comparison of second moments between FP, CA, and GA methods for kernel β_C

t	$I = 177$		$I = 581$		$I = 870$		GA
	FP	CA	FP	CA	FP	CA	
0	1.50	1.50	1.50	1.50	1.50	1.50	1.50
0.1	1.70	1.70	1.70	1.70	1.70	1.70	1.70
0.2	2.05	2.04	2.04	2.04	2.04	2.04	2.04
0.3	2.73	2.72	2.71	2.71	2.71	2.71	2.70
0.4	4.27	4.19	4.18	4.17	4.17	4.17	4.11
0.5	33.26	9.26	8.23	8.17	8.18	8.16	7.91
0.6	39546.75	5195.11	228.89	133.07	112.56	73.64	23.27

second moment seems to diverge for both the fixed pivot and cell average techniques. However, the values obtained using the fixed pivot and cell average techniques differ significantly at later times and the fixed pivot values are much larger as usual.

As mentioned earlier the value of t^{gel} depends on the initial condition, now we consider the same coagulation kernel with the following initial condition

$$n(0, x) = 0.5\delta(x - 1) + 0.25\delta(x - 2). \tag{3.75}$$

The values of the second moment at different times have been summarized in Table 3.11. The variation of second moment is the same as that obtained by Piskunov et al. [89]. The values of the second moment increase rapidly after $t = 0.6$, this indicates the appearance of critical time. The overall cell average values of the second moment are slightly larger than that obtained from the GA method but smaller than the fixed pivot values.

Finally we can conclude that the cell average technique gives better results than the fixed pivot technique in each case. The results by the cell average technique are comparable with the GA method. However, comparison with the GA method is not the main concern of this work.

Computational time

As mentioned earlier, the computations for both the fixed pivot and cell average techniques were carried out in the programming software MATLAB on a Pentium-4 machine with 1.5 GHz and

3.2. THE CELL AVERAGE TECHNIQUE

Table 3.12: Computation time in seconds for both techniques (Programming software MATLAB, Pentium-4 machine with 1.5 GHz and 512 MB RAM)

Case	Kernel	Initial condition	I	I_{agg}	FP technique	CA technique
1	Constant	Mono-disperse	15	0.98	1.18	0.39
		Exponential	45	0.98	1.24	1.28
2	Sum	Mono-disperse	22	0.85	0.56	0.76
		Exponential	48	0.85	0.95	1.65
3	Product	Mono-disperse	22	0.40	0.72	0.28
		Exponential	51	0.18	0.64	0.56

512 MB RAM. We have realized computations for several cases: three different kernels and two different initial conditions. A comparison of CPU time taken for both the schemes under the same demands on accuracy and other conditions is drawn in Table 3.12. Although the average computation time for one step is higher for the cell average technique, the table indicates that the total computation times are comparable. It shows the faster convergence toward the final solution by the cell average technique in comparison to the fixed pivot technique. However, for the sum kernel the computation time by the cell average technique is larger. On the other hand in case of the product kernel the fixed pivot technique takes more time. The fixed pivot technique takes more time for both initial conditions, because of the numerical problems near mathematical gelation. Nevertheless, the difference between computational times varies less than by a factor of 1.5. The cell average technique takes considerably more time in the case of the exponential initial distribution with the sum kernel than for any of the other cases. But, this is reasonable because of the highly precise prediction of the results by the cell average technique in this case. If we take a look at the Figure 3.22, the prediction of the size distribution as well as the second moment by the cell average technique is extremely accurate and the deviation between the numerical results by the techniques is more pronounced.

It should be noted that due to the large over-prediction of large particles by the fixed pivot technique we have to take a very large range of volume in order to cover all the particles and conserve mass. The number of particles produced by the cell average technique in the large volume range is insignificant and we may take a smaller computational domain without losing mass. The larger volume range of the fixed pivot technique, of course, generates more equations and thus more computation time. The computation time that we give can therefore still be reduced by the cell average technique by taking a smaller range of volumes, i.e. fewer equations. Here we have not done this in order to compare results on the same computational domain.

Relative error

As pointed out before, in all previous sections we have always made computations on coarse grids of the type $x_{i+1/2} = 2x_{i-1/2}$. In this section we study the effect of discretizations on numerical results. We choose a family of geometric discretizations of the type $x_{i+1/2} = 2^{1/q}x_{i-1/2}$. By varying the value of q we can get different discretizations of the domain. We computed the second moment for different q using both the fixed pivot and cell average techniques. The

CHAPTER 3. NEW NUMERICAL METHODS: ONE-DIMENSIONAL

Table 3.13: Comparison of relative error of second moment for mono-disperse initial distribution and sum kernel, $I_{\text{agg}} = 0.85$

Grid points I	Relative error	
	FP technique	CA technique
20	2.16	6.42E-2
40	0.33	3.57E-2
60	0.14	4.14E-3
120	3.49E-2	1.74E-3
240	7.93E-3	7.36E-4

Table 3.14: Comparison of relative error of second moment for exponential initial distribution and sum kernel, $I_{\text{agg}} = 0.85$

Grid points I	Relative error	
	FP technique	CA technique
40	4.23	0.28
80	0.49	1.67E-2
120	0.19	6.99E-3
240	4.51E-2	5.07E-3
400	1.75E-2	2.44E-3

relative error has been calculated by dividing the error $\|\mu_2^{\text{ana}} - \mu_2^{\text{num}}\|$ by $\|\mu_2^{\text{ana}}\|$, where $\|\cdot\|$ is the L_2 norm. The L_2 norm of a vector $x = (x_1, x_2, \dots, x_n)$ is given as $(\sum_{k=0}^n x_k^2)^{1/2}$. The values μ_2^{ana} and μ_2^{num} are the analytical and numerical values of the second moment respectively.

We calculated the relative error for the mono-disperse and the exponential initial distributions for the case of the sum kernel. The degree of aggregation in both cases is taken to be 0.85. Table 3.13 and 3.14 show the relative error in the second moment using different grid points for the mono-disperse and exponential initial distributions respectively. As can be seen from both tables, the difference between the two techniques is considerable. Moreover the tables clearly show that both techniques produce nearly the same results for fine grids.

Experimental order of convergence

Tables 3.15(a) and 3.15(b) show the EOC (3.53) test of the cell average and fixed pivot techniques respectively. It is computed for a test problem with an exponential initial condition and the sum coagulation kernel. The degree of aggregation is chosen to be 0.95. As can be seen from the tables, the convergence of the two methods differs significantly. The fixed pivot method is only of first order whereas the cell average method is clearly of second order for this problem.

The cell average formulation presented here maintains the consistency with the zeroth and the first moments. It should be noted that the formulation can easily be changed for the consistency with any two moments. Since we are dealing with the number density population balance

3.2. THE CELL AVERAGE TECHNIQUE

equation the consistency with the total number is very important. Let us consider a general case of the exact prediction of the zeroth moment and the r th moment. In this case it is easy to modify the equations (3.63), (3.64) in the form

$$V_{\text{agg},i} = \sum_{\substack{j \geq k \\ j,k \\ x_{i-1/2} \leq (x_j + x_k) < x_{i+1/2}}} \left(1 - \frac{1}{2}\delta_{j,k}\right) \beta_{j,k} N_j N_k (x_j + x_k)^r, \quad (3.76)$$

$$\bar{v}_i = \left(\frac{V_{\text{agg},i}}{B_{\text{agg},i}}\right)^{1/r}. \quad (3.77)$$

Consider the case when the average value \bar{v}_i is bigger than x_i , the fractions must be calculated from the following system of equations

$$\begin{aligned} a_1 + a_2 &= \hat{B}_{\text{agg},i} \\ a_1 x_i^r + a_2 x_{i+1}^r &= \hat{B}_{\text{agg},i} \bar{v}_i^r. \end{aligned} \quad (3.78)$$

Solving these equations, the fractions a_1 and a_2 are given by

$$a_1 = \hat{B}_{\text{agg},i} \frac{\bar{v}_i^r - x_{i+1}^r}{x_i^r - x_{i+1}^r}, \text{ and } a_2 = \hat{B}_{\text{agg},i} \frac{\bar{v}_i^r - x_i^r}{x_{i+1}^r - x_i^r}. \quad (3.79)$$

As discussed before, the λ_i for this case can be defined as

$$\lambda_i^\pm(x) = \frac{x^r - x_{i\pm 1}^r}{x_i^r - x_{i\pm 1}^r}. \quad (3.80)$$

The formulation (3.67) with the average values \bar{v}_i from the equation (3.77) and the functions λ_i from the equation (3.80) gives consistency with respect to the zeroth and r th moments. Up to now we have considered the consistency with the zeroth and one extra moment. Similarly the cell average formulation can be derived for any two moments. Nevertheless, the first two moments are of special interest for many applications, so that we refrain here from discussion of the exact prediction of more moments. The extension of the scheme for the consistency of more moments is possible by distributing the birth to more nodes but it may lead to a formulation that loses positivity of the solution. All these issues and remedies to resolve the positivity problem will be discussed in Subsection 3.2.3.

We conclude this section with the observation that the numerical results have shown the ability of the cell average technique to predict very well the time evolution of the second moment as well as the complete particle size distribution. The technique follows a two step strategy—one to calculate average size of the newborn particles in a class and the other to assign them to neighboring nodes such that the properties of interest are exactly preserved. The main significance from the applicational point of view of the improved efficiency is that it can be used as a tool for the calculation up to (or near to) the gelation point, as we have already seen that the fixed pivot technique diverges before the gelation point due to the over-prediction. A comparison of the numerical results for the fixed pivot and the cell average technique with the analytical results indicates that the cell average technique improves the under-prediction in the moderate size range and the over-prediction in the large size range. Furthermore, we applied the cell average technique to physically relevant problems and the results have been compared with the fixed pivot and GA techniques. The numerical results for these problems are comparable to the GA method while the fixed pivot technique gives over-prediction in each case.

CHAPTER 3. NEW NUMERICAL METHODS: ONE-DIMENSIONAL

Table 3.15: EOC of the cell average and fixed pivot techniques for exponential initial distribution and sum kernel, $I_{agg} = 0.95$

(a) The fixed pivot technique			(b) The cell average technique		
Grid points, I	Error, L_1	EOC	Grid points, I	Error, L_1	EOC
30	2.43E-2	-	30	2.54E-2	-
60	1.16E-2	1.06	60	9.38E-3	1.44
120	6.31E-3	0.87	120	2.93E-3	1.68
240	2.84E-3	1.14	240	7.63E-4	1.94

Comment on choice of grid

The right choice of grids is a very important factor in the computation of population balances. Batterham et al. [7] divided the particle size domain into intervals of equal sizes for the process of aggregation. They pointed out that covering a modest range of particle size domains results in a very large set of ordinary differential equations. Bleck [9] proposed a geometric grid for the discretization of PBEs for aggregation. By using a geometric grid, the computational cost of course can be highly reduced, but on the other hand the prediction of numerical results becomes poorer. Moreover, the suitability of grid type also depends on the particular problem. Nevertheless, there is a trade-off between accuracy and computational cost and one has to find a compromise. The effect of grids on the solution can be well observed in the following example.

Let us consider a problem proposed by Boehm et al. [10] where the initial conditions are bimodal. They have considered the following non-dimensional form of the following discrete population balance equation

$$\frac{dN_j}{dT} = \sum_{j=1}^{i-1} N_j N_{i-j} - 2N_i \sum_{j=1}^{\infty} N_j. \tag{3.81}$$

The initial conditions are

$$N_1(0) = \check{a}, \quad N_J(0) = \check{b}, \quad N_j(0) = 0, \quad \text{for } J \in \mathbb{N}, j \neq 1, J. \tag{3.82}$$

where $\check{a}, \check{b} > 0$ and $\check{a} + \check{b} = 1$.

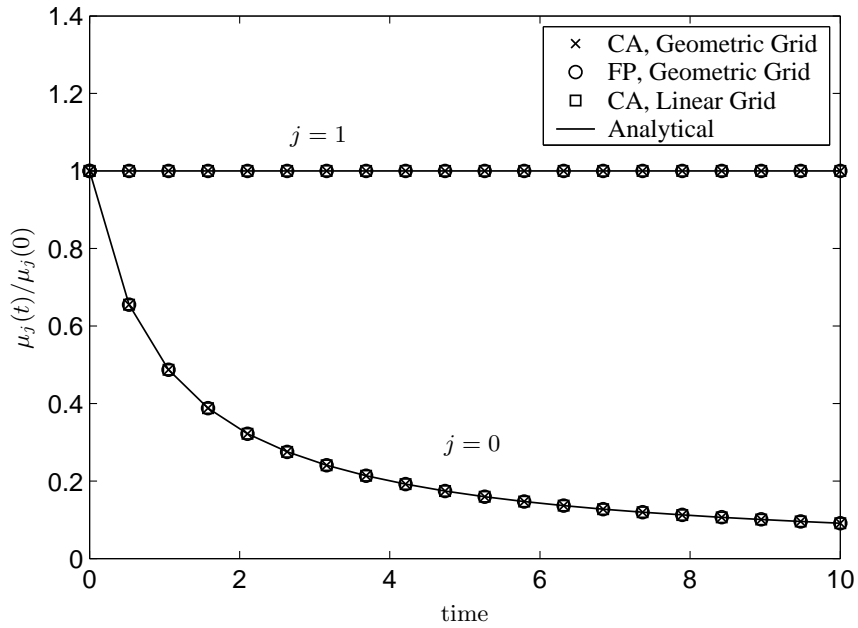
They obtained the following analytical solution of the above problem

$$N_j(T) = \frac{1}{(1+T^2)} \sum_{l=0}^{\frac{j}{J-1}} \frac{(j-lJ-l)!}{(j-lJ)!(l)!} \check{a}^{j-lJ} \check{b}^l \left(\frac{T}{1+T} \right)^{j-1-l(J-1)}. \tag{3.83}$$

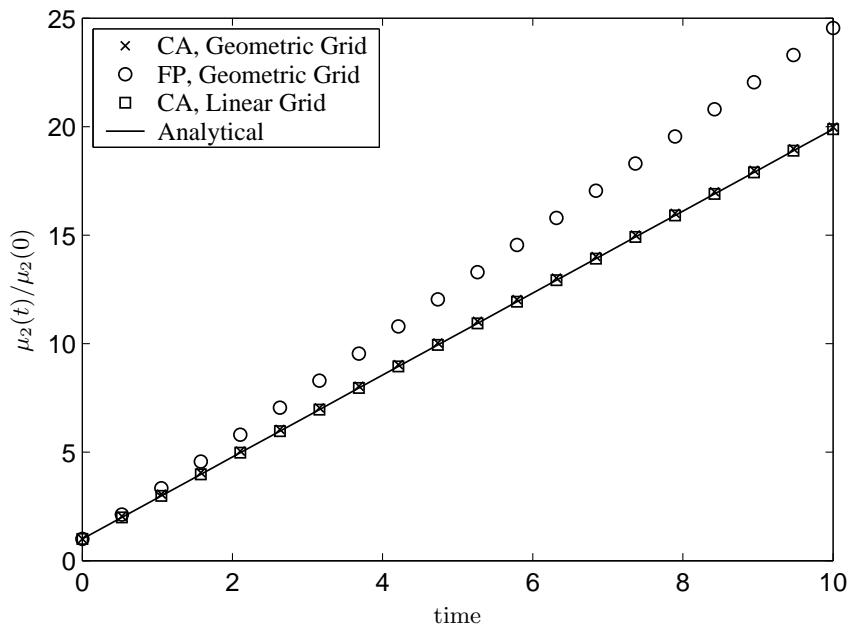
Boehm et al. [10] also presented a recurrence relation for the solution where $j \geq J$

$$(1 + 1/T)N_{j+1}(T) = \check{a}N_j(T) + \check{b}N_{j+1-J}(T). \tag{3.84}$$

3.2. THE CELL AVERAGE TECHNIQUE



(a) Variation of the first two moments.



(b) Variation of the second moment.

Figure 3.29: A comparison of numerical and analytical moments obtained by using linear and geometric grids, $q = 1$, for bi-disperse initial condition and constant kernel.

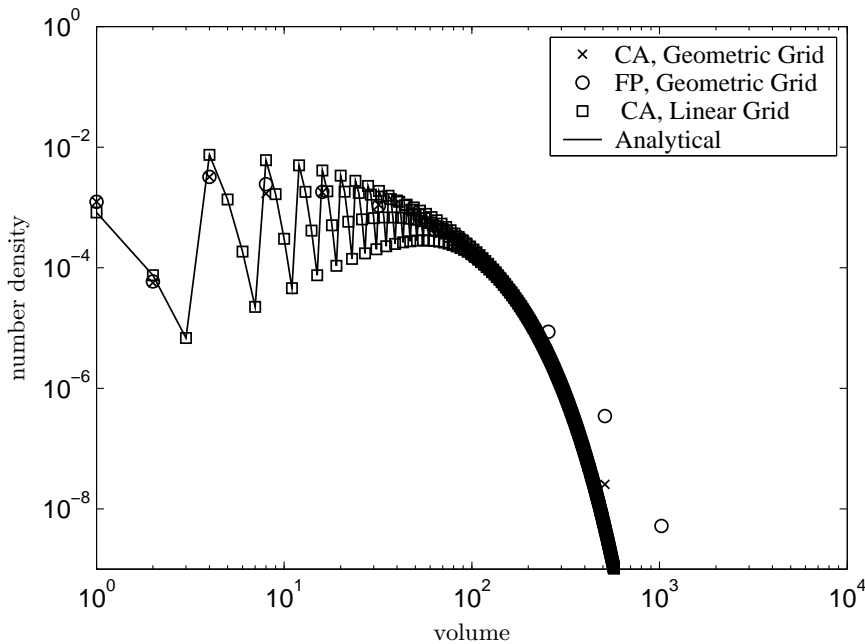


Figure 3.30: A comparison of numerically and analytically calculated particle size distribution obtained by using linear and geometric grids, $q = 1$, for bi-disperse initial condition and constant kernel.

We solved this problem numerically using linear grids, $x_i = ix_1$, and geometric grids, $x_{i+1} = 2x_i$. We used the fixed pivot technique and the cell average technique for the computation. As we mentioned before that both techniques produce the same results while using on liner grid. The results have been obtained for $\check{a} = 0.1$, $\check{b} = 0.9$, and $T = 10$. If we look at the moments, Figure 3.29, the results are in good agreement with the exact solution. As expected, the zeroth and first moments, Figure 3.29(a), are exactly preserved in each case. While the difference of the second moment between the numerical and analytical results is still comparable. As aggregation proceeds, the difference of second moment between numerical results obtained by geometric grid using the fixed pivot technique and analytical results becomes more pronounced as shown in Figure 3.29(b). Interestingly, the prediction of the second moment by the cell average technique is very close to the analytical results.

The corresponding prediction for size distribution is plotted in Figure 3.30. The figure shows that the results are not accurate in the case of geometric grids. The scheme does not capture any details of the distribution. Since the original problem is fully discrete and the linear grids fit exactly to cover all the new particles which are formed during the process, this scheme can capture these details. As shown in the Figure 3.30, the numerical approximation by the linear grid clearly allows a correct tracking of the PSD in the entire range. As expected, however, the cell average technique gives less over-prediction in the number density distribution compares to that obtained by the fixed pivot technique. Once more, it has been demonstrated that the cell average technique is more accurate than the fixed pivot technique.

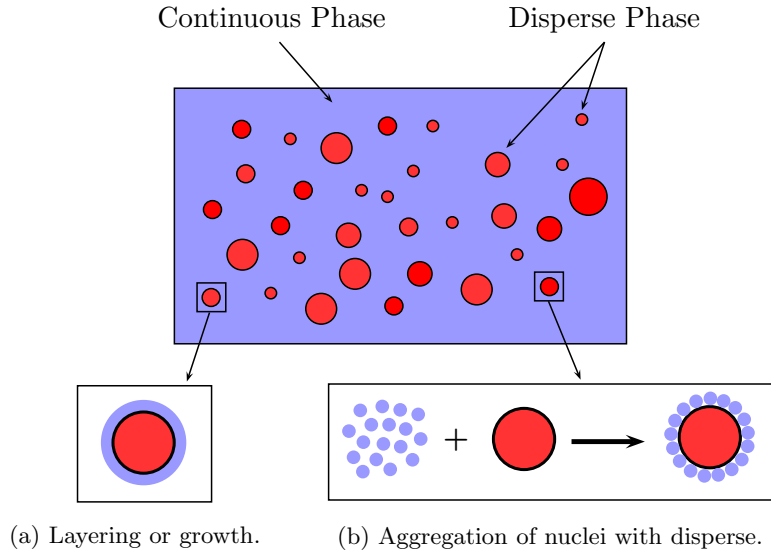


Figure 3.31: Interaction of disperse phase with continuous phase.

The only problem with linear grids is that they take more computational time. For the linear grid we have to solve a set of 1000 ODEs while in case of the geometric grids the set reduces to 11 ODEs. The situation may be dealt with by choosing the linear grid in the small size range where oscillations have been observed and the geometric in the large size range where the distribution decays exponentially. A similar grid criterion has been chosen by Kumar and Ramkrishna [57] in a problem of simultaneous breakup and aggregation in order to improve the accuracy of numerical predictions.

3.2.3 Pure Growth

As we have seen in the previous chapter that most of the methods for solving growth PBEs suffer from numerical diffusion. The finite volume schemes are good alternatives to solve growth PBEs, but they are usually consistent only with a single moment. Moreover, the extension of the existing finite volume schemes to arbitrary grids is extremely complicated. The moving mesh techniques are exceptionally good but they are difficult to combine with other processes. We have derived a two-moment consistent discrete formulation for the pure aggregation and pure breakage PBEs and we do expect the same here. Therefore the aim is to derive a scheme which is consistent at least with the first two moments, easy to combined with other the processes and can be applied on general grids.

In order to accomplish the goal, a completely new perspective to treat the growth process has been introduced. The growth of a particle can be treated as adherence of small nuclei on the particle surface. Traditionally, growth process is described as continuous transfer of mass from the continuous phase to the disperse phase, see Figure 3.31 (a). Here we consider this process as a combination of two processes. At first, the continuous phase transforms into small nuclei. Then, these nuclei aggregate discretely with the disperse phase. This is shown in Figure 3.31 (b). In this way, the numerical treatment of the growth process becomes easier.

Thus, the process can be modeled as aggregation of existing particles with the imaginary nuclei. The aggregation rate will of course be directly proportional to the growth rate of particles. Like the aggregation population balance equation, the mathematical model of the growth process then take the following form

$$\frac{\partial n(t, x)}{\partial t} = \beta(x - x_0, x_0)n(x - x_0)n(x_0) - \beta(x, x_0)n(x)n(x_0). \quad (3.85)$$

Here $x_0 > 0$ is the size of the nuclei. In practice we assume that this is a small value. The first term represents the birth at x due to aggregation of nuclei of size x_0 with the particles of size $x - x_0$. Similarly the second term describes the death of particles at x due to aggregation of particles of size x with the nuclei of size x_0 .

Unlike the conventional aggregation population balance equation, the equation (3.85) does not contain any integral in the birth and death terms because we have fixed the size of the nuclei and therefore a single possible event only is responsible to change the particles at x . Here we assume that the mass $m_0 (= x_0 n(x_0))$ of the nuclei has a nonzero limit, i.e. $m_0 > 0$ for $x_0 \rightarrow 0$. In the limit $x_0 \rightarrow 0$ this equation leads to the classical form of growth PBE. Let us consider the equation (3.85) in the form

$$\frac{\partial n(t, x)}{\partial t} = -x_0 n(x_0) \left(\frac{\beta(x, x_0)n(x) - \beta(x - x_0, x_0)n(x - x_0)}{x_0} \right), \quad (3.86)$$

and take the limit $x_0 \rightarrow 0$. This gives

$$\begin{aligned} \frac{\partial n(t, x)}{\partial t} &= -m_0 \frac{\partial}{\partial x} (\beta(x, x_0)n(x)) \\ &= -\frac{\partial}{\partial x} (m_0 \beta(x, x_0)n(x)). \end{aligned} \quad (3.87)$$

If we compare this equation directly with the classical PBE for growth, we get the following relationship between the aggregation kernel β and the mass of the infinitesimally small nuclei

$$G(t, x) = m_0 \beta(x, x_0). \quad (3.88)$$

Now the cell average formulation can easily be derived for the equation (3.85). The numerical discretization of this different form of the classical growth PBE will then become easy, consistent with two moments and versatile to applied on any type of grids. We shall now formulate the cell average technique for the PBE (3.85).

Numerical discretization

The cell average formulation is easy to derive for the new growth PBE. First we calculate the total birth and death rates in the cell i as

$$B_{\text{growth}, i} = \int_{x_{i-1/2}}^{x_{i+1/2}} \beta(x - x_0, x_0)n(x - x_0)n(x_0) dx, \quad (3.89)$$

and

$$D_{\text{growth}, i} = \int_{x_{i-1/2}}^{x_{i+1/2}} \beta(x, x_0)n(x)n(x_0) dx. \quad (3.90)$$

3.2. THE CELL AVERAGE TECHNIQUE

We make the assumption that x_0 is small enough so that $x_i + x_0 < x_{i+1/2}$ for all $i = 1, 2, \dots, I$. This assumption ensures that particles just get larger inside the cells and they do not leave their cells. Then substituting the number density $n(t, x) = \sum_{j=1}^I N_j \delta(x - x_j)$ into the above birth and death terms gives

$$\begin{aligned} B_{\text{growth},i} &= \int_{x_{i-1/2}}^{x_{i+1/2}} \beta(x - x_0, x_0) \sum_{j=1}^I N_j \delta(x - x_0 - x_j) n(x_0) dx \\ &= \beta(x_i, x_0) N_i n(x_0), \end{aligned} \quad (3.91)$$

and

$$\begin{aligned} D_{\text{growth},i} &= \int_{x_{i-1/2}}^{x_{i+1/2}} \beta(x, x_0) \sum_{j=1}^I N_j \delta(x - x_j) n(x_0) dx \\ &= \beta(x_i, x_0) N_i n(x_0). \end{aligned} \quad (3.92)$$

The discrete birth and death rate terms are the same in this case. Since we assume that the particles are concentrated only at the pivots, the mass of the particles in the cell will increase and the total number of particles will remain the same. Similarly the volume flux into the i th cell is calculated by

$$V_{\text{growth},i} = \beta(x_i, x_0) N_i n(x_0) (x_i + x_0). \quad (3.93)$$

In order to apply the cell average technique, the volume average will simply be computed by

$$\bar{v}_i = \frac{V_{\text{growth},i}}{B_{\text{growth},i}} = x_i + x_0. \quad (3.94)$$

Now the birth has to be modified according to the cell average strategy as

$$\begin{aligned} B_{\text{growth},i}^{\text{CA}} &= B_{\text{growth},i-1} \lambda_i^- (\bar{v}_{i-1}) H(\bar{v}_{i-1} - x_{i-1}) + B_{\text{growth},i} \lambda_i^- (\bar{v}_i) H(x_i - \bar{v}_i) \\ &\quad + B_{\text{growth},i} \lambda_i^+ (\bar{v}_i) H(\bar{v}_i - x_i) + B_{\text{growth},i+1} \lambda_i^+ (\bar{v}_{i+1}) H(x_{i+1} - \bar{v}_{i+1}). \end{aligned} \quad (3.95)$$

Since $\bar{v}_i \geq x_i$, the modified birth term can be simplified further

$$B_{\text{growth},i}^{\text{CA}} = B_{\text{growth},i-1} \lambda_i^- (\bar{v}_{i-1}) + B_{\text{growth},i} \lambda_i^+ (\bar{v}_i). \quad (3.96)$$

The final formulation of rate of change of number after substituting the expressions of λ and $B_{\text{growth},i}$ in equation (3.96) takes the following form

$$\begin{aligned} \frac{dN_i}{dt} &= \beta(x_{i-1}, x_0) N_{i-1} n(x_0) \left(\frac{\bar{v}_{i-1} - x_{i-1}}{x_i - x_{i-1}} \right) \\ &\quad + \beta(x_i, x_0) N_i n(x_0) \left(\frac{x_{i+1} - \bar{v}_i}{x_{i+1} - x_i} \right) - \beta(x_i, x_0) N_i n(x_0). \end{aligned} \quad (3.97)$$

The aggregation kernel is given by the relationship given in equation (3.88). The parameter m_0 in equation (3.88) can be adjusted equal to 1 by fixing a small value of the size of nuclei x_0 and choosing $n(x_0) = 1/x_0$. Consequently, the relationship in equation (3.88) changes to $G(t, x) = \beta(x, x_0)$.

The formulation (3.97) can also be rewritten as

$$\frac{dN_i}{dt} = \beta(x_{i-1}, x_0)N_{i-1}n(x_0) \left(\frac{\bar{v}_{i-1} - x_{i-1}}{x_i - x_{i-1}} \right) + \beta(x_i, x_0)N_in(x_0) \left(\frac{x_i - \bar{v}_i}{x_{i+1} - x_i} \right). \quad (3.98)$$

Substituting the value of average volume from equation (3.94), it further simplifies to

$$\frac{dN_i}{dt} = \beta(x_{i-1}, x_0)N_{i-1}n(x_0)x_0 \left(\frac{1}{x_i - x_{i-1}} \right) - \beta(x_i, x_0)N_in(x_0)x_0 \left(\frac{1}{x_{i+1} - x_i} \right). \quad (3.99)$$

Using the definition of growth rate G , we obtain the following two point formula

$$\frac{dN_i}{dt} = G(x_{i-1})\frac{N_{i-1}}{x_i - x_{i-1}} - G(x_i)\frac{N_i}{x_{i+1} - x_i}. \quad (3.100)$$

This formula looks similar to the first order upwind discretization discussed in Chapter 2. The discretization (3.100) and the first order upwind discretization are exactly the same for the case of equidistant grids and a constant growth rate. This discretization is always consistent with the first two moments independently of type of grids used in the computation. On the other hand the first order upwind discretization loses the first moment consistency while applied on non-homogeneous grids or with a non-constant growth rate. For a constant growth rate $G(x) = G_0$ and equidistant grids the formulation (3.100) reduces to the upwind discretization in the following form

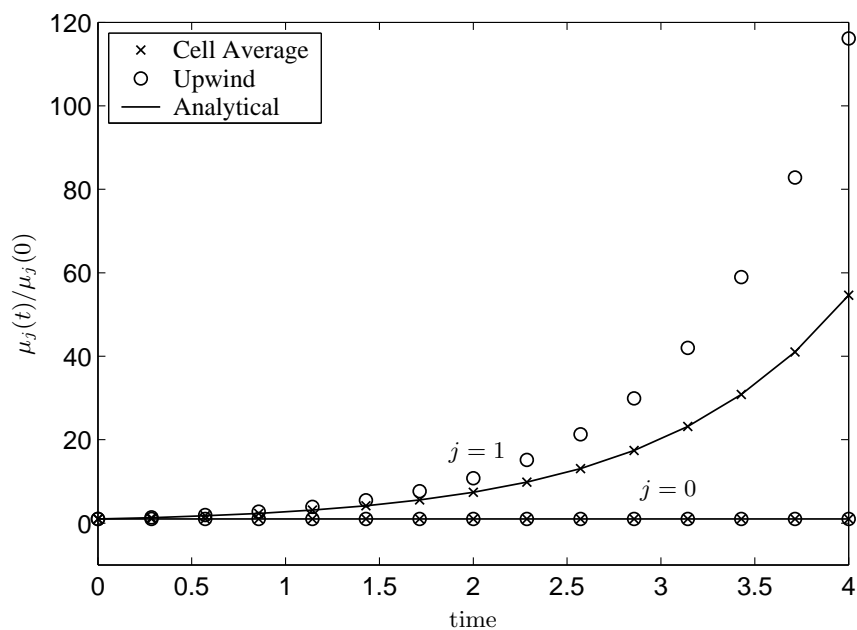
$$\frac{dN_i}{dt} = \frac{G_0}{\Delta x} (N_{i-1} - N_i), \quad (3.101)$$

where Δx is the distance between the grids.

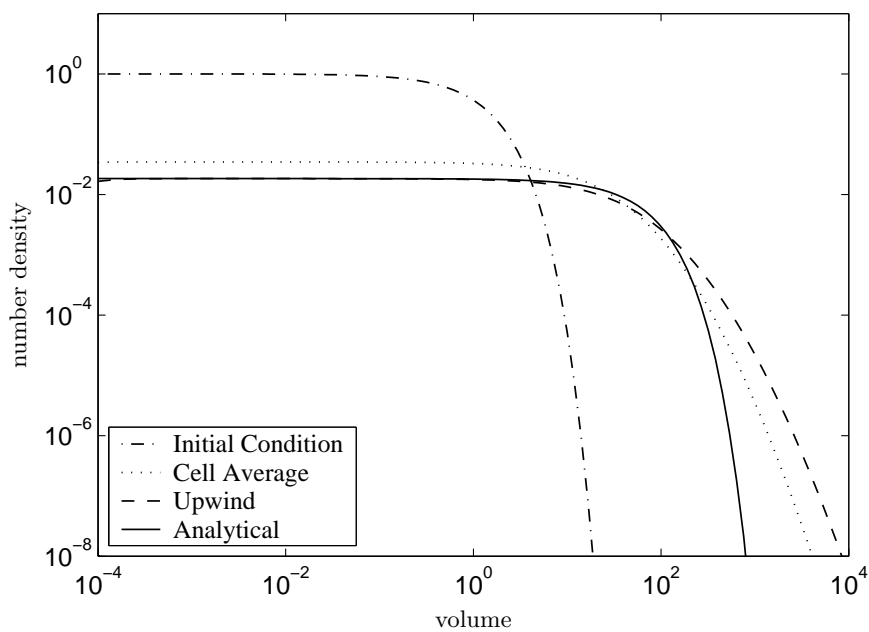
To conclude, the new form of PBE (3.85) treats the growth process as aggregation of existing particle with new small nuclei. The resulting numerical discretization of the growth process becomes very simple and consistent with first two moments. Additionally, it will be shown later that the new numerical formulation makes it easy to combine the growth process with other processes. Next we will observe that the new discretization of the growth is a little diffusive but it predicts the first two moments exactly without any computational difficulties like appearance of negative values or any other instabilities.

It should be noted that the objective of this work is not to provide a numerical scheme for pure growth problems but to propose a rather simple and general scheme which can be used to solve combined processes effectively. Several finite volume and finite element schemes can be found in the literature, also mentioned in the previous chapter, which may be used to solve the growth PBEs but all of them either have problems with consistency of moments or they are not easy to combine with other particulate processes. In the next section we will show that the coupling of the growth process with other particulate processes using the cell average technique becomes trivial and considerably better results for combined processes can be obtained without extra much computational effort. Nevertheless it is necessary first to check the accuracy of the derived scheme for some analytically solvable pure growth problems.

3.2. THE CELL AVERAGE TECHNIQUE

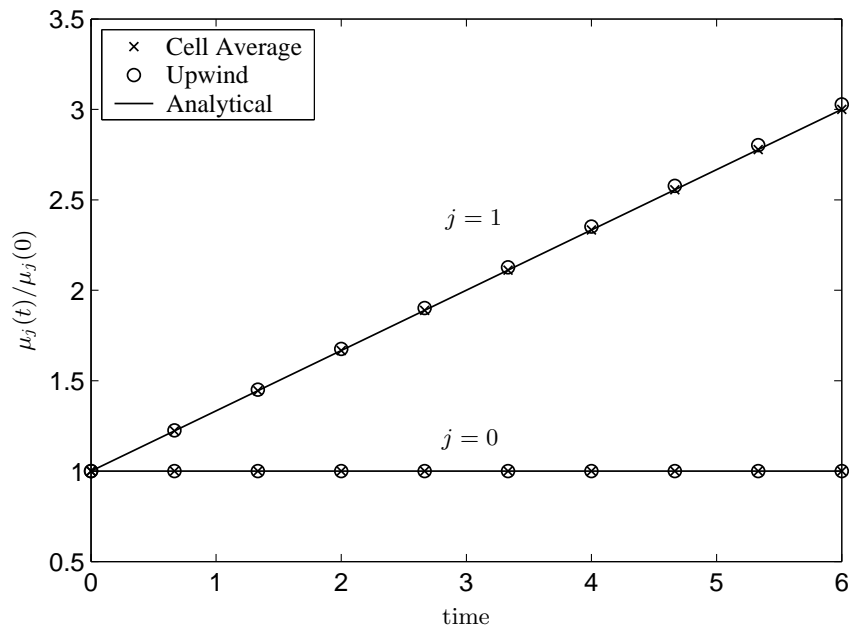


(a) Variation of the first two moments.

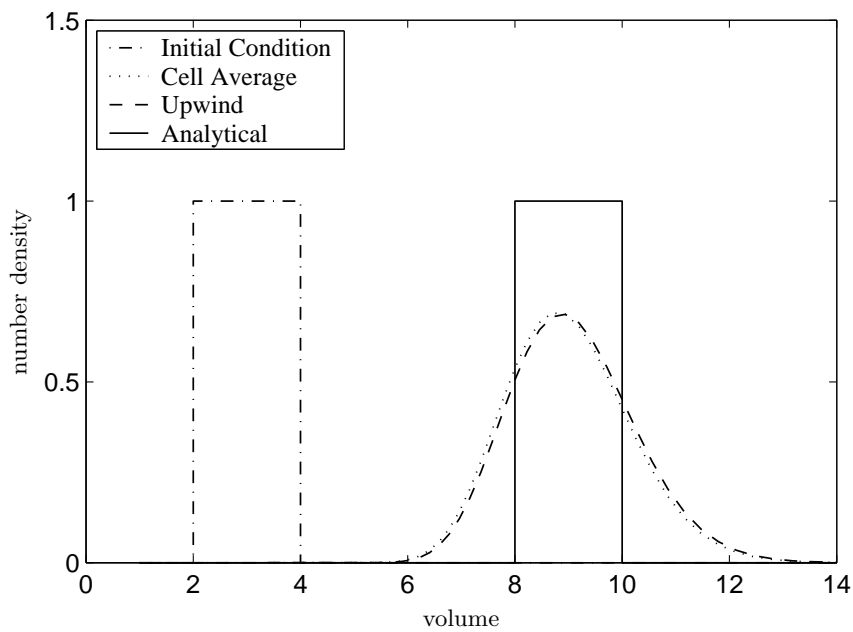


(b) Particle size distribution.

Figure 3.32: A comparison analytical and numerical results for pure growth using exponentially distributed initial particle size distribution and linear growth rate, grid points 130.



(a) Variation of the first two moments.



(b) Particle size distribution.

Figure 3.33: A comparison analytical and numerical results for pure growth using step function as initial particle size distribution and constant growth rate, grid points 95.

Numerical results

We have considered two test cases to access the ability of the scheme to handle pure growth problems. In the first test case we take exponentially distributed particle size distribution (3.69) with a linear growth rate $G(x) = x$. The second test case considers the step function as initial condition with a constant growth rate. The analytical results for the number density and different moments for a initial condition $n_0(x)$ are given in Appendix A.3. The volume domain is discretized geometrically into small cells by the rule $x_{i+1/2} = 2^{1/q}x_{i-1/2}$. The parameter q adjusts the coarseness of the mesh.

Figure 3.32(a) shows numerical results for the first two moments calculated using the cell average technique and the first order upwind discretization. Since the cell average formulation is consistent with the first two moments, the prediction of the first two moments using the cell average technique is exact. On the other hand the upwind discretization shows a diverging behavior of the first moment. The prediction of the zeroth moment by the upwind discretization is excellent due to automatic conserving property of the upwind discretization. The corresponding particle size distribution at the final time is plotted in Figure 3.33(b). The prediction of the particle size distribution by the two techniques is quite similar. A small over-prediction of the results by the cell average technique has been observed at the small as well as at large volumes. The number density at the small volumes by the upwind discretization is pretty good whereas it is consistently over-predicting at the large volumes.

The numerical results for the second test case have been presented in Figure 3.33. For the constant growth rate numerical results obtained using both techniques are quite similar. Nevertheless, once more, the prediction of the first moment by the upwind discretization, shown in Figure 3.33(a), is slightly over-estimated. Whereby both the moments calculated using the cell average technique are exactly matching with the analytical results. Figure 3.33(b) shows that the numerical results for the particle size distribution are highly diffusive. It is due to the fact that we have chosen a discontinuous initial condition. Most of the numerical schemes smear out near discontinuities and higher gradients. Very fine grids near discontinuities are often required to capture the complete details of the distribution.

As we have seen that the numerical results of the particle size distribution for pure growth problems by the cell average technique as well as by the upwind discretization are not very accurate. A better accuracy may be obtained by making the formulation consistent with the first three moments. Next we establish the cell average technique consistent with the first three moments and observe the computational difficulties with the formulation.

Consistency with the first three moments: Consistency with three moments may be achieved by assigning newborn particles to three nodes. The most appropriate choice could be the node of the cell particles belong to and two nodes of the adjoining cells. Consider that some newborn particles appear in i th cell at \bar{v}_i , see Figure 3.34. Now the objective is to assign these particles to the nodes x_{i-1}, x_i and x_{i+1} in such a way that the first three moments are exactly conserved. Assuming that fractions a_1, a_2 and a_3 are assigned to the nodes x_{i-1}, x_i and x_{i+1}

CHAPTER 3. NEW NUMERICAL METHODS: ONE-DIMENSIONAL

respectively. Then these fractions must satisfy the following equalities

$$\begin{aligned} a_1 + a_2 + a_3 &= 1, \\ x_{i-1}a_1 + x_i a_2 + x_{i+1}a_3 &= \bar{v}_i, \\ x_{i-1}^2 a_1 + x_i^2 a_2 + x_{i+1}^2 a_3 &= \bar{v}_i^2. \end{aligned}$$

The above set of equations results in

$$a_1 = \frac{(\bar{v}_i - x_i)(\bar{v}_i - x_{i+1})}{(x_{i-1} - x_i)(x_{i-1} - x_{i+1})}, \quad (3.102)$$

$$a_2 = \frac{(\bar{v}_i - x_{i+1})(\bar{v}_i - x_{i-1})}{(x_i - x_{i+1})(x_i - x_{i-1})}, \quad (3.103)$$

and

$$a_3 = \frac{(\bar{v}_i - x_{i-1})(\bar{v}_i - x_i)}{(x_{i+1} - x_{i-1})(x_{i+1} - x_i)}. \quad (3.104)$$

These fractions seem unrealistic since either a_1 is negative in case of $\bar{v}_i > x_i$ or a_3 is negative for $\bar{v}_i < x_i$. In the pure growth case, the volume average \bar{v}_i is always bigger than x_i , i.e. $\bar{v}_i > x_i$ and therefore $a_1 < 0$. Let us first obtain the formulation for the rate of change of numbers in a cell with these fractions. Similar to the previous case of two moment consistency we obtain

$$\begin{aligned} \frac{dN_i}{dt} &= \frac{(\bar{v}_{i-1} - x_{i-2})(\bar{v}_{i-1} - x_{i-1})}{(x_i - x_{i-2})(x_i - x_{i-1})} B_{\text{growth},i-1} + \frac{(\bar{v}_i - x_{i+1})(\bar{v}_i - x_{i-1})}{(x_i - x_{i+1})(x_i - x_{i-1})} B_{\text{growth},i} \\ &\quad + \frac{(\bar{v}_{i+1} - x_{i+1})(\bar{v}_{i+1} - x_{i+2})}{(x_i - x_{i+1})(x_i - x_{i+2})} B_{\text{growth},i+1} - \beta(x_i, x_0) N_i n(x_0). \end{aligned} \quad (3.105)$$

All parameters appearing the above formulation have already been defined earlier. The above-mentioned three-point method is unstable due to the appearance of negative values of particle numbers. It is due to the fact that the reassignment process makes the formulation consistent with respect to the first three moments by removing some particles from one node and assigning them to others. In other words, the assignment process takes negative growth at some nodes and that, in some situations, is responsible for appearance of negative values. Setting negative N_i to zero causes an increase of total particle number and other higher moments as well as fluctuations in particle size distribution. We have tested the new formulation for the same problem considered in Figure 3.33. As can be seen in Figure 3.35(a) that the prediction of the first two moments is very poor by the three moments consistent strategy. Figure 3.35(b) shows the fluctuations of the particle size distribution. As mentioned before, it should be pointed out that these fluctuations and negative values are not produced by the ODE solver but the formulation itself produces negative values which causes instability in the solution.

The positivity in the formulation can be preserved by using a combination of the two strategies, consistency with two and three moments, to distribute the particles. This may be accomplished in different ways. We have used a simple criterion to switch between the two strategies. A particle birth distribution from i th cell using a three moment consistent strategy together with possible birth at $(i - 1)$ node is indicated in Figure 3.36. It is shown in the figure that the three

3.2. THE CELL AVERAGE TECHNIQUE

- Cell representative (node)
- Position of newborn particles

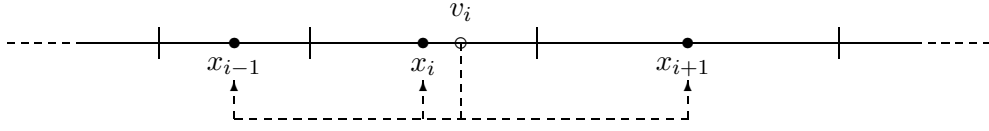


Figure 3.34: Assignment of particles for the consistency of the first three moments.

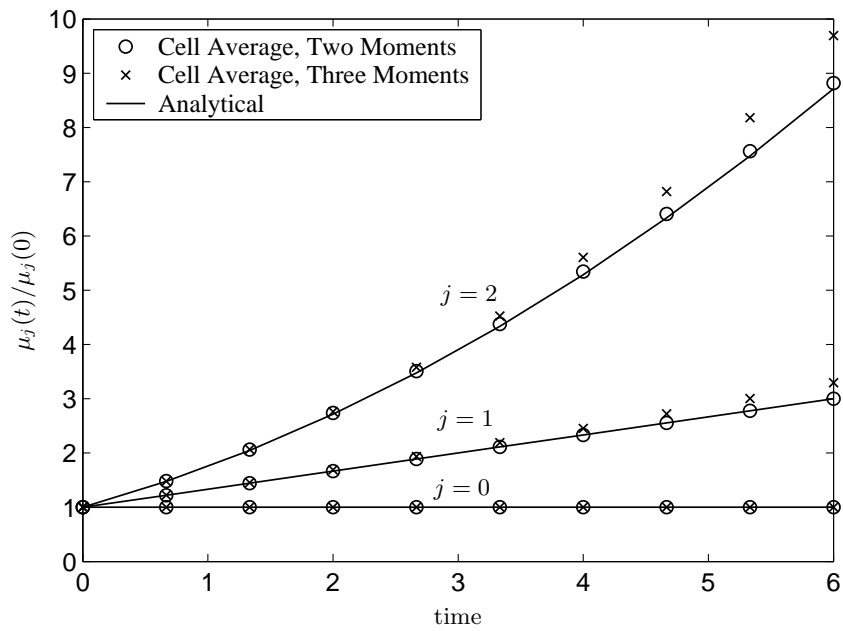
moment consistent strategy of particles in the i th cell results in a negative birth rate at the $(i - 1)$ node. If the total positive birth at the $(i - 1)$ th node which is contributed from the $(i - 1)$ th cell and $(i - 2)$ th cell is not large enough then this redistribution strategy results in negative values of number density at $(i - 1)$ th node. A simple remedy to avoid negative values is to redistribute particles using a two moment consistent strategy. We summarize the schemes used in this work in following steps.

1. Choose a small number ϵ ($\approx 10^{-3}$).
2. Calculate the birth and death rates $B_{\text{growth},i}$ and $D_{\text{growth},i}$ for all i .
3. If N_{i-1} and N_{i-2} are smaller than ϵ , reassigned birth $B_{\text{growth},i}$ by two moment consistent strategy otherwise by three moment consistent strategy. Do it for all i to get net birth at each node, i.e. $B_{\text{growth},i}^{\text{mod}}$.
4. Compute $\frac{dN_i}{dt} = B_{\text{growth},i}^{\text{mod}} - D_{\text{growth},i}$.

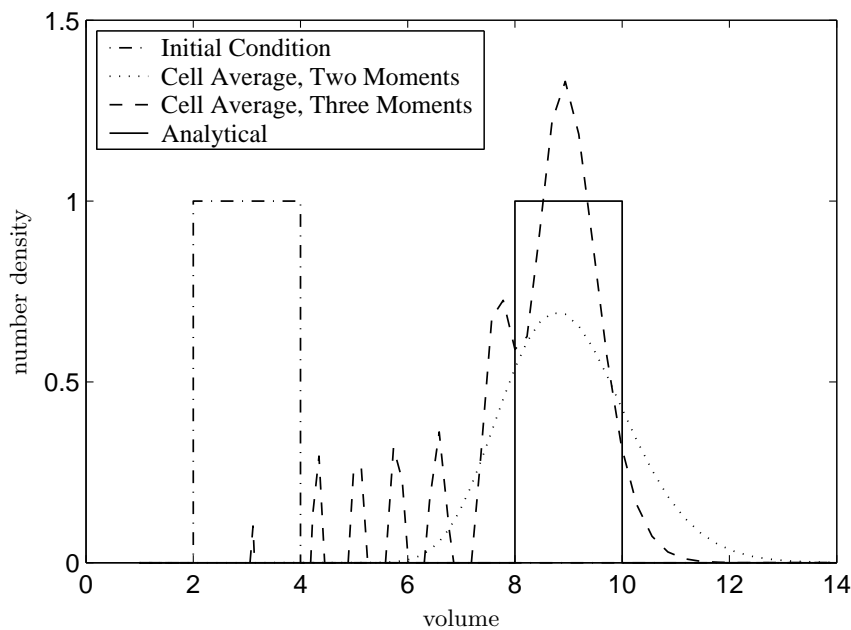
We have used the above switching strategy in our computations. The value of the parameter ϵ in different problems can be adjusted accordingly to avoid negative values. It should be pointed out that this switching criterion is by no means the best possible. The approach used here is one of the simplest switching criteria. A more sophisticated criterion can be adapted to achieve the positivity of the solution.

We now present some results to illustrate the above concept of switching the two strategies of consistency. We applied the above algorithm on the same test case as before. The value of the parameter ϵ is taken to be 10^{-3} . The results have been plotted in Figure 3.37. These figures reveal that using a simple criterion of combination of two distribution mechanisms has improved the accuracy considerably without any extra efforts. The prediction of the first three moments by the new strategy is extremely accurate while a small over-prediction in the second moment by the two moment consistent formulation is observed. The numerical results for the particle size distribution by the new formulation are considerably better than two moment consistent formulation. The prediction of the particle size distribution is highly accurate without any fluctuations or appearance of negative values.

We can conclude that the strategy to use two formulations comes out as a good alternative to solve a growth population balance equation. As we have seen in the previous chapter that all



(a) Variation of the first three moments.



(b) Particle size distribution.

Figure 3.35: A comparison analytical and numerical results for pure growth using step function as initial particle size distribution and constant growth rate, grid points 95.

3.2. THE CELL AVERAGE TECHNIQUE

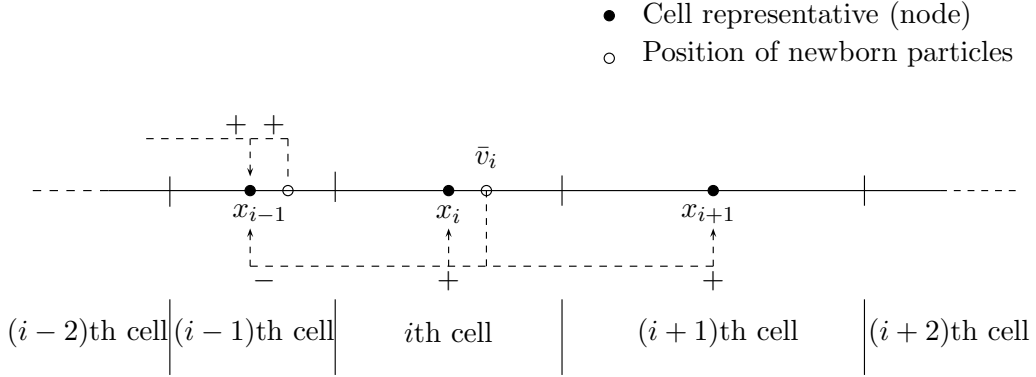


Figure 3.36: Reasons for negative values in a three moment consistent formulation.

numerical schemes which are theoretically consistent with respect to the first three moments produce much more fluctuations as well as negative values and consequently loose consistency with respect to all moments. Moreover, the fundamental concept of the scheme, the coupling with other processes, is an extra advantage of the scheme. In a following section we will demonstrate the coupling efficiency and accuracy of the numerical results for growth combined with other processes. Now we proceed to apply the cell average technique for different combinations of processes where analytical results are easily available.

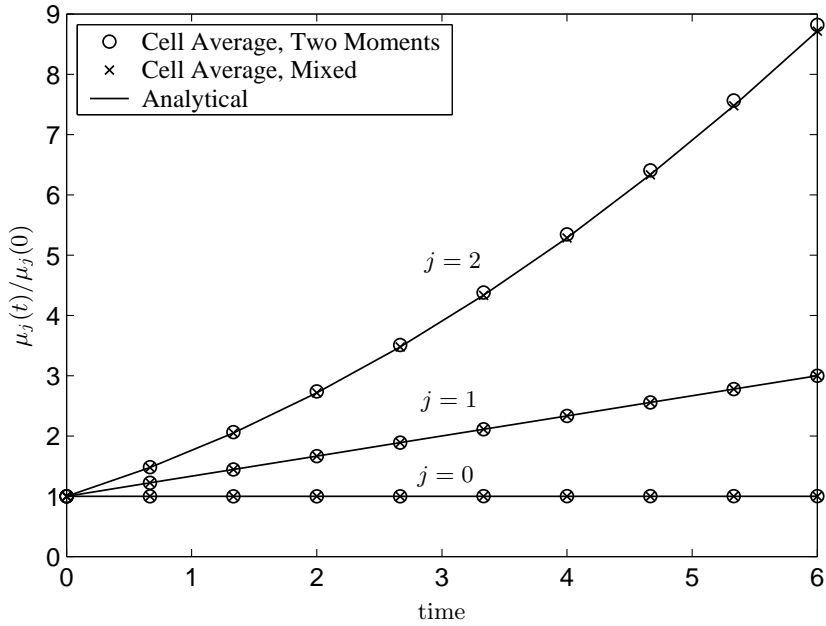
3.2.4 Simultaneous Aggregation and Breakage

This subsection is devoted to the numerical treatment of combined aggregation and breakage processes. When both aggregation and breakage processes take place together, the discrete birth and death rates for combined processes in most of the numerical schemes are generally considered by algebraically summing the individual birth and death rates. In other words, conventionally the easiest way to couple the two processes is to just add the corresponding discretizations in the following way.

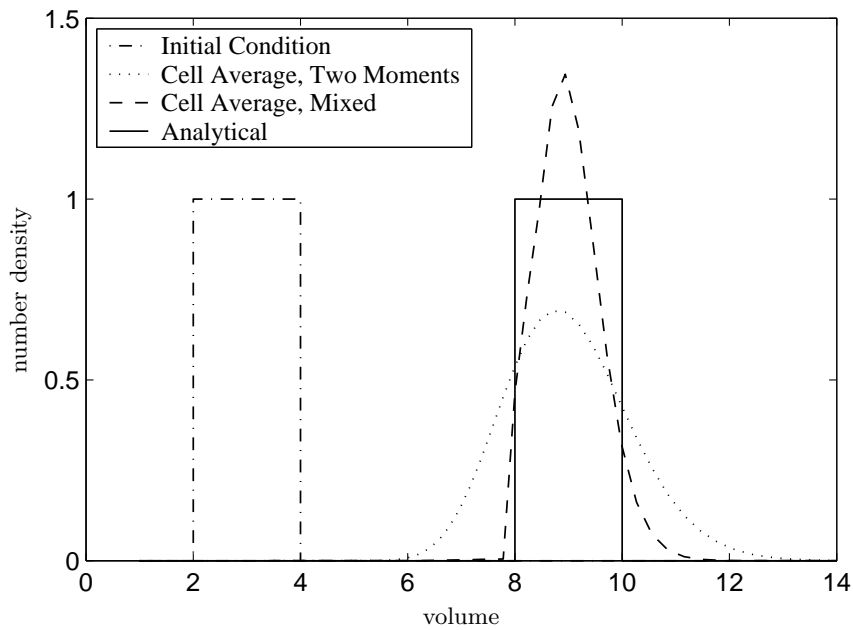
$$\frac{dN_i}{dt} = B_{\text{agg},i}^{\text{CA}} + B_{\text{break},i}^{\text{CA}} - D_{\text{agg},i} - D_{\text{break},i}, \quad (3.106)$$

where the abbreviations CA, agg, and break stands for cell average, aggregation and breakage respectively. In this formulation birth and death rates have been added to get a formulation for combined processes.

The preceding formulation is of course consistent with the first two moments if this holds for breakage and aggregation separately. In order to couple the two discretizations more efficiently we take advantage of the cell average technique. The accuracy can further be improved by using the idea of cell average for the combined problem simply by considering the total birth and death rates from combined processes. Thereby, we shall treat both processes together in a similar way as we have treated the individual processes. First we collect all the newborn particles in a cell independently of the events that make them appear in the cell. In our case here the events are aggregation and breakage processes. Then we take the volume average of all newborn particles in the cell. The remaining steps are the same we used for the individual processes of aggregation



(a) Variation of the first three moments.



(b) Particle size distribution.

Figure 3.37: A comparison analytical and numerical results for pure growth using step function as initial particle size distribution and constant growth rate, grid points 95.

3.2. THE CELL AVERAGE TECHNIQUE

or breakage. Mathematically, we construct the discrete formulation for the coupled problem as

$$\frac{dN_i}{dt} = B_{\text{agg+break},i}^{\text{CA}} - D_{\text{agg+break},i}. \quad (3.107)$$

Here the terms $B_{\text{agg+break},i}^{\text{CA}}$ and $D_{\text{agg+break},i}$ represent the birth and death rates of particles in the cell i due to aggregation and breakage respectively. The total birth and death rates in i th cell is given by

$$B_{\text{agg+break},i} = B_{\text{agg},i} + B_{\text{break},i}, \quad (3.108)$$

and

$$D_{\text{agg+break},i} = D_{\text{agg},i} + D_{\text{break},i}. \quad (3.109)$$

Now the birth rate $B_{\text{agg+break},i}$ has to be modified to make the formulation consistent with respect to the first two moments. Thus, the modified birth term or the cell average birth term will be then computed as

$$\begin{aligned} B_{\text{agg+break},i}^{\text{CA}} = & B_{\text{agg+break},i-1} \lambda_i^- (\bar{v}_{i-1}) H(\bar{v}_{i-1} - x_{i-1}) + B_{\text{agg+break},i} \lambda_i^- (\bar{v}_i) H(x_i - \bar{v}_i) \\ & + B_{\text{agg+break},i} \lambda_i^+ (\bar{v}_i) H(\bar{v}_i - x_i) + B_{\text{agg+break},i+1} \lambda_i^+ (\bar{v}_{i+1}) H(x_{i+1} - \bar{v}_{i+1}). \end{aligned} \quad (3.110)$$

The truly new ingredient is that the average value \bar{v}_i will be computed as

$$\bar{v}_i = \frac{V_{\text{agg},i} + V_{\text{break},i}}{B_{\text{agg},i} + B_{\text{break},i}}. \quad (3.111)$$

The terms $B_{\text{agg},i}$, $B_{\text{break},i}$, $D_{\text{agg},i}$, $D_{\text{break},i}$, $V_{\text{agg},i}$, $V_{\text{break},i}$ and also the λ_i are the same as given in the previous sections. Next we will test the coupled formulation on two test problems. The modified birth term (3.110) and the death term (3.109) can be substituted in equation (3.107) to get the final formulation. We will see that the new way of coupling is not only more accurate but also computationally less expensive. This is evident since in the latter case we are distributing particles once while in the conventional approach particles are distributed twice; once due to aggregation and then due to breakage.

Numerical results

We compared the fixed pivot technique [57] and the cell average technique with analytically solvable problems proposed by Patil and Andrews [81]. Later these solutions were slightly simplified by Lage [61] to the form we use here. A list of analytical solutions used here has been included in Appendix A.4. They considered a special case of simultaneous aggregation and breakage where the number of particles stays constant with a uniform binary breakage $b(x, y) = 2/y$, linear selection function $S(x) = S_0 x$ and constant aggregation kernel $\beta(x, y) = \beta_0$. They used the following two types of initial conditions

$$n(0, x) = N_0 \left[2 \frac{N_0}{x_0} \right]^2 x \exp \left(-2 \frac{N_0}{x_0} x \right), \quad (3.112)$$

and

$$n(0, x) = N_0 \frac{N_0}{x_0} \exp \left(-\frac{N_0}{x_0} x \right). \quad (3.113)$$

Note that next to conservation of mass these problems have the special properties that the processes of aggregation and breakage balance to conserve total number also. The data (3.113) are a steady state solution.

We have discretized the volume domain geometrically using the rule $x_{i+1/2} = 2x_{i-1/2}$. Figures 3.38(a) and 3.38(b) show a comparison of the particle size distributions for the initial condition (3.112) at time $t = 0.4$ and $t = 6$ respectively. As can be seen from the figures, the cell average technique is able to approximate the PSD to a very high degree of accuracy. On the other hand a small over-prediction is observed at the smaller volumes by the fixed pivot technique.

Let us now consider the steady state data (3.113). The results for this case are presented in Figure 3.39. The prediction by the cell average technique is again excellent in this case while a similar over-prediction by the fixed pivot technique can be observed. Actually this over-prediction grows with time, i.e. the fixed pivot technique is not stable with respect to steady states. Furthermore, the same numerical results for both the initial conditions at the final time have been plotted on a log-log scale in Figure 3.40. Once again we can see here that the prediction of PSD by the cell average technique is superior to the prediction with the fixed pivot technique.

We shall now demonstrate the difference between conventional coupling (3.106) of the cell average technique applied separately to aggregation and breakage and the new cell average coupling (3.107). Note that we are not considering the fixed pivot technique in this comparison. Since the numerical results are indistinguishable from the analytical results for the steady state initial condition (3.113), we have only compared the numerical results for the unsteady initial condition (3.112). The numerical results have been plotted in Figure 3.41. The L_1 error between the numerical and analytical results of PSD has also been reported in the figure. Due to the simplicity of the problem, uniform binary breakage, the difference between the two types of coupling is not so significant. Nevertheless, the cell average type coupling (3.107) gives better results which can be observed at the steep part of the PSD as well as from the L_1 error. Another difference has been observed in computational time. The cell average type coupling (3.107) takes about 38 seconds CPU time while conventional coupling (3.106) takes 52 seconds CPU time on a Pentium-4 machine with 1.5 GHz and 512 MB RAM.

To summarize, the cell average technique provides highly accurate results already on a very coarse grid. The accuracy can of course be further increased by making the grid finer. The cell average technique with the new coupling makes the technique even more useful for combined aggregation and breakage by being not only more accurate but also computationally less expensive.

3.2.5 Simultaneous Aggregation and Nucleation

As in the previous section we have just considered that the particles are appearing in cells independently of the event that make them appear and presented a cell average formulation for combined aggregation and breakage processes. A similar approach has to be applied here for the case of simultaneous aggregation and nucleation. The process of nucleation may be introduced into the modeling in two ways. A common approach is via a boundary condition at particle

3.2. THE CELL AVERAGE TECHNIQUE

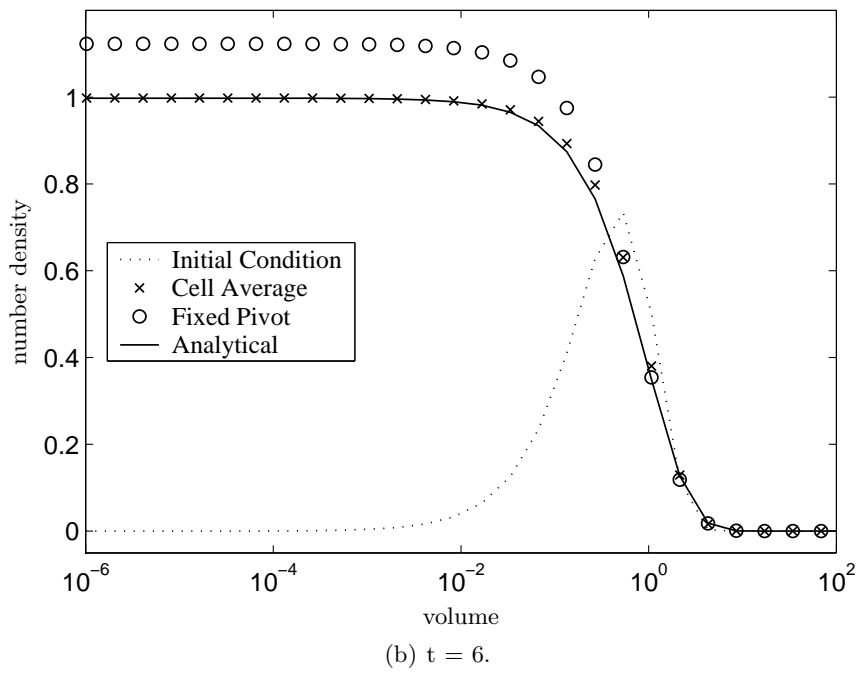
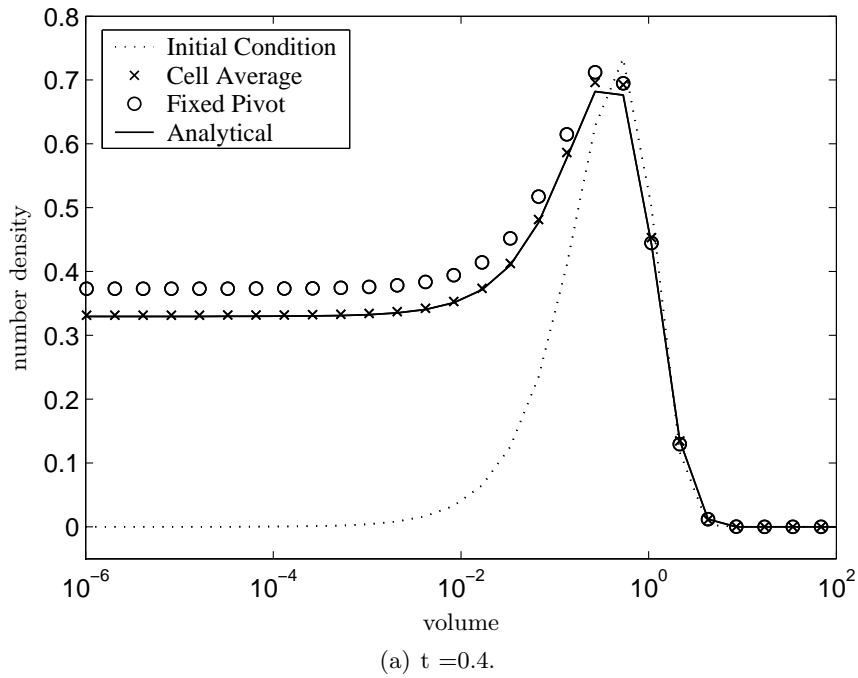
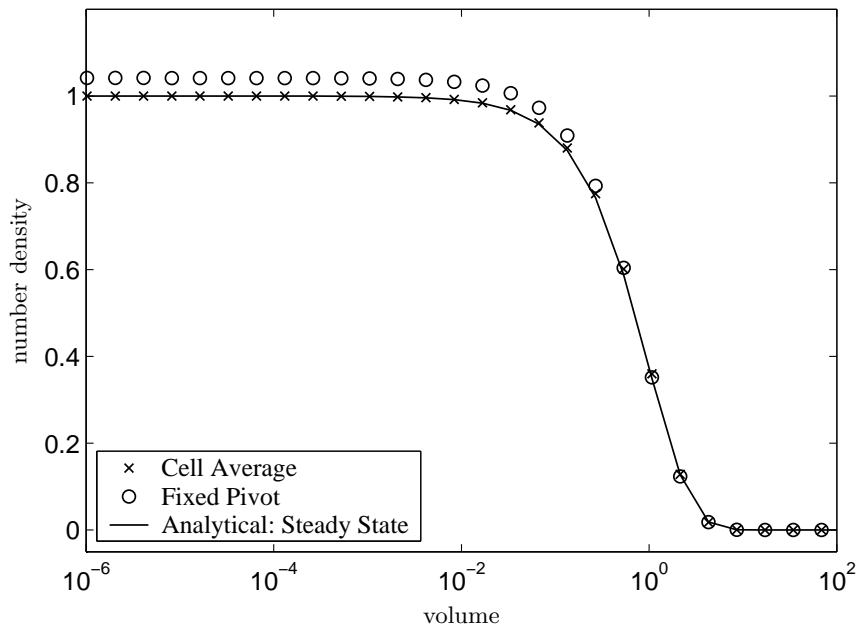
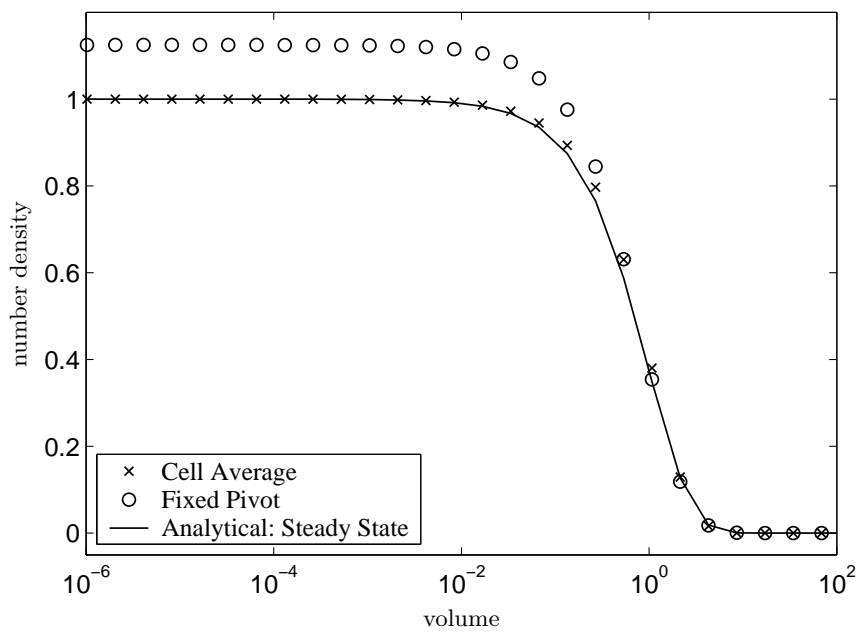


Figure 3.38: A comparison of particle size distributions for binary breakage and aggregation with initial condition (3.112), grid points 38.

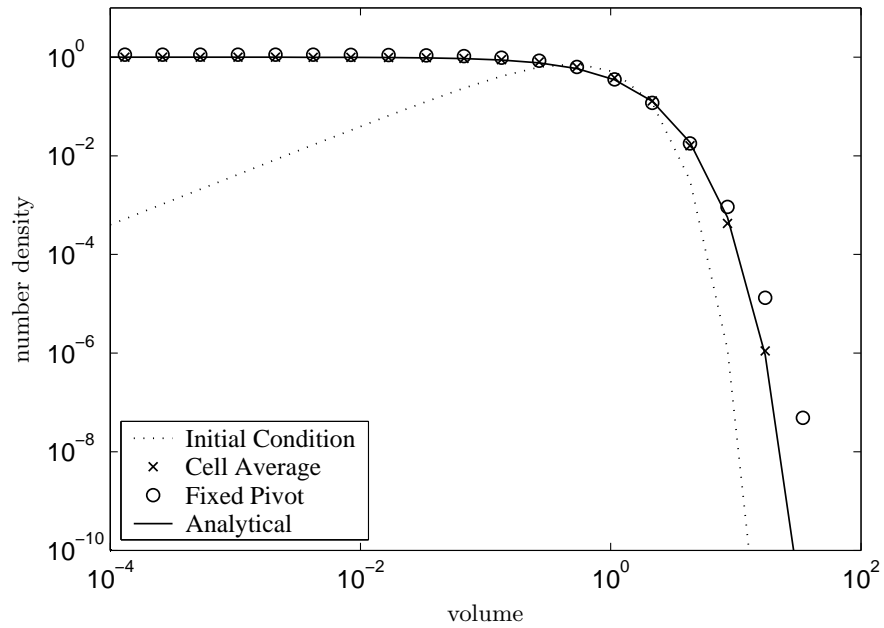


(a) $t = 0.4$.

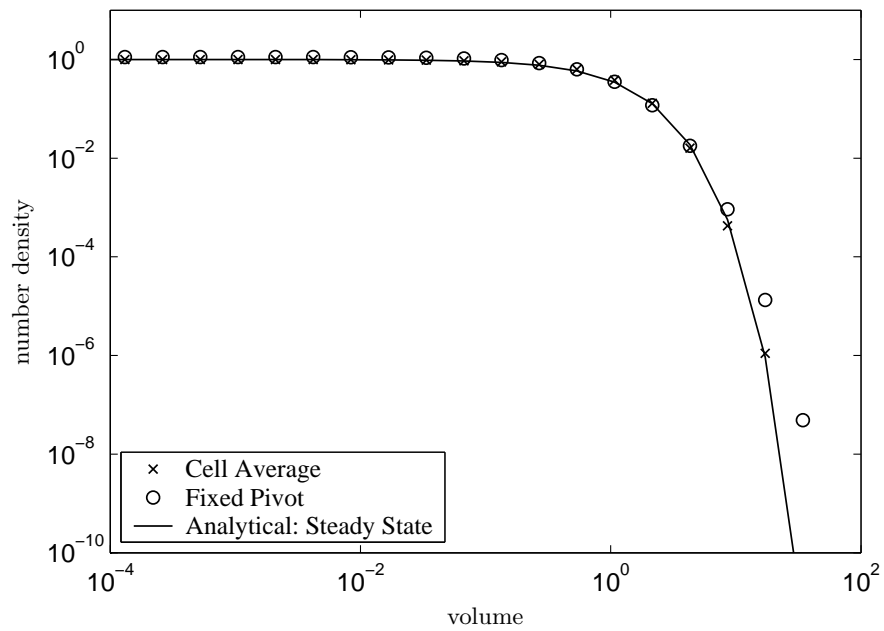


(b) $t = 6$.

Figure 3.39: A comparison of particle size distributions for binary breakage and aggregation with initial condition (3.113), grid points 38.



(a) Initial condition (3.112).



(b) Initial condition (3.113).

Figure 3.40: A comparison of particle size distributions at $t = 6$ for binary breakage and aggregation plotted on log-log scale, grid points 38.

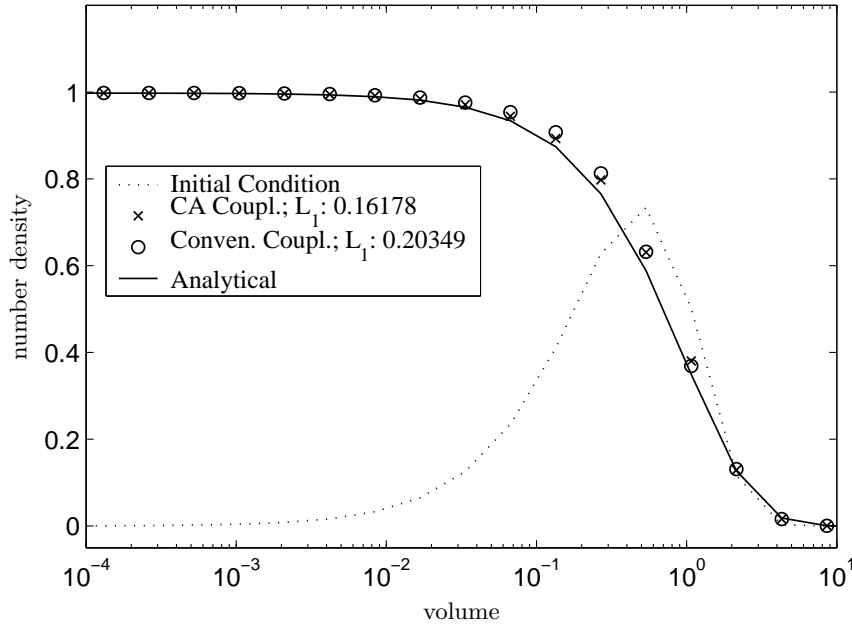


Figure 3.41: A comparison of particle size distributions for binary breakage and aggregation showing the difference between conventional coupling and cell average coupling, grid points 38.

size 0 if the nucleation is mono-disperse. Here we want to consider the alternative of a source located near particle size 0. In a continuum theory both are valid approaches.

Before we proceed to the final form of the cell average technique, we want to comment on the conventional coupling of these processes. Let us discuss the case of discretization of Kumar and Ramkrishna [59] for simultaneous aggregation and nucleation, they considered

$$\frac{dN_i}{dt} = \text{discretization due to aggregation} + \int_{x_{i-1/2}}^{x_{i+1/2}} B_{\text{nuc}}(t, x) dx. \quad (3.114)$$

Note that in above formulation we may gain or loose mass if the nucleation does not take place exactly at the representative sizes x_i . It is possible that the particles could again be distributed to neighboring cells for the consistency of moments in the fixed pivot technique. We are not interested here to explore more about this issue. We now present how to deal with these problems with the cell average techniques efficiently. Similar to previous section, we wish to have the following discretization

$$\frac{dN_i}{dt} = B_{\text{agg+nuc},i}^{\text{CA}} - D_{\text{agg},i}. \quad (3.115)$$

Since nucleation is the birth of the particles, there is no nucleation term to be considered in the death term. An analogous contribution to the death term would come if we considered harvesting of certain particle sizes. The numerical treatment would be analogous. Now the

birth by nucleation and aggregation can be described as follows

$$\begin{aligned}
 B_{\text{agg+nuc},i}^{\text{CA}} = & B_{\text{agg+nuc},i-1} \lambda_i^- (\bar{v}_{i-1}) H(\bar{v}_{i-1} - x_{i-1}) + B_{\text{agg+nuc},i} \lambda_i^- (\bar{v}_i) H(x_i - \bar{v}_i) \\
 & + B_{\text{agg+nuc},i} \lambda_i^+ (\bar{v}_i) H(\bar{v}_i - x_i) + B_{\text{agg+nuc},i+1} \lambda_i^+ (\bar{v}_{i+1}) H(x_{i+1} - \bar{v}_{i+1}). \quad (3.116)
 \end{aligned}$$

where

$$B_{\text{agg+nuc},i} = B_{\text{agg},i} + \int_{x_{i-1/2}}^{x_{i+1/2}} B_{\text{nuc}}(t, x) dx. \quad (3.117)$$

The average values are computed as

$$\bar{v}_i = \frac{V_{\text{agg},i} + \int_{x_{i-1/2}}^{x_{i+1/2}} x B_{\text{nuc}}(t, x) dx}{B_{\text{agg},i} + \int_{x_{i-1/2}}^{x_{i+1/2}} B_{\text{nuc}}(t, x) dx}. \quad (3.118)$$

All other notations appearing in the formulation are already defined in previous sections. So treating nucleation and aggregation as particle birth in cells in a similar fashion we have gained the consistency with the first two moments. It should be noted that if the nucleation is mono-disperse, usually the appearance of smallest particle, and the smallest representative is chosen such that it matches exactly with the size of the the mono-disperse particles, then the above formulation can be rewritten as

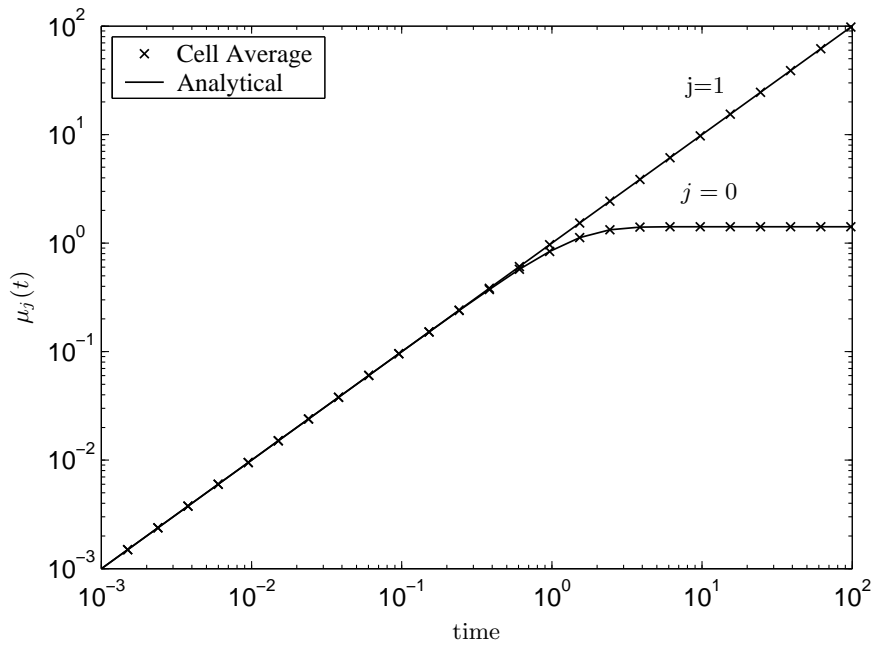
$$\begin{aligned}
 \frac{dN_1}{dt} &= B_{\text{agg},1}^{\text{CA}} - D_{\text{agg},1} + B_{\text{nuc}}(t, x_1), \\
 \text{and} & \\
 \frac{dN_i}{dt} &= B_{\text{agg},i}^{\text{CA}} - D_{\text{agg},i}, \quad i = 2, 3, \dots, I. \quad (3.119)
 \end{aligned}$$

The formulation (3.115) may be used for a general poly-disperse nucleation and the formulation (3.119), a particular case of (3.115), is used for mono-disperse nucleation.

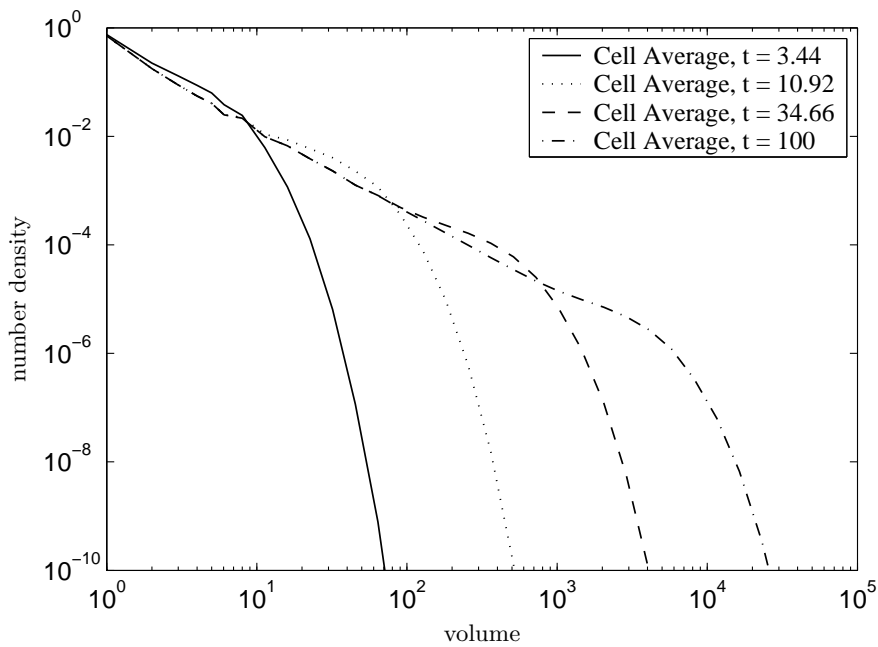
Numerical results

We have tested the formulation for simultaneous nucleation and aggregation. A simple case of zero initial population with constant aggregation kernel and mono-disperse nucleation is considered. Such systems with zero initial population usually lead to oscillations in the particle size distribution. But we will see by numerical results that the cell average technique is completely free of oscillations. Analytical solutions for the first two moments of this problem reported by Alexopoulos and Kiparissides [4] have been included in Appendix A.5. The formulation (3.119) is used for the computation in this particular case.

In Figure 3.42(a), a comparison is made between the exact solutions of the first two moments and the numerical solution calculated using the cell average formulation (3.119) for the case $\beta_0 = 1$ and $B_{\text{nuc}}(t, x_1) = 1$. The volume domain is discretized geometrically into 30 cells starting with 10^{-6} . As can be seen from the figure that the numerical results are in excellent agreement with the analytical results. It should be mentioned that after a certain time, the total number of particles in the system is invariant. A dynamic equilibrium with respect to the total number has been reached at that time. In other words the particle nucleation rate



(a) Moments.



(b) Particle size distribution.

Figure 3.42: Numerical results for simultaneous nucleation and aggregation, grid points 30.

becomes equal to the total particle aggregation rate. On the other hand, the total mass of the particles which is proportional to the first moment increases linearly with respect to the process time. Unfortunately an analytical solution for the complete PSD is not easily available, only numerical results at different times have been depicted in Figure 3.42(b). A quite complicated but systematic behavior of the results has been observed. Clearly the particle size distribution is free from oscillations.

3.2.6 Simultaneous Growth and Aggregation

This section is devoted to the numerical treatment of the simultaneous growth and aggregation processes. As we have seen that the cell average technique can be applied to solve a pure growth problem by the application of a different form of growth PBE. Similar to other combined processes, in this case we like to have the following form of the cell average formulation

$$\frac{dN_i}{dt} = B_{\text{agg+growth},i}^{\text{CA}} - D_{\text{agg+growth},i}. \quad (3.120)$$

Here the birth and death terms in above equation are given as

$$\begin{aligned} B_{\text{agg+growth},i}^{\text{CA}} = & B_{\text{agg+growth},i-1} \lambda_i^- (\bar{v}_{i-1}) H(\bar{v}_{i-1} - x_{i-1}) + B_{\text{agg+growth},i} \lambda_i^- (\bar{v}_i) H(x_i - \bar{v}_i) \\ & + B_{\text{agg+growth},i} \lambda_i^+ (\bar{v}_i) H(\bar{v}_i - x_i) + B_{\text{agg+growth},i+1} \lambda_i^+ (\bar{v}_{i+1}) H(x_{i+1} - \bar{v}_{i+1}), \end{aligned} \quad (3.121)$$

and

$$D_{\text{agg+growth},i} = D_{\text{agg},i} + D_{\text{growth},i}, \quad (3.122)$$

where

$$B_{\text{agg+growth},i} = B_{\text{agg},i} + B_{\text{growth},i}. \quad (3.123)$$

The volume average of particles appearing due to growth and aggregation in the cell i is calculated as

$$\bar{v}_i = \frac{V_{\text{agg},i} + V_{\text{growth},i}}{B_{\text{agg},i} + B_{\text{growth},i}}. \quad (3.124)$$

The discrete equation (3.120) has been used in our simulations to calculate the evolution of particle size distribution and its moments.

For comparison we describe an alternative by which the two processes can be coupled in a different manner which is more accurate but more expensive. For the simultaneous aggregation and growth, one may use cell average technique for the aggregation and a Lagrangian approach for the growth to obtain a better accuracy of the numerical results. Finally, we solve the following set of ordinary differential equations for the simultaneous growth and aggregation

$$\frac{dN_i}{dt} = B_{\text{agg},i}^{\text{CA}} - D_{\text{agg},i}, \quad (3.125)$$

together with

$$\frac{dx_i}{dt} = G(x_i), \quad (3.126)$$

and

$$\frac{dx_{i+1/2}}{dt} = G(x_{i+1/2}). \quad (3.127)$$

The first equation is for the rate of change of particle due to aggregation while the last two equations describe the motion of the representatives and boundaries respectively. A similar approach can be used to coupled growth process with other processes like breakage or simultaneous breakage and aggregation. In this work we only presented numerical results for the cell average technique where analytical solutions are easily available but it can be formulated in a similar fashion for other combinations of processes.

Numerical results

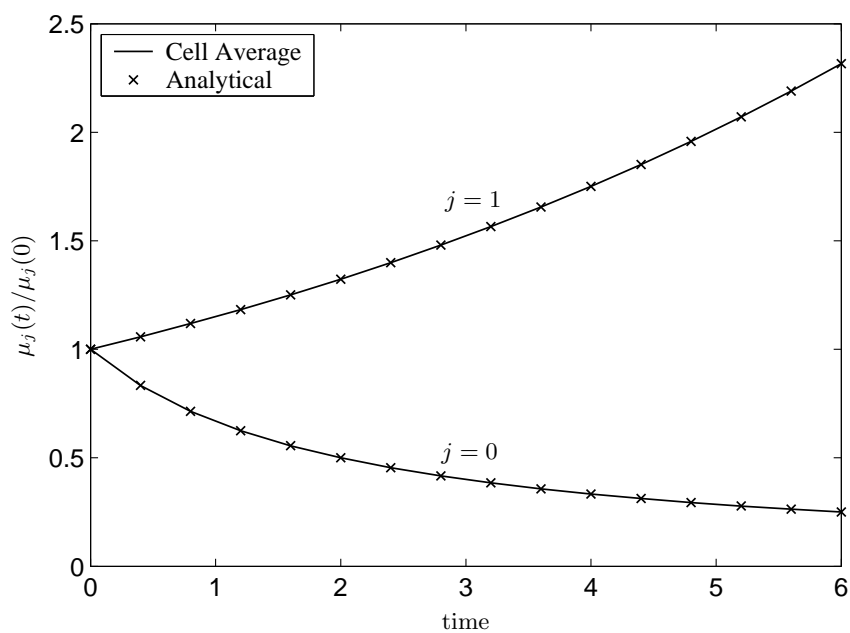
In order to demonstrate the effectiveness of the cell average technique we have applied it to two test problems with a linear growth rate $G(x) = G_0x$. The constant kernel $\beta(x, y) = \beta_0$ and the sum kernel $\beta(x, y) = \beta_0(x + y)$ for aggregation are used in the first and second test problems respectively. An exponentially decreasing particle size distribution has been used as initial condition. The initial condition and analytical solutions for the particle size distribution as well as its moments are given in Appendix A.6. The particle volume domain was partitioned into 60 non-homogeneous cells with the rule $x_{i+1/2} = 2^{1/q}x_{i-1/2}$.

Numerical results for the first test problems have been plotted in Figure 3.43. The variation of the first two moments with time is presented in Figure 3.43(a). The numerical and analytical solutions for moments are in excellent agreement. On the other hand numerical results for the particle size distribution at final time, shown in Figure 3.43(b), are slightly over-estimated. A better accuracy, of course, can be achieved by refining the grids.

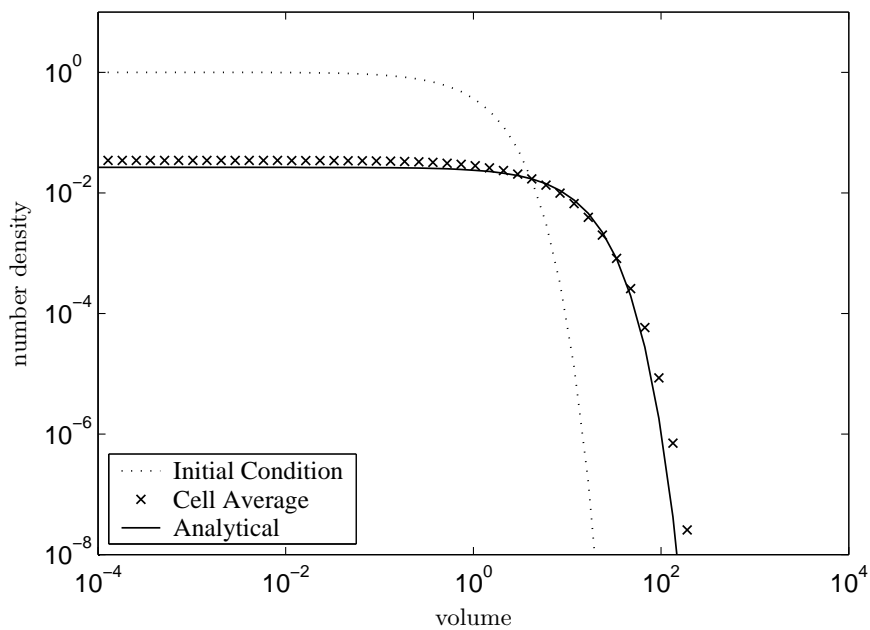
A similar computation has been performed for the second test case of size-dependent aggregation kernel. Once more the numerical solution of the first two moments overlaps the analytical solutions excellently, see Figure 3.44(a). The number density distribution at final time together with the initial condition is plotted in Figure 3.44(b). As can be seen from the figure that a very good agreement between the analytical and numerical solutions has been obtained.

We can conclude that the cell average technique can be used for coupled processes effectively. The coupling of growth processes with aggregation and breakage has been a big issue in areas related to particulate systems. Different authors proposed different coupling techniques but all of them either are complicated Kumar and Ramkrishna [59], less accurate and unstable Hounslow et al. [34] or applicable to limited problems Hu et al. [35], Prakash et al. [90]. The application of the cell average technique to combined different processes is easy as well as consistent and produces comparatively good results.

As mentioned before that growth processes can be coupled with other processes by computing growth using Lagrangian approach and aggregation or breakage using the cell average technique. In this way numerical diffusion by the growth can significantly be reduced and considerably better results can be obtained. In order to illustrate this coupling we have considered the same test cases as before. Since the prediction of the first two moments in this case is similar to the previous case, we omitted them to present here. Only the particle size distributions

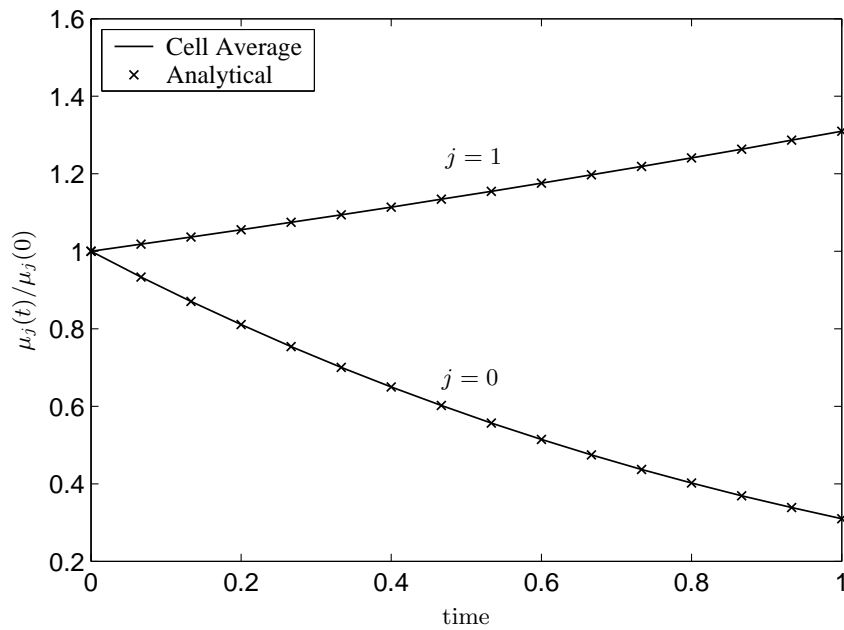


(a) First two moments.

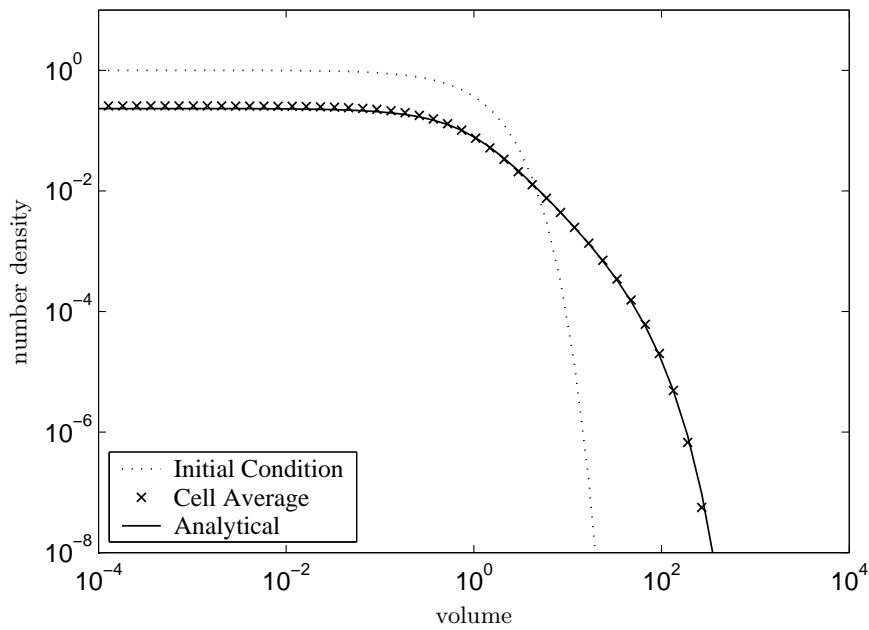


(b) Particle size distribution.

Figure 3.43: Simultaneous growth and aggregation using the cell average technique, $\beta(x, y) = \beta_0$ and $G(x) = G_0x$, grid points 65.



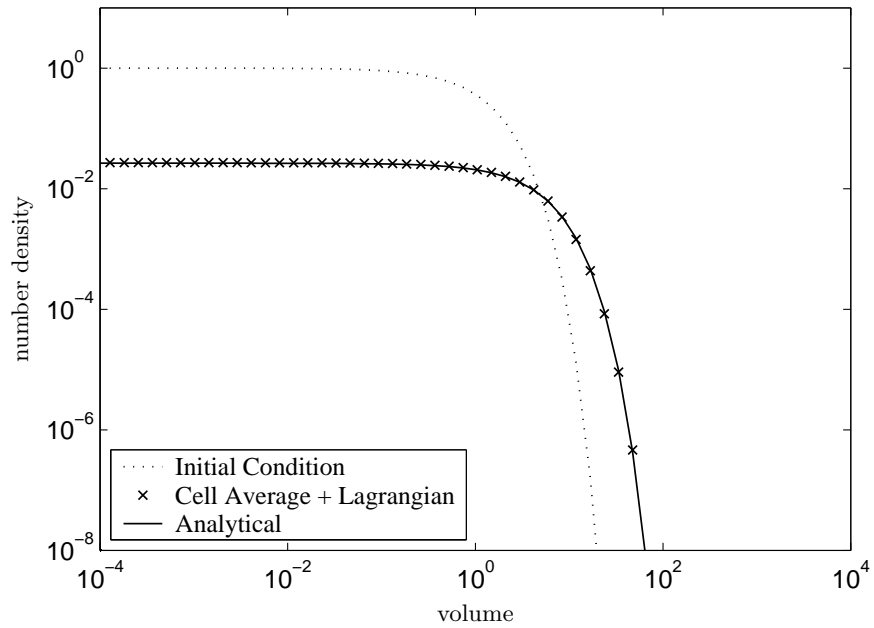
(a) First two moments.



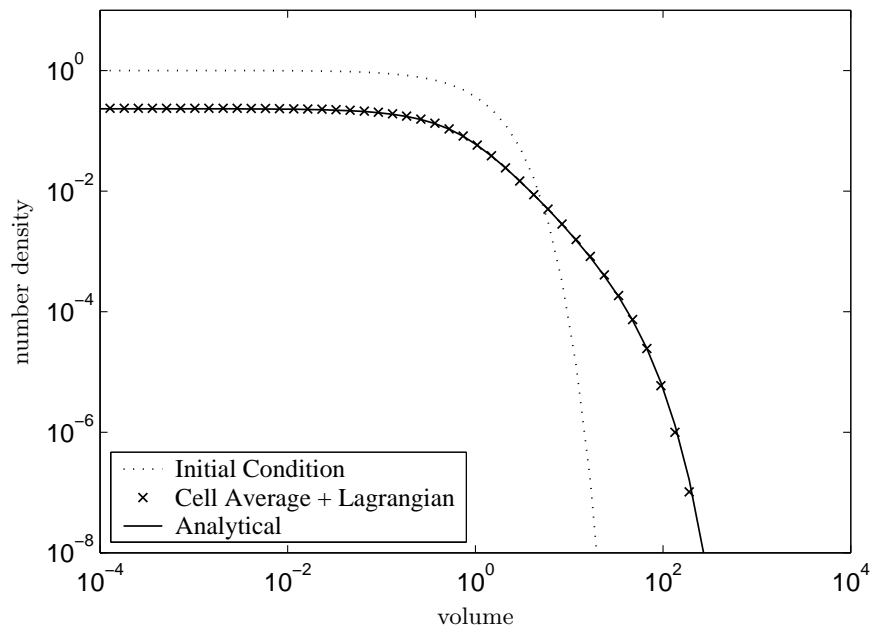
(b) Particle size distribution.

Figure 3.44: Simultaneous growth and aggregation using the cell average technique, $\beta(x, y) = \beta_0(x + y)$ and $G(x) = G_0x$, grid points 65.

3.2. THE CELL AVERAGE TECHNIQUE



(a) Particle size distribution with $\beta(x, y) = \beta_0$ and $G(x) = G_0x$.



(b) Particle size distribution with $\beta(x, y) = \beta_0(x + y)$ and $G(x) = G_0x$.

Figure 3.45: Simultaneous growth and aggregation using the cell average technique for aggregation and Lagrangian approach for growth, grid points 65.

corresponding to Figures 3.43(b) and 3.44(b) have been plotted in Figures 3.45(a) and 3.45(b). Clearly, it can be seen from the figures that the accuracy of the numerical results has been improved in both cases.

3.2.7 Simultaneous Growth and Nucleation

Similar to the case of simultaneous aggregation and nucleation, see Subsection 3.2.5, it is easy to couple the growth and nucleation processes. The cell average formulation in this case is given as

$$\frac{dN_i}{dt} = B_{\text{growth+nuc},i}^{\text{CA}} - D_{\text{growth},i}. \quad (3.128)$$

Now the birth by nucleation and growth can be described as follows

$$\begin{aligned} B_{\text{growth+nuc},i}^{\text{CA}} = & B_{\text{growth+nuc},i-1} \lambda_i^- (\bar{v}_{i-1}) H(\bar{v}_{i-1} - x_{i-1}) + B_{\text{growth+nuc},i} \lambda_i^- (\bar{v}_i) H(x_i - \bar{v}_i) \\ & + B_{\text{growth+nuc},i} \lambda_i^+ (\bar{v}_i) H(\bar{v}_i - x_i) + B_{\text{growth+nuc},i+1} \lambda_i^+ (\bar{v}_{i+1}) H(x_{i+1} - \bar{v}_{i+1}), \end{aligned} \quad (3.129)$$

where

$$B_{\text{growth+nuc},i} = B_{\text{growth},i} + \int_{x_{i-1/2}}^{x_{i+1/2}} B_{\text{nuc}}(t, x) dx. \quad (3.130)$$

The average values are computed as

$$\bar{v}_i = \frac{V_{\text{growth},i} + \int_{x_{i-1/2}}^{x_{i+1/2}} x B_{\text{nuc}}(t, x) dx}{B_{\text{growth},i} + \int_{x_{i-1/2}}^{x_{i+1/2}} B_{\text{nuc}}(t, x) dx}. \quad (3.131)$$

We now proceed to test the formulation by comparing the numerical results with the analytical solution for a selected problem.

Numerical results

Nucleation with no particles initially present is difficult to simulate. The analytical solution together with the initial condition is included in Appendix A.7. The volume domain has been partitioned into 100 geometrically spaced cells. A comparison between the analytical and numerical solution is shown in Figure 3.46. As can be seen from the figure the numerical results are slightly diffusive. Very fine grids are needed to capture the details near discontinuity. Some improvements using a three-point formula discussed in Subsection 3.2.3 can be obtained, but no attempts have been made here in that direction.

As we have seen in previous sections that the coupling of growth with other processes using a Lagrangian approach produces excellent results. An attempt in this direction has been made by Kumar and Ramkrishna [59]. Numerical treatment of simultaneous growth and nucleation using the Lagrangian approach is not trivial because smallest representative sizes together with their boundaries will move and there may not be a cell to place subsequently formed nuclei. This definitely forces us to add more cells as the PSD moves to the right and therefore it leads to serious difficulties in numerics. As mentioned in the previous chapter the formulation of Kumar and Ramkrishna [59] was inconsistent with the mass of the particles due to nucleation. It was later improved by Spicer et al. [106] by considering the effect of the mass of new formed nuclei on the movement of cell representatives.

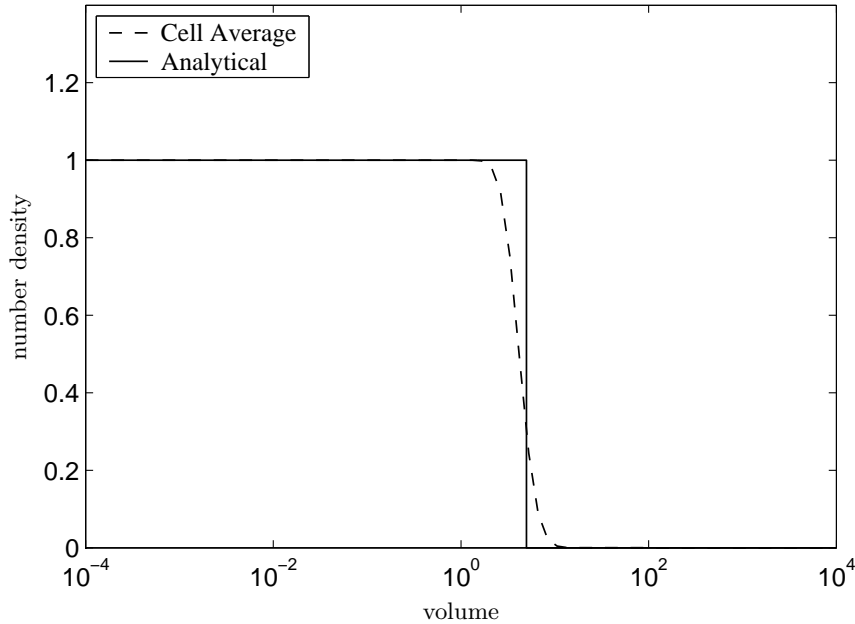


Figure 3.46: A comparison of particle size distributions with no particles initially present in the system, grid points 120.

3.2.8 Choice of Representative Sizes

Now we shall divert our attention to the concept of choosing representative sizes and find out some similarities of the fixed pivot and cell average schemes. In practice, the representative size of a cell may be chosen arbitrarily. The center of the cell, an easy choice, is a common choice for the representative size. On the basis of the position of the representative sizes we have the following lemma which tells us about the similarity of two techniques.

Lemma 3.2.1. *If we choose the representative sizes x_i as a boundary of cells then both the cell average and fixed pivot schemes become the same, i.e.*

$$\left(\frac{dN_i}{dt}\right)^{CA} = \left(\frac{dN_i}{dt}\right)^{FP} \quad \text{if } x_i = x_{i\pm 1/2}. \quad (3.132)$$

Proof. Consider some particles n_1, n_2, \dots, n_m of respective sizes x_1, x_2, \dots, x_m appear in the i th cell due to aggregation, breakage or any other event. Let us suppose that the representative size x_i of this cell lies at the left boundary $x_{i-1/2}$. In order to make particles appearance consistent with their number and mass, only a fraction of them has to be assigned at x_i . We calculate the fraction assigned at x_i using the cell average and the fixed pivot techniques. It is evident that the particles have to be distributed between x_i and x_{i+1} according to both techniques. The assigned fraction of particles at x_i according to the fixed pivot technique is given as

$$a^{FP} = \left(\frac{x_{i+1} - x_1}{x_{i+1} - x_i}\right) n_1 + \left(\frac{x_{i+1} - x_2}{x_{i+1} - x_i}\right) n_2 + \dots + \left(\frac{x_{i+1} - x_m}{x_{i+1} - x_i}\right) n_m. \quad (3.133)$$

According to the cell average technique, the fraction is given by

$$a^{\text{CA}} = \left(\frac{x_{i+1} - \bar{v}_i}{x_{i+1} - x_i} \right) (n_1 + n_2 + \dots + n_m), \quad (3.134)$$

where the average value \bar{v}_i is computed as

$$\bar{v}_i = \frac{x_1 n_1 + x_2 n_2 + \dots + x_m n_m}{n_1 + n_2 + \dots + n_m}. \quad (3.135)$$

Clearly substitution of the average \bar{v}_i from equation (3.135) into equation (3.134) gives the required result (3.133), i.e. $a^{\text{FP}} = a^{\text{CA}}$. To summarize, if the representative size of a cell lies at one of the boundaries then taking average and assigning a fraction of all particles to the neighboring representatives is the same as assigning particles of each size separately without taking average of them. \square

3.3 Mathematical Analysis

In this section we study the consistency, stability and convergence of the cell average technique. Non-uniform grids are usually very complicated for analyzing these features and therefore we consider here uniform grids only. Furthermore the cell average formulation for aggregation problems is highly non-linear and therefore we restrict ourselves to study thoroughly the breakage problems. Moreover, convergence analysis of the fixed pivot technique will be investigated and comparisons will be made with the cell average technique. In order to make the analysis more transparent, the same study has been performed for a simple approach of solving the population balance equation.

Before we proceed to analyze the schemes, it is convenient to review some theorems and definitions at this time. The cell average as well as the fixed pivot formulations take the following form

$$\frac{d\hat{N}(t)}{dt} = B(\hat{N}(t)) - D(\hat{N}(t)). \quad (3.136)$$

Here $\hat{N}(t)$ is a continuous time grid function on computation volume domain Ω with components $\hat{N}_i(t)$, $j = 1, 2, \dots, I$. The component $\hat{N}_i(t)$ is a numerical approximation of the total number in i th cell $N_i(t)$. The function B and D are vectors of birth and death rates in each cell. Unless stated otherwise, the notation Δx is used for the width of a cell of a uniform grid. The \mathbb{R}^m norm is denoted by $\|\cdot\|$ in the entire work.

Definition 3.3.1. *The **spatial truncation error** is defined by the residual left by substituting the exact solution $N(t)$ into equation (3.136) as*

$$\sigma(t) = \frac{dN(t)}{dt} - (B(N(t)) - D(N(t))). \quad (3.137)$$

The scheme (3.136) is called consistent of order p if, for $\Delta x \rightarrow 0$,

$$\|\sigma(t)\| = \mathcal{O}(\Delta x^p), \quad \text{uniformly for all } t. \quad (3.138)$$

Definition 3.3.2. The *global discretization error* is defined by $\epsilon(t) = N(t) - \hat{N}(t)$. The scheme (3.136) is called convergent of order p if, for $\Delta x \rightarrow 0$,

$$\|\epsilon(t)\| = \mathcal{O}(\Delta x^p), \quad \text{uniformly for all } t. \quad (3.139)$$

Definition 3.3.3. The *logarithmic norm* of a matrix A in $\mathbb{R}^{m \times m}$ is defined as, see Hundsdorfer and Verwer [37],

$$\tilde{\mu}(A) = \lim_{\tau \rightarrow 0} \frac{\|I + \tau A\| - 1}{\tau}. \quad (3.140)$$

The logarithmic norms of a matrix A corresponding to certain p norms on \mathbb{R}^m are given by

$$\tilde{\mu}_1(A) = \max_j \left(\operatorname{Re}(a_{jj}) + \sum_{i \neq j} |a_{ij}| \right), \quad p = 1, \quad (3.141)$$

We denote the real part of a complex number z by $\operatorname{Re}(z)$.

$$\tilde{\mu}_2(A) = \max \{ \lambda : \lambda \in \sigma((A + A^*)/2) \}, \quad p = 2, \quad (3.142)$$

$$\tilde{\mu}_\infty(A) = \max_i \left(\operatorname{Re}(a_{ii}) + \sum_{j \neq i} |a_{ij}| \right), \quad p = \infty. \quad (3.143)$$

The following theorem is useful for calculating the norm of the exponential of a matrix. The proof can be found in Hundsdorfer and Verwer [37].

Theorem 3.3.4. If $A \in \mathbb{R}^{m \times m}$ and $\omega \in \mathbb{R}$ then we have

$$\tilde{\mu}(A) \leq \omega \iff \|e^{tA}\| \leq e^{t\omega}, \quad \text{for all } t \geq 0. \quad (3.144)$$

Proof. See Hundsdorfer and Verwer [37], Chapter 1, Theorem 2.4. \square

Now we include a useful definition and theorem for stability and convergence from Hundsdorfer and Verwer [37]. In case of pure breakage problem the equation (3.136) takes the following linear semi-discrete form

$$\frac{d\hat{N}}{dt} = A\hat{N}(t). \quad (3.145)$$

Definition 3.3.5. The semi-discrete system (3.145) is called stable if we have on all grids

$$\|e^{tA}\| \leq K e^{\omega t} \quad \text{for } 0 \leq t \leq T, \quad (3.146)$$

with constant $K \geq 1$ and $\omega \in \mathbb{R}$ both independent of Δx .

Theorem 3.3.6. (Hundsdorfer and Verwer [37]). Consider the linear semi-discrete system (3.145) and assume the stability condition (3.146) is valid. Suppose further that $\|\sigma(t)\| \leq C\Delta x^q$ for $0 \leq t \leq T$ (consistency of order q) and $\|\epsilon(0)\| \leq C_0\Delta x^q$ with constant $C, C_0 > 0$. Then we have convergence of order $p = q$ with the error bounds

$$\|\epsilon(t)\| \leq KC_0 e^{\omega t} \Delta x^q + \frac{KC}{\omega} (e^{\omega t} - 1) \Delta x^q \quad \text{if } \omega \neq 0, 0 \leq t \leq T, \quad (3.147)$$

and

$$\|\epsilon(t)\| \leq KC_0 \Delta x^q + KCt \Delta x^q \quad \text{if } \omega = 0, 0 \leq t \leq T. \quad (3.148)$$

Proof. See Hundsdorfer and Verwer [37], Chapter 1, Theorem 4.1. \square

Quadrature error for non-uniform grids

Let us begin with the following integration formula

$$I = \int_{\check{a}}^{\check{b}} f(x) dx. \quad (3.149)$$

Let $\check{a} = x_{1-1/2} < x_{1+1/2} < x_{2+1/2} < \dots < x_{i-1/2} < x_{i+1/2} \dots < x_{n+1/2} = \check{b}$ be a partition of the interval $[\check{a}, \check{b}]$ with $\Delta x_i = x_{i+1/2} - x_{i-1/2}$. Here the partition does not have to be equidistant. We assume that $f \in C^p([\check{a}, \check{b}])$ and that on $[x_{i-1/2}, x_{i+1/2}]$ we have a quadrature rule of order p

$$\int_{x_{i-1/2}}^{x_{i+1/2}} f(x) dx = Q_p^i f + \check{c} f^{(p)}(\xi_i) \Delta x_i^{p+1}. \quad (3.150)$$

Now summing the equation (3.150) over the interval $[\check{a}, \check{b}]$ to give

$$I = \sum_{i=1}^n Q_p^i f + R_n f, \quad (3.151)$$

where $R_n f$ is the quadrature error defined by

$$\begin{aligned} R_n f &= \check{c} \sum_{i=1}^n f^{(p)}(\xi_i) \Delta x_i^{p+1} \\ &= \check{c} \left(\sum_{i=1}^n \Delta x_i^{p+1} \right) \left(\sum_{i=1}^n f^{(p)}(\xi_i) \Delta x_i^{p+1} / \sum_{i=1}^n \Delta x_i^{p+1} \right). \end{aligned} \quad (3.152)$$

The last term in parentheses is a convex combination. Therefore, application of the intermediate value theorem gives for some $\xi \in [\check{a}, \check{b}]$

$$R_n f = \check{c} \sum_{i=1}^n \Delta x_i^{p+1} f^{(p)}(\xi). \quad (3.153)$$

Setting $\Delta x_{\max} = \max(\Delta x_1, \Delta x_2, \dots, \Delta x_n)$, error bounds can be estimated by

$$\begin{aligned} |R_n f| &\leq \max_{x \in [\check{a}, \check{b}]} |f^{(p)}(x)| \sum_{i=1}^n \Delta x_i^{p+1} \\ &\leq \max_{x \in [\check{a}, \check{b}]} |f^{(p)}(x)| n \Delta x_{\max}^{p+1}. \end{aligned} \quad (3.154)$$

For the convergence analysis it is reasonable to put the following condition on Δx_{\max} and n

$$n \cdot \Delta x_{\max} \leq C,$$

for some fixed constant $C > 0$. In terms of Δx_{\max} , the error bounds are given by

$$\boxed{|R_n f| \leq \check{c} C \Delta x_{\max}^p \max_{x \in [\check{a}, \check{b}]} |f^{(p)}(x)|}$$

Also in terms of degree of freedom, error is estimated by

$$\boxed{|R_n f| \leq \check{c} C^{p+1} n^{-p} \max_{x \in [\check{a}, \check{b}]} |f^{(p)}(x)|}$$

Special cases: Error bounds can easily be obtained for different quadrature rules for example, rectangle rule, midpoint rule, trapezoidal rule, Simpson's rule etc. For detailed information for uniform grids readers are referred to Hämmerlin and Hoffmann [28]. Substituting values of c and p in the preceding error formula, we can obtain the error estimates for various cases given below:

- Rectangle rule: $\check{c} = \frac{1}{2}, p = 1,$
- Midpoint rule: $\check{c} = \frac{1}{24}, p = 2,$
- Trapezoidal rule: $\check{c} = \frac{1}{12}, p = 2,$
- Simpson's rule: $\check{c} = \frac{1}{180}, p = 4.$

The cell average and the fixed pivot techniques were derived by approximating the number density by Dirac-delta distributions and the integrals appearing in the population balance equations were transformed into sums. Since quadrature rules are easy to analyze, we construct here the same cell average and the fixed pivot formulations using the quadrature rules.

3.3.1 The Fixed Pivot Technique

In this section we study the consistency, convergence and stability of the fixed pivot technique. For mathematical convenience, we have assumed that the first grid point x_1 can be chosen in such a way that it remains always smaller or equal to the size of the smallest particle that can appear during the breakage process. In practice this may be performed by designing the breakage function accordingly. Furthermore, we have used \hat{N}_i for the numerical approximation of the number of particles in a cell N_i in order to distinguish between exact and numerical values. Let us first discuss some basic facts of the technique by the following proposition.

Proposition 3.3.7. *Assuming that x_1 is the smallest particle size that can appear during the breakage, then the fixed pivot formulation (2.39) conserves the total volume with time; that is,*

$$\frac{d}{dt} \sum_{i=1}^I (x_i \hat{N}_i) = 0. \quad (3.155)$$

Proof. Multiplying the formulation (2.39) by x_i and summing over all i we get

$$\frac{d}{dt} \sum_{i=1}^I (x_i \hat{N}_i) = x_i \sum_{k=i}^I \eta_{i,k} S_k(t) N_k(t) - x_i S_i(t) N_i(t), \quad (3.156)$$

with η from (2.40). Substituting the value of η , the above equation takes the following form

$$\begin{aligned} \frac{d}{dt} \sum_{i=1}^I (x_i \hat{N}_i) &= \sum_{i=1}^I x_i \sum_{k=i}^I S_k N_k \int_{x_i}^{x_{i+1}} a_1(x, x_i) b(x, x_k) dx \\ &+ \sum_{i=1}^I x_i \sum_{k=i}^I S_k N_k \int_{x_{i-1}}^{x_i} a_2(x, x_i) b(x, x_k) dx - \sum_{i=1}^I x_i S_i N_i. \end{aligned} \quad (3.157)$$

It is evident that for $k = i$,

$$S_i N_i \int_{x_i}^{x_{i+1}} a_1(x, x_i) b(x, x_i) dx = 0, \quad \text{since } b(x, x_i) = 0 \text{ for } x > x_i. \quad (3.158)$$

We shall use this value of integral to simplify the equation (3.157). Also x_1 and x_I are the smallest and the largest sizes of particles in the system, the equation (3.157) can be simplified further to get

$$\begin{aligned} \frac{d}{dt} \sum_{i=1}^I (x_i \hat{N}_i) &= \sum_{i=1}^{I-1} x_i \sum_{k=i+1}^I S_k N_k \int_{x_i}^{x_{i+1}} a_1(x, x_i) b(x, x_k) dx \\ &\quad + \sum_{i=2}^I x_i \sum_{k=i}^I S_k N_k \int_{x_{i-1}}^{x_i} a_2(x, x_i) b(x, x_k) dx - \sum_{i=2}^I x_i S_i N_i. \end{aligned} \quad (3.159)$$

It can be rewritten as

$$\begin{aligned} \frac{d}{dt} \sum_{i=1}^I (x_i \hat{N}_i) &= \sum_{i=1}^{I-1} x_i \sum_{k=i+1}^I S_k N_k \int_{x_i}^{x_{i+1}} a_1(x, x_i) b(x, x_k) dx \\ &\quad + \sum_{i=1}^{I-1} x_{i+1} \sum_{k=i+1}^I S_k N_k \int_{x_i}^{x_{i+1}} a_2(x, x_{i+1}) b(x, x_k) dx - \sum_{i=2}^I x_i S_i N_i. \end{aligned} \quad (3.160)$$

Using the local conservation property (2.43), we obtain

$$\begin{aligned} \frac{d}{dt} \sum_{i=1}^I (x_i \hat{N}_i) &= \sum_{i=1}^{I-1} \sum_{k=i+1}^I S_k N_k \int_{x_i}^{x_{i+1}} x b(x, x_k) dx - \sum_{i=2}^I x_i S_i N_i \\ &= \sum_{i=2}^I S_i N_i \int_{x_1}^{x_i} x b(x, x_i) dx - \sum_{i=2}^I x_i S_i N_i. \end{aligned} \quad (3.161)$$

The application of the property of the breakage function (2.36) provides

$$\frac{d}{dt} \sum_{i=1}^I (x_i \hat{N}_i) = \sum_{i=2}^I S_i N_i x_i - \sum_{i=2}^I x_i S_i N_i = 0. \quad (3.162)$$

This proves the conservation property (3.155). □

Remark 3.3.8. *It should be noted from the proof of Proposition 3.3.7 that the integrals*

$$\int_{x_i}^{x_{i+1}} x b(x, x_k) dx,$$

and respectively

$$\int_{x_i}^{x_{i+1}} b(x, x_k) dx,$$

in the fixed pivot formulation must be computed exactly or at least approximated by a higher order scheme in order to ensure mass conservation.

Proposition 3.3.9. *Assuming that x_1 is the smallest particle size that can appear during the breakage, then for the fixed pivot formulation (2.39) the total number is a increasing function of time; that is,*

$$\frac{d}{dt} \sum_{i=1}^I (\hat{N}_i) > 0. \quad (3.163)$$

Proof. Proceeding as before in Proposition 3.3.7 and using the property (2.35) as well as the equality constraint (2.42), it is easy to obtain

$$\begin{aligned} \frac{d}{dt} \sum_{i=1}^I (\hat{N}_i) &= \sum_{i=2}^I S_i N_i \int_{x_1}^{x_i} b(x, x_i) dx - \sum_{i=2}^I x_i S_i N_i \\ &= \sum_{i=2}^I S_i N_i (\bar{N}(x_i) - 1). \end{aligned} \quad (3.164)$$

The physical restriction that a particle breaks into at least two particles requires that $\bar{N}(x_i) \geq 2$ and thus inequality (3.163) holds. This proves that the total number of particles in a breakage process always increases. \square

Remark 3.3.10. *If we calculate the analytical expression for the rate of change of total number of particles then we get exactly the continuous analog of the discrete expression (3.164). Thus, we begin with the following equation*

$$\frac{d}{dt} \int_0^\infty n(t, x) dx = \int_0^\infty \int_x^\infty b(x, \epsilon) n(t, \epsilon) S(\epsilon) d\epsilon dx - \int_0^\infty S(x) n(t, x) dx. \quad (3.165)$$

Changing the order of integration we obtain by $\int_0^\epsilon b(x, \epsilon) dx = \bar{N}(\epsilon)$, see equation (2.35),

$$\begin{aligned} \frac{d}{dt} \int_0^\infty n(t, x) dx &= \int_0^\infty \int_0^\epsilon b(x, \epsilon) n(t, \epsilon) S(\epsilon) dx d\epsilon - \int_0^\infty S(x) n(t, x) dx \\ &= \int_0^\infty n(t, \epsilon) S(\epsilon) \bar{N}(\epsilon) d\epsilon - \int_0^\infty S(\epsilon) n(t, \epsilon) d\epsilon \\ &= \int_0^\infty S(\epsilon) n(t, \epsilon) (\bar{N}(\epsilon) - 1) d\epsilon. \end{aligned} \quad (3.166)$$

We now consider a fundamental lemma useful for analyzing the scheme.

Lemma 3.3.11. *Let $f(x)$ be a continuously differentiable function in $[x_i - \Delta x, x_i + \Delta x]$. If $\lambda_1(x)$ and $\lambda_2(y)$ are continuously differentiable functions in $[x_i, x_i + \Delta x]$ and $[x_i - \Delta x, x_i]$ respectively such that*

$$\lambda_1(x_i) + \lambda_2(x_i) \neq 1,$$

then

$$\int_{x_i - \Delta x/2}^{x_i + \Delta x/2} f(x) dx = \int_{x_i}^{x_i + \Delta x} \lambda_1(x) f(x) dx + \int_{x_i - \Delta x}^{x_i} \lambda_2(x) f(x) dx + \mathcal{O}(\Delta x).$$

Proof. The application of Taylor series expansion about x_i gives

$$\begin{aligned} & \int_{x_i-\Delta x/2}^{x_i+\Delta x/2} f(x) dx - \int_{x_i}^{x_i+\Delta x} \lambda_1(x)f(x) dx - \int_{x_i-\Delta x}^{x_i} \lambda_2(x)f(x) dx \\ &= \Delta x f(x_i) + \mathcal{O}(\Delta x^3) - \Delta x \lambda_1(x_i)f(x_i) - \Delta x \lambda_2(x_i)f(x_i) + \mathcal{O}(\Delta x^2) \\ &= \Delta x f(x_i)(1 - \lambda_1(x_i) - \lambda_2(x_i)) + \mathcal{O}(\Delta x^2) \\ &= \mathcal{O}(\Delta x). \end{aligned}$$

Hence the lemma is proved. \square

Consistency

The analytical expressions for the birth and death rates on truncated domains are given by

$$B_i = \int_{x_{i-1/2}}^{x_{i+1/2}} \int_x^{x_{I+1/2}} b(x, \epsilon) S(\epsilon) n(t, \epsilon) d\epsilon dx, \quad (3.167)$$

and

$$D_i = \int_{x_{i-1/2}}^{x_{i+1/2}} S(x)n(t, x) dx. \quad (3.168)$$

According to Kumar and Ramkrishna [57], the birth term of the fixed pivot technique is defined as

$$\begin{aligned} B_i^{\text{mod}} &= \int_{x_i}^{x_{i+1}} a_1(x) \int_x^{x_{I+1/2}} b(x, \epsilon) S(\epsilon) n(t, \epsilon) d\epsilon dx \\ &+ \int_{x_{i-1}}^{x_i} a_2(x) \int_x^{x_{I+1/2}} b(x, \epsilon) S(\epsilon) n(t, \epsilon) d\epsilon dx. \end{aligned} \quad (3.169)$$

Here the function a_1 and a_2 are given as

$$a_1(x) = \frac{x_{i+1} - x}{x_{i+1} - x_i}, \quad a_2(x) = \frac{x - x_{i-1}}{x_i - x_{i-1}}.$$

and therefore

$$a_1(x_i) + a_2(x_i) = 2 \neq 1.$$

Using Lemma 3.3.11, the following relation between (3.167) and (3.169) holds

$$B_i = B_i^{\text{mod}} + \mathcal{O}(\Delta x). \quad (3.170)$$

Changing the order of integration in equation (3.169), the equation (3.170) follows

$$\begin{aligned} B_i &= \int_{x_i}^{x_{i+1}} \int_{x_i}^{\epsilon} a_1(x)b(x, \epsilon)S(\epsilon)n(t, \epsilon) dx d\epsilon + \sum_{k=i+1}^I \int_{x_k}^{x_{k+1}} \int_{x_i}^{x_{i+1}} a_1(x)b(x, \epsilon)S(\epsilon)n(t, \epsilon) dx d\epsilon \\ &+ \int_{x_{i-1}}^{x_i} \int_{x_{i-1}}^{\epsilon} a_2(x)b(x, \epsilon)S(\epsilon)n(t, \epsilon) dx d\epsilon \\ &+ \sum_{k=i}^I \int_{x_k}^{x_{k+1}} \int_{x_{i-1}}^{x_i} a_2(x)b(x, \epsilon)S(\epsilon)n(t, \epsilon) dx d\epsilon + \mathcal{O}(\Delta x). \end{aligned} \quad (3.171)$$

3.3. MATHEMATICAL ANALYSIS

We now make an assumption of constant density within the cell, i.e. $N_i(t) = n(t, x_i)\Delta x$. The left rectangular rule for the outer integral gives first order accuracy and therefore we get the following simplified formulation

$$\begin{aligned}
B_i &= S(x_i)N_i \int_{x_i}^{x_i} a_1(x)b(x, x_i) dx + \sum_{k=i+1}^I S(x_k)N_k \int_{x_i}^{x_{i+1}} a_1(x)b(x, x_k) dx \\
&\quad + S(x_{i-1})N_{i-1} \int_{x_{i-1}}^{x_{i-1}} a_2(x)b(x, x_{i-1}) dx + \sum_{k=i}^I S(x_k)N_k \int_{x_{i-1}}^{x_i} a_2(x)b(x, x_k) dx + \mathcal{O}(\Delta x) \\
&= \sum_{k=i+1}^I S(x_k)N_k \int_{x_i}^{x_{i+1}} a_1(x)b(x, x_k) dx + \sum_{k=i}^I S(x_k)N_k \int_{x_{i-1}}^{x_i} a_2(x)b(x, x_k) dx + \mathcal{O}(\Delta x) \\
&= B_i^{\text{FP}} + \mathcal{O}(\Delta x).
\end{aligned} \tag{3.172}$$

The death term can be discretized using the midpoint rule as

$$D_i = S(x_i)N_i + \mathcal{O}(\Delta x^3) = D_i^{\text{FP}} + \mathcal{O}(\Delta x^3). \tag{3.173}$$

Combining the birth and death terms we obtain the first order consistency. Then we have

$$\|\sigma(t)\| = \mathcal{O}(\Delta x), \quad \text{uniformly for all } t. \tag{3.174}$$

Remark 3.3.12. *Note that if we distribute particles immediately after breakage (the fixed pivot technique) then the formulation provides us at the most 1st order accuracy. This motivates us to distribute particles in a different way by taking first the average volume and then distributing them only once (the cell average technique).*

Stability and convergence

The fixed pivot technique (2.39) can be rewritten in a matrix form (3.145) by defining the matrix A as

$$A = \begin{bmatrix} \eta_{11}S_1 - S_1 & \eta_{12}S_2 & \dots & \eta_{1I}S_I \\ 0 & \eta_{22}S_2 - S_2 & \dots & \eta_{2I}S_I \\ \cdot & & & \cdot \\ \cdot & & & \cdot \\ 0 & 0 & \dots & \eta_{II}S_I - S_I \end{bmatrix}.$$

Let us define a diagonal matrix D with the representative points as

$$D = \begin{bmatrix} x_1 & 0 & \dots & 0 \\ 0 & x_2 & \dots & 0 \\ \cdot & & & \cdot \\ \cdot & & & \cdot \\ 0 & 0 & \dots & x_I \end{bmatrix}.$$

CHAPTER 3. NEW NUMERICAL METHODS: ONE-DIMENSIONAL

Note that $x_i > 0$, for all i . We now consider the matrix $M = DAD^{-1}$ given by

$$M = \begin{bmatrix} \eta_{11}S_1 - S_1 & \frac{x_1}{x_2}\eta_{12}S_2 & \dots & \frac{x_1}{x_I}\eta_{1I}S_I \\ 0 & \eta_{22}S_2 - S_2 & \dots & \frac{x_2}{x_I}\eta_{2I}S_I \\ \cdot & & & \cdot \\ \cdot & & & \cdot \\ 0 & 0 & \dots & \eta_{II}S_I - S_I \end{bmatrix}.$$

Now we evaluate the logarithmic norm of the matrix $M = (m_{ij})_{I \times I}$ as

$$\tilde{\mu}_1(M) = \max_j \left(\operatorname{Re}(m_{jj}) + \sum_{i \neq j} |m_{ij}| \right). \quad (3.175)$$

Since all elements of the matrix M are real and all non-diagonal elements are non-negative, the logarithmic norm can again be rewritten as

$$\tilde{\mu}_1(M) = \max_j \left(\sum_{1 \leq i \leq I} m_{ij} \right). \quad (3.176)$$

Using the assumption that the flux through the boundary of the domain is zero, the sum of all column elements of matrix M is given by

$$\begin{aligned} \sum_{i=1}^I m_{ij} &= \sum_{i=1}^j \frac{x_i}{x_j} \eta_{ij} S_j - S_j \\ &= \frac{S_j}{x_j} \sum_{i=1}^j x_i \eta_{ij} - S_j. \end{aligned} \quad (3.177)$$

The sum appearing in the above equation can be calculated as

$$\begin{aligned} \sum_{i=1}^j x_i \eta_{ij} &= \sum_{i=1}^j x_i \left(\int_{x_i}^{x_{i+1}} a_1(x, x_i) b(x, x_j) dx + \int_{x_{i-1}}^{x_i} a_2(x, x_i) b(x, x_j) dx \right) \\ &= \sum_{i=1}^{j-1} \int_{x_i}^{x_{i+1}} x_i a_1(x, x_i) b(x, x_j) dx + \sum_{i=2}^j \int_{x_{i-1}}^{x_i} x_i a_2(x, x_i) b(x, x_j) dx \\ &= \sum_{i=1}^{j-1} \int_{x_i}^{x_{i+1}} x_i a_1(x, x_i) b(x, x_j) dx + \sum_{i=1}^{j-1} \int_{x_i}^{x_{i+1}} x_{i+1} a_2(x, x_{i+1}) b(x, x_j) dx. \end{aligned} \quad (3.178)$$

Using the properties of fractions $x_i a_1(x, x_i) + x_{i+1} a_2(x, x_{i+1}) = x$ and breakage function (2.36), we get

$$\begin{aligned} \sum_{i=1}^j x_i \eta_{ij} &= \sum_{i=1}^{j-1} \int_{x_i}^{x_{i+1}} x b(x, x_j) dx \\ &= \int_{x_1}^{x_j} x b(x, x_j) dx \\ &= x_j. \end{aligned} \quad (3.179)$$

Substituting the above sum into the equation (3.177), we obtain

$$\sum_i m_{ij} = \frac{S_j}{x_j} x_j - S_j = 0. \quad (3.180)$$

Consequently, we obtain

$$\tilde{\mu}_1(M) = 0. \quad (3.181)$$

Application of Theorem 3.3.4 provides

$$\|e^{tM}\|_1 \leq 1. \quad (3.182)$$

We now establish the stability of the scheme as follows

$$\begin{aligned} \|e^{At}\|_1 &= \|D^{-1} D e^{At} D^{-1} D\|_1 \\ &\leq \|D^{-1}\|_1 \cdot \|D e^{At} D^{-1}\|_1 \cdot \|D\|_1 \\ &= \|D^{-1}\|_1 \cdot \|e^{tM}\|_1 \cdot \|D\|_1 \\ &\leq \|D^{-1}\|_1 \cdot \|D\|_1 \\ &= \frac{x_I}{x_1} := K \geq 1. \end{aligned} \quad (3.183)$$

Here we calculated the matrix norm as follows

$$\|D\|_1 = \max_{1 \leq j \leq I} \sum_{i=1}^I |d_{ij}|. \quad (3.184)$$

Since D and D^{-1} are diagonal matrices with positive values, thus the norm of matrices D and D^{-1} are simply given by

$$\|D\|_1 = \max \{x_1, x_2, \dots, x_I\} = x_I, \quad (3.185)$$

and

$$\|D^{-1}\|_1 = \max \left\{ \frac{1}{x_1}, \frac{1}{x_2}, \dots, \frac{1}{x_I} \right\} = \frac{1}{x_1}. \quad (3.186)$$

Finally from (3.183), we have

$$\|e^{At}\|_1 \leq K. \quad (3.187)$$

This shows the stability of the fixed pivot technique with the stability constant $\omega = 0$. This predicts linear growth of the global discretization error $\epsilon(t)$. Thus, from Theorem 3.3.6 we have convergence of order 1 with error bounds

$$\|\epsilon(t)\|_1 \leq K c_0 \Delta x + K C t \Delta x, \quad (3.188)$$

with constants $C, C_0 > 0$. Computational evidence indicates that the first order in Δx cannot be improved.

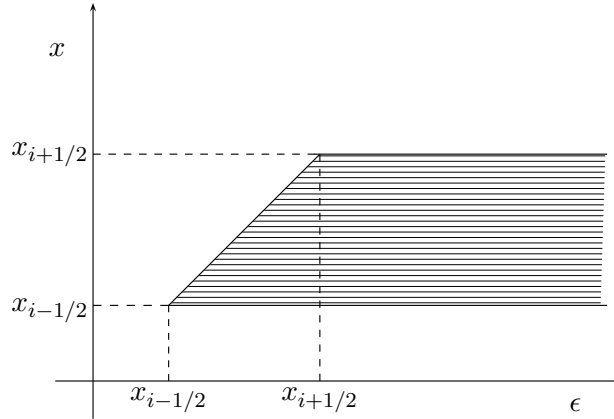


Figure 3.47: Integration limits.

3.3.2 Direct Approach

Although the fixed pivot technique is only first order accurate, it is consistent with the first two moments. The consistency with respect to moments has been guaranteed by imposing the conservation properties during the formulation. It is also of interest to investigate the scheme if we just replace integrals appearing in the population balance equation by quadrature rules without applying any conservation properties. We call this the *direct approach*. We shall begin with the birth and death rates (3.167) and (3.168).

Let us first consider the birth term B_i . Changing the order of integration, see Figure 3.47, gives

$$B_i = \int_{x_{i-1/2}}^{x_{i+1/2}} S(\epsilon)n(t, \epsilon) \int_{x_{i-1/2}}^{\epsilon} b(x, \epsilon) dx d\epsilon + \int_{x_{i+1/2}}^{x_{I+1/2}} S(\epsilon)n(t, \epsilon) \int_{x_{i-1/2}}^{x_{i+1/2}} b(x, \epsilon) dx d\epsilon. \quad (3.189)$$

Applying the midpoint rule for the outer integral, we obtain

$$\begin{aligned} B_i &= S(x_i)N_i \int_{x_{i-1/2}}^{x_i} b(x, x_i) dx + \sum_{k=i+1}^I S(x_k)N_k \int_{x_{i-1/2}}^{x_{i+1/2}} b(x, x_k) dx + \mathcal{O}(\Delta x^3) \\ &= \sum_{k=i}^I S(x_k)N_k \int_{x_{i-1/2}}^{p_k^i} b(x, x_k) dx + \mathcal{O}(\Delta x^2) =: \hat{B}_i + \mathcal{O}(\Delta x^2), \end{aligned} \quad (3.190)$$

where $p_k^i = x_i$ for $k = i$ and $p_k^i = x_{i+1/2}$ elsewhere. The death term D_i after applying the midpoint rule becomes

$$D_i = S(x_i)N_i + \mathcal{O}(\Delta x^3) =: \hat{D}_i + \mathcal{O}(\Delta x^3). \quad (3.191)$$

More precisely, the final formulation for direct approach is given by

$$\frac{d\hat{N}_i}{dt} = \sum_{k=i}^I S(x_k)\hat{N}_k \int_{x_{i-1/2}}^{p_k^i} b(x, x_k) dx - S(x_i)\hat{N}_i. \quad (3.192)$$

Next we will show that the direct formulation (3.192) is not mass conserving. Unless mentioned otherwise, the assumption that x_1 is the smallest particle size that can appear during the breakage has been pre-assumed in our analysis.

Proposition 3.3.13. *The direct formulation (3.192) does not conserve the total volume in general; that is,*

$$\frac{d}{dt} \sum_{i=1}^I (x_i \hat{N}_i) \neq 0. \quad (3.193)$$

Proof. Multiplying the formulation (3.192) by x_i and summing over i we obtain

$$\frac{d}{dt} \sum_{i=1}^I (\hat{N}_i x_i) = \sum_{i=1}^I x_i \sum_{k=i}^I S_k \hat{N}_k \int_{x_{i-1/2}}^{p_k^i} b(x, x_k) dx - \sum_{i=1}^I x_i S_i \hat{N}_i. \quad (3.194)$$

Changing the order of sums and using the fact $\int_{x_{1/2}}^{x_k} x b(x, x_k) dx = x_k$ we get

$$\begin{aligned} \frac{d}{dt} \sum_{i=1}^I (\hat{N}_i x_i) &= \sum_{k=1}^I S_k \hat{N}_k \sum_{i=1}^k x_i \int_{x_{i-1/2}}^{p_k^i} b(x, x_k) dx - \sum_{i=1}^I x_i S_i \hat{N}_i \\ &= \sum_{k=1}^I S_k \hat{N}_k \left[\sum_{i=1}^k x_i \int_{x_{i-1/2}}^{p_k^i} b(x, x_k) dx - x_k \right] \\ &= \sum_{k=1}^I S_k \hat{N}_k \left[\sum_{i=1}^k x_i \int_{x_{i-1/2}}^{p_k^i} b(x, x_k) dx - \sum_{i=1}^k \int_{x_{i-1/2}}^{p_k^i} x b(x, x_k) dx \right] \\ &= \sum_{k=1}^I S_k \hat{N}_k \left[\sum_{i=1}^k \int_{x_{i-1/2}}^{p_k^i} b(x, x_k) (x_i - x) dx \right] \neq 0. \end{aligned} \quad (3.195)$$

This proves (3.193). □

Proposition 3.3.14. *Assuming that x_1 is the smallest particle size that can appear during the breakage, then for the direct approach (3.192) the total number is a increasing function of time; that is,*

$$\frac{d}{dt} \sum_{i=1}^I (\hat{N}_i) > 0. \quad (3.196)$$

Proof. It follows analogously as the preceding proof using the property of the breakage function (2.42) that

$$\begin{aligned} \frac{d}{dt} \sum_{i=1}^I (\hat{N}_i) &= \sum_{k=1}^I S_k \hat{N}_k \left[\sum_{i=1}^k \int_{x_{i-1/2}}^{p_k^i} b(x, x_k) dx - 1 \right] \\ &= \sum_{k=1}^I S_k \hat{N}_k [\bar{N}(x_k) - 1] \geq 0. \end{aligned} \quad (3.197)$$

This proves the required result. □

Consistency, stability and convergence

Clearly the consistency order of the scheme is 2 which can directly be perceived from equations (3.190) and (3.191). Thus

$$\|\sigma(t)\| = \mathcal{O}(\Delta x^2), \quad \text{uniformly for all } t. \quad (3.198)$$

The direct scheme (3.192) can be transformed into a matrix form (3.145) with

$$A = \begin{bmatrix} S_1 \int_{x_{1-1/2}}^{x_1} b(x, x_1) dx - S_1 & S_2 \int_{x_{1-1/2}}^{x_1+1/2} b(x, x_2) dx & \dots & S_I \int_{x_{1-1/2}}^{x_1+1/2} b(x, x_I) dx \\ 0 & S_2 \int_{x_{2-1/2}}^{x_2} b(x, x_2) dx - S_2 & \dots & S_I \int_{x_{2-1/2}}^{x_2+1/2} b(x, x_I) dx \\ \cdot & \cdot & \cdot & \cdot \\ 0 & 0 & \dots & S_I \int_{x_{I-1/2}}^{x_I} b(x, x_I) dx - S_I \end{bmatrix}.$$

The logarithmic matrix norm of $A = (a_{ij})_{I \times I}$ is given by

$$\begin{aligned} \tilde{\mu}_1(A) &= \max_{1 \leq j \leq I} \left(\operatorname{Re}(a_{jj}) + \sum_{i \neq j} |a_{ij}| \right) \\ &= \max_{1 \leq j \leq I} \left(S_j \left(\int_{x_{1-1/2}}^{x_j} b(x, x_j) dx - 1 \right) \right) \\ &= \max_{1 \leq j \leq I} (S_j (\overline{N}(x_j) - 1)) \\ &\leq \max_{1 \leq j \leq I} (S_j \overline{N}(x_j)) := \omega. \end{aligned} \quad (3.199)$$

Using the properties of logarithmic norm we get

$$\|e^{tA}\|_1 \leq e^{t\omega}. \quad (3.200)$$

It proves the stability of the scheme and therefore using Theorem 3.3.6 we get the second order convergence. The error bounds are given by

$$\|\epsilon(t)\|_1 = C_0 e^{\omega t} \Delta x^2 + \frac{C}{\omega} (e^{\omega t} - 1) \Delta x^2, \quad 0 \leq t \leq T, \quad (3.201)$$

with constants C and C_0 .

3.3.3 The Cell Average Technique

Finally we will investigate the convergence analysis of the cell average scheme. The cell average technique takes the following form

$$\frac{d\hat{N}_i}{dt} = \hat{B}_i^{\text{CA}} - \hat{D}_i. \quad (3.202)$$

where

$$\begin{aligned} \hat{B}_i^{\text{CA}} &= \hat{B}_{i-1} \lambda_i^- (\bar{v}_{i-1}) H(\bar{v}_{i-1} - x_{i-1}) + \hat{B}_i (\lambda_i^- (\bar{v}_i) H(x_i - \bar{v}_i) + \lambda_i^+ (\bar{v}_i) H(\bar{v}_i - x_i)) \\ &\quad + \hat{B}_{i+1} \lambda_i^+ (\bar{v}_{i+1}) H(x_{i+1} - \bar{v}_{i+1}). \end{aligned} \quad (3.203)$$

The terms \hat{B}_i and \hat{D}_i have been described in the previous section by equations (3.190) and (3.191) respectively.

Proposition 3.3.15. *The formulation (3.202) provides the total volume as a constant function of time. In other words the total volume remains constant with time. So we obtain conservation of mass*

$$\frac{d}{dt} \sum_{i=1}^I (x_i \hat{N}_i) = 0.$$

Proof. Multiplying x_i to equation (3.202) and summing over i , we obtain

$$\begin{aligned} \frac{d}{dt} \sum_{i=1}^I (\hat{N}_i x_i) &= \sum_{i=1}^I x_i \hat{B}_{i-1} \lambda_i^- (\bar{v}_{i-1}) H(\bar{v}_{i-1} - x_{i-1}) + \sum_{i=1}^I x_i \hat{B}_i [\lambda_i^- (\bar{v}_i) H(x_i - \bar{v}_i) + \\ &\quad \lambda_i^+ (\bar{v}_i) H(\bar{v}_i - x_i)] + \sum_{i=1}^I x_i \hat{B}_{i+1} \lambda_i^+ (\bar{v}_{i+1}) H(x_{i+1} - \bar{v}_{i+1}) - \sum_{i=1}^I x_i S_i \hat{N}_i \\ &= \sum_{i=1}^I \hat{B}_i \bar{v}_i - \sum_{i=1}^I x_i S_i \hat{N}_i \\ &= \sum_{i=1}^I \sum_{k=i}^I S_k \hat{N}_k \int_{x_{i-1/2}}^{p_k^i} x b(x, x_k) dx - \sum_{i=1}^I x_i S_i \hat{N}_i \\ &= \sum_{k=1}^I S_k \hat{N}_k \sum_{i=1}^k \int_{x_{i-1/2}}^{p_k^i} x b(x, x_k) dx - \sum_{i=1}^I x_i S_i \hat{N}_i. \end{aligned}$$

Using the property of the breakage function (2.36) we obtain

$$\frac{d}{dt} \sum_{i=1}^I (\hat{N}_i x_i) = \sum_{k=1}^I S_k \hat{N}_k x_k - \sum_{i=1}^I x_i S_i \hat{N}_i = 0.$$

This implies that the mass or total volume is conserved during the process. \square

Proposition 3.3.16. *Assuming that x_1 is the smallest particle size that can appear during the breakage, then for the cell average formulation (3.202) the total number is a increasing function of time; that is,*

$$\frac{d}{dt} \sum_{i=1}^I (\hat{N}_i) > 0. \quad (3.204)$$

Proof. The proof is analogous to the proof of the above proposition. It also follows from the proof of the Proposition 3.3.9. Finally we obtain the following expression

$$\frac{d}{dt} \sum_{i=1}^I (\hat{N}_i) = \sum_{i=2}^I S_i N_i (\bar{N}(x_i) - 1) > 0. \quad (3.205)$$

This is the required result. \square

Remark 3.3.17. *Once again, it should be emphasized that the integrals $\int_{x_{i-1/2}}^{p_k^i} x b(x, x_k) dx$ and respectively $\int_{x_{i-1/2}}^{p_k^i} b(x, x_k) dx$ in the formulation (3.202) must be computed exactly or approximated by a higher order scheme in order to ensure mass conservation.*

Now we consider an important lemma useful for further analysis.

Lemma 3.3.18. *Let $\Omega := [0, x_{\max}]$ and $\mathbb{R}_+ :=]0, +\infty[$. If $S(x)$, $n(t, x)$ and $b(x, y)$ are continuously differentiable functions in Ω , $\mathbb{R}_+ \times \Omega$ and $\Omega \times \Omega$ respectively. Then the following hold*

- (a) $S_{i\pm 1} = S_i + \mathcal{O}(\Delta x)$.
- (b) $N_{i\pm 1} = N_i + \mathcal{O}(\Delta x^2)$.
- (c) $b(x_{i\pm 1}, y_{i\pm 1}) = b(x_i, y_i) + \mathcal{O}(\Delta x)$.

Moreover,

$$S_{i\pm 1}N_{i\pm 1}b(x_{i\pm 1}, y_{i\pm 1}) = S_iN_ib(x_i, y_i) + \mathcal{O}(\Delta x).$$

Proof. Note that S_i is $S(x_i)$ and N_i is given by (1.1). The results (a) and (c) are trivial and can be proved simply by Taylor series expansion of $S(x_i \pm \Delta x)$ and $b(x_i \pm \Delta x, y_i \pm \Delta x)$. For (b), we have

$$N_{i\pm 1} - N_i = \int_{x_{i\pm 1} - \Delta x/2}^{x_{i\pm 1} + \Delta x/2} n(t, x) dx - \int_{x_i - \Delta x/2}^{x_i + \Delta x/2} n(t, x) dx.$$

Again Taylor series expansion and the midpoint rule produces

$$\begin{aligned} N_{i\pm 1} - N_i &= n(t, x_i)\Delta x + n'(t, x_i) \int_{x_{i\pm 1} - \Delta x/2}^{x_{i\pm 1} + \Delta x/2} (x - x_i) dx + \mathcal{O}(\Delta x^3) - n(t, x_i)\Delta x + \mathcal{O}(\Delta x^3) \\ &= \pm n'(t, x_i)\Delta x^2 + \mathcal{O}(\Delta x^3). \end{aligned}$$

Clearly, it gives

$$N_{i\pm 1} = N_i + \mathcal{O}(\Delta x^2).$$

Finally, it follows that

$$S_{i\pm 1}N_{i\pm 1}b(x_{i\pm 1}, y_{i\pm 1}) = S_iN_ib(x_i, y_i) + \mathcal{O}(\Delta x).$$

This completes the proof. □

Consistency

Clearly from the equation (3.191), the approximation of the death term in the cell average formulation (3.202) is third order accurate. We have to check the consistency order of the birth term. We simplify the birth term (3.203) by taking each term separately. Consider the first term without the Heaviside function $H(x)$ and substitute the λ from (3.8), we get

$$\lambda_i^-(\bar{v}_{i-1})\hat{B}_{i-1} = \frac{\bar{v}_{i-1} - x_{i-1}}{x_i - x_{i-1}}\hat{B}_{i-1} = \frac{1}{\Delta x} \left[\bar{v}_{i-1}\hat{B}_{i-1} - x_{i-1}\hat{B}_{i-1} \right]. \quad (3.206)$$

Note that, for notational convenience we are not using the subscript *break* in all formulations. Substituting the values of \hat{B}_{i-1} from (3.190) and \bar{v}_{i-1} from (3.30) into the preceding equation to get

$$\lambda_i^-(\bar{v}_{i-1})\hat{B}_{i-1} = \frac{1}{\Delta x} \left[\sum_{k=i-1}^I S_k N_k \int_{x_{i-3/2}}^{p_k^{i-1}} x b(x, x_k) dx - x_{i-1} \sum_{k=i-1}^I S_k N_k \int_{x_{i-3/2}}^{p_k^{i-1}} b(x, x_k) dx \right].$$

As stated before, p_k^{i-1} takes the value x_{i-1} for $k = i - 1$ and $x_{i-1/2}$ for $k > i - 1$. Now using the midpoint rule we obtain

$$\begin{aligned} \lambda_i^-(\bar{v}_{i-1})\hat{B}_{i-1} &= \frac{1}{\Delta x} \left[S_{i-1}N_{i-1}(x_{i-1} - \Delta x/4)b(x_{i-1} - \Delta x/4, x_{i-1})(\Delta x/2) \right. \\ &\quad + \left(\sum_{k=i}^I S_k N_k x_{i-1} b(x_{i-1}, x_k) \Delta x \right) - x_{i-1} S_{i-1} N_{i-1} b(x_{i-1} - \Delta x/4, x_{i-1})(\Delta x/2) \\ &\quad \left. + x_{i-1} \sum_{k=i}^I S_k N_k b(x_{i-1}, x_k) \Delta x + \mathcal{O}(\Delta x^3) \right]. \end{aligned}$$

After some simplifications, this gives

$$\lambda_i^-(\bar{v}_{i-1})\hat{B}_{i-1} = -\frac{\Delta x}{8} S_{i-1} N_{i-1} b(x_{i-1} - \Delta x/4, x_{i-1}) + \mathcal{O}(\Delta x^2). \quad (3.207)$$

We now consider the third term

$$\begin{aligned} \hat{B}_i \lambda_i^+(\bar{v}_i) &= \frac{\bar{v}_i - x_{i+1}}{x_i - x_{i+1}} \hat{B}_i \\ &= \frac{1}{\Delta x} \left[x_{i+1} \sum_{k=i}^I S_k N_k \int_{x_{i-1/2}}^{p_k^i} b(x, x_k) dx - \sum_{k=i}^I S_k N_k \int_{x_{i-1/2}}^{p_k^i} x b(x, x_k) dx \right]. \end{aligned}$$

Again, making use of the midpoint rule we obtain

$$\begin{aligned} \hat{B}_i \lambda_i^+(\bar{v}_i) &= \frac{1}{\Delta x} \left[x_{i+1} S_i N_i b(x_i - \Delta x/4, x_i)(\Delta x/2) + x_{i+1} \sum_{k=i+1}^I S_k N_k b(x_i, x_k) \Delta x \right. \\ &\quad \left. - S_i N_i (x_i - \Delta x/4) b(x_i - \Delta x/4, x_i)(\Delta x/2) + \sum_{k=i+1}^I S_k N_k x_i b(x_i, x_k) \Delta x + \mathcal{O}(\Delta x^3) \right]. \end{aligned}$$

This gives

$$\begin{aligned} \hat{B}_i \lambda_i^+(\bar{v}_i) &= \frac{1}{\Delta x} \left[h B_i + \frac{\Delta x^2}{8} S_i N_i b(x_i - \Delta x/4, x_i) \right] + \mathcal{O}(\Delta x^2) \\ &= \hat{B}_i + \frac{\Delta x}{8} S_i N_i b(x_i - \Delta x/4, x_i) + \mathcal{O}(\Delta x^2). \end{aligned} \quad (3.208)$$

Similarly, the remaining two terms can be approximated as

$$\hat{B}_i \lambda_i^-(\bar{v}_i) = \hat{B}_i - \frac{\Delta x}{8} S_i N_i b(x_i - \Delta x/4, x_i) + \mathcal{O}(\Delta x^2), \quad (3.209)$$

and

$$\lambda_i^+(\bar{v}_{i+1})\hat{B}_{i+1} = \frac{\Delta x}{8} S_{i+1} N_{i+1} b(x_{i+1} - \Delta x/4, x_{i+1}) + \mathcal{O}(\Delta x^2). \quad (3.210)$$

Now we simplify the birth term (3.203) for some particular values of \bar{v}_i . The definition (3.12) of $H(x)$ gives a total of $3^3 = 27$ different possibilities, depending on $x > 0$, $x = 0$, $x < 0$, in which the equation (3.203) can be further simplified. Now we consider some special cases which will give second order accuracy due to cancellation.

- **Cases 1-8.** If $\bar{v}_{i-1} \geq x_{i-1}$, $\bar{v}_i \geq x_i$ and $\bar{v}_{i+1} \geq x_{i+1}$.

In these cases the birth term reduces to

$$\hat{B}_i^{\text{CA}} = \hat{B}_{i-1} \lambda_i^- (\bar{v}_{i-1}) + \hat{B}_i \lambda_i^+ (\bar{v}_i). \quad (3.211)$$

After substituting the values on the right hand side from the equations (3.207) and (3.208), we obtain

$$\hat{B}_i^{\text{CA}} = \hat{B}_i + \frac{\Delta x}{8} [-S_{i-1} N_{i-1} b(x_{i-1} - \Delta x/4, x_{i-1}) + S_i N_i b(x_i - \Delta x/4, x_i)] + \mathcal{O}(\Delta x^2).$$

Now the application of the Lemma 3.3.18 provides

$$\begin{aligned} \hat{B}_i^{\text{CA}} &= \hat{B}_i + \frac{\Delta x}{8} [-S_i N_i b(x_i - \Delta x/4, x_i) + \mathcal{O}(\Delta x) + S_i N_i b(x_i - \Delta x/4, x_i)] + \mathcal{O}(\Delta x^2) \\ &= \hat{B}_i + \mathcal{O}(\Delta x^2). \end{aligned}$$

- **Cases 9-16.** If $\bar{v}_{i-1} \leq x_{i-1}$, $\bar{v}_i \leq x_i$ and $\bar{v}_{i+1} \leq x_{i+1}$.

In these cases clearly from equation (3.203) we have

$$\hat{B}_i^{\text{CA}} = \hat{B}_i \lambda_i^- (\bar{v}_i) + \hat{B}_{i+1} \lambda_i^+ (\bar{v}_{i+1}). \quad (3.212)$$

Again substitution from the equations (3.209) and (3.210) gives

$$\hat{B}_i^{\text{CA}} = \hat{B}_i + \frac{\Delta x}{8} [S_{i+1} N_{i+1} b(x_{i+1} - \Delta x/4, x_{i+1}) - S_i N_i b(x_i - \Delta x/4, x_i)] + \mathcal{O}(\Delta x^2).$$

Now Lemma 3.3.18 leads to

$$\begin{aligned} \hat{B}_i^{\text{CA}} &= \hat{B}_i + \frac{\Delta x}{8} [S_i N_i b(x_i - \Delta x/4, x_i) - S_i N_i b(x_i - \Delta x/4, x_i) + \mathcal{O}(\Delta x)] + \mathcal{O}(\Delta x^2) \\ &= \hat{B}_i + \mathcal{O}(\Delta x^2). \end{aligned}$$

- **Cases 17-20.** If $\bar{v}_{i-1} \leq x_{i-1}$, $\bar{v}_i = x_i$ and $\bar{v}_{i+1} \geq x_{i+1}$.

These cases give

$$\begin{aligned} \hat{B}_i^{\text{CA}} &= \frac{1}{2} \left(\hat{B}_i - \frac{\Delta x}{8} S_i N_i b(x_i - \Delta x/4, x_i) \right) \\ &\quad + \frac{1}{2} \left(\hat{B}_i + \frac{\Delta x}{8} S_i N_i b(x_i - \Delta x/4, x_i) \right) + \mathcal{O}(\Delta x^2) \\ &= \hat{B}_i + \mathcal{O}(\Delta x^2). \end{aligned}$$

- **Case 21.** If $\bar{v}_{i-1} > x_{i-1}$, $\bar{v}_i = x_i$ and $\bar{v}_{i+1} < x_{i+1}$.

Proceeding as before we get

$$\begin{aligned} \hat{B}_i^{\text{CA}} &= \hat{B}_i + \frac{\Delta x}{8} [-S_{i-1} N_{i-1} b(x_{i-1} - \Delta x/4, x_{i-1}) \\ &\quad + S_{i+1} N_{i+1} b(x_{i+1} - \Delta x/4, x_{i+1})] + \mathcal{O}(\Delta x^2) \\ &= \hat{B}_i + \mathcal{O}(\Delta x^2). \end{aligned}$$

Table 3.16: Cases which give second order convergence

Cases	Cell, $(i - 1)$	Cell, i	Cell, $(i + 1)$	Order
1 – 8	$\bar{v}_{i-1} \geq x_{i-1}$	$\bar{v}_i \geq x_i$	$\bar{v}_{i+1} \geq x_{i+1}$	$\mathcal{O}(\Delta x^2)$
9 – 16	$\bar{v}_{i-1} \leq x_{i-1}$	$\bar{v}_i \leq x_i$	$\bar{v}_{i+1} \leq x_{i+1}$	$\mathcal{O}(\Delta x^2)$
17 – 20	$\bar{v}_{i-1} \leq x_{i-1}$	$\bar{v}_i = x_i$	$\bar{v}_{i+1} \geq x_{i+1}$	$\mathcal{O}(\Delta x^2)$
21	$\bar{v}_{i-1} > x_{i-1}$	$\bar{v}_i = x_i$	$\bar{v}_{i+1} < x_{i+1}$	$\mathcal{O}(\Delta x^2)$

Table 3.17: Cases which give first order convergence

Cases	Cell, $(i - 1)$	Cell, i	Cell, $(i + 1)$	Order
22	$\bar{v}_{i-1} < x_{i-1}$	$\bar{v}_i < x_i$	$\bar{v}_{i+1} > x_{i+1}$	$\mathcal{O}(\Delta x)$
23	$\bar{v}_{i-1} < x_{i-1}$	$\bar{v}_i > x_i$	$\bar{v}_{i+1} > x_{i+1}$	$\mathcal{O}(\Delta x)$
24	$\bar{v}_{i-1} < x_{i-1}$	$\bar{v}_i > x_i$	$\bar{v}_{i+1} < x_{i+1}$	$\mathcal{O}(\Delta x)$
25	$\bar{v}_{i-1} > x_{i-1}$	$\bar{v}_i < x_i$	$\bar{v}_{i+1} > x_{i+1}$	$\mathcal{O}(\Delta x)$
26	$\bar{v}_{i-1} > x_{i-1}$	$\bar{v}_i < x_i$	$\bar{v}_{i+1} < x_{i+1}$	$\mathcal{O}(\Delta x)$
27	$\bar{v}_{i-1} > x_{i-1}$	$\bar{v}_i > x_i$	$\bar{v}_{i+1} < x_{i+1}$	$\mathcal{O}(\Delta x)$

In all other cases one has first order accuracy only, i.e.,

$$\hat{B}_i^{\text{CA}} = \hat{B}_i + \mathcal{O}(\Delta x). \quad (3.213)$$

All the cases have been summarized in Tables 3.16 and 3.17. The consistency order depends upon the problem. However, it has been found that in many relevant breakage problems it gives second order accuracy, see for example the test cases discussed in this chapter. Thus, we have

$$\|\sigma(t)\| = \mathcal{O}(\Delta x^p), \quad \text{uniformly for all } t. \quad (3.214)$$

where p is either 1 or 2.

Remark 3.3.19. For the case of a uniform breakage function $b(x, y) = 2/y$ (binary breakage) and a ternary breakage problem with breakage function $b(x, y) = \frac{6}{y} \left(1 - \frac{x}{y}\right)$, we have proved that $\bar{v}_i \leq x_i$, see equations (3.33) and (3.39). Due to the cases 9 – 16, we get second order accuracy for these problems.

Stability and convergence

The cell average formulation (3.202) can be rewritten in a simplified form as

$$\begin{aligned}
 \frac{d\hat{N}_i}{dt} &= \lambda_i^-(\bar{v}_{i-1})H(\bar{v}_{i-1} - x_{i-1}) \sum_{k=i-1}^I S_k \hat{N}_k \int_{x_{i-3/2}}^{p_k^{i-1}} b(x, x_k) dx \\
 &\quad + [\lambda_i^-(\bar{v}_i)H(x_i - \bar{v}_i) + \lambda_i^+(\bar{v}_i)H(\bar{v}_i - x_i)] \sum_{k=i}^I S_k \hat{N}_k \int_{x_{i-1/2}}^{p_k^i} b(x, x_k) dx \\
 &\quad + \lambda_i^+(\bar{v}_{i+1})H(x_{i+1} - \bar{v}_{i+1}) \sum_{k=i+1}^I S_k \hat{N}_k \int_{x_{i+1/2}}^{p_k^{i+1}} b(x, x_k) dx - S_i \hat{N}_i. \tag{3.215}
 \end{aligned}$$

For notational convenience, it can be rewritten in a more simplified form as

$$\frac{d\hat{N}_i}{dt} = a_{i-1}^1 \sum_{k=i-1}^I b_{i-1,k} \hat{N}_k + a_i^2 \sum_{k=i}^I b_{i,k} \hat{N}_k + a_{i+1}^3 \sum_{k=i+1}^I b_{i+1,k} \hat{N}_k - S_i \hat{N}_i. \tag{3.216}$$

Here for simplification we use the notation

$$b_{i,k} = S_k \int_{x_{i-1/2}}^{p_k^i} b(x, x_k) dx, \tag{3.217}$$

and the a_i^j are the coefficients of the respective terms in (3.215) given as

$$\begin{aligned}
 a_{i-1}^1 &= \lambda_i^-(\bar{v}_{i-1})H(\bar{v}_{i-1} - x_{i-1}) \\
 a_i^2 &= \lambda_i^-(\bar{v}_i)H(x_i - \bar{v}_i) + \lambda_i^+(\bar{v}_i)H(\bar{v}_i - x_i) \\
 a_{i+1}^3 &= \lambda_i^+(\bar{v}_{i+1})H(x_{i+1} - \bar{v}_{i+1}).
 \end{aligned}$$

We can also write the above system (3.216) in a matrix form (3.145) given below

$$\frac{d\hat{N}}{dt} = A\hat{N}, \quad \text{with } \hat{N} = [\hat{N}_1, \hat{N}_2, \dots, \hat{N}_I]^T. \tag{3.218}$$

Here the matrix A is given by

$$A = \begin{bmatrix} a_1^2 b_{1,1} - S_1 & a_1^2 b_{1,2} + a_2^3 b_{2,2} & \dots & a_1^2 b_{1,I} + a_2^3 b_{2,I} \\ a_1^1 b_{1,1} & a_1^1 b_{1,2} + a_2^2 b_{2,2} - S_2 & \dots & a_1^1 b_{1,I} + a_2^2 b_{2,I} + a_3^3 b_{3,I} \\ 0 & a_2^1 b_{2,2} & \dots & a_2^1 b_{2,I} + a_3^2 b_{3,I} + a_4^3 b_{4,I} \\ \vdots & & & \vdots \\ 0 & 0 & \dots & a_{I-1}^1 b_{I-1,I} + a_I^2 b_{I,I} - S_I \end{bmatrix}.$$

Similar to the previous cases, the logarithmic norm (3.141) of the matrix $A = (a_{ij})_{I \times I}$ is computed as

$$\tilde{\mu}_1(A) = \max_{1 \leq j \leq I} \left(\sum_{i=1}^I a_{ij} \right). \tag{3.219}$$

It is easy to show that the sum of column elements of the matrix A is given by

$$\sum_{i=1}^I a_{ij} = \underbrace{(a_1^1 + a_1^2)}_{=1} b_{1,j} + \underbrace{(a_2^1 + a_2^2 + a_2^3)}_{=1} b_{2,j} + \dots + \underbrace{(a_j^1 + a_j^2 + a_j^3)}_{=1} b_{j,j} - S_j. \quad (3.220)$$

It can be further simplified as

$$\begin{aligned} \sum_{i=1}^I a_{ij} &= \sum_{i=1}^j b_{i,j} - S_j \\ &= S_j \int_{x_1}^{x_j} b(x, x_j) dx - S_j. \end{aligned} \quad (3.221)$$

Now using the property (2.35) we get

$$\sum_{i=1}^I a_{ij} = S_j \bar{N}(x_j) - S_j. \quad (3.222)$$

Consequently, we obtain the following bounds from equations (3.219) and (3.222)

$$\begin{aligned} \tilde{\mu}_1(A) &= \max_{1 \leq j \leq I} (\bar{N}(x_j) - 1) S_j \\ &\leq \max_{1 \leq j \leq I} (\bar{N}(x_j) S_j) := \omega. \end{aligned} \quad (3.223)$$

Clearly from Theorem 3.3.4 we obtain the stability condition as

$$\|e^{tA}\|_1 \leq e^{\omega t}. \quad (3.224)$$

This shows that the cell average technique is stable and hence from Theorem 3.3.6 we have convergence of order p , with $p = 1$ or $p = 2$ according to our discussion above. The error bound followed by Theorem 3.3.6 is given as

$$\|\epsilon(t)\|_1 = C_0 e^{\omega t} \Delta x^p + \frac{C}{\omega} (e^{\omega t} - 1) \Delta x^p, \quad 0 \leq t \leq T, \quad (3.225)$$

with constants $C, C_0 > 0$.

Remark 3.3.20. *Note that all formulations considered in this section are positivity preserving. If $N_i(t)$ is zero then dN_i/dt is always positive due to the presence of the birth term only. If $N_i(t) \neq 0$ then a positive solution can always be obtained by choosing an appropriate time step.*

In summary, the fixed pivot technique being consistent with respect to the first two moments is clearly a first order scheme for breakage problems. On the other hand a direct approach which is consistent only with the zeroth moment gives second order convergence. It must be noted that the choice of representatives as midpoints of the cells leads to second order accuracy in the cell average method as well as in the direct approach. This is due to the fact that the application of the midpoint rule in both methods provides second order accuracy. Additionally, all schemes discussed here produce the same numerical results for the zeroth moment. The cell average technique, also consistent with the first two moments, provides second order accuracy in most of the cases.

3.4 The Finite Volume Scheme

We have seen in the previous chapter that Filbet and Laurençot [21] developed a finite volume scheme for the numerical solution of pure aggregation problems. For the application of the finite volume scheme they used a different form, a mass conservation law, of the population balance equation. They obtained remarkably good results. Therefore the objective here is to develop a similar approach for the numerical treatment of the pure breakage population balance equation. Furthermore, the aim is to apply the finite volume scheme for combined aggregation and breakage problems.

Here we present a new approach of solving the population balance equation using a finite volume method. A new form of breakage population balance equation is derived in order to apply the finite volume scheme effectively. Furthermore, a detailed comparison between discretized methods and finite volume methods has been made. The discretized methods predict certain moments of the population exactly independence of grid size while the accuracy of complete particle size distribution as well as its moments depends on grid size in finite volume scheme. The effectiveness of the methods have been demonstrated by several test problems where analytical solutions are available. Finally, it is concluded that the finite volume methods are good alternative for solving such problems. However, discretized methods are easy to implement and faster than the finite volume method

3.4.1 Pure Breakage

As mentioned before, a finite volume approach for solving population balance equations has been introduced by Filbet and Laurençot [21]. They took the advantage of conservative form of aggregation equation which was first introduced by Tanaka et al. [110]. We will follow Filbet and Laurençot [21] in order to introduced finite volume scheme for breakage equations.

A typical conservation law is given by the following equation

$$\frac{\partial n}{\partial t} + \frac{\partial F(n)}{\partial x} = 0, \tag{3.226}$$

where $n(x, t) \in \mathbb{R}$ is the unknown conservative variable and the function $F : \mathbb{R} \rightarrow \mathbb{R}$ is called flux function. Finite volume methods are a class of discretization schemes used to solve mainly conservation laws, see LeVeque [66]. Conservation laws describe many physical processes. It has been observed that many differential equations which we would like to solve come from conservation laws which are integrals over volumes. We discretize the space into small cells $\Lambda_j = [x_{j-1/2}, x_{j+1/2}]$, and time in discrete level t_m . The finite volume idea has been carried over to the discretization of such equations by instead of interpreting n_j^m as an approximation to a point value in a cell, i.g. $n(t_m, x_j)$, rather taking an approximation of the cell average of the solution on cell j and time t_m

$$n_j^m \sim \frac{1}{\Delta x} \int_{x_{j-1/2}}^{x_{j+1/2}} n(t_m, x) dx. \tag{3.227}$$

Integrating the conservation law on a cell in space-time $\Lambda_j \times [t_n, t_{m+1}]$ we obtain

$$n_j^{m+1} = n_j^m - \frac{\Delta t}{\Delta x} (F_{j+1/2} - F_{j-1/2}), \quad (3.228)$$

where $F_{j+1/2}$, called *numerical flux*, is an approximation of the flux function. We will apply this idea of finite volume scheme in the next section. Next we derive a new form of the breakage PBE and a finite volume scheme for solving the equation. Besides the derivation of the scheme we will investigate some properties of the solution. At the end numerical results will be validated with some analytically solvable test cases.

Breakage PBE as a mass conservation law

In a batch system the breakage process can be defined as the flow of mass from bigger particles to smaller particles and can be modeled by the following mass conservation law

$$\frac{\partial xn(x)}{\partial t} + \frac{\partial F(x)}{\partial x} = 0, \quad (3.229)$$

where $n(x)$ is the number density and $F(x)$ is the mass flux across mass x . Now the objective is to model the flux function F and to solve the preceding equation using the idea of finite volume schemes.

Furthermore, the kinetics of breakage are governed by two functions, the selection function $S(t, \epsilon)$, which describes the rate at which particles are selected to break and the breakage function, $b(t, \epsilon, u)$, which describes the sizes into which the selected particle breaks. The breakage function $b(t, \epsilon, u)$ is the probability density function for the formation of particles of size u from particle of size ϵ . The selection function $S(t, \epsilon)$ gives the death rate of particles of size ϵ as $n(t, \epsilon)S(t, \epsilon)$. Clearly this death results to the flow of mass towards smaller particles. So the total mass flux at x for $x < \epsilon$, resulting from this death is

$$- \int_0^x ub(\epsilon, u)S(\epsilon)n(\epsilon) du. \quad (3.230)$$

The negative sign appears due to the negative direction of mass flow. Considering all the breakage events which produce a flux at x , we obtain the mass flux $F(x)$ as

$$F(x) = - \int_x^\infty \int_0^x ub(\epsilon, u)S(\epsilon)n(\epsilon) du d\epsilon. \quad (3.231)$$

The equation (3.229) together with equation (3.231) is a mass conservation law for breakage process. It is easy to transform the equation (3.229) to standard form of number density population balance equation. The following steps show the transformation of this conservation laws to the standard population balance equation for breakage. Putting the value of $F(x)$ into equation (3.229), we get

$$\frac{\partial xn(x)}{\partial t} = \frac{\partial}{\partial x} \int_x^\infty \int_0^x ub(\epsilon, u)S(\epsilon)n(\epsilon) du d\epsilon. \quad (3.232)$$

Applying the Leibnitz integration rule, this gives

$$\begin{aligned} \frac{\partial xn(x)}{\partial t} &= \int_x^\infty \frac{\partial}{\partial x} \int_0^x ub(\epsilon, u)S(\epsilon)n(\epsilon) du d\epsilon - \int_0^x ub(x, u)S(x)n(x) du \\ &= \int_x^\infty xb(\epsilon, x)S(\epsilon)n(\epsilon) d\epsilon - S(x)n(x) \int_0^x ub(x, u) du. \end{aligned} \quad (3.233)$$

The last integral $\int_0^x ub(x, u) du$, the total volume of fragments formed, must be equal to the volume of the selected particle x i.e. $x = \int_0^x ub(x, u) du$. Now the equation (3.233) turns into the following well known breakage equation

$$\frac{\partial n(x)}{\partial t} = \int_x^\infty b(\epsilon, x)S(\epsilon)n(\epsilon) d\epsilon - S(x)n(x). \quad (3.234)$$

Numerical discretization

Similar to the finite volume discretization for aggregation discussed in Chapter 2 we get the following formulation

$$g_i^{m+1} = g_i^m - \frac{\Delta t}{\Delta x_i} (J_{i+1/2}^m - J_{i-1/2}^m), \quad (3.235)$$

where g_i^m denotes an approximation of the cell average of $g(t^m, x) = xn(t^m, x)$ on cell i at time t_m , and $J_{i+1/2}^m$ approximates the flux at the boundary of the cell. It is the so called numerical flux. The numerical flux may be approximated as follows

$$\begin{aligned} F(x_{i+1/2}) &= - \int_{x_{i+1/2}}^{x_I} \int_0^{x_{i+1/2}} ub(\epsilon, u)S(\epsilon)n(\epsilon) du d\epsilon \\ &= - \sum_{k=i+1}^I \int_{\Lambda_k} S(\epsilon)n(\epsilon) \int_0^{x_{i+1/2}} ub(\epsilon, u) du d\epsilon \\ &= - \sum_{k=i+1}^I g_k^m \int_{\Lambda_k} \frac{S(\epsilon)}{\epsilon} d\epsilon \int_0^{x_{i+1/2}} ub(x_k, u) du + \mathcal{O}(\Delta x^2) \\ &=: J_{i+1/2}^m + \mathcal{O}(\Delta x^2). \end{aligned} \quad (3.236)$$

The formulation (3.235) is used to calculate the particle mass density g_i^m at time t_m . The particle number density in our comparisons will then easily be calculated as

$$n_i^m = \frac{g_i^m}{x_i}. \quad (3.237)$$

Before we proceed to test the formulation we do some stability analysis.

Stability condition

It is necessary to investigate the stability of the proposed numerical formulation. The fundamental concept behind the stability is the preservation of the positivity and conservation of the mass. The formulation should preserve the positivity of the solution and conserve the mass. For the stability we have the following proposition.

Proposition 3.4.1. *Assuming that $x_{1/2}$ is the smallest particle that can appear during breakage i.e. the value of the integral $\int_0^{x_{1/2}} ub(x_k, u) du$, for all k is zero. Then, under the following CFL condition on the time step*

$$\Delta t \sup_i \left(\frac{1}{\Delta x_i} \int_{\Lambda_i} \frac{S(\epsilon)}{\epsilon} d\epsilon \int_0^{x_{i+1/2}} ub(x_i, u) du \right) \leq 1 \quad (3.238)$$

the function g is nonnegative i.e. $g_i^m \geq 0$ for all i and m . Furthermore, it satisfies the following conservative property

$$\sum_{i=1}^I \Delta x_i g_i^{m+1} = \sum_{i=1}^I \Delta x_i g_i^m. \quad (3.239)$$

Since we have $g_i^m \geq 0$ this is l^1 -stability.

Moreover, if $\phi : [0, +\infty[\rightarrow [0, +\infty[$ is a non-increasing function, then we have

$$\sum_{i=1}^I \Delta x_i \phi(x_i) g_i^{m+1} \geq \sum_{i=1}^I \Delta x_i \phi(x_i) g_i^m. \quad (3.240)$$

For instance, this implies increase of total number when taking $\phi(x) = 1/x$, which is an obvious property of pure breakage processes.

Proof. Let us assume that g_i^m is nonnegative and we will show that g_i^{m+1} is nonnegative. We consider the following equality

$$J_{i+1/2}^m = - \sum_{k=i+1}^I g_k^m A_i B_{i,k}, \quad (3.241)$$

where

$$A_i = \int_{\Lambda_k} \frac{S(\epsilon)}{\epsilon} d\epsilon, \quad B_{i,k} = \int_0^{x_{i+1/2}} ub(x_k, u) du. \quad (3.242)$$

We can rewrite the equation (3.241) as follow

$$\begin{aligned} J_{i+1/2}^m &= - \sum_{k=i}^I g_k^m A_i B_{i,k} + g_i^m A_i B_{i,i} \\ &= J_{i-1/2}^m + g_i^m A_i B_{i,i}. \end{aligned} \quad (3.243)$$

Here we make use of the stability condition (3.238), that is

$$A_i B_{i,i} \leq \frac{\Delta x_i}{\Delta t}. \quad (3.244)$$

Combining equations (3.243) and (3.244), we obtain

$$J_{i+1/2}^m - J_{i-1/2}^m \leq g_i^m \frac{\Delta x_i}{\Delta t}. \quad (3.245)$$

Now from equation (3.235) we have

$$g_i^{m+1} \geq g_i^m - g_i^m \frac{\Delta t}{\Delta x_i} \frac{\Delta x_i}{\Delta t}. \quad (3.246)$$

It gives

$$g_i^{m+1} \geq 0. \quad (3.247)$$

Multiplying Δx_i to equation (3.235) and summing over i gives

$$\sum_{i=1}^I \Delta x_i g_i^{m+1} = \sum_{i=1}^I \Delta x_i g_i^m - \Delta t \sum_{i=1}^I (J_{i+1/2}^m - J_{i-1/2}^m). \quad (3.248)$$

As a consequence of $\int_0^{x_{1/2}} ub(x_k, u) du = 0$, clearly the flux through the lower boundary of the first cell is zero i.e. $J_{1/2} = 0$. The preceding equation turns into the conservation property, the required result (3.239).

Furthermore, multiplying the equation (3.235) by a non-increasing function $\phi(x_i)$ as well as by Δx_i and summing over i , we get

$$\sum_{i=1}^I \Delta x_i \phi(x_i) g_i^{m+1} = \sum_{i=1}^I \Delta x_i \phi(x_i) g_i^m - \sum_{i=1}^I \Delta x_i \phi(x_i) \frac{\Delta t}{\Delta x_i} (J_{i+1/2}^m - J_{i-1/2}^m). \quad (3.249)$$

Again using the assumption that $J_{1/2} = 0$ and negativity of J , we obtain

$$\begin{aligned} \sum_{i=1}^I \Delta x_i \phi(x_i) g_i^{m+1} &= \sum_{i=1}^I \Delta x_i \phi(x_i) g_i^m - \Delta t \sum_{i=2}^I J_{i-1/2}^m (\phi(x_{i-1}) - \phi(x_i)) \\ &\geq \sum_{i=1}^I \Delta x_i \phi(x_i) g_i^m, \end{aligned} \quad (3.250)$$

and hence (3.240). □

Remark 3.4.2. *To fix the size of smallest particle during the breakage is physically relevant and it can be forced by the breakage function that particles smaller than the fixed smallest particle size do not appear during the process. If this is not the case then the numerical flux through the first boundary $x_{1/2}$ will not be zero and we may loose particles at the boundary of the first cell. Then the conservation property (3.239) takes the following form*

$$\sum_{i=1}^I \Delta x_i g_i^{m+1} \leq \sum_{i=1}^I \Delta x_i g_i^m, \quad (3.251)$$

and the inequality (3.240) may not hold in that case.

The integral appearing in the numerical flux function, i.e. the coefficients A_i and $B_{i,k}$ can be evaluated analytically in some simple cases otherwise a second order quadrature formula can be used to maintain second order accuracy of the numerical formulation.

We now start with the derivation of the semi-discrete form of the finite volume scheme (3.235). Using the fully discrete scheme (3.235), the semi-discrete approximation can be directly written as

$$\frac{dg_i(t)}{dt} = -\frac{1}{\Delta x_i}(J_{i+1/2} - J_{i-1/2}), \quad i = 1, 2, \dots, I. \quad (3.252)$$

where

$$J_{i+1/2} = -\sum_{k=i+1}^I g_k(t) \int_{\Lambda_k} \frac{S(\epsilon)}{\epsilon} d\epsilon \int_0^{x_{i+1/2}} ub(x_k, u) du. \quad (3.253)$$

The equation (3.252) can be rewritten in matrix form as

$$\frac{dg(t)}{dt} = Ag(t), \quad (3.254)$$

with $g = [g_1, g_2, \dots, g_I]$ and

$$A = \begin{bmatrix} \frac{1}{\Delta x_1} (d_{1,1-1/2}) & \frac{1}{\Delta x_1} (d_{2,1-1/2} - d_{2,1+1/2}) & \dots & \frac{1}{\Delta x_1} (d_{I,1-1/2} - d_{I,1+1/2}) \\ 0 & \frac{1}{\Delta x_2} (d_{2,2-1/2}) & \dots & \frac{1}{\Delta x_2} (d_{I,2-1/2} - d_{I,2+1/2}) \\ \cdot & \cdot & \cdot & \cdot \\ 0 & 0 & \dots & \frac{1}{\Delta x_I} (d_{I,I-1/2}) \end{bmatrix}.$$

For convenience we use

$$d_{k,i+1/2} = -\int_{\Lambda_k} \frac{S(\epsilon)}{\epsilon} d\epsilon \int_0^{x_{i+1/2}} ub(x_k, u) du.$$

In order to retain the overall high accuracy, the semi-discrete scheme (3.252) can be combined with any higher order time integration method. We have used the fourth order Runge-Kutta scheme, ODE45 in MATLAB. Before proceeding further to establish the consistency, stability and convergence of the scheme, we have the following proposition to show some characteristic features of the numerical solution.

Proposition 3.4.3. *The semi-discrete formulation (3.252) is mass conserving. Thus, we have*

$$\frac{d}{dt} \sum_i (\Delta x_i g_i(t)) = 0. \quad (3.255)$$

Furthermore, if $\phi : [0, +\infty[\rightarrow [0, +\infty[$ is a non-increasing function, then

$$\frac{d}{dt} \sum_i (\phi(x_i) \Delta x_i g_i(t)) \geq 0. \quad (3.256)$$

Proof. The volume conservation property (3.255) can easily be proved directly from the equation (3.252) by multiplying Δx_i and summing over i . Similarly, for the property (3.256), we multiply the equation (3.252) by $\phi(x_i) \Delta x_i$ and summing over i to get

$$\begin{aligned} \frac{d}{dt} \sum_i (\phi(x_i) \Delta x_i g_i(t)) &= -\sum_i \phi(x_i) (J_{i+1/2} - J_{i-1/2}) \\ &= -\sum_i \underbrace{J_{i-1/2}}_{\leq 0} \underbrace{(\phi(x_{i-1}) - \phi(x_i))}_{\geq 0} \geq 0. \end{aligned} \quad (3.257)$$

This proves the inequality (3.256). □

Consistency, stability and convergence

The consistency of the semi-discrete scheme (3.252) can easily be confirmed from the equation (3.236). It comes out from there that the numerical flux is second order accurate. Subsequently, we obtain for the spatial truncation error (3.137)

$$\|\sigma(t)\| = \mathcal{O}(\Delta x^2), \quad \text{uniformly for all } t. \quad (3.258)$$

In order to establish the stability of the scheme we now compute the logarithmic norm (3.141) of the matrix A as

$$\tilde{\mu}_1(A) = \max_j \left(\operatorname{Re}(a_{jj}) + \sum_{i \neq j} |a_{ij}| \right). \quad (3.259)$$

Since all elements of the matrix A are real and all non-diagonal elements are non-negative, the above logarithmic norm takes the following form

$$\tilde{\mu}_1(A) = \max_j \left(\sum_i a_{ij} \right). \quad (3.260)$$

Using the assumption that x_1 is the smallest size of particles that can appear in the breakage process, we can set $a_{k,1-1/2} = 0$ for all k . Then, it is easy to show that

$$\sum_i a_{ij} = \sum_{i=2}^j d_{j,i-1/2} \left(\frac{1}{\Delta x_j} - \frac{1}{\Delta x_{j-1}} \right). \quad (3.261)$$

We make an assumption that $\Delta x_1 \leq \Delta x_2 \leq \dots \leq \Delta x_I$. Then it follows that

$$\sum_i a_{ij} \leq 0, \quad (3.262)$$

and hence

$$\tilde{\mu}_1(A) \leq 0. \quad (3.263)$$

Consequently, Theorem (3.3.4) can be used to get

$$\|e^{tA}\| \leq 1, \quad (3.264)$$

which ensures the stability of the scheme. The error bound can be obtained by the application of Theorem 3.3.6 as

$$\|\epsilon(t)\| = C_0 \Delta x^2 + Ct \Delta x^2, \quad 0 \leq t \leq T, \quad (3.265)$$

with constants C_0 and C .

Table 3.18: EOC (3.53) of the finite volume scheme for binary breakage problems

(a) $S(x) = x, t = 1000$			(b) $S(x) = x^2, t = 2000$		
Grid points, I	Error, L_1	EOC	Grid points, I	Error, L_1	EOC
61	33.8559	-	61	0.8526	-
122	8.8548	1.93	122	0.2200	1.95
244	2.2363	1.98	244	0.0551	2.00
488	0.5612	1.99	488	0.0138	2.00

Comparison with exact solutions

In this section we compare our results obtained by the finite volume scheme with analytical results. We calculate the absolute error by the following expression

$$L_1 = \sum_i |(n_i^{\text{ana}} - n_i^{\text{num}}) \cdot \Delta x_i|. \tag{3.266}$$

Similar to Subsection 3.2.1, for the computation mono-disperse initial condition with size unity has been taken. Two types of problems have been considered:

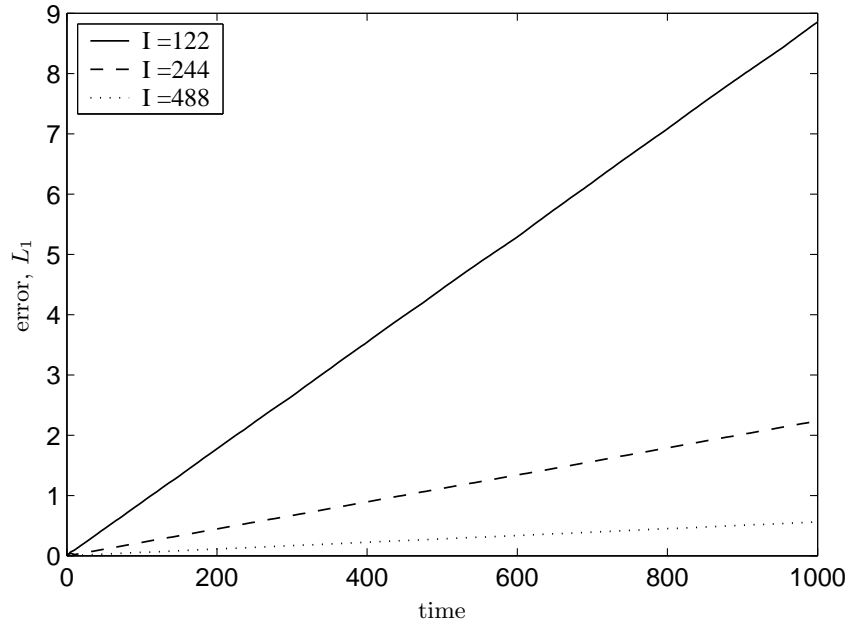
1. Binary breakage, $b(x, y) = 2/y$ with selection function, $S(x) = x$; and
2. Binary breakage, $b(x, y) = 2/y$ with selection function, $S(x) = x^2$.

The analytical solutions for both problems have been given in Appendix A.1. Figures 3.48(a) and 3.48(b) present the absolute error for the first and the second problems respectively. We have computed different numerical solutions using different number of grid points $I = 122, 244$ and 448. Figures show that the prediction by the numerical technique is in good agreement with the analytical results. The corresponding analysis for order of convergence has been summarized in Tables 3.18(a) and 3.18(b). Moreover, it can be seen from the figures and the tables that the numerical technique converges to the analytical results as the number of cells tends to a large value. Furthermore, the tables show that the scheme is second order accurate.

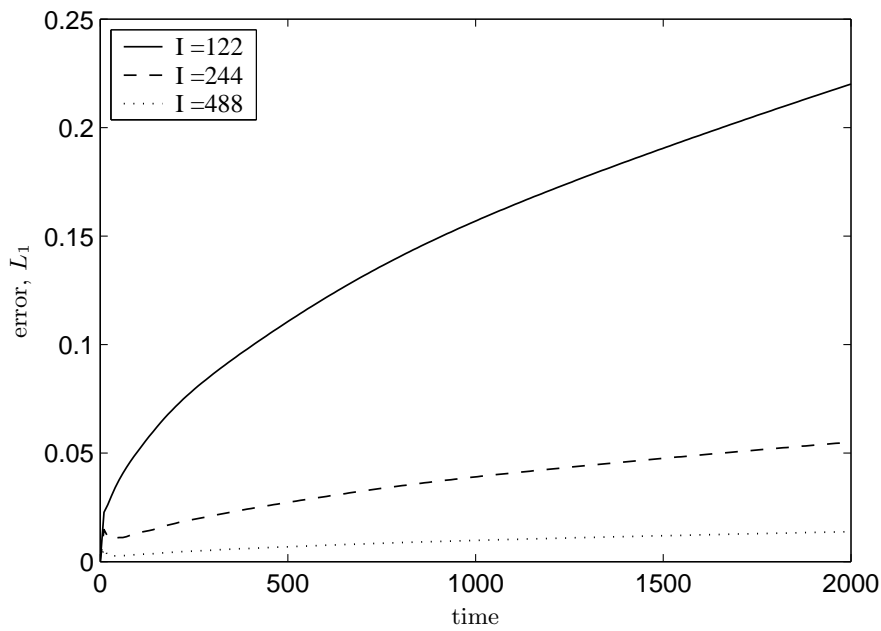
Discussion and comparison with the cell average technique

In this section we compare the numerical results obtained by discretized method and the finite volume method. The discretized methods are well known and widely used due to their simplicity and preserving properties. In this work we consider the cell average technique which predicts the zeroth and the first moments of the PSD exactly irrespective of the number of grid points chosen for the discretization.

We investigate the same test cases as above. The numerical results reflect the same behavior for each case and therefore we show here the comparisons for the first case only. We consider the binary breakage with mono-disperse particles of size unity as an initial condition and linear selection function. Figure 3.49 shows the absolute error in PSD with respect to grid points. The



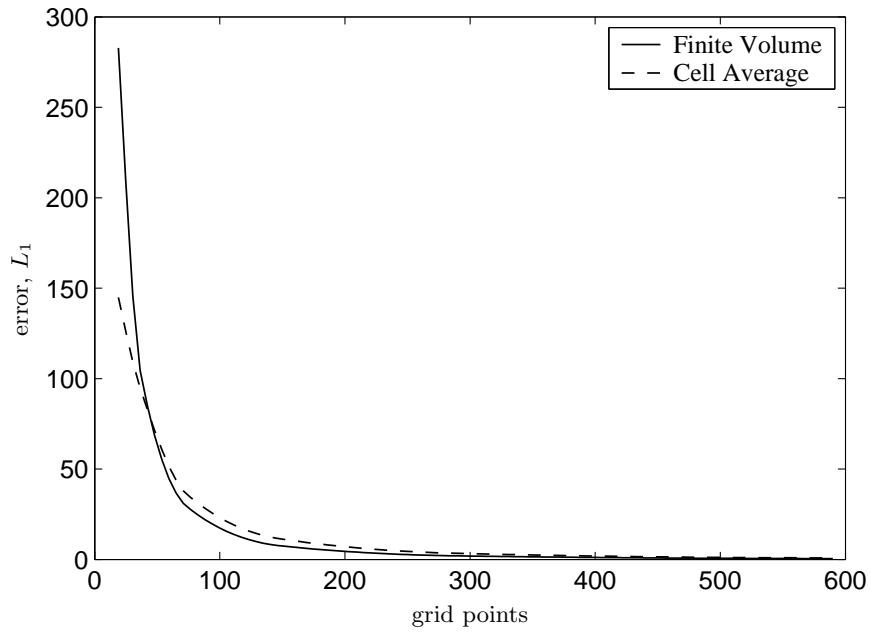
(a) $S(x) = x, t = 1000$.



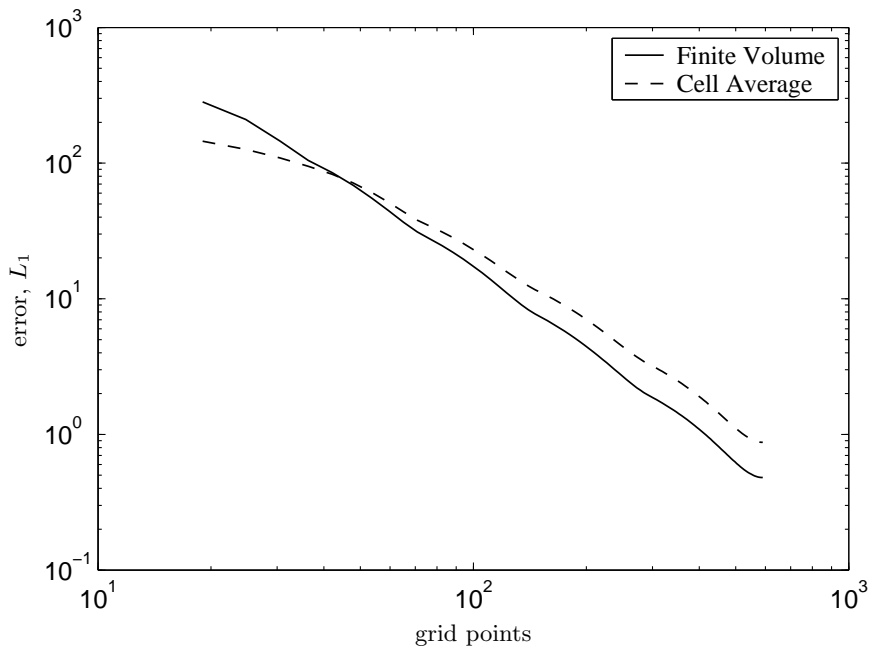
(b) $S(x) = x^2, t = 2000$.

Figure 3.48: Evolution of absolute error in binary breakage using the finite volume scheme.

3.4. THE FINITE VOLUME SCHEME

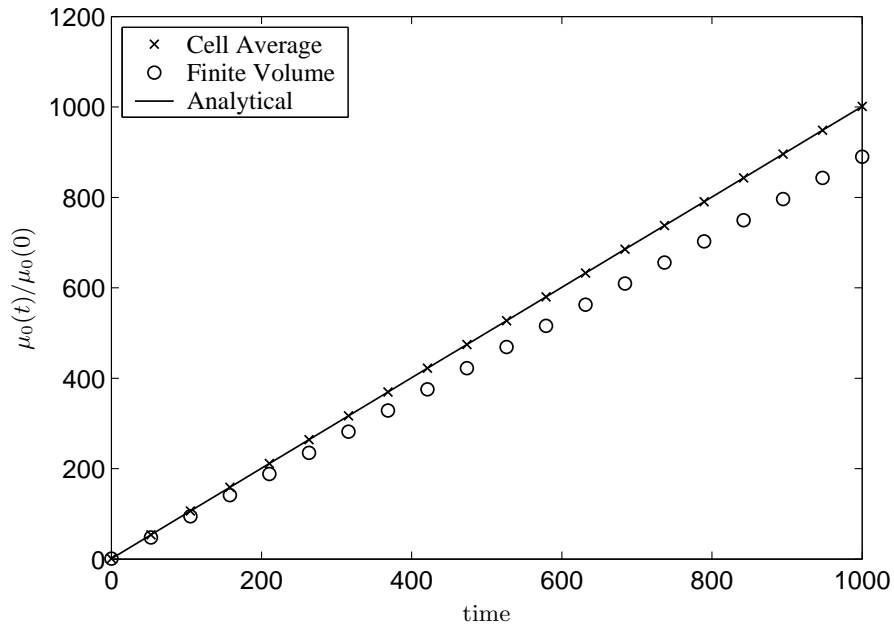


(a) Linear scale.

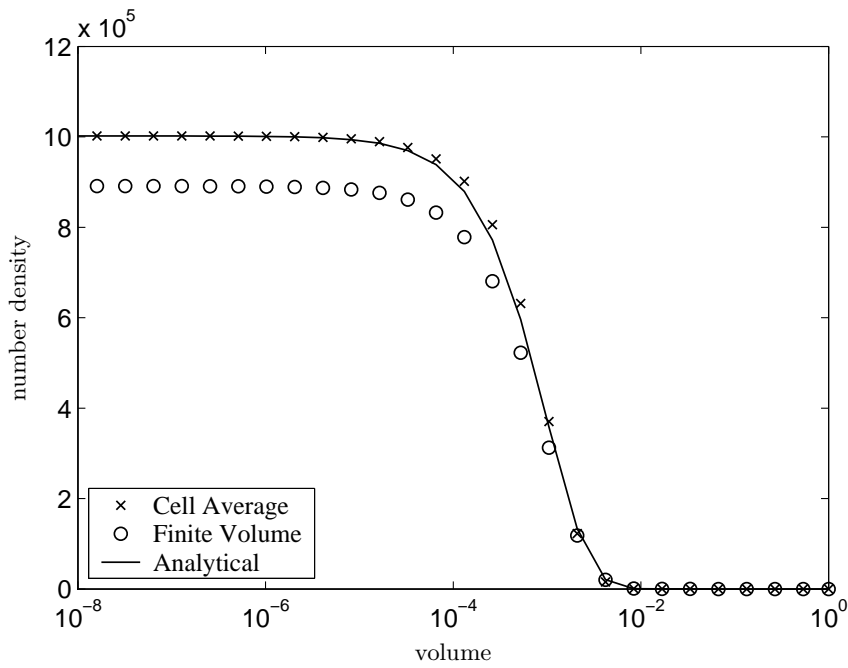


(b) Log scale.

Figure 3.49: Evolution of absolute error with number of grid points chosen for computation, $S(x) = x$, $t = 1000$.



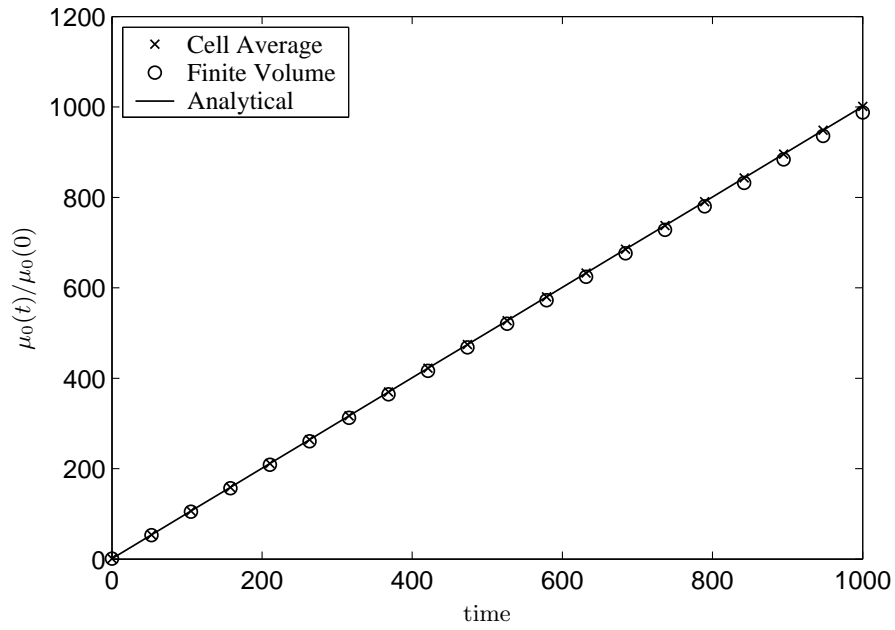
(a) First moment.



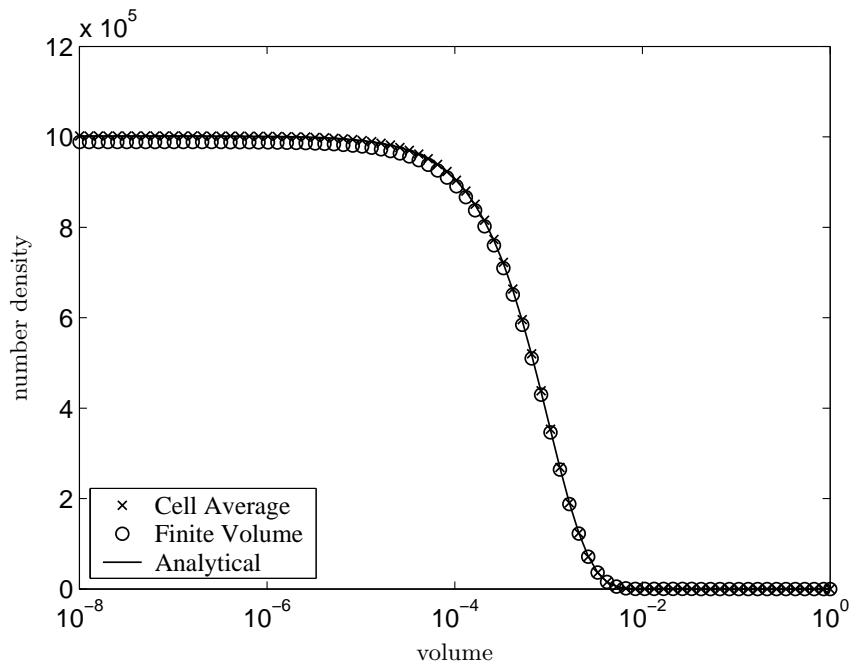
(b) Particle size distribution.

Figure 3.50: A comparison of numerical results, grid points = 31, $S(x) = x$, $t = 1000$.

3.4. THE FINITE VOLUME SCHEME



(a) First moment.



(b) Particle size distribution.

Figure 3.51: A comparison of numerical results, grid points = 91, $S(x) = x$, $t = 1000$.

grid refinement has been performed by dividing each section into two equal parts. As evident from the figure, the error is larger with the finite volume scheme at small number of grid points than the error with the cell average technique. But as we increase the number of grid points the prediction of PSD by the finite volume method becomes more accurate than the cell average technique.

Further comparison concerning the accuracy has been achieved by direct comparison of total number and particle number density in Figures 3.50(a) and 3.50(b) respectively. The computation has been performed by dividing the volume domain into 31 cells by the rule $x_{i+1/2} = 2x_{i+1/2}$. As expected, due to the preserving properties of the cell average technique, the prediction of the total number by the cell average technique is highly accurate while the prediction by the finite volume technique is poor. Figure 3.50(b) shows the under-prediction of the number density by the finite volume scheme for small volumes. It must be noted that the absolute error in PSD by the finite volume scheme was comparable or even less to the cell average technique, but the predictions of total number differ considerably. Figures 3.51(a) and 3.51(b) show the same results for the refined volume domain, $I = 91$. Even with such fine grids the prediction for the total number is poor with the finite volume scheme.

We conclude this section with the observation that the new numerical solution of a general breakage equation has been studied. For further treatment the population balance equation is first transformed to a mass conservation law which has a straightforward numerical solution using the finite volume scheme. It has been tested for two analytically solvable breakage problems. The numerical results obtained by the finite volume scheme have been compared with the cell average technique. It has been shown that the finite volume scheme predicts the PSD more accurately but the prediction of total number is quite poor.

3.4.2 Simultaneous Aggregation and Breakage

We have seen that the finite volume method can be applied to the numerical solution of pure breakage as well as pure aggregation problems. The detailed description of the scheme for pure aggregation problems can be found in Filbet and Laurençot [21]. A short overview has already been presented in the previous chapter. The finite volume scheme for simultaneous aggregation and breakage can be obtained easily by adding the corresponding numerical fluxes of the two processes. Analogous to pure breakage and pure aggregation cases, we get the following formulation in this case

$$g_i^{m+1} = g_i^m - \frac{\Delta t}{\Delta x_i} \left(J_{i+1/2}^m - J_{i-1/2}^m \right). \quad (3.267)$$

Here the numerical flux J is given by the algebraical sum of both individual fluxes as

$$\begin{aligned} J_{i+1/2}^m = & \sum_{k=1}^i \Delta x_k g_k^m \left(\sum_{j=\alpha_{i,k}}^I \int_{\Lambda_j} \frac{\beta(u, x_k)}{u} du g_j^n + \int_{x_{i+1/2}-x_k}^{x_{\alpha_{i,k}-1/2}} \frac{a(u, x_k)}{u} du g_{\alpha_{i,k}-1}^m \right) \\ & - \sum_{k=i+1}^I g_k^m \int_{\Lambda_k} \frac{S(\epsilon)}{\epsilon} d\epsilon \int_0^{x_{i+1/2}} ub(x_k, u) du. \end{aligned} \quad (3.268)$$

The first and the second terms on the right hand side are the numerical flux corresponding to the aggregation and the breakage respectively. Before we proceed to test the scheme for analytically solvable problems, it is necessary to get a stability condition on the time step. Let us first summarize the stability condition for the pure aggregation problem derived by Filbet and Laurençot [21] by the following proposition.

Proposition 3.4.4. *Pure aggregation (Filbet and Laurençot [21]): Under the stability condition on the time step*

$$\Delta t \sup_{i,m} \left(\int_{\delta}^{x_I} \frac{\beta(x_i, u)}{u} g(t^m, u) du \right) \leq 1, \quad (3.269)$$

where $\delta = \min(\Delta x_i/2; i = 1, \dots, I)$, the function g is nonnegative and its total volume is a non-increasing function of time; that is,

$$\sum_{i=1}^I \Delta x_i g_i^{m+1} \leq \sum_{i=1}^I \Delta x_i g_i^m, \quad \forall m. \quad (3.270)$$

Proof. See Filbet and Laurençot [21], Proposition 2.1. □

Note that the inequality (3.270) is only due to the loss of particles that are too large for our particle domain. By fixing the maximum size of the computational domain so that it does not loose any particles during the aggregation process we get the following corollary.

Corollary 3.4.5. *If we fix the computational domain bigger than or equal to the largest particle size that can appear during the aggregation process, then under the same stability condition (3.269) the monotonicity condition (3.270) becomes an equality. that is, we obtain conservation of mass*

$$\sum_{i=1}^I \Delta x_i g_i^{m+1} = \sum_{i=1}^I \Delta x_i g_i^m, \quad \forall m. \quad (3.271)$$

Proof. It easily follows from Proposition 3.4.1. The basic fact about the mass conservation equality (3.271) is that by fixing the computational domain to be big enough so that it contains all particles during the aggregation process without loosing mass. The numerical flux $J_{I+1/2}$ through the end boundary $x_{I+1/2}$ then becomes zero and therefore mass remains constant. □

Remark 3.4.6. *Theoretically, the biggest size of the particle during the batch aggregation process can easily be fixed from the initial condition. It cannot be bigger than the total volume of particles. In a limit case we may get a single particle of total volume at the end of the aggregation process.*

As a consequence of Propositions 3.4.1 and 3.4.4 we can derive the following proposition for the combined aggregation and breakage problem.

Proposition 3.4.7. *Simultaneous aggregation and breakage: Under the stability condition on the time step*

$$\Delta t \sup_{i,m} \left(\int_{\delta}^{x_I} \frac{\beta(x_i, u)}{u} g(t^m, u) du + \frac{1}{\Delta x_i} \int_{\Lambda_i} \frac{S(\epsilon)}{\epsilon} d\epsilon \int_0^{x_{i+1/2}} ub(x_i, u) du \right) \leq 1, \quad (3.272)$$

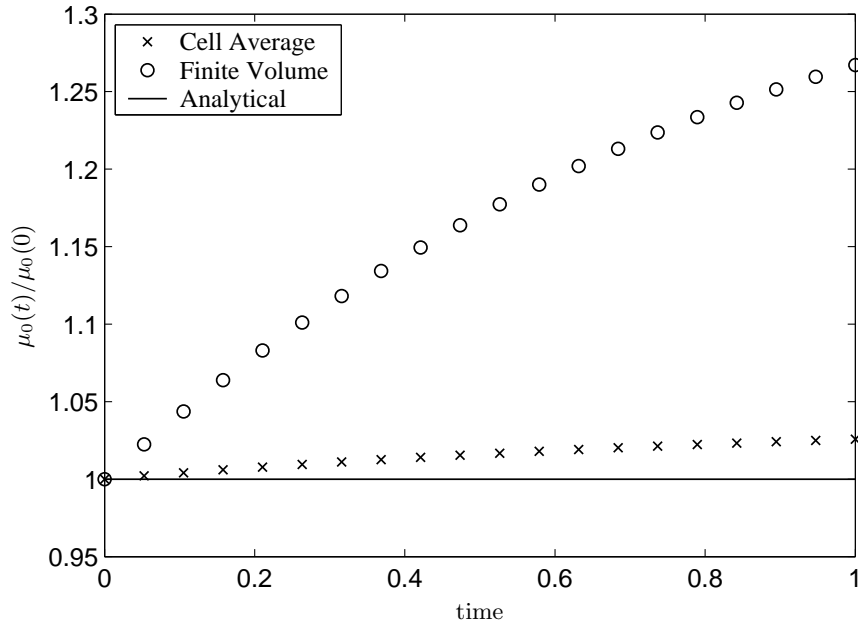


Figure 3.52: A comparison of the first moment for simultaneous breakage and aggregation, grid points 38.

and the assumption that the flux through the boundaries of the domain is zero, the function g is nonnegative and its total volume remains constant with time; that is,

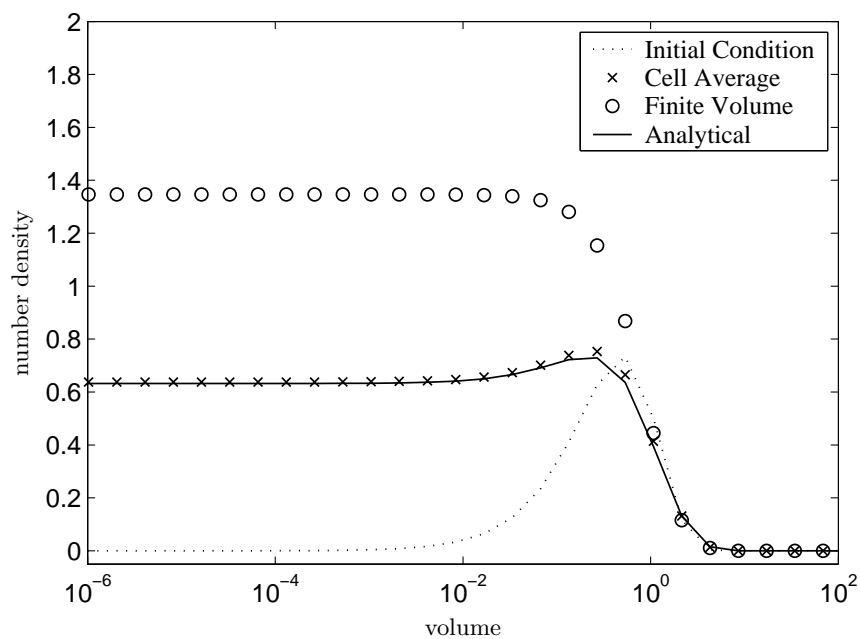
$$\sum_{i=1}^I \Delta x_i g_i^{m+1} = \sum_{i=1}^I \Delta x_i g_i^m, \quad \forall m. \tag{3.273}$$

Proof. See Appendix B.7. □

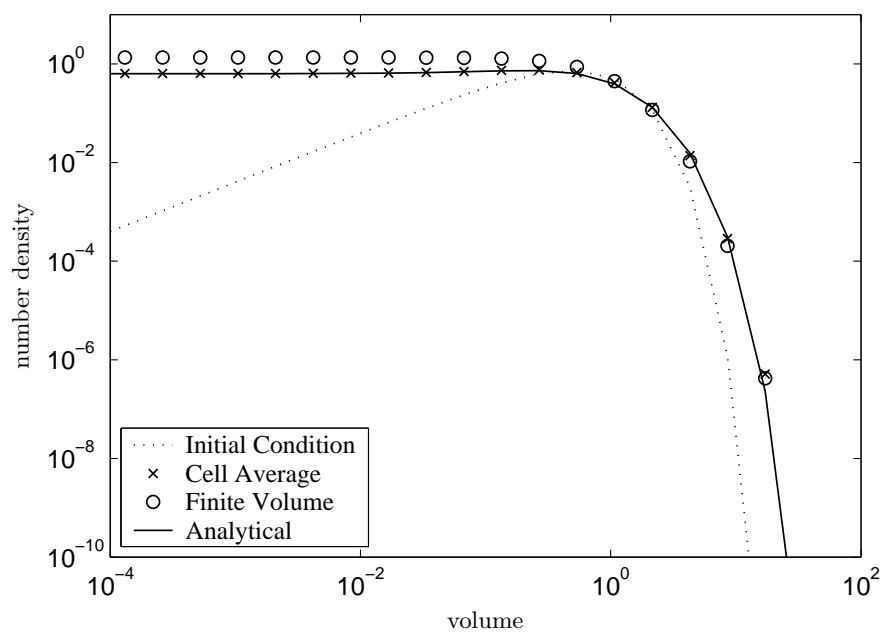
Numerical results

In order to test the numerical formulation derived above we take the same test cases with similar computational parameters as considered in Subsection 3.2.4. The initial conditions are (3.112) and (3.113). Here we have compared the zeroth moment additionally to check the consistency with respect to moments of the finite volume scheme. It must be noted that the first two moments remain constant in both test cases. The prediction of the first moment by both techniques is the same and it stays constant during the process.

The first test case is an unsteady state problem. The numerical results for the zeroth moments in this case are shown in Figure 3.52. As expected the zeroth moment by the cell average technique remains nearly constant. Due to numerical error in the initial condition, a little increase of the zeroth moment at the beginning by the cell average technique is observed and then it stays constant. On the other hand, the prediction of the zeroth moment by the finite volume scheme is extremely poor. The first moment is increasing with time. The prediction of the complete

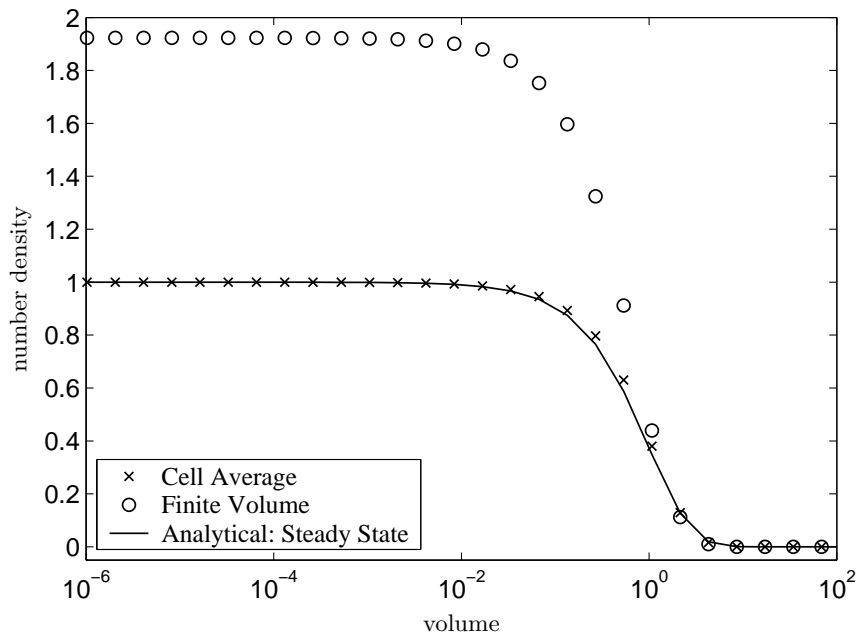


(a) Semi-log scale.

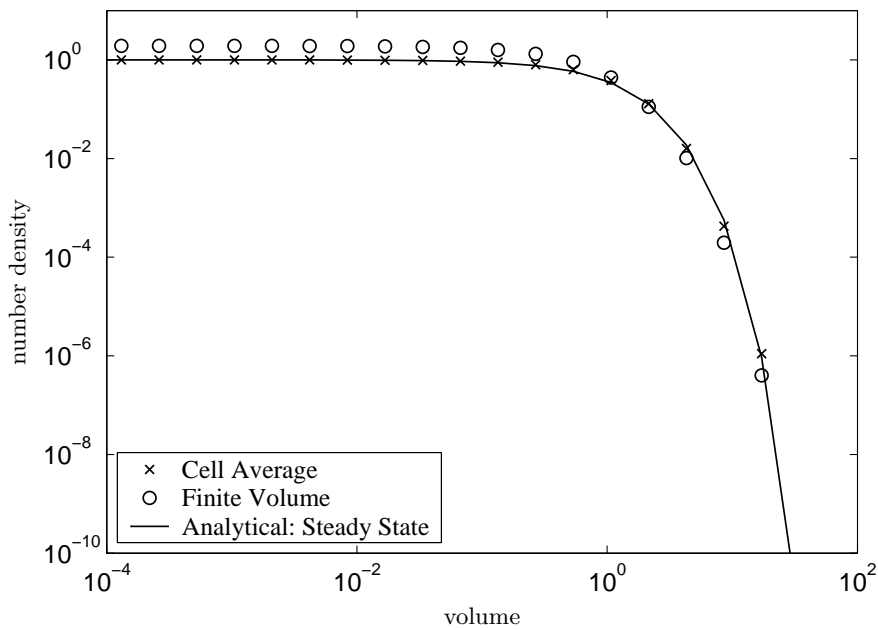


(b) Log-log scale.

Figure 3.53: A comparison of particle size distributions for simultaneous breakage and aggregation, grid points 38.



(a) Semi-log scale.



(b) Log-log scale.

Figure 3.54: A comparison of particle size distributions for simultaneous breakage and aggregation, grid points 38.

3.4. THE FINITE VOLUME SCHEME

particle size distribution is plotted in Figure 3.53. The numerical results by the finite volume scheme are overestimating at the smaller volumes while the cell average predicts them with high accuracy. The prediction of the number density at the larger volumes by both techniques is matching, see Figure 3.53(b). The computation has been performed for a very short time because after that it becomes a steady state solution and the numerical results are similar to the second test case shown in Figure 3.54.

The second test case is a steady state solution corresponding to the initial condition (3.113). The numerical results for the zeroth moment are exactly similar to the previous case presented in Figure 3.52. Once again, the prediction of the zeroth moment by the finite volume scheme is very poor. The complete particle size distribution calculated by both techniques together with the steady state solution is shown in Figure 3.54. Once again the numerical results for the number density by the finite volume scheme are over predicting while the prediction by the cell average technique is extremely accurate. The accuracy of the numerical results can of course be improved by refining the grid.

We conclude this section with the observation that the consistency of the cell average technique dominates over the finite volume scheme. Moreover the numerical results of the particle size distribution by the cell average technique using a coarse grid are more accurate than the finite volume scheme. More precisely, numerical results of the particle size distribution using a fine grid are comparable to that obtained by the cell average technique but the prediction of the total number by the finite volume scheme is quite poor. A more sophisticated finite volume formulation is needed to predict more moments of distribution accurately.

Chapter 4

New Numerical Methods: Multi-Dimensional

4.1 Introduction

In this chapter, we provide a general perspective of multi-dimensional population balances for pure aggregation problems and discretized methods to solve them. There are two reasons to consider the pure aggregation process. First, numerical methods for multi-dimensional aggregation problems are highly demanding and secondly that derivation of a numerical scheme for solving multi-dimensional aggregation problems is most difficult. The solution of a multi-dimensional problem is computationally highly expensive and therefore we will derive a numerical scheme for a two-dimensional PBE. Nevertheless, the idea of the numerical scheme could easily be extended to n -dimensional problems. Moreover, the same idea can be used to model a multi-dimensional problem for breakage. Furthermore there are two different approaches to deal with an n -dimensional PBE: computation on a reduced model and on a complete model. In contrast to the complete model we perform computations on a set of n one-dimensional PBEs in the reduced model approach. The computational time reduces drastically in the reduced model approach but it is not possible to capture the complete information of the particle property distribution (PPD). We will discuss both the approaches in detail.

Frequently the state of a dispersed phase is described in terms of extensive properties. Extensive properties, such as mass, mole number or enthalpy are defined as the properties which depend directly on the size of a thermodynamic system. If such a system is divided into several parts, the extensive property changes according to the size of these parts. It is often useful to give an extensive property in a form which is not directly proportional to the size of system, in other words to convert an extensive property into an intensive property. For certain applications it might be necessary to determine intensive properties of the disperse phase such as density, concentration or temperature. For example, to model the mass transfer between disperse and gas phase, the temperature of the disperse phase it is necessary to calculate the equilibrium state at the phase boundary. In general an intensive property is defined as the quotient of some extensive property with respect to another extensive property.

The traditional one-dimensional population balance models assume that granule size, usually volume, is the only independent granule property that influences the granule growth process. A

one-dimensional PBE for growth, agglomeration and breakage has been applied to numerous processes in chemical engineering such as crystallization, granulation and agglomeration, see Bramley et al. [12], Ding et al. [16]. However several other independent granule properties can strongly influence granulation behavior. Such properties include porosity, binder content, enthalpy and compositions etc. For a more general case of liquid spray granulation, one-dimensional population balance models can be found, see e.g. Saleh et al. [98]. As mentioned before, the impact of operating conditions on the particle property distribution has been investigated by various authors, Adetayo et al. [2], Watano et al. [119], Schaafsma [100]. Watano et al. [119] observed that the moisture content in solids is one of the most important particle properties to control the agglomeration process. This again leads to the conclusion that properties such as particle size and moisture content have to be considered simultaneously in a population balance model.

An application of a multi-dimensional PBE appears from simultaneous agglomeration and drying in fluidized bed granulation, see Peglow et al. [84]. Since the kinetics for heat and mass transfer require the temperature and moisture content of particles, one needs to extend the vector of internal coordinates. The concept of population balance cannot be applied to any intensive property of the solid phase. Thus, the intensive properties of solid phase have been expressed in terms of adequate extensive properties: the enthalpy of particles and the liquid mass of particles.

Iveson [40] presented a four dimensional population balance model for wet granulation which includes size, porosity, binder content and compositions as four independent granule properties. He also mentioned the limitations of spatially uniform conditions of a one-dimensional population balance model. Segregation is a common problem in many commercial granulators. It may alter the frequency and velocity of collisions between granules of different sizes. Therefore this effect needs to be modeled either by spatially dependent PBEs or by calculating a global average collision frequency between different sized granules. In addition to wet granulation, two-dimensional PBEs have been applied in various other areas including modeling the coagulation and structural rearrangement of sintering aerosol particles, Xiong and Pratsinis [123] as well as tracking the growth of crystals with anisotropic growth rates of different faces, Puel et al. [92].

An n -dimensional particle property distribution is defined by $f(x_1, x_2, \dots, x_n)$, where n independent granule characteristics are denoted by x_1, x_2, \dots, x_n . Assuming spatially uniform conditions throughout the system, an n -dimensional PBE for binary aggregation can be formulated as

$$\frac{\partial f(x_1, x_2, \dots, x_n)}{\partial t} = B_{\text{agg}}(x_1, x_2, \dots, x_n) - D_{\text{agg}}(x_1, x_2, \dots, x_n). \quad (4.1)$$

The first term on the right hand side is corresponding to the birth of particles of property (x_1, x_2, \dots, x_n) due to aggregation of smaller particles. The last term describes the death of particles of property (x_1, x_2, \dots, x_n) due to collision and adhesion to other particles in the system. These are given by

$$B_{\text{agg}} = \frac{1}{2} \int_{\epsilon_1=0}^{m_1} \dots \int_{\epsilon_n=0}^{m_n} \hat{\beta}(\epsilon_1, \eta_1, \dots, \epsilon_n, \eta_n) f(\epsilon_1, \dots, \epsilon_n) f(\eta_1, \dots, \eta_n) d\epsilon_1 \dots d\epsilon_n, \quad (4.2)$$

with

$$\eta_i = \eta_i(\epsilon_1, x_1, \dots, \epsilon_n, x_n), \quad i = 1, 2, \dots, n, \quad (4.3)$$

and

$$D_{\text{agg}} = f(x_1, \dots, x_n) \int_{\epsilon_1=0}^{w_1} \dots \int_{\epsilon_n=0}^{w_n} \hat{\beta}(\epsilon_1, x_1, \dots, \epsilon_n, x_n) f(\epsilon_1, \dots, \epsilon_n) d\epsilon_1 \dots d\epsilon_n. \quad (4.4)$$

The aggregation kernel of a multi-dimensional PBE is denoted by $\hat{\beta}$. The birth term describes all the possible aggregation events that form a particle with properties x_1, x_2, \dots, x_n . Similarly death term represents all possible collisions that form an aggregate with particles of size x_1, x_2, \dots, x_n . In the preceding multi-dimensional balance equation limits of integration will change according to the particles properties and the way of defining them in a particular model. Before we propose a numerical scheme to solve such equations we mention some examples of multi-dimensional PBE.

Application 1: Wet granulation of a binary mixture of two solids

Iveson [40] modeled a four-dimensional PBE for wet granulation of a binary mixture of solids "a" and "b". As mentioned above he considered four independent granule characteristics: The granule solid phase mass m , the binder to solid mass ratio w , the granule porosity ϵ , the solid mass phase fraction of component "a" x . The birth term takes the following form

$$B_{\text{agg}}(m, \epsilon, w, x) = \frac{1}{2} \int_{m_1=0}^m \int_{w_1=0}^\infty \int_{\epsilon_1=0}^1 \int_{x_1=0}^1 \hat{\beta}(m_1, m_2, w_1, w_2, \epsilon_1, \epsilon_2, x_1, x_2) \\ \times f(m_1, w_1, \epsilon_1, x_1) f(m_2, w_2, \epsilon_2, x_2) dm_1 dw_1 d\epsilon_1 dx_1, \quad (4.5)$$

with the following additional conservation equations

$$m_2 = m - m_1, \\ w_2 = \frac{wm - w_1m_1}{m_2}, \\ x_2 = \frac{xm - x_1m_1}{m_2},$$

and

$$\left(\frac{\epsilon}{1-\epsilon} \right) \left(\frac{mx}{\rho_a} + \frac{m(1-x)}{\rho_b} \right) \\ = \left(\frac{\epsilon_1}{1-\epsilon_1} \right) \left(\frac{m_1x_1}{\rho_a} + \frac{m_1(1-x_1)}{\rho_b} \right) + \left(\frac{\epsilon_2}{1-\epsilon_2} \right) \left(\frac{m_2x_2}{\rho_a} + \frac{m_2(1-x_2)}{\rho_b} \right).$$

The death rate is given by

$$D_{\text{agg}}(m, \epsilon, w, x) = f(m, w, \epsilon, x) \int_{m_1=0}^\infty \int_{w_1=0}^\infty \int_{\epsilon_1=0}^1 \int_{x_1=0}^1 \hat{\beta}(m_1, m, w_1, w, \epsilon_1, \epsilon, x_1, x) \\ \times f(m_1, w_1, \epsilon_1, x_1) dm_1 dw_1 d\epsilon_1 dx_1. \quad (4.6)$$

The PBE associated with these four dimensional birth and death terms becomes very complex to solve numerically.

Application 2: Simultaneous agglomeration and drying in fluidized beds

A multidimensional PBE used for modeling of simultaneous agglomeration and drying in fluidized beds is now presented. For such processes, the enthalpy, moisture content and size are of special interest. For a detailed description readers are referred to Peglow et al. [84] as well as Peglow [82]. In this case particle property density f depends on mass of granule v , moisture content within granule $c \in]0, v[$ and enthalpy of granule h . A three-dimensional PBE with aggregation only has been derived. The birth and death terms are given as

$$B_{\text{agg}}(v, c, h) = \frac{1}{2} \int_{\epsilon=0}^v \int_{\gamma=\max(0, c-v+\epsilon)}^{\min(c, \epsilon)} \int_{\eta=0}^h \hat{\beta}(v - \epsilon, \epsilon, c - \gamma, \gamma, h - \eta) f(t, v - \epsilon, c - \gamma, h - \eta) f(t, \epsilon, \gamma, \eta) d\eta d\gamma d\epsilon, \quad (4.7)$$

and

$$D_{\text{agg}}(v, c, h) = \int_{\epsilon=0}^{\infty} \int_{\gamma=0}^{\epsilon} \int_{\eta=0}^{\infty} \hat{\beta}(v, \epsilon, c, \gamma, h, \eta) f(t, v, c, h) f(t, \epsilon, \gamma, \eta) d\eta d\gamma d\epsilon. \quad (4.8)$$

The appearance of complicated integral limits in second integral of birth term will be explained later. They appear due to the fact that the moisture content of one of the aggregating particles can not be bigger than the mass (volume) of the newborn granule and also cannot be smaller than $c - v + \epsilon$ to produce a particle of size v and moisture content c .

Application 3: Tracer studies of high shear granulation

Similar to the previous case, Hounslow et al. [33] applied a two-dimensional PBE to study the tracer mass distribution in a high shear granulation. They considered that every granule is identified by two distinct properties: the size of granule and the mass of tracer within the granule. The associated birth and death terms in this case are

$$B_{\text{agg}}(v, c) = \frac{1}{2} \int_{\epsilon=0}^v \int_{\gamma=\max(0, c-v+\epsilon)}^{\min(c, \epsilon)} \hat{\beta}(v - \epsilon, \epsilon, c - \gamma, \gamma) f(v - \epsilon, c - \gamma) f(\epsilon, \gamma) d\gamma d\epsilon, \quad (4.9)$$

and

$$D_{\text{agg}}(v, c) = \int_{\epsilon=0}^{\infty} \int_{\gamma=0}^{\epsilon} \hat{\beta}(v, \epsilon, c, \gamma) f(v, c) f(\epsilon, \gamma) d\gamma d\epsilon. \quad (4.10)$$

In order to solve PBEs associated with these birth and death terms Hounslow et al. [33] reduced the PBE to a set of two one-dimensional PBEs. They also proposed a solution strategy to solve the resulting coupled equations. We will explain the procedure to reduce the model and then propose a better scheme to solve them in a next section.

Application 4: Coagulation of a two component mixture

Lushnikov [70] investigated coagulation of a two component mixture. Let $f(m, n)$ be the concentration of the particles consisting of m and n monomers of the first and the second kind respectively. Then the governing birth and death terms are given by

$$B_{\text{agg}}(m, n) = \frac{1}{2} \int_{\epsilon=0}^m \int_{\gamma=0}^n \hat{\beta}(m - \epsilon, \epsilon, n - \gamma, \gamma) f(m - \epsilon, n - \gamma) f(\epsilon, \gamma) d\gamma d\epsilon, \quad (4.11)$$

and

$$D_{\text{agg}}(m, n) = \int_{\epsilon=0}^{\infty} \int_{\gamma=0}^{\infty} \hat{\beta}(m, \epsilon, n, \gamma) f(m, n) f(\epsilon, \gamma) d\gamma d\epsilon. \quad (4.12)$$

Lushnikov [70] also presented analytical solutions for some simple aggregation kernels. Those analytical solutions are useful to assess the efficiency of numerical schemes.

Below we propose a numerical scheme for the solutions of a multi-dimensional PBE. As mentioned before we will investigate numerical methods on two major classes of multi-dimensional PBE: reduced models and complete models. The reduced model is based on a reduction of a complete n -dimensional population balance to a set of n one-dimensional PBEs. Model reduction is done to get an approximation of some average values at low computational cost. On the other hand a complete model provides the entire property distribution at a very high computational cost.

4.2 Reduced Model

This section is devoted to the modeling of reduced system of PBEs and their numerical solutions. For convenience we consider here a two-dimensional PBE to show the procedure of model reduction. However the same procedure can be applied for any higher dimensional system. The same holds for numerical procedure. We will test our numerical scheme on a two-dimensional PBE due to easily available analytical solutions.

4.2.1 Mathematical Modeling

A two-dimensional particle property distribution is defined as $f(t, v, c)$, where v and c are two distinct properties, granule volume (size) and tracer volume respectively. Thus, the total number in a domain D is given by

$$\int_D f(t, v, c) dv dc. \quad (4.13)$$

It should be noted that granule volume v contains volume of tracer and volume of particles, that is, $c \leq v$. The two-dimensional PBE can be obtained by extending the classical one-dimensional PBE [36] to two-dimensional space as

$$\begin{aligned} \frac{\partial f(t, v, c)}{\partial t} = & \frac{1}{2} \int_0^v \int_{\max(0, c-v+\epsilon)}^{\min(c, \epsilon)} \hat{\beta}(t, v - \epsilon, \epsilon, c - \gamma, \gamma) f(t, v - \epsilon, c - \gamma) f(t, \epsilon, \gamma) d\gamma d\epsilon \\ & - \int_0^{\infty} \int_0^{\epsilon} \hat{\beta}(t, v, \epsilon, c, \gamma) f(t, v, c) f(t, \epsilon, \gamma) d\gamma d\epsilon. \end{aligned} \quad (4.14)$$

The limits of the second integral in the birth term can easily be explained. Note that the first aggregating particle has volume $v - \epsilon$ and tracer contents $c - \gamma$. Therefore it is evident from the definition of tracer mass that

$$c - \gamma \leq v - \epsilon \Rightarrow \gamma \geq c - v + \epsilon,$$

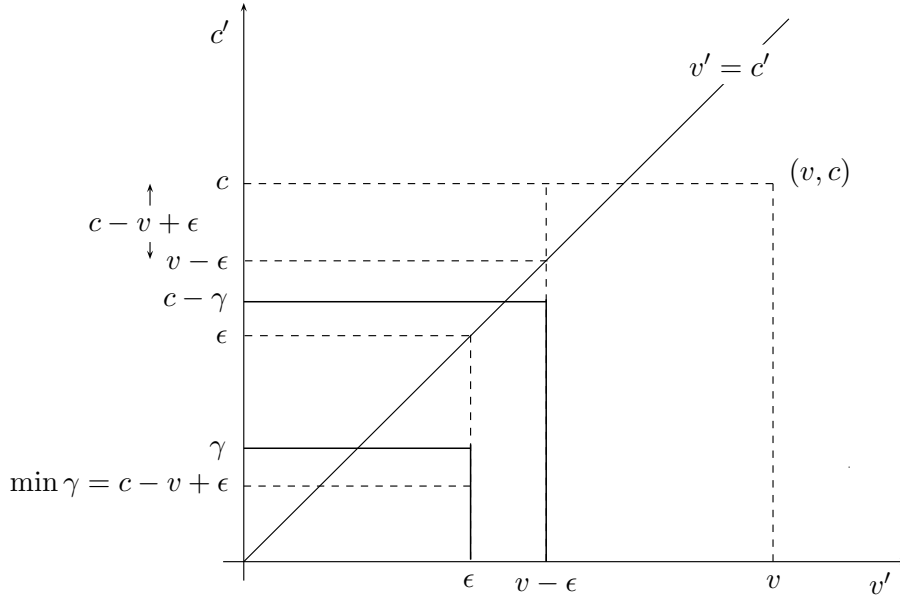


Figure 4.1: Limits of integrals in 2-D PBE.

and obviously

$$\gamma \geq 0.$$

These two bounds give the lower limits. Similarly the second set of aggregation particles have volume ϵ and tracer contents γ . Clearly the following relation holds

$$\gamma \leq \epsilon.$$

Since the resultant aggregate has tracer content c , therefore

$$\gamma \leq c.$$

These relations provides the upper integral limits. The limits of integration can also be perceived from Figure 4.1. The above 2-D PBE (4.14) must be supplemented with an initial condition

$$f(0, v, c) = f_0(v, c). \quad (4.15)$$

The first and the second terms on the right hand side of the equation (4.14) account for the formation and the loss of the particles with the properties v and c . Let us assume that the aggregation kernel $\hat{\beta}$ depends only on time and size of the granules, but not on the tracer contents within the granules, i.e. $\hat{\beta} = \hat{\beta}(t, v, \epsilon)$. Then the 2-D PBE can be converted into two 1-D PBEs corresponding to the conventional number density $n(t, v)$ and mass of tracer within granules $m(t, v)$. The number density $n(t, v)$, may be obtained from f by integrating over all possible tracer masses

$$n(t, v) = \int_0^v f(t, v, c) dc. \quad (4.16)$$

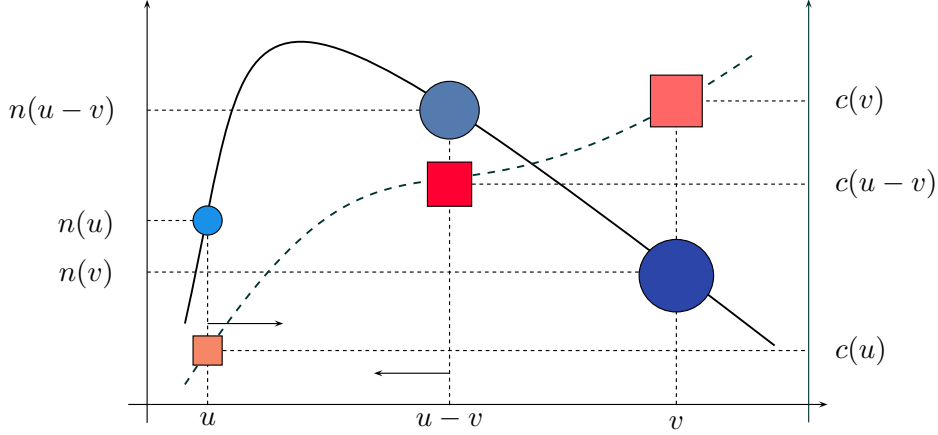


Figure 4.2: Birth of tracer mass.

The mass of tracer within the granules of size v is given analogously by

$$m(t, v) = \int_0^v cf(t, v, c) dc. \quad (4.17)$$

Reduction to 1-D PBE for granule size distribution (GSD)

Integrating the equation (4.14) over all possible values of c , we have

$$\begin{aligned} \frac{\partial n(t, v)}{\partial t} &= \frac{1}{2} \int_0^v \int_0^v \int_{\max(0, c-v+\epsilon)}^{\min(c, \epsilon)} \hat{\beta}(t, v - \epsilon, \epsilon, c - \gamma, \gamma) f(t, v - \epsilon, c - \gamma) f(t, \epsilon, \gamma) d\gamma d\epsilon dc \\ &\quad - \int_0^v \int_0^\infty \int_0^\epsilon \hat{\beta}(t, v, \epsilon, c, \gamma) f(t, v, c) f(t, \epsilon, \gamma) d\gamma d\epsilon dc. \end{aligned} \quad (4.18)$$

Reversing the order of integration, we obtain

$$\begin{aligned} \frac{\partial n(t, v)}{\partial t} &= \frac{1}{2} \int_0^v \int_0^\epsilon \int_\gamma^{v-\epsilon+\gamma} \hat{\beta}(t, v - \epsilon, \epsilon, c - \gamma, \gamma) f(t, v - \epsilon, c - \gamma) f(t, \epsilon, \gamma) dc d\gamma d\epsilon \\ &\quad - \int_0^\infty \int_0^\epsilon \int_0^v \hat{\beta}(t, v, \epsilon, c, \gamma) f(t, v, c) f(t, \epsilon, \gamma) dc d\gamma d\epsilon. \end{aligned} \quad (4.19)$$

If we assume that the aggregation kernel depends only on time and the size of both granules, i.e. $\hat{\beta}(t, v, \epsilon, c, \gamma) = \beta(t, v, \epsilon)$, then by substituting $c - \gamma = p$ and using the definition of density function n , we get

$$\frac{\partial n(t, v)}{\partial t} = \frac{1}{2} \int_0^v \beta(t, v - \epsilon, \epsilon) n(t, v - \epsilon) n(t, \epsilon) d\epsilon - n(t, v) \int_0^\infty \beta(t, v, \epsilon) n(t, \epsilon) d\epsilon. \quad (4.20)$$

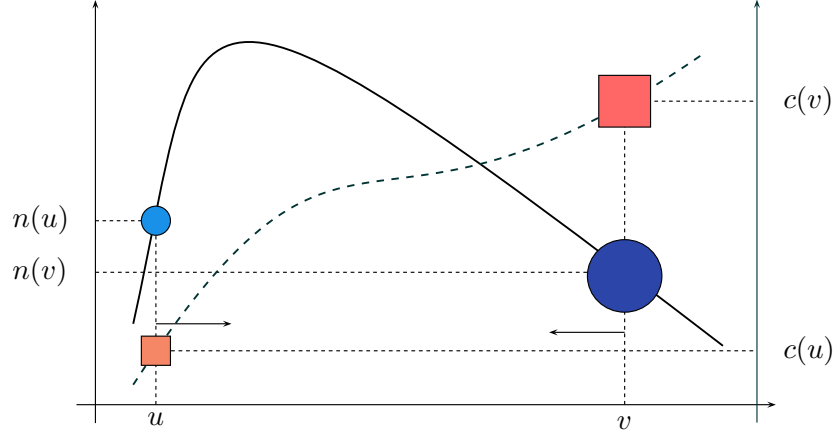


Figure 4.3: Death of tracer mass.

Reduction to 1-D PBE for tracer mass distribution (TMD)

Proceeding as before, multiplication of the equation (4.14) by c and integrating over all possible values of c yields

$$\begin{aligned} \frac{\partial m(t, v)}{\partial t} = & \frac{1}{2} \int_0^v c \int_0^v \int_{\max(0, c-v+\epsilon)}^{\min(c, \epsilon)} \hat{\beta}(t, v - \epsilon, \epsilon, c - \gamma, \gamma) f(t, v - \epsilon, c - \gamma) f(t, \epsilon, \gamma) d\gamma d\epsilon dc \\ & - \int_0^v c \int_0^\infty \int_0^\epsilon \hat{\beta}(t, v, \epsilon, c, \gamma) f(t, v, c) f(t, \epsilon, \gamma) d\gamma d\epsilon dc. \end{aligned} \quad (4.21)$$

Again, reversing the order of integration and some simple substitution gives

$$\frac{\partial m(t, v)}{\partial t} = \int_0^v \beta(t, v - \epsilon, \epsilon) m(t, v - \epsilon) n(t, \epsilon) d\epsilon - m(t, v) \int_0^\infty \beta(t, v, \epsilon) n(t, \epsilon) d\epsilon. \quad (4.22)$$

Equations (4.20) and (4.22) are ordinary integro-differential equations which have to be solved numerically. Hounslow et al. [34] developed a discretized method for solving GSD and later they extended the discretization for the solution of TMD, see Hounslow et al. [33]. The discretized PBE of TMD was applicable only for special geometric grid of the type $x_{i-1/2} = 2x_{i+1/2}$. In the next section we first briefly discuss the discretization of TMD and then propose a new idea for the better accuracy and implementation.

The preceding PBE for the tracer mass can also directly be obtained from the classical one-dimensional PBE (4.20). Note that the tracer mass distribution $m(t, v)$, which represents the total tracer mass contained in particles of size v , can be defined as the product of the number density of particles size v with the mass of tracer $c(t, v)$ in each particle.

$$m(t, v) = c(t, v)n(t, v). \quad (4.23)$$

It follows that the rate of change of total tracer mass contained in particles of size v as a results of coagulation is therefore given by (see Figures 4.2 and 4.3)

$$\begin{aligned} \frac{\partial m(t, v)}{\partial t} = & \frac{1}{2} \int_0^v \beta(t, v - \epsilon, \epsilon) [c(t, v - \epsilon) + c(t, \epsilon)] n(t, v - \epsilon) n(t, \epsilon) d\epsilon \\ & - n(t, v) c(t, v) \int_0^\infty \beta(t, v, \epsilon) n(t, \epsilon) d\epsilon. \end{aligned} \quad (4.24)$$

Using the definition of $m(t, v)$ from equation (4.23), we obtain the required PBE (4.22).

Here we have shown that a two-dimensional PBE can be reduced to a set of two one-dimensional PBEs. A similar criteria can be applied to higher dimensional PBEs to get a reduced system. Now it will then be possible to solve the set of reduced PBEs at moderate computational cost. In the following section we shall first briefly discuss Hounslow's discretized PBE for TMD and consistency problems associated with the discretization. Then a new approach to solve the coupled problem will be presented and some comparisons between them will be demonstrated.

4.2.2 Numerical Methods

Hounslow et al. [33] proposed a discretized population balance for both the reduced equations (4.20), (4.22) and calculated the temporal change of particle size distribution and tracer mass distribution (TMD) simultaneously. The discretization of the tracer PBE was similar to their well-known discretized PBE [34]. It has been found by Peglow et al. [86] that the discretized tracer population balance equation (DTPBE) for the tracer mass is not entirely consistent with the associated discretized population balance equation (DPBE) for granule size distribution. Our interest here is first to discuss the discretized tracer PBE and to show the inconsistency. These inconsistencies are then remedied in a new formulation that retains the advantages of the original DTPBE such as conservation of total tracer mass, prediction of tracer-weighted mean particle volume and so on. Furthermore, the DTPBE has been extended to an adjustable discretization based on that of Litster et al. [69]. Various comparisons are made of the validity of the extended and modified formulation.

The discretization of the equation (4.22) is totally different than the discretization of PBE (4.20) discussed in Chapter 2. We can not get a set of discrete equations directly from Hounslow's DPBEs (2.10). The reason is obviously mechanism number 5 discussed in Chapter 2. Hounslow et al. [34] did not consider this mechanism when formulating discretization for PSD since it has no effect on number of particles. Here we will discuss only mechanism number 5 in detail, all others are the same discussed in Chapter 2.

Mechanism 1. The resulting expression for the rate of change of particles due to this mechanism is given by

$$B_i^{[1]} = \sum_{j=1}^{i-2} 3 \cdot 2^{j-i} \beta_{i-1,j} N_{i-1} N_j. \quad (4.25)$$

So the rate of change of binder mass in the i th interval due to this mechanism is given by

$$B_{i,T}^{[1]} = \sum_{j=1}^{i-2} 3 \cdot 2^{j-i} \beta_{i-1,j} (M_{i-1} N_j + N_{i-1} M_j). \quad (4.26)$$

Mechanism 2. Birth rate of the tracer due to this mechanism is

$$\begin{aligned} B_{i,T}^{[2]} &= \frac{1}{2} \beta_{i-1,i-1} (M_{i-1} N_{i-1} + N_{i-1} M_{i-1}) \\ &= \beta_{i-1,i-1} M_{i-1} N_{i-1}. \end{aligned} \quad (4.27)$$

Mechanism 3. Death rate of the tracer in the i th interval can be obtained from the death rate of granules as

$$D_{i,T}^{[3]} = M_i \sum_{j=1}^{i-1} 3 \cdot 2^{j-i-1} \beta_{i,j} N_j. \quad (4.28)$$

Mechanism 4. In the similar way we can obtain death rate of tracer due to this mechanism in the i th interval.

$$D_{i,T}^{[4]} = M_i \sum_{j=i}^I \beta_{i,j} N_j. \quad (4.29)$$

Mechanism 5. As discussed before, this mechanism is completely different than others. It has no influence on number of particles while mass within the interval increases. Particles can grow within the i th interval only when a particle in the i th interval aggregates with a particle in the j th ($j < i$) interval. If a particle of size a in the j th interval collides with particles in the size range $2^i \leq v < (2^{i+1} - a)$ of i th interval, the resulting particle will be in the i th class. The number of particles in the i th interval available for collision is $(2^i - a)N_i/2^i$. The differential rate of change of tracer mass in the i th interval is given by

$$dB_{i,j,T}^{[5]} = \beta_{i,j} \frac{(2^i - a)N_i}{2^i} \frac{N_j}{2^j} da \left(\frac{M_j}{N_j} \right). \quad (4.30)$$

Thus, the rate of birth in the i th interval resulting from collision between i th and j th interval is given by

$$\begin{aligned} dB_{i,j,T}^{[5]} &= \beta_{i,j} \int_{2^j}^{2^{j+1}} \frac{(2^i - a)N_i}{2^i} \frac{M_j}{2^j} da \\ &= \beta_{i,j} N_i M_j (1 - 3 \cdot 2^{j-i-1}). \end{aligned} \quad (4.31)$$

Summing over all j , the total rate of birth due to this mechanism can be expressed as

$$B_{i,T}^{[5]} = \sum_{j=1}^{i-1} \beta_{i,j} N_i M_j (1 - 3 \cdot 2^{j-i-1}). \quad (4.32)$$

Collecting expressions from all the mechanisms and introducing a correction factor, the final set of equations is

$$\begin{aligned} \frac{dM_i}{dt} &= \sum_{j=1}^{i-2} k \cdot 3 \cdot 2^{j-i} \beta_{i-1,j} (M_{i-1} N_j + N_{i-1} M_j) + \beta_{i-1,i-1} M_{i-1} N_{i-1} \\ &\quad - M_i \sum_{j=1}^{i-1} k \cdot 3 \cdot 2^{j-i-1} \beta_{i,j} N_j - M_i \sum_{j=i}^I \beta_{i,j} N_j \\ &\quad + \sum_{j=1}^{i-1} \beta_{i,j} N_i M_j (1 - k \cdot 3 \cdot 2^{j-i-1}). \end{aligned} \quad (4.33)$$

Total rate of change of mass is given by (for simplicity we use constant β_0)

$$\begin{aligned} \sum_i \frac{dM_i}{dt} &= \sum_{i=1}^I \sum_{j=1}^{i-2} k \cdot 3 \cdot 2^{j-i} \beta_{i-1,j} (M_{i-1} N_j + N_{i-1} M_j) + \sum_{i=1}^I \beta_{i-1,i-1} M_{i-1} N_{i-1} \\ &\quad - \sum_{i=1}^I M_i \sum_{j=1}^{i-1} k \cdot 3 \cdot 2^{j-i-1} \beta_{i,j} N_j - \sum_{i=1}^I M_i \sum_{j=i}^M \beta_{i,j} N_j \\ &\quad + \sum_{i=1}^I \sum_{j=1}^{i-1} \beta_{i,j} N_i M_j (1 - k \cdot 3 \cdot 2^{j-i-1}). \end{aligned}$$

It can be rewritten as

$$\begin{aligned} \sum_i \frac{dM_i}{dt} &= \sum_{i=1}^I M_{i-1} \sum_{j=1}^{i-2} k \cdot 3 \cdot 2^{j-i} \beta_{i-1,j} N_j - \sum_{i=1}^I M_i \sum_{j=1}^{i-1} k \cdot 3 \cdot 2^{j-i-1} \beta_{i,j} N_j \\ &\quad + \sum_{i=1}^I N_{i-1} \sum_{j=1}^{i-2} k \cdot 3 \cdot 2^{j-i} \beta_{i-1,j} M_j - \sum_{i=1}^I N_i \sum_{j=1}^{i-1} k \cdot 3 \cdot 2^{j-i-1} \beta_{i,j} M_j \\ &\quad + \sum_{i=1}^I \beta_{i-1,i-1} M_{i-1} N_{i-1} + \sum_{i=1}^I \sum_{j=1}^{i-1} \beta_{i,j} N_i M_j - \sum_{i=1}^I \sum_{j=i}^I \beta_{i,j} N_j M_i \\ &= 0, \end{aligned}$$

for any value of k . Hounslow et al. [34] put $k = 2/3$, the same volume correction factor as they derived in DPBs. For $k = 2/3$ it reduces to

$$\begin{aligned} \frac{dM_i}{dt} &= \sum_{j=1}^{i-2} 2^{j-i+1} \beta_{i-1,j} (M_{i-1} N_j + N_{i-1} M_j) \\ &\quad + \beta_{i-1,i-1} M_{i-1} N_{i-1} + N_i \sum_{j=1}^{i-1} (1 - 2^{j-i}) \beta_{i,j} M_j \\ &\quad - M_i \sum_{j=1}^{i-1} 2^{j-i} \beta_{i,j} N_j - M_i \sum_{j=i}^I \beta_{i,j} N_j. \end{aligned} \tag{4.34}$$

A similar discretization corresponding to the fixed pivot technique can also be obtained in this case. The advantage of the fixed pivot technique over the Hounslow's discretization is the generality regarding grids. The fixed pivot formulation can be applied on any types of grid. The fixed pivot discretization of the equation (4.22) is given by

$$\begin{aligned} \frac{dM_i(t)}{dt} &= \sum_{\substack{j \geq k \\ j, k \\ x_{i-1} \leq x < x_{i+1}}} (1 - \frac{1}{2} \delta_{j,k}) \eta(x) \beta_{j,k} [M_j(t) N_k(k) + N_j(t) M_k(k)] \\ &\quad - M_i(t) \sum_{k=1}^I \beta_{i,k} N_k(t). \end{aligned} \tag{4.35}$$

Note that both discretizations (4.34) and (4.35) become the same while applied on a geometric grid. It is of interest to explain the simplicity of mass formulation by the application of the fixed pivot technique, while it was complicated in Hounslow's approach to get the discrete equation for tracer mass from the discrete equation for GSD. We have to consider one more interaction mechanism in case of Hounslow's approach. However, the point can be made clear if we look at birth and death terms separately. In Hounslow case, birth and death terms predict net rate of birth and death in a section individually, while in the fixed pivot technique it is different. Nevertheless, both techniques predict correct net rate of change of particles. In the fixed pivot technique, all collisions with particles of i th section result in death which is not true, only some of them result in death. If any particle from lower classes collides with a particle of i th class and the resultant particle still stays in i th class, there is no birth with respect to the number of particles in this interaction mechanism. Particles are getting larger within the interval while the number of particles remains constant. This mechanism simply leads to an increment of mass in the interval. In the fixed pivot technique, these interactions first leads to death and then to birth during the process of reassignment of particles. The reason why the formulation is trivial in the case of the fixed pivot technique is now clear. On the other hand in case of Hounslow's discretization one has to take those collisions into account which have no influence in number of particles in a section but have significant effects in tracer mass. So, formulation for tracer mass distribution can not directly be obtained from number distribution.

One can use the DTPBE (4.34) of Hounslow et al. [33] or alternatively (4.35) for the computation of various extensive properties (amount of water within the particle, enthalpy of particles etc.) of aggregating systems. The equations predict the total amount of extensive properties exactly but it fails to predict intensive properties which are proportional to the ratio of extensive properties and mass of granules. For the purpose of illustration let us consider an example where a particle system is described by the two properties: volume of particles and amount of water within the particles. Our interest is to calculate the particle moisture content as the ratio of water mass to particle mass - an intensive property. We assume that the density is constant and particle volume is equal to the particle mass. For simplicity let us assume that initially the water mass inside a particle is equal to the dry particle mass. In other words, the ratio between water mass and dry particle mass or equivalently the particle moisture content is constant over the particle size range and is equal to one. Since agglomeration is the only governing mechanism which changes the particle size, the particle moisture content should be constant throughout the process.

Let us consider the following initial condition for the PSD with volume as the distributed property

$$n(t, x) = \frac{N_0}{x_0} \exp\left(-\frac{x}{x_0}\right). \quad (4.36)$$

In the DTPBE of Hounslow et al. [33] the particle size domain is divided into discrete size ranges using a geometric discretization of the type $x_{i+1/2} = 2x_{i-1/2}$. Integration of equation (4.36) over the interval $[x_{i-1/2}, x_{i+1/2}]$ gives the total number of particles within the interval

$$N_i = \frac{N_0}{2} \left[\exp\left(-\frac{x_{i-1/2}}{x_0}\right) - \exp\left(-\frac{x_{i+1/2}}{x_0}\right) \right]. \quad (4.37)$$

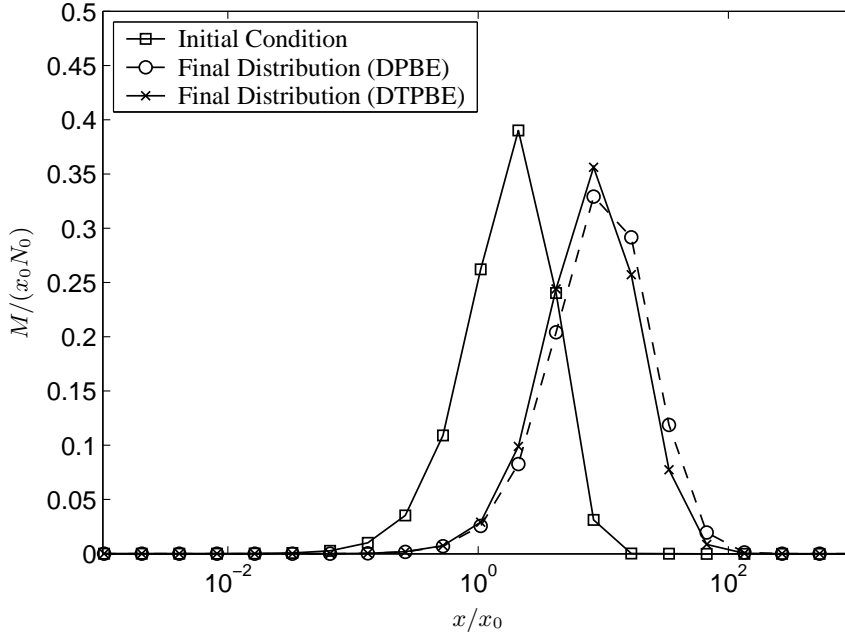


Figure 4.4: Initial and final distribution calculated Hounslow’s DTPBE and DPBE.

The dry mass of particles in an interval $[x_{i-1/2}, x_{i+1/2}]$ is approximated as

$$M_{p,i} = N_i \left(\frac{x_{i-1/2} + x_{i+1/2}}{2} \right). \quad (4.38)$$

Here we make an assumption of constant density, so that the mass could be replaced by volume. The initial condition for water mass distribution is chosen in such a way that the total mass of water $M_{w,i}$ within the particles in the interval $[x_{i-1/2}, x_{i+1/2}]$ is equal to the total mass of dry particles in this interval, that is

$$M_{w,i} = M_{p,i}. \quad (4.39)$$

Here the subscripts w and p denotes the water and particles respectively.

The computation is made for a size independent kernel and $N_0 = x_0 = 1$. We calculated the particle mass and the water content within the particles as a function of particle volume using Hounslow’s discrete PBE, see Hounslow et al. [34], and Hounslow’s DTPBE, see Hounslow et al. [33], respectively. The numerical results at $I_{agg} = 0.8$ together with the initial condition have been plotted in Figure 4.4. Clearly the DTPBE fails to predict the water distribution within the particles correctly since both water distribution and mass distribution must be the same during the process. Furthermore, Figure 4.5 includes initial and final ratio of water mass and particle mass within the intervals. It can be seen from the figure that the final ratio is not constant. However, it should be pointed out that both discretized formulations conserve mass.

Improved Hounslow’s discretization

Let us discuss this ratio problem in detail. Consider the birth contribution in the i th interval due to collision of particles from the j th and k th cells. In DTPBE this birth contribution is

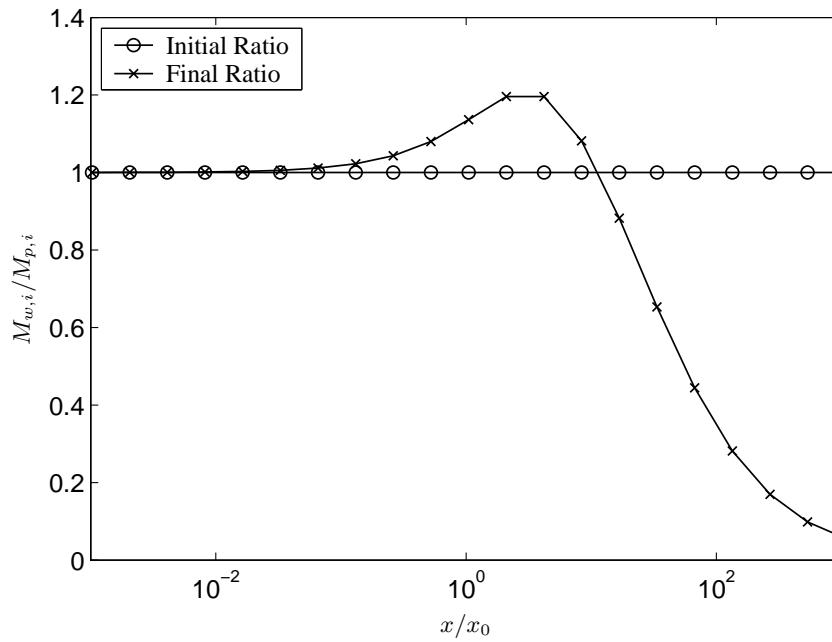


Figure 4.5: Initial and final ratio of water mass and particle mass distribution.

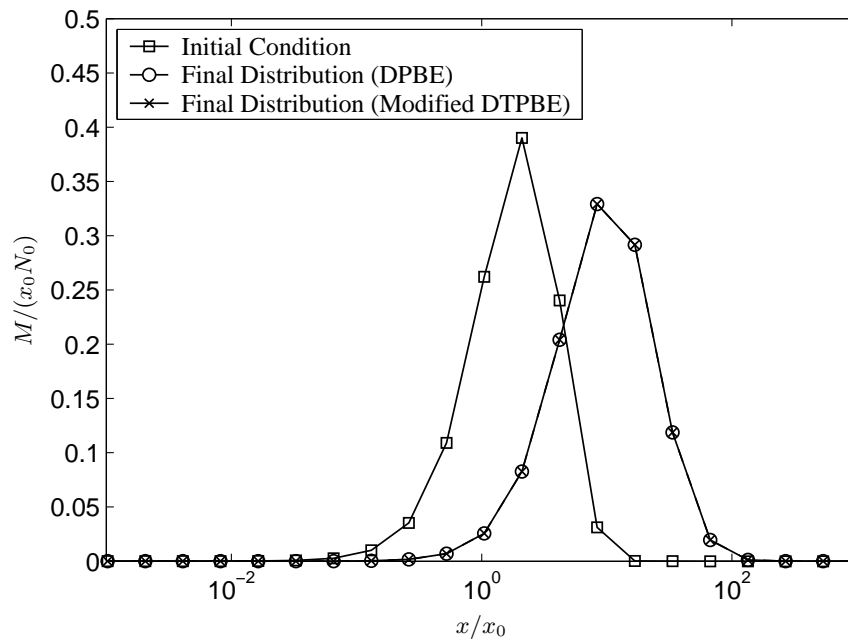


Figure 4.6: Initial and final distribution calculated Hounslow's DPBE and modified DTPBE.

CHAPTER 4. NEW NUMERICAL METHODS: MULTI-DIMENSIONAL

replaced by $N_j M_k + M_j N_k$ as a tracer mass birth contribution which is the actual amount of tracer coming from the j th and k th cells. The cause for the non-constant ratio is that the assignment of the tracer mass is different from that of granule mass in the i th interval. Let us observe that the actual amount of granule mass corresponds to $N_j N_k$ birth in the i th cell. If x_i represents the mean volume (or mass) of the i th interval then $N_j N_k (x_j + x_k)$ is the total mass carried with $N_j N_k$ particles from the j th and k th cells. On the other hand, corresponding to $N_j N_k$ particles in the i th cell we assign $N_j N_k x_i$ mass to the i th cell. Clearly

$$N_j N_k (x_j + x_k) \neq N_j N_k x_i, \text{ for all } i, j, k. \quad (4.40)$$

The authors did not assign the mass of tracer in the same ratio as granule mass. This inconsistency can be repaired by introducing some correction factors. For instance, a correction factor K in this case can be introduced in the following way

$$\frac{\text{Assigned tracer mass}}{\text{Actual tracer mass}} = \frac{\text{Assigned granule mass}}{\text{Actual granule mass}} = \frac{x_j}{x_j + x_k} = K. \quad (4.41)$$

By introducing correction factors in each term of the DTPBE, we obtain the following set of equations

$$\begin{aligned} \frac{dM_i}{dt} = & \sum_{j=1}^{i-2} 2^{j-i+1} \beta_{i-1,j} (M_{i-1} N_j + N_{i-1} M_j) K_1 + N_i \sum_{j=1}^{i-1} (1 - 2^{j-i}) \beta_{i,j} M_j K_2 \\ & + \beta_{i-1,i-1} N_{i-1} M_{i-1} - M_i \sum_{j=1}^{i-1} 2^{j-i} \beta_{i,j} N_j K_3 - M_i \sum_{j=i}^I \beta_{i,j} N_j, \end{aligned} \quad (4.42)$$

with correction factors

$$K_1 = \frac{2}{2^{j-i+1}}, \quad K_2 = \frac{1}{2^{j-i} + 1}, \quad K_3 = \frac{2}{2^{j-i} + 1}. \quad (4.43)$$

The correction factors corresponding to the third and the last terms of (4.42) are 1. It can be easily shown that the total tracer mass is still conserved, see Appendix B.8. This modified formulation has been now applied to the same problem as before. As expected, Figure 4.6 shows the same prediction by both the DPBE and the modified DTPBE.

The discretized equation outlined above, which is valid for the geometric grid of type $x_{i+1/2} = 2x_{i-1/2}$, is now generalized to adjustable discretizations of the form $x_{i+1/2} = 2^{1/q} x_{i-1/2}$. Besides 5 interaction mechanisms described in Litster et al. [69], one more interaction mechanism will be considered in the case of tracer mass distribution. We call this new interactions mechanism a Type 6 interaction. In these interactions, particles in interval i and j aggregate, and the resulting particles still stay in the i th interval, see Figure 4.7. These interactions have not changed the number of particles in the interval but the tracer mass, or the mass of granules itself, in the interval is increased due to the particles coming from the lower intervals. This mechanism was not considered in the birth term of the adjustable discretization of the number density PBE since it does not change the number of particles in the cell. This is a birth mechanism with respect to mass. All 4 interactions which produce birth in the i th cell are summarized in Table 4.1. A similar table for death mechanisms and other detailed descriptions can be found in Litster et al.

Table 4.1: Birth (Type 1, 2, 3, and 6) mechanisms

q	Size Interval 1		Size Interval 2			Type 6 (Birth)
	Type 1 (Birth)	Type 2 (Birth)	Type 3 (Birth)	Type 4 (Birth)	Type 5 (Birth)	
1	i	-	-	-	-	$1 \leq j \leq i-1$
	$i-1$	$1 \leq j \leq i-2$	$i-1$	-	-	-
2	i	-	-	-	-	$1 \leq j \leq i-3$
	$i-1$	$1 \leq j \leq i-4$	-	-	$i-3 \leq j \leq i-2$	-
	$i-2$	$i-4 \leq j \leq i-3$	$i-2$	-	-	-
3	i	-	-	-	-	$1 \leq j \leq i-6$
	$i-1$	$1 \leq j \leq i-7$	-	-	$i-6 \leq j \leq i-4$	-
	$i-2$	$i-7 \leq j \leq i-5$	-	-	$i-4 \leq j \leq i-3$	-
	$i-3$	$i-5 \leq j \leq i-4$	$i-3$	-	-	-
4	i	-	-	-	-	$1 \leq j \leq i-10$
	$i-1$	$1 \leq j \leq i-11$	-	-	$i-10 \leq j \leq i-7$	-
	$i-2$	$i-11 \leq j \leq i-8$	-	-	$i-7 \leq j \leq i-5$	-
	$i-3$	$i-8 \leq j \leq i-6$	-	-	$i-5 \leq j \leq i-4$	-
	$i-4$	$i-6 \leq j \leq i-5$	$i-4$	-	-	-
q	i	-	-	-	-	$1 \leq j \leq i-S_1+1$
	$i-p; (1 \leq p \leq q-1)$	$i-S_{p-1} \leq j \leq i-S_p$	-	-	$i+1-S_p \leq j \leq i+1-S_{p+1}$	-
	$i-q$	$i-S_{q-1} \leq j \leq i-S_q$	$i-q$	-	-	-

CHAPTER 4. NEW NUMERICAL METHODS: MULTI-DIMENSIONAL

[69] and Wynn [120]. Following Litster et al. [69] and Wynn [120], all 6 interaction mechanisms (birth and death) can be put together in the following expression. The final extended and consistent model is given by

$$\begin{aligned}
 \frac{dM_i}{dt} = & \sum_{j=1}^{i-S_1} \frac{2^{(j-i+1)/q}}{2^{1/q} - 1} \beta_{i-1,j} (M_{i-1}N_j + N_{i-1}M_j)K_1 + \beta_{i-q,i-q}N_{i-q}M_{i-q} \\
 & + \sum_{p=1}^{q-1} \sum_{j=i+1-S_p}^{i+1-S_{p+1}} \frac{2^{1/q} - 2^{(j-i)/q} - 2^{-p/q}}{2^{1/q} - 1} \beta_{i-p,j} (M_{i-p}N_j + N_{i-p}M_j)K_2 \\
 & + \sum_{p=2}^q \sum_{j=i-S_{p-1}}^{i-S_p} \frac{2^{(j-i+1)/q} - 1 + 2^{-(p-1)/q}}{2^{1/q} - 1} \beta_{i-p,j} (M_{i-p}N_j + N_{i-p}M_j)K_3 \\
 & + \sum_{j=1}^{i-S_1+1} \left(1 - \frac{2^{(j-i)/q}}{2^{1/q} - 1} \right) \beta_{i,j}N_iM_jK_4 \\
 & - \sum_{j=1}^{i-S_1+1} \frac{2^{(j-i)/q}}{2^{1/q} - 1} \beta_{i,j}M_iN_jK_5 - \sum_{j=i-S_1+2}^I \beta_{i,j}M_iN_j, \tag{4.44}
 \end{aligned}$$

where

$$S_p = \text{Int} \left[1 - \frac{q \ln(1 - 2^{-p/q})}{\ln 2} \right], \tag{4.45}$$

and

$$K_1 = \frac{2^{(i-j)/q}}{1 + 2^{(i-j-1)/q}}, \tag{4.46}$$

$$K_2 = K_3 = \frac{2^{(i-j)/q}}{1 + 2^{(i-j-p)/q}}, \tag{4.47}$$

$$K_4 = \frac{1}{1 + 2^{(j-i)/q}}, \tag{4.48}$$

$$K_5 = \frac{2^{1/q} - 1}{2^{(j-i)/q}} - \frac{-2^{i/q} + 2^{(2i-j)/q}(2^{1/q} - 1)}{2^{i/q} + 2^{j/q}}. \tag{4.49}$$

The function $\text{Int}[x]$ gives the integer part of x . Let us call this formulation the modified DTPBE. The inclusion of the correction factors allows us to predict the change of the mass of tracer according to the change of mass of particles. In Hounslow's previous approach, see Hounslow et al. [33], the change of number of particles within an interval was considered to determine the change of tracer. Setting all corrections factors $K_1 - K_5$ to 1, the set of equations (4.42) and (4.44) reduces exactly to those given by Hounslow et al. [33] and its extended version for geometric grids of the type $x_{i+1/2} = 2^{1/q}x_{i-1/2}$ respectively.

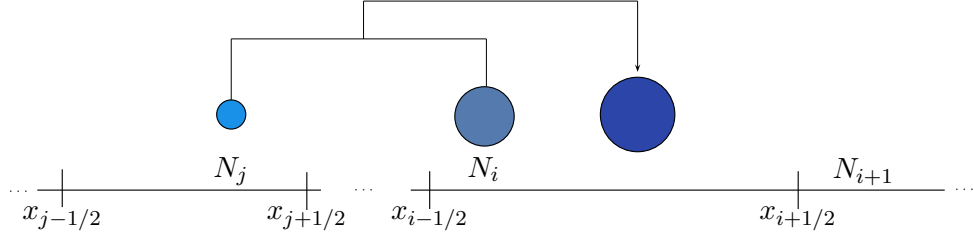


Figure 4.7: Birth mechanism with respect to mass only.

Though the DTPBE of Hounslow et al. [33] is extended to adjustable discretizations of type $x_{i+1/2} = 2^{1/q}x_{i-1/2}$, one can not apply it on general grids. The objective now is to propose a general discretization for tracer PBEs. Before we proceed to the next section it is worth to make some comparisons between Hounslow's original DTPBE and the modified, adjustable and consistent discretization DTPBE. Detailed comparisons are made in Peglow et al. [86]. We consider only a few of them here.

In order to compare the extended and modified formulation with Hounslow's original DTPBE we consider the same problem which was considered in Hounslow et al. [33] for a CST with size-independent aggregation. They considered a well-mixed continuous process initially at steady state to which a spike of mono-disperse tracer was added. The continuous form of the tested problem is the following

$$\frac{\partial n(t, v)}{\partial t} = \frac{1}{2} \int_0^v \beta(t, v - \epsilon, \epsilon) n(t, v - \epsilon) n(t, \epsilon) d\epsilon - n(t, v) \int_0^\infty \beta(t, v, \epsilon) n(t, \epsilon) d\epsilon + B^0 \delta(v) - \frac{n(t, v)}{\tau}, \quad (4.50)$$

$$n(t, 0^-) = 0, \quad \left. \frac{\partial n(t, v)}{\partial t} \right|_{t=0} = 0, \quad (4.51)$$

$$\frac{\partial m(t, v)}{\partial t} = \int_0^v \beta(t, v - \epsilon, \epsilon) m(t, v - \epsilon) n(t, \epsilon) d\epsilon - m(t, v) \int_0^\infty \beta(t, v, \epsilon) n(t, \epsilon) d\epsilon - \frac{m(t, v)}{\tau}, \quad (4.52)$$

$$m(t, 0^-) = 0, \quad m(0, v) = \delta(v - v_0). \quad (4.53)$$

Ilievski and Hounslow [38] provided the solutions of decay of total tracer mass and tracer weighted mean particle volume \bar{v}_T for the size-independent kernel $\beta(u, v) = \beta_0$, the sum kernel $\beta(u, v) = \beta_0 \times (u + v)$, and the product kernel $\beta(u, v) = \beta_0 \times u \times v$. The tracer weighted mean particle volume \bar{v}_T is defined as

$$\bar{v}_T(t) = \frac{\int_0^\infty v m(t, v) dv}{\int_0^\infty m(t, v) dv}. \quad (4.54)$$

The analytical solutions of \bar{v}_T for these kernels have been collected in Appendix A.9. They mentioned that \bar{v}_T gives meaningful values up to one-third degree of aggregation for a sum

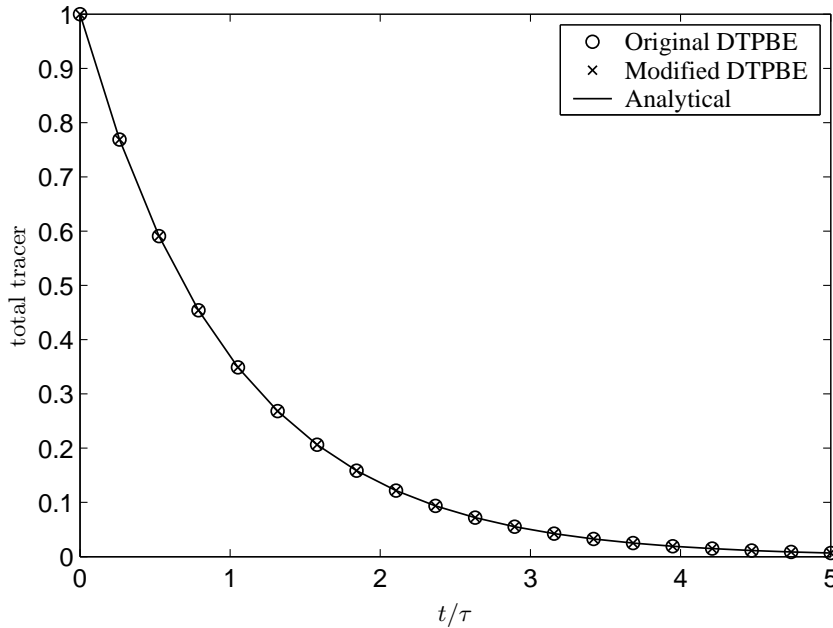


Figure 4.8: Progress of total tracer mass for size-independent aggregation, $I_{\text{agg}} = 1/4$.

kernel and is valid up to one-eighth degree of aggregation for a product kernel. The decay of total mass of tracer M_T in each case takes the following form

$$M_T = M_0 \exp(-t/\tau). \tag{4.55}$$

Figure 4.8 compares the total tracer mass calculated using both formulations. The prediction of total tracer mass is exactly the same for both formulations. A comparison of tracer-weighted mean particle volumes, as drawn in Figure 4.9, illustrates that a good prediction is only possible by the original version. For a better prediction of numerical results we have to use a finer grid. This is true for the DTPBE and for the DBPE as well. The numerical solutions obtained for different discretizations are plotted in Figure 4.10. However, already for $q = 5$ the results are in quite good agreement with the analytical solutions.

In Figures 4.11 and 4.12, a similar comparison of tracer weighted mean particle volume for the size-dependent sum kernel. The decay of total mass is the same in each case, we refrain from plotting that comparison here. For this kernel both formulations deviate significantly from analytical solutions, see Figure 4.11. The effectiveness of the grid for different values of q has been shown in Figure 4.12. Once again the numerical results are satisfactory by $q = 5$. A similar observation has been made for the product kernel shown in Figures 4.13 and 4.14.

To conclude, the consistency of numerical solutions of the tracer mass distribution results in lower accuracy. The accuracy has been investigated only for a constant aggregation kernel. It gets even worse for other kernels like a sum and product kernels, see Peglow et al. [86]. The low accuracy and restriction to geometric type grids the above numerical formulations motivate us to propose a better scheme. Therefore the aim is now to develop a numerical scheme for the tracer PBE which is more accurate and general.

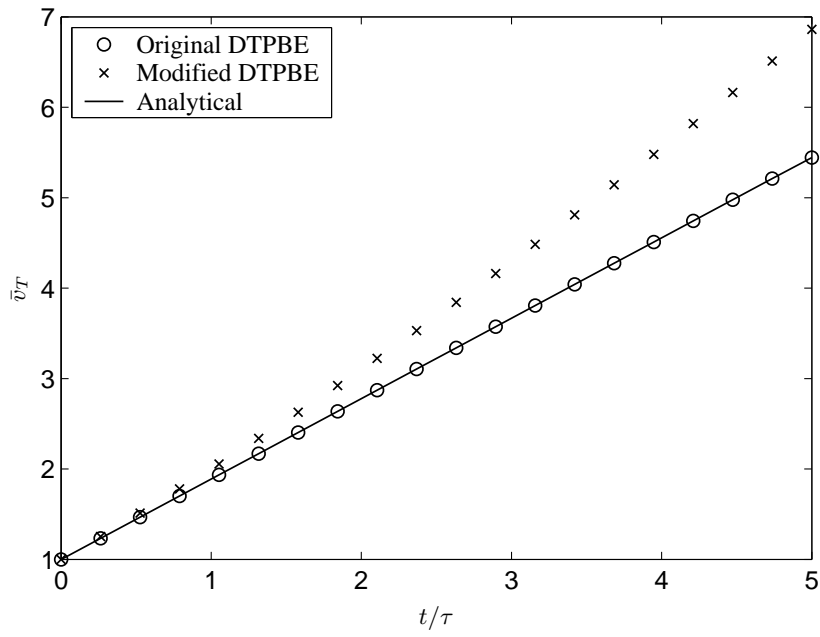


Figure 4.9: Progress of tracer-weighted mean particle volume for size independent aggregation, $I_{\text{agg}} = 1/4$.

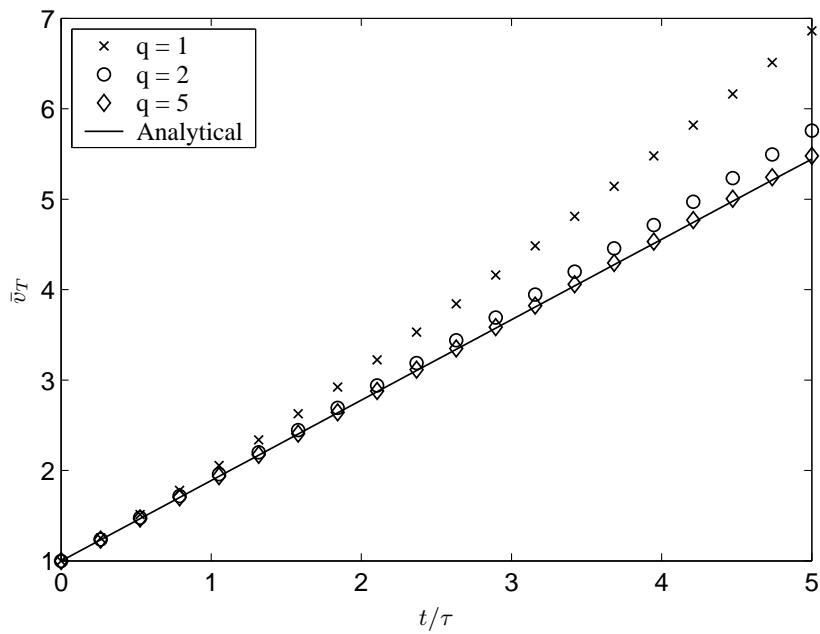


Figure 4.10: Progress of tracer-weighted mean particle volume for size independent aggregation, $I_{\text{agg}} = 1/4$.

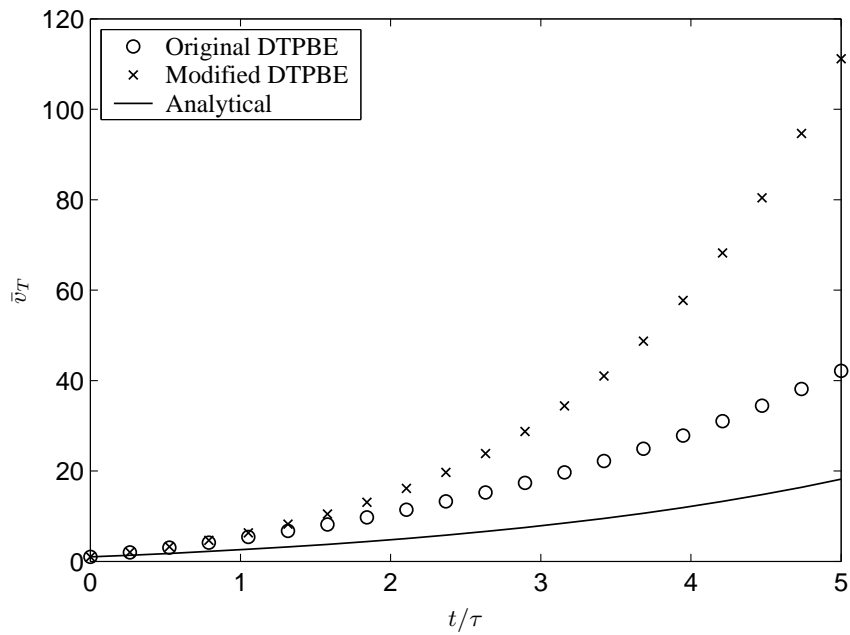


Figure 4.11: Progress of tracer-weighted mean particle volume with the sum aggregation kernel, $I_{agg} = 1/4$.

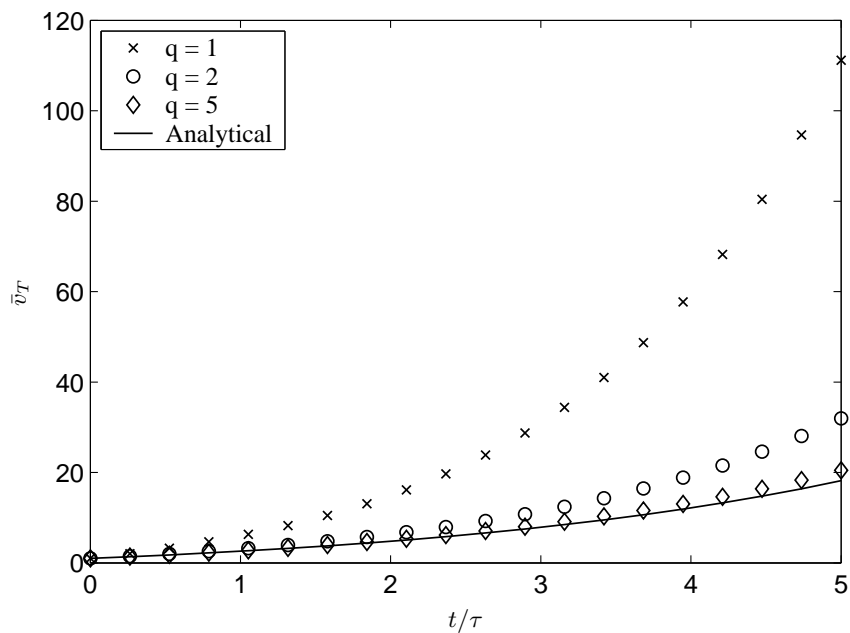


Figure 4.12: Progress of tracer-weighted mean particle volume with the sum aggregation kernel, $I_{agg} = 1/4$.

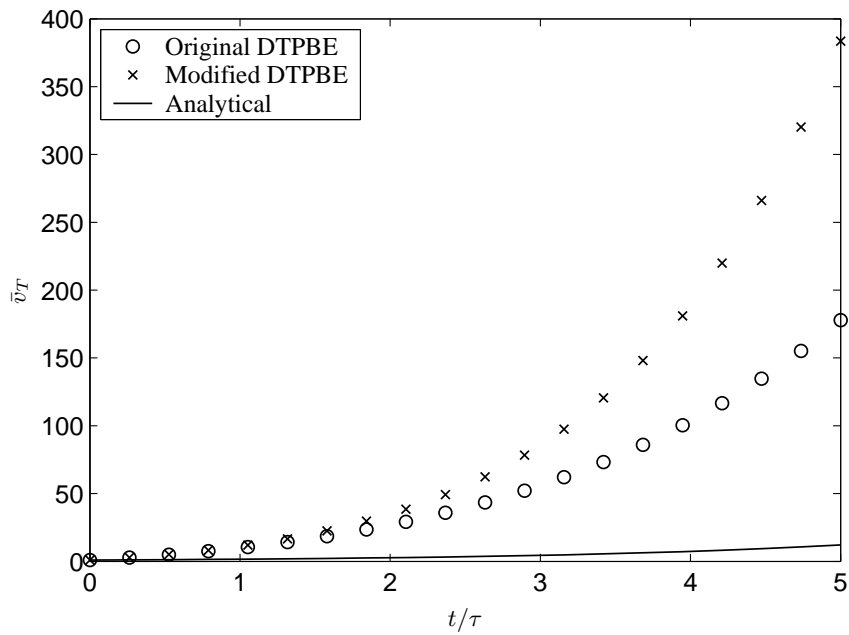


Figure 4.13: Progress of tracer-weighted mean particle volume with the product aggregation kernel, $I_{\text{agg}} = 1/4$.

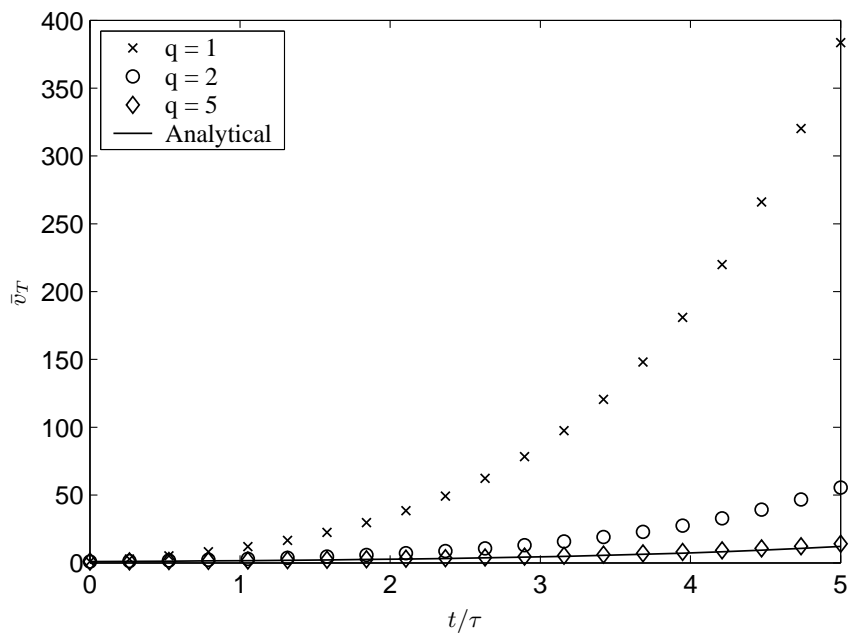


Figure 4.14: Progress of tracer-weighted mean particle volume with the product aggregation kernel, $I_{\text{agg}} = 1/4$.

New numerical scheme

The new discretized scheme is based on the *cell average technique* discussed in Section 3.2. The entire size domain in this technique is divided into several small cells. The particles within a cell are assumed to be concentrated at a representative size. The idea was to take the average of all new born particles within the cell and then assign them to the neighboring nodes such that pre-chosen properties are exactly preserved. The same idea can be adapted for the discretization of the TPBE. Since all the particles are assumed to be concentrated at representatives sizes x_i , the number and tracer mass density can be expressed as

$$n(t, v) = \sum_{j=1}^I N_j(t) \delta(v - x_j). \quad (4.56)$$

and

$$M(t, v) = \sum_{j=1}^I M_j(t) \delta(v - x_j). \quad (4.57)$$

Birth term: Substitution of n and M into the birth term of equation (4.22) gives

$$B_{i,T} = \sum_{\substack{j \geq k \\ v_i \leq (x_j + x_k) < v_{i+1}}} \left(1 - \frac{1}{2} \delta_{j,k} \right) \beta_{j,k} (M_j N_k + N_j M_k). \quad (4.58)$$

Analogous to the cell average technique the assignment of a fraction of this tracer birth and collection of all birth contributions from neighboring cells, the modified tracer birth rate at x_i is given by

$$\begin{aligned} B_{i,T}^{\text{CA}} = & B_{i-1,T} \lambda_i^-(\bar{v}_{i-1}) \eta_i(\bar{v}_{i-1}) H(\bar{v}_{i-1} - x_{i-1}) + B_{i,T} \lambda_i^-(\bar{v}_i) \eta_i(\bar{v}_i) H(x_i - \bar{v}_i) \\ & + B_{i,T} \lambda_i^+(\bar{v}_i) \eta_i(\bar{v}_i) H(\bar{v}_i - x_i) + B_{i+1,T} \lambda_i^+(\bar{v}_{i+1}) \eta_i(\bar{v}_{i+1}) H(x_{i+1} - \bar{v}_{i+1}), \end{aligned} \quad (4.59)$$

where

$$\eta_i(a) = x_i/a. \quad (4.60)$$

The factor η assigns the tracer mass in the same ratio as granule mass. This factor can be illustrated by a simple example, consider the birth contribution of granules $B_{i-1} \lambda_i^-(\bar{v}_{i-1})$ from the cell $i-1$ to the cell i . The total volume (mass) fraction carried with these particles is given as $B_{i-1} \lambda_i^-(\bar{v}_{i-1}) \bar{v}_{i-1}$. On the other hand, corresponding to $B_{i-1} \lambda_i^-(\bar{v}_{i-1})$ particles we assign $B_{i-1} \lambda_i^-(\bar{v}_{i-1}) x_i$ volume to the cell i . Now we wish to distribute the tracer mass same as granule mass

$$\frac{\text{Assigned granule mass}}{\text{Actual granule mass}} = \frac{B_{i-1} \lambda_i^-(\bar{v}_{i-1}) x_i}{B_{i-1} \lambda_i^-(\bar{v}_{i-1}) \bar{v}_{i-1}} = \frac{\text{Assigned tracer mass}}{\text{Actual tracer mass}}.$$

It follows that

$$\frac{\text{Assigned tracer mass}}{\text{Actual tracer mass}} = \frac{x_i}{\bar{v}_{i-1}} := \eta_i(\bar{v}_{i-1}).$$

Similarly we can construct the other two factors appearing in the formulation (4.59). A detailed discussion about this factor can also be found in Peglow et al. [86].

Death term: Substituting n and M in the death term of equation (4.22), we obtain

$$D_{i,T} = M_i \sum_{j=1}^I \beta(x_i, x_j) N_j. \quad (4.61)$$

The detailed calculations of tracer birth and death terms term have been put in Appendix B.9. The final set of discrete equations for tracer mass is given as

$$\frac{dM_i}{dt} = B_{i,T}^{\text{CA}} - D_{i,T}. \quad (4.62)$$

Now the discretized (4.62) together with the cell average discretization (3.67) of the number density PBE (4.20) will be used for the calculation of TMD and GSD. These new discretized equations will be compared with the modified Hounslow discretized model by application to several analytically tractable problems in the next cell.

4.2.3 Test Cases

In order to show the effectiveness of the new discretization of TPBE we consider two different types of problems, aggregation in a batch mode of operation and the problem which was considered in [33] for a mixed-suspension-mixed-product-removal (MSMPR) system considered in previous section. The new discretized scheme will be compared with the modified DTPBE developed in previous section.

Aggregation in a batch system

First we take a trivial test case. We consider two properties of the system: granule volume and the concentration of primary particles in a granule. For the sake of simplicity and the availability of analytical solutions let us take the discrete problem of mono-disperse charge particles with dimensionless size unity. Aldous [3] provides the particle size distribution for size-independent kernel $\beta_{i,j} = 1$ and $N_0 = 1$ as

$$N_i(t) = \frac{4}{(t+2)^2} \left(\frac{t}{t+2} \right)^{i-1}. \quad (4.63)$$

Here N_i is the number concentration of clusters containing i primary particles. Here the size of a granule v is identified by the number of primary particles i in the granule. The total number of primary particles in clusters containing i primary particles, say $N_{p,i}$ which corresponds to $M(t,v)$ in continuous setting, is trivial in this case and given by

$$N_{p,i}(t) = i * N_i(t). \quad (4.64)$$

The mean volume size of the primary particle distribution in this case is computed by

$$\bar{v}_p(t) = \frac{\sum_i i N_{p,i}}{\sum_i N_{p,i}} = 1 + t, \quad \text{for all } t. \quad (4.65)$$

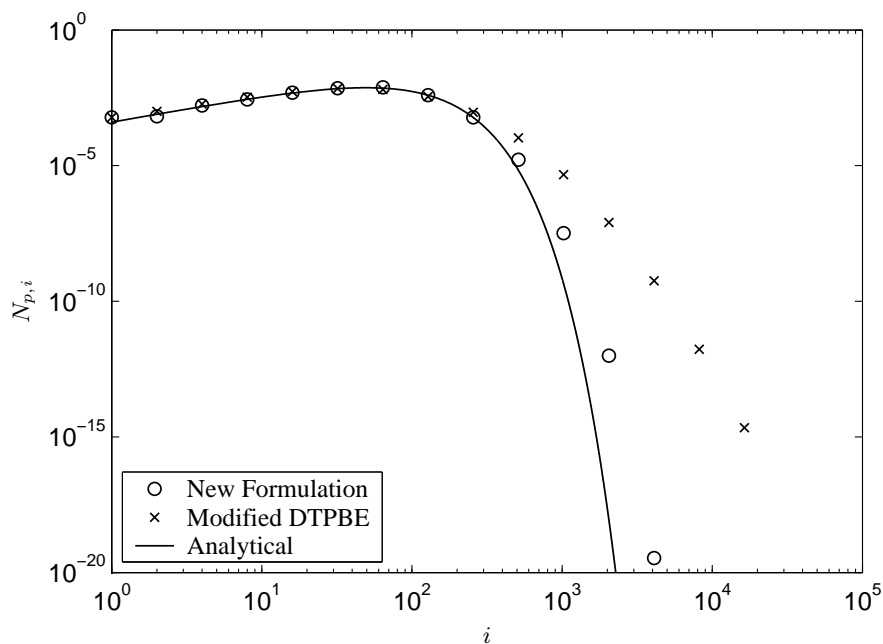


Figure 4.15: Comparison of primary particle number distribution for constant kernel, $I_{agg} = 0.98$.

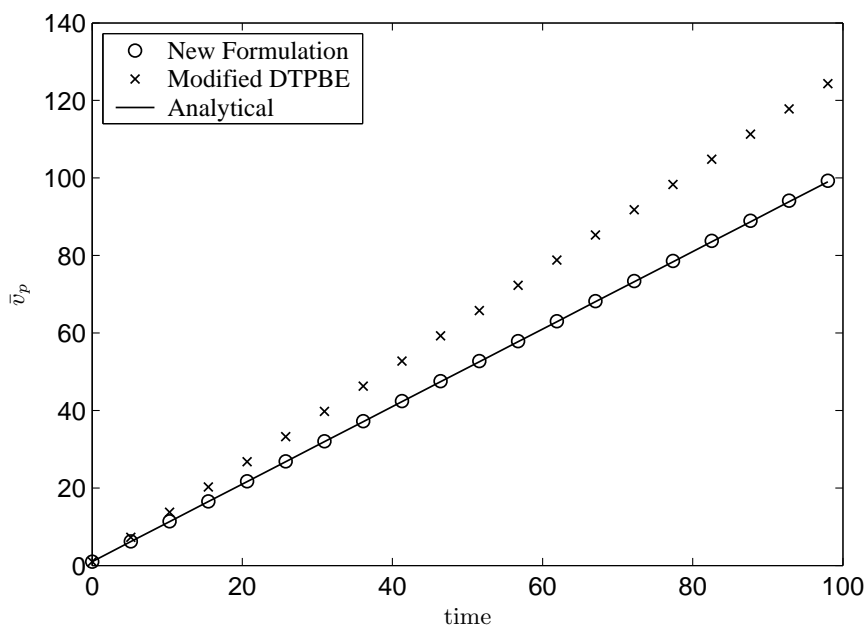
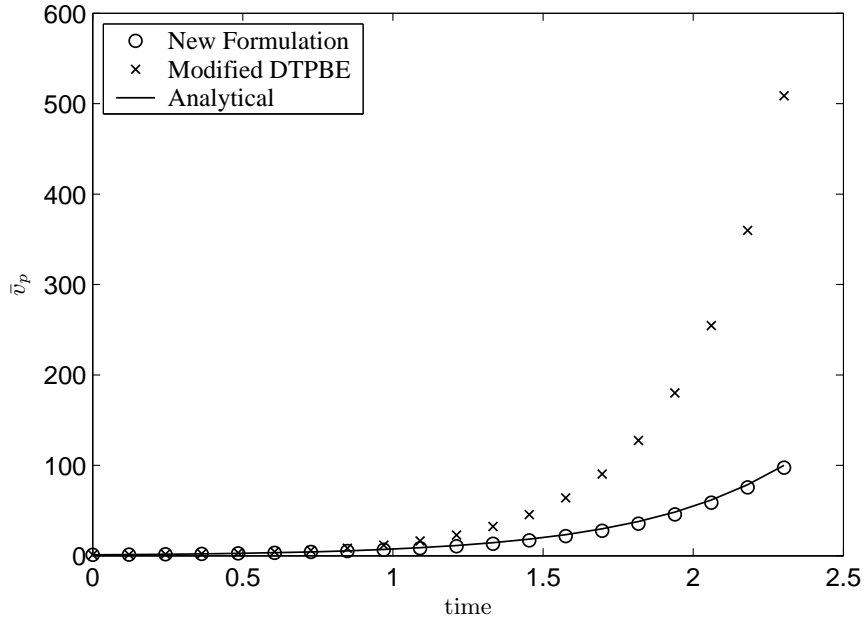
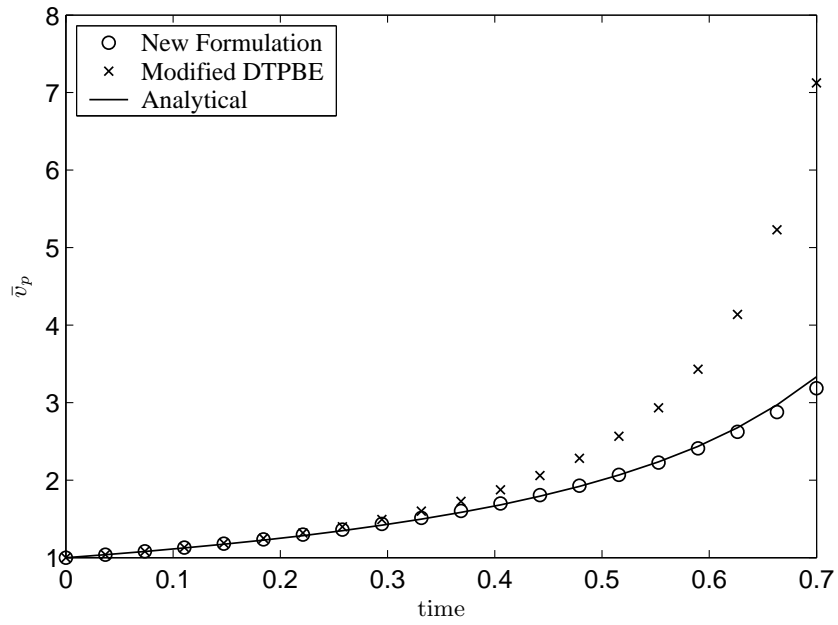


Figure 4.16: Progress of mean particle volume for size-independent aggregation in a batch system, $I_{agg} = 0.98$.



(a) Sum kernel, $I_{agg} = 0.90$.



(b) Product kernel, $I_{agg} = 0.35$.

Figure 4.17: Progress of mean particle volume for aggregation in a batch system.

Table 4.2: Computation time in seconds for both techniques (batch problem)

Case	Kernel	q	Modified DTPBE	New technique
1	Constant	1	1.04	0.68
		2	3.42	1.28
		3	7.34	2.04
2	Sum	1	1.09	1.07
		2	4.10	1.67
		3	9.18	5.01
3	Product	1	0.92	0.60
		2	4.12	1.57
		3	8.34	2.65

Now N_i and $N_{p,i}$ have been calculated simultaneously using discretized PBE for GSD and TMD respectively. Although the analytical solution $N_{p,i}$ is trivial and there is no need to use a DTPBE for this case, we just consider this case in order to check the ability of the new scheme to handle it. A comparison of primary particle number distribution has been depicted in Figure 4.15. The numerical results are obtained for a coarse geometric grid of the type $x_{i+1/2} = 2x_{i-1/2}$ in this section since both the formulations produce the same results for a fine grid. The degree of aggregation, see Subsection 3.2.2, is chosen to be 0.98 in this case. The modified DTPBE gives over-prediction in the large size range. This over-prediction can clearly be seen once again in the corresponding Figure 4.16. The mean volume size of the primary particle is shown in this figure. The figures conclude that both the formulations differ significantly from each other.

Since for a large degree of aggregation analytical solutions for a sum and a product kernel are difficult to calculate, we are plotting only mean volume size in these cases. For the sum kernel $\beta_{i,j} = i + j$, the mean volume size takes the following form

$$\bar{v}_p(t) = \frac{\sum_i i N_{p,i}}{\sum_i N_{p,i}} = \exp(2t), \quad \text{for all } t. \quad (4.66)$$

For the product kernel $\beta_{i,j} = ij$, the mean volume is given by

$$\bar{v}_p(t) = \frac{\sum_i i N_{p,i}}{\sum_i N_{p,i}} = \frac{1}{1-t}, \quad 0 \leq t < 1. \quad (4.67)$$

The temporal change of the primary particle mean volume for the sum kernel $\beta_{i,j} = i + j$, has been drawn in Figure 4.17(a). The computation has been carried out for a degree of aggregation $I_{agg} = 0.90$. The figure shows that the prediction at very short times is the same for both formulations, but at later times prediction by the new formulation is considerably better than that predicted by the modified DTPBE. In Figure 4.17(b), the same comparison is made for a product kernel $\beta_{i,j} = i \times j$. The results have been obtained for $I_{agg} = 0.35$. A similar conclusion can be reached for this case.

The computations were carried out in the programming software MATLAB on a Pentium-4 processor with 1.5 GHz and 512 MB RAM. The set of ordinary differential equations resulting from the discretized formulation is solved by a Runge-Kutta fourth order method with adaptive

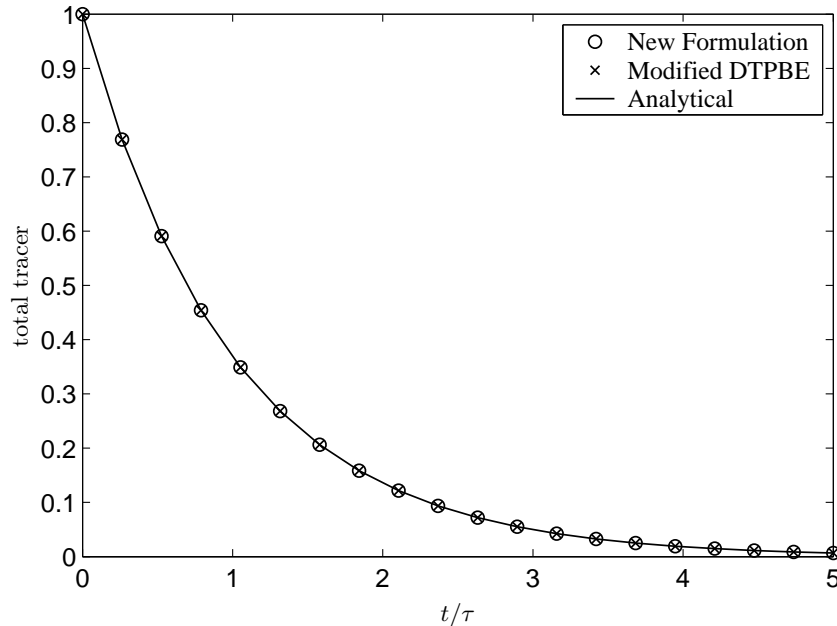


Figure 4.18: Decay of total tracer mass for size-independent aggregation in Ilievski and Hounslow's problem, $I_{\text{agg}} = 1/4$.

step-size control. We have considered several cases in order to check the computation time for both formulations. A comparison of CPU time taken by both formulations for the same demand of accuracy and other conditions is given in Table 4.2. The table indicates that the computation times are comparable for coarse grids but the modified DTPBE takes considerably more time for fine grids in each case.

Aggregation of a mono-disperse feed in MSMPR

Here we take the same problem which has been considered in the previous section in Figures 4.8 and 4.9. Analytical solutions have been summarized in Appendix A.9. Three different types of aggregation kernels have been investigated for numerical computation.

Figure 4.18 shows that both formulations predict exactly the same total tracer mass and are in excellent agreement with analytical results. The prediction of the total tracer mass is similar and is in excellent agreement with analytical results for all other kernels as well. In Figure 4.19, the numerical and analytical temporal changes of tracer weighted mean particle volume $\bar{v}_T(t)$ have been compared. The numerical solutions by the cell average technique are in very close agreement with analytical results at small times while the modified DTPBE gives over-prediction at large times. Both the numerical solutions converges to the analytical solutions using finer grids. More rigorous comparisons are made in J. Kumar et al. [54].

Figures 4.20 and 4.21 compare the prediction of tracer weighted mean particle volume for the sum and the product kernels respectively. Similar findings as before have been observed in this case. The numerical results by the new formulation are in good agreement with analytical

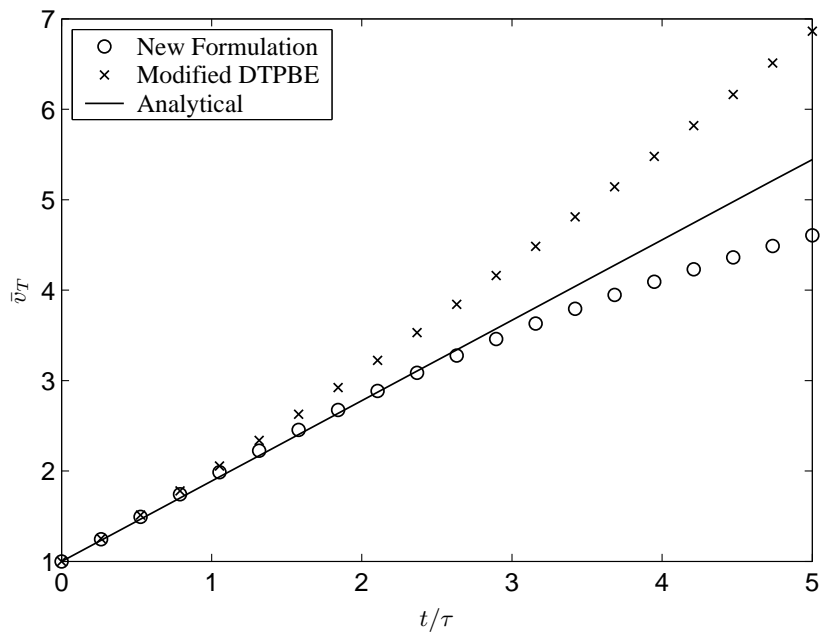


Figure 4.19: Progress of tracer-weighted mean particle volume for a size-independent aggregation kernel in Ilievski and Hounslow’s problem, $I_{agg} = 1/4$.

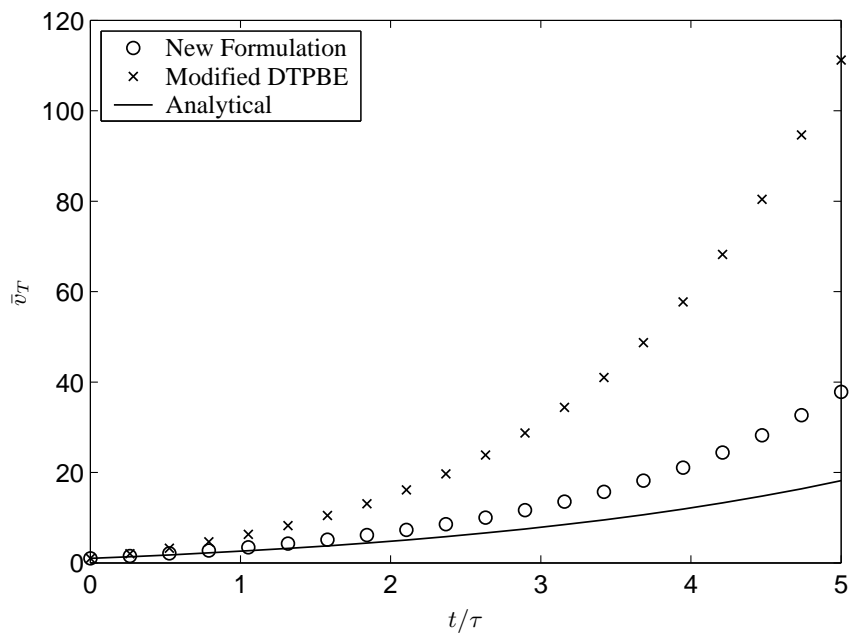


Figure 4.20: Progress of tracer-weighted mean particle volume for a sum aggregation kernel in Ilievski and Hounslow’s problem, $I_{agg} = 1/4$.

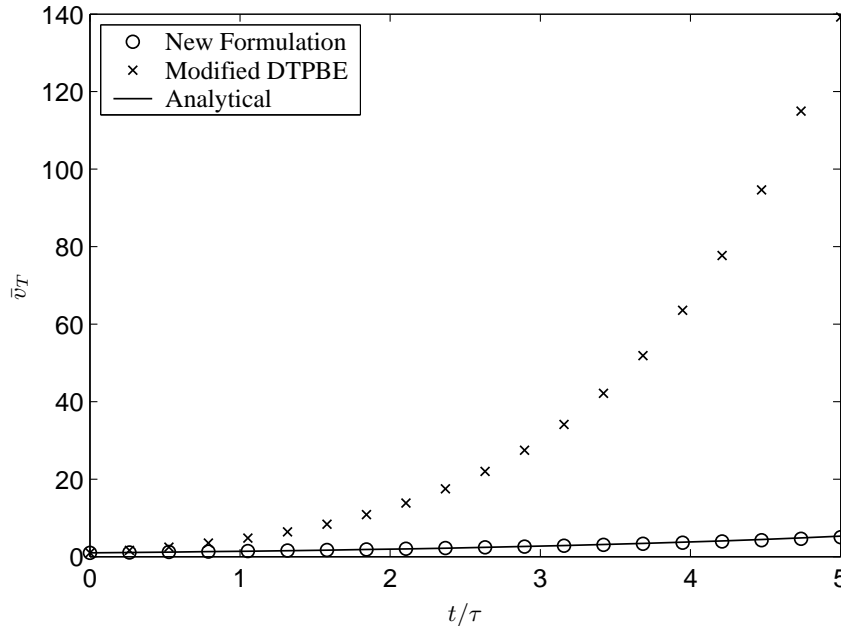


Figure 4.21: Progress of tracer-weighted mean particle volume for a product aggregation kernel in Ilievski and Hounslow’s problem, $I_{\text{agg}} = 1/4$.

results. The prediction is very poor by the modified DTPBE even at small times and a diverging behavior of solution can be observed at large times.

To summarize, the main advantages of the new discretized method discussed above are less computational time and flexibility with type of grids. Moreover, a better accuracy has been observed in all test problems. The new discretization is also easy to implement in any programming language. Additionally, unlike Hounslow’s discretization for TMD, the new formulation is a straightforward extension of the discretized scheme of GSD.

In the following section we shall formulate a numerical scheme for the computation of the complete particle property distribution. The reduced model approach considered up to now in this chapter is limited to produce only some average quantities; in other words, it assumes that a particle of the same size contains the same amount of another distributed property. Whereas in many applications one needs to get information about the complete property distribution. Therefore, we shall extend the previously discussed one-dimensional schemes to multi-dimensional problems.

4.3 Complete Model

As we have observed that by reduced model approach it is possible to simulate the process at low computational cost. But there we estimate only the particle size distribution and amount of the second property as a function of size of particle. Consider a particle property number distribution as shown in a Figure 4.22. The same size particles $v_1 = v_2$ have different content of the second property and therefore different distribution function f_1 and f_2 . Therefore a reduced

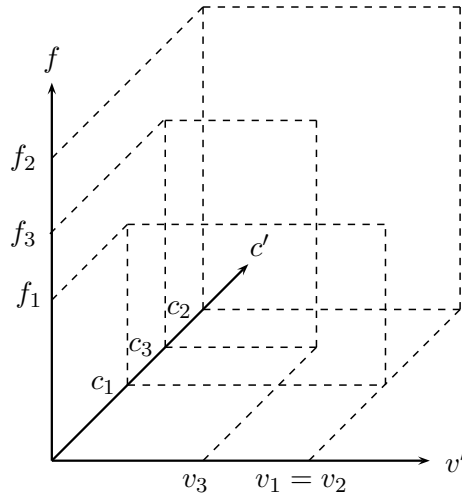


Figure 4.22: A complete two-dimensional particle property distribution.

model approach is not adequate to simulate such processes. We need to calculate the complete property distribution by a numerical scheme applicable for a complete two-dimensional PBE. Here we consider a two-dimensional PBE for aggregation which is an extension of the one-dimensional PBE is given as [70]

$$\begin{aligned} \frac{\partial f(x, y)}{\partial t} = & \frac{1}{2} \int_0^x \int_0^y \hat{\beta}(x - \epsilon, \epsilon, y - \gamma, \gamma) f(x - \epsilon, y - \gamma) f(x, y) d\gamma d\epsilon \\ & - \int_0^\infty \int_0^\infty \hat{\beta}(x, \epsilon, y, \gamma) f(x, y) f(\epsilon, \gamma) d\gamma d\epsilon, \end{aligned} \quad (4.68)$$

where x and y are two extensive properties of the particle and $\hat{\beta}$ is an aggregation kernel. The first term is corresponding to the birth of particles of properties x and y due to aggregation of smaller particles. The last term describes the death of particles (x, y) due to collision and adhesion to particles.

4.3.1 Numerical Methods

Numerical solution of the above PBE is difficult due to the double integral and the non-linear behavior of the equation. There are only few numerical techniques available in the literature to compute the complete property distribution. Some numerical techniques can be found in the following literature [39, 62, 112, 122, 123]. But all of them either have problems regarding the preservation of properties of the distribution or they are computationally very expensive. The accurate computation of total mass and number is essential in many applications. In order to overcome the computational load, an attempt has been made in the previous section. The reduced model is, of course, computationally less expensive but it is not possible to capture the complete two-dimensional behavior of the population with the model. In the reduced model, it has been assumed that particles of the same size contain the same amount of the second property. Therefore the objective of this work is to calculate the complete two-dimensional distribution of the population at a relatively low computational cost.

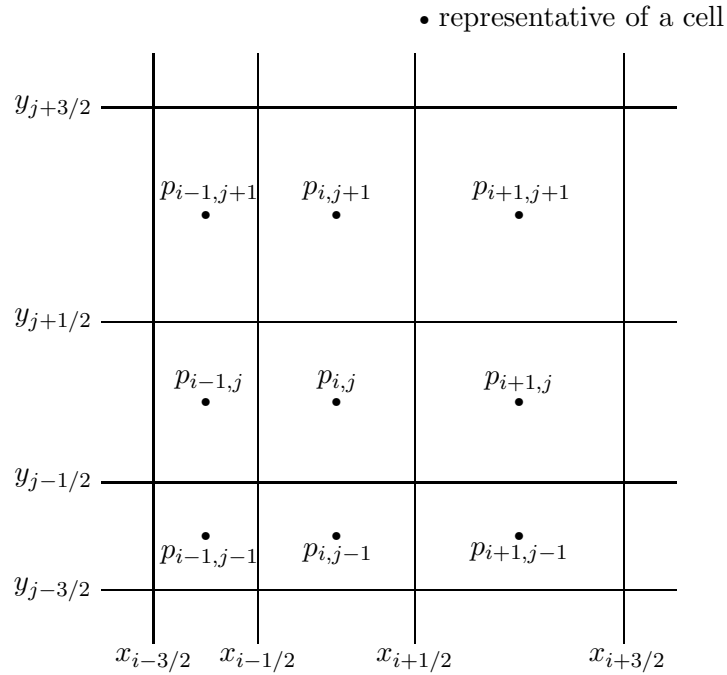


Figure 4.23: Domain discretization.

We present a new numerical technique to solve the two-dimensional PBE (4.68). For simplicity only we have considered a numerical scheme applicable for a two-dimensional PBE. But it can easily be extended to higher dimensional problems. The numerical technique is an extension of the cell average technique which was discussed in Section 3.2 for solving the one-dimensional PBE. This is based on taking averages of all newborn particles in cells. The entire property domain is first divided into small cells. The division may be inhomogeneous, for example geometric or any other appropriate choice. Each cell will have its representative where all the particles of this cell are assumed to be concentrated. The solution strategy follows two steps, one to calculate averages of the properties of the newborn particles in a cell and the other to assign them to the neighboring 4 nodes such that some properties of the distribution are exactly preserved.

Furthermore a similar extension of the fixed pivot technique [57] will be derived and comparisons will be made between the two extended techniques. We will see that the extended cell average technique is more accurate and less diffusive than the extended fixed pivot technique. Moreover, prediction of higher moments is better by the extended cell average technique. On the other hand, the extended fixed pivot technique predicts one extra moment exactly.

Extended cell average technique

We now present the extension of the cell average technique to the two-dimensional PBE (4.68). The entire two-dimensional property domain is divided into small cells $C_{i,j}$. A typical domain discretization is shown in Figure 4.23. The particles within a cell are assumed to be concentrated at a representative node $P_{i,j}$ of the cell $C_{i,j}$. The size of cells could be chosen arbitrarily. It should be noted that each node $P_{i,j}$ is associated with two properties x_i and y_j in case of

CHAPTER 4. NEW NUMERICAL METHODS: MULTI-DIMENSIONAL

a two-dimensional problem. Particulate processes such as aggregation, breakage and growth, produce particles of properties that are not associated with any nodes (except on a uniform linear grid). The idea of the cell average technique is to calculate the average properties of all newborn particles in a cell and observe the position of the averages values. If the two-dimensional average value lies exactly at the node of the cell, which is again rarely possible, then we assign all newborn particles to the node, otherwise these newborn particles must be reassigned to the neighboring nodes depending upon the position of average properties in the cell. The reassignment process is done in such a way that some pre-chosen moments are exactly preserved.

We now formulate the cell average idea mathematically. Let us define the discrete number density N_{ij} , i.e. the total number of particles in a cell by integrating the number density over both properties as

$$N_{ij} = \int_{x_{i-}}^{x_{i+}} \int_{y_{j-}}^{y_{j+}} f(t, x, y) dx dy. \quad (4.69)$$

For notational convenience $x_{i\pm 1/2}$ and $y_{j\pm 1/2}$ are replaced by $x_{i\pm}$ and $y_{i\pm}$ respectively. The moment of the distribution are defined by

$$\mu_{ij}(t) = \int_0^\infty \int_0^\infty x^j y^j f(t, x, y) dx dy.$$

Integrating equation (4.68) over both the properties we obtain

$$\begin{aligned} \frac{dN_{ij}}{dt} &= \frac{1}{2} \int_{x_{i-}}^{x_{i+}} \int_{y_{j-}}^{y_{j+}} \int_0^x \int_0^y \hat{\beta}(x - \epsilon, \epsilon, y - \gamma, \gamma) f(x - \epsilon, y - \gamma) f(\epsilon, \gamma) d\gamma d\epsilon dy dx \\ &\quad - \int_{x_{i-}}^{x_{i+}} \int_{y_{j-}}^{y_{j+}} \int_0^\infty \int_0^\infty \hat{\beta}(x, \epsilon, y, \gamma) f(x, y) f(\epsilon, \gamma) d\gamma d\epsilon. \end{aligned} \quad (4.70)$$

Since particles within a cell C_{ij} are assumed to be concentrated at the representative node $P_{i,j} = (x_j, y_j)$, the number density can be expressed using Dirac point masses as

$$f(t, x, y) = \sum_{i=1}^{I_x} \sum_{j=1}^{I_y} N_{ij} \delta(x - x_i) \delta(y - y_j). \quad (4.71)$$

Here I_x and I_y are the total number of cells in the x and y property directions respectively. Putting the value of f from (4.71) into equation (4.70), we obtain the following equation, see Appendix B.10,

$$\frac{dN_{ij}}{dt} = B_{ij} - D_{ij}. \quad (4.72)$$

The birth and death terms are given as

$$B_{ij} = \sum_{\substack{k \geq l \\ k, l \\ x_{i-} \leq (x_k + x_l) < x_{i+}}} \sum_{\substack{m \geq n \\ m, n \\ y_{j-} \leq (y_m + y_n) < y_{j+}}} \left(1 - \frac{1}{2} \delta_{k,l} \delta_{m,n} \right) \hat{\beta}_{klmn} N_{km} N_{ln}, \quad (4.73)$$

and

$$D_{ij} = \sum_{p=1}^{I_x} \sum_{q=1}^{I_y} \hat{\beta}_{ipjq} N_{ij} N_{pq}, \quad (4.74)$$

where

$$\hat{\beta}_{klmn} = \hat{\beta}(x_j, x_l, y_m, y_n), \quad (4.75)$$

and $\delta_{m,n}$ is Kronecker delta.

For uniform linear grids, equation (4.72) reduces exactly to the discrete PBE for two-dimensional problems. This could of course be used for numerical computation on uniform linear grids at a very high computational cost. Due to the high computational costs of linear grids, other inhomogeneous such as geometric grids are preferred. Inhomogeneity in the grids causes inconsistency of moments in this formulation. In order to resolve this problem, the birth term has to be modified (reassignment of particles to neighboring nodes) so that the formulation becomes consistent with certain moments. This issue has already been discussed in detail for one-dimensional problems.

The birth term (4.73) approximates the total birth rate in the cell C_{ij} . Note that the newborn particles in the cell C_{ij} may be distributed everywhere. Since a birth takes place by aggregation of smaller particles, it is easy to compute the net flux of the property x , $V_{x,i}$, into cell C_{ij} as a result of these aggregation as

$$V_{x,i} = \sum_{\substack{k \geq l \\ k,l \\ x_{i-} \leq (x_k + x_l) < x_{i+}}} \sum_{\substack{m \geq n \\ m,n \\ y_{j-} \leq (y_m + y_n) < y_{j+}}} \left(1 - \frac{1}{2} \delta_{k,l} \delta_{m,n} \right) \hat{\beta}_{klmn} N_{km} N_{ln} (x_k + x_l). \quad (4.76)$$

Similarly, the net flux of the property y , $V_{y,j}$, can be computed as

$$V_{y,j} = \sum_{\substack{k \geq l \\ k,l \\ x_{i-} \leq (x_k + x_l) < x_{i+}}} \sum_{\substack{m \geq n \\ m,n \\ y_{j-} \leq (y_m + y_n) < y_{j+}}} \left(1 - \frac{1}{2} \delta_{k,l} \delta_{m,n} \right) \hat{\beta}_{klmn} N_{km} N_{ln} (y_m + y_n). \quad (4.77)$$

Consequently, the average property values of all newborn particles in the cell $C_{i,j}$ can be calculated as

$$\bar{x}_i = \frac{V_{x,i}}{B_{ij}}, \quad (4.78)$$

and

$$\bar{y}_j = \frac{V_{y,j}}{B_{ij}}. \quad (4.79)$$

If these average values \bar{x}_i and \bar{y}_j are different from the representatives x_i and y_j , particles have to be reassigned to the neighboring nodes. Note that in the case of linear (equidistant) grids in both directions \bar{x}_i and \bar{y}_j are always equal to x_i and y_i . Therefore, in that case all particles will

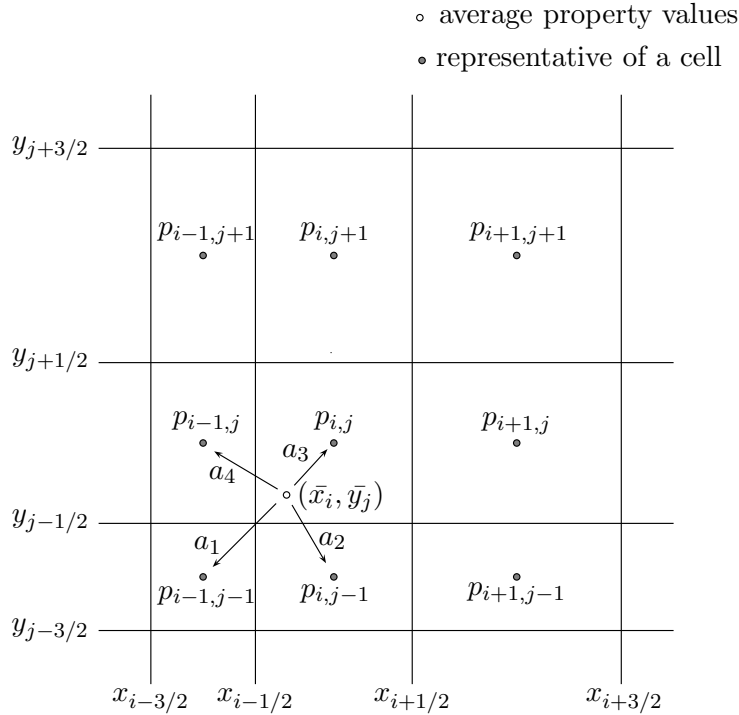


Figure 4.24: Distribution of particles to neighboring nodes.

be assigned to the same cell they belong to without any assignment to neighboring nodes. An obvious question arises: Which and how many neighboring nodes must be chosen for assignment of particles? The number of nodes for assignment of course depends on the choice of number of moments we want to preserve during assignment of particles. Here we are interested in preserving total number and total mass of each properties and therefore we have chosen, probably the most appropriate and easy choice, the four surrounding nodes of the position of average properties. There are a total of 9 nodes which may get a birth contribution from newborn particles in cell C_{ij} . The choice of 4 neighboring nodes depends on the position of (\bar{x}_i, \bar{y}_j) in the cell C_{ij} .

Let us consider that the average property values as shown in Figure 4.24. Clearly in this case the particles will be assigned to the nodes $p_{i-1,j-1} = (x_{i-1}, y_{j-1})$, $p_{i,j-1} = (x_i, y_{j-1})$, $p_{i,j} = (x_i, y_j)$ and $p_{i-1,j} = (x_{i-1}, y_j)$. Let us suppose that the particle fractions a_1 , a_2 , a_3 and a_4 have been assigned to the neighboring nodes $p_{i-1,j-1}$, $p_{i,j-1}$, $p_{i,j}$ and $p_{i-1,j}$ respectively. For the consistency of zeroth μ_{00} and first moments μ_{10} or μ_{01} , these fractions must satisfy the following relations

$$\begin{aligned}
 a_1 + a_2 + a_3 + a_4 &= B_{ij}, \\
 a_1 x_{i-1} + a_2 x_i &= (a_1 + a_2) \bar{x}_i, \\
 a_3 x_i + a_4 x_{i-1} &= (a_3 + a_4) \bar{x}_i, \\
 a_1 y_{j-1} + a_4 y_j &= (a_1 + a_4) \bar{y}_j, \\
 a_2 y_{j-1} + a_3 y_j &= (a_2 + a_3) \bar{y}_j.
 \end{aligned}$$

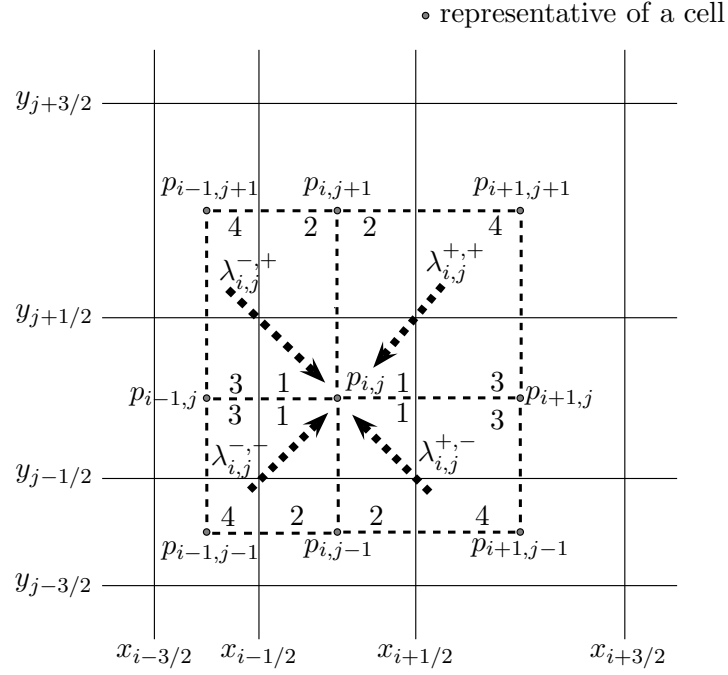


Figure 4.25: Collection of particles from neighboring nodes.

The above system of equations (4 variables and 5 equations) has a unique solution. The last four equations are dependent equations. This system of equations can easily be solved to give

$$a_1 = \frac{(x_i - \bar{x}_i)(y_j - \bar{y}_j)}{(x_i - x_{i-1})(y_j - y_{j-1})} B_{ij}, \quad (4.80)$$

$$a_2 = \frac{(\bar{x}_i - x_{i-1})(y_j - \bar{y}_j)}{(x_i - x_{i-1})(y_j - y_{j-1})} B_{ij}, \quad (4.81)$$

$$a_3 = \frac{(\bar{x}_i - x_{i-1})(\bar{y}_j - y_{j-1})}{(x_i - x_{i-1})(y_j - y_{j-1})} B_{ij}, \quad (4.82)$$

$$a_4 = \frac{(x_i - \bar{x}_i)(\bar{y}_j - y_{j-1})}{(x_i - x_{i-1})(y_j - y_{j-1})} B_{ij}. \quad (4.83)$$

Furthermore, it is easy to show that the assignment process of particles is also consistent with the first cross moment μ_{11} , see Appendix B.11. Thus, the fractions also satisfy the following equality

$$a_1 x_{i-1} y_{j-1} + a_2 x_i y_{j-1} + a_3 x_i y_j + a_4 x_{i-1} y_j = B_{ij} \bar{x}_i \bar{y}_j. \quad (4.84)$$

It must be pointed out here that the particles assignment process is consistent with the first cross moment μ_{11} but we have lost this consistency during the averaging process, i.e.

$$\sum_{\substack{k \geq l \\ k, l}} \sum_{\substack{m \geq n \\ m, n}} \left(1 - \frac{1}{2} \delta_{k,l} \delta_{m,n}\right) \hat{\beta}_{klmn} N_{km} N_{ln} (x_k + x_l)(y_m + y_n) \neq B_{ij} \bar{x}_i \bar{y}_j.$$

$x_{i-} \leq (x_k + x_l) < x_{i+} \quad y_{j-} \leq (y_m + y_n) < y_{j+}$

CHAPTER 4. NEW NUMERICAL METHODS: MULTI-DIMENSIONAL

It is clear now that the formulation is consistent with μ_{00} , μ_{10} and μ_{01} only, but not with μ_{11} . Now the aim is to collect all birth contributions coming from surrounding cells and the cell C_{ij} itself. There are 8 surrounding cells which may give rise to birth in cell C_{ij} . Similar to the one-dimensional case it is convenient to define a function λ as

$$\lambda_{i,j}^{\pm,\pm}(x, y) = \frac{(x - x_{i\pm 1})(y - y_{j\pm 1})}{(x_i - x_{i\pm 1})(y_j - y_{j\pm 1})}. \quad (4.85)$$

Now a_1 , a_2 , a_3 and a_4 can be rewritten using $\lambda_{i,j}^{\pm,\pm}$ as

$$a_1 = \lambda_{i-1,j-1}^{+,+}(\bar{x}_i, \bar{y}_j) B_{ij}, \quad (4.86)$$

$$a_2 = \lambda_{i,j-1}^{-,+}(\bar{x}_i, \bar{y}_j) B_{ij}, \quad (4.87)$$

$$a_3 = \lambda_{i,j}^{-,-}(\bar{x}_i, \bar{y}_j) B_{ij}, \quad (4.88)$$

$$a_4 = \lambda_{i-1,j}^{+,-}(\bar{x}_i, \bar{y}_j) B_{ij}. \quad (4.89)$$

Collecting all birth contributions to the node $P_{i,j}$, the final formulation takes the following form

$$\begin{aligned} \frac{dN_{ij}}{dt} = & \sum_{p=0}^1 \sum_{q=0}^1 B_{i-p,j-q} \lambda_{i,j}^{-,-}(x_{i-p}, y_{j-q}) H [(-1)^p(x_{i-p} - \bar{x}_{i-p})] H [(-1)^q(y_{j-q} - \bar{y}_{j-q})] \\ & + \sum_{p=0}^1 \sum_{q=0}^1 B_{i-p,j+q} \lambda_{i,j}^{-,+}(x_{i-p}, y_{j+q}) H [(-1)^p(x_{i-p} - \bar{x}_{i-p})] H [(-1)^{q+1}(y_{j+q} - \bar{y}_{j+q})] \\ & + \sum_{p=0}^1 \sum_{q=0}^1 B_{i+p,j+q} \lambda_{i,j}^{+,+}(x_{i+p}, y_{j+q}) H [(-1)^{p+1}(x_{i+p} - \bar{x}_{i+p})] H [(-1)^{q+1}(y_{j+q} - \bar{y}_{j+q})] \\ & + \sum_{p=0}^1 \sum_{q=0}^1 B_{i+p,j-q} \lambda_{i,j}^{+,-}(x_{i+p}, y_{j-q}) H [(-1)^{p+1}(x_{i+p} - \bar{x}_{i+p})] H [(-1)^q(y_{j-q} - \bar{y}_{j-q})] \\ & - \sum_{p=1}^{I_x} \sum_{q=1}^{I_y} \hat{\beta}_{ipjq} N_{ij} N_{pq}. \end{aligned} \quad (4.90)$$

Here H is the Heaviside function defined as in previous chapter. Figure 4.25 explains the birth terms in the above formulation. Four major terms (double sum in each) in the birth are corresponding to the four different domains, shown by dotted lines, in Figure 4.25. Each major term has a contribution from four cells, numbered 1, 2, 3, 4, shown in the figure i.e. each major term has four terms again. There are a total of 16 terms and many of them may be zero at a particular time depending upon the average property values in each cell.

It is also of interest to mention the discrete formulation of a one-dimensional PBE in the form presented above and see the similarity between them. The discrete formulation for the one-

dimensional case can be rewritten as

$$\begin{aligned} \frac{dN_i}{dt} = & \sum_{p=0}^1 B_{i-p} \lambda_i^-(\bar{x}_{i-p}) H [(-1)^p (x_{i-p} - \bar{x}_{i-p})] + \sum_{p=0}^1 B_{i+p} \lambda_i^+(\bar{x}_{i+p}) H [(-1)^{p+1} (x_{i+p} - \bar{x}_{i+p})] \\ & - \sum_{q=1}^I \beta_{iq} N_i N_q. \end{aligned} \quad (4.91)$$

Here the parameter λ is given as

$$\lambda_i^\pm(x) = \frac{(x - x_{i\pm 1})}{(x_i - x_{i\pm 1})}. \quad (4.92)$$

Clearly the two-dimensional formulation is a direct extension of the one-dimensional case. We have written the formulation (4.90) in such a way that it could be easily extended to higher dimensional (more than two) problems. For example in the three dimensional case each birth term will be extended corresponding to the third z variable and the total major birth term (triple sum in each) will be 8 in that case. Nevertheless the formulation will become computationally very expensive and therefore some other dimensionality reduction methods or Monte Carlo methods would be preferred for higher dimensional cases.

Extended fixed pivot technique

Now it is easy to formulate the extended version of the fixed pivot technique for two-dimensional problems. The basic difference between the two techniques is the averaging of properties. The reassignment strategy is the same in both the techniques. If a newborn particle appears due to aggregation or breakage in the dotted domain in Figure 4.26 then it will be partly assigned to the node $P_{i,j}$ in such a way that the number and mass is preserved. Note that this domain is not the same as that of the cell average technique, all surrounding cells were taken into account for the assignment in the cell average technique. On the other hand, in the fixed pivot technique a part of the surrounding cells is being taken into consideration for the assignment. In the cell average technique, particle birth reassignment was done once for each cell whereas in the fixed pivot technique reassignment is done for each birth separately.

Consider that a birth takes place at (x, y) in the sub-domain A shown in the Figure 4.26. It is clear that particles appeared at (x, y) will be assigned to $P_{i-1,j-1}$, $P_{i,j-1}$, $P_{i,j}$ and $P_{i-1,j}$. Suppose that fractions a_1 , a_2 , a_3 and a_4 of this birth have been assigned to $P_{i-1,j-1}$, $P_{i,j-1}$, $P_{i,j}$ and $P_{i-1,j}$ respectively. Similar to the cell average technique, for the exact prediction of total number and total mass of each component these fraction will be given by

$$a_1 = \frac{(x_i - x)(y_j - y)}{(x_i - x_{i-1})(y_j - y_{j-1})}, \quad (4.93)$$

$$a_2 = \frac{(x - x_{i-1})(y_j - y)}{(x_i - x_{i-1})(y_j - y_{j-1})}, \quad (4.94)$$

$$a_3 = \frac{(x - x_{i-1})(y - y_{j-1})}{(x_i - x_{i-1})(y_j - y_{j-1})}, \quad (4.95)$$

$$a_4 = \frac{(x_i - x)(y - y_{j-1})}{(x_i - x_{i-1})(y_j - y_{j-1})}. \quad (4.96)$$

Let us denote the fraction of the birth assigned to the node $P_{i,j}$ from the new particles appeared at (x, y) in the dotted domain shown in Figure 4.26 by a function $\eta(x, y)$. Thus, the function $\eta(x, y)$ is given by

$$\eta(x, y) = \begin{cases} \frac{(x - x_{i-1})(y - y_{j-1})}{(x_i - x_{i-1})(y_j - y_{j-1})}, & x_{i-1} \leq x < x_i \text{ and } y_{j-1} \leq c < y_j, \quad (\text{sub-domain } A) \\ \frac{(x - x_{i-1})(y_{j+1} - y)}{(x_i - x_{i-1})(y_{j+1} - y_j)}, & x_{i-1} \leq x < x_i \text{ and } y_j \leq c < y_{j+1}, \quad (\text{sub-domain } B) \\ \frac{(x_{i+1} - x)(y_{j+1} - y)}{(x_{i+1} - x_i)(y_{j+1} - y_j)}, & x_i \leq y < x_{i+1} \text{ and } y_j \leq c < y_{j+1}, \quad (\text{sub-domain } C) \\ \frac{(x_{i+1} - x)(y - y_{j-1})}{(x_{i+1} - x_i)(y_j - y_{j-1})}, & x_i \leq y < x_{i+1} \text{ and } y_{j-1} \leq c < y_j, \quad (\text{sub-domain } D). \end{cases} \quad (4.97)$$

Now the continuous PBE (4.68) is integrated over the cell C_{ij} and the birth term is modified to make the formulation consistent with the total number and mass. It takes the following form

$$\begin{aligned} \frac{dN_{ij}}{dt} &= \frac{1}{2} \int_{x_{i-1}}^{x_{i+1}} \int_{y_{j-1}}^{y_{j+1}} \eta(x, y) \int_0^x \int_0^y \hat{\beta}(x - \epsilon, \epsilon, y - \gamma, \gamma) f(x - \epsilon, y - \gamma) f(\epsilon, \gamma) d\gamma d\epsilon dy dx \\ &\quad - \int_{x_{i-}}^{x_{i+}} \int_{y_{j-}}^{y_{j+}} \int_0^\infty \int_0^\infty \hat{\beta}(x, \epsilon, y, \gamma) f(x, y) f(\epsilon, \gamma) d\gamma d\epsilon. \end{aligned} \quad (4.98)$$

Substituting the $f(x, y)$ using Dirac point masses from equation (4.71) and after some manipulations similar to the cell average technique, one arrives at the following discrete equations

$$\begin{aligned} \frac{dN_{ij}}{dt} &= \sum_{\substack{k \geq l \\ k, l \\ x_{i-1} \leq (x_k + x_l) < x_{i+1} \\ y_{j-1} \leq (y_m + y_n) < y_{j+1}}} \sum_{\substack{m \geq n \\ m, n}} \left(1 - \frac{1}{2} \delta_{k,l} \delta_{m,n} \right) \eta(x_k + x_l, y_m + y_n) \hat{\beta}_{klmn} N_{km} N_{ln} \\ &\quad - \sum_{k=1}^{I_x} \sum_{l=1}^{I_y} \hat{\beta}_{ikjl} N_{ij} N_{kl}. \end{aligned} \quad (4.99)$$

Note that besides the correct prediction of total mass and number the fixed pivot technique is consistent with the first cross moment μ_{11} which we have lost in the cell average technique during averaging process. It is due to the fact that we reassigned particles in the fixed pivot technique immediately after their birth to the appropriate grids according to the rule discussed above. We have already seen that the reassignment rule is also consistent with the first cross moment. In the next section we will see some comparisons of the two techniques with analytically available solutions.

4.3.2 Test Cases

In order to show the effectiveness of the two numerical techniques, we now present some comparisons of the numerical solutions with analytical solutions of two components processes. The aim

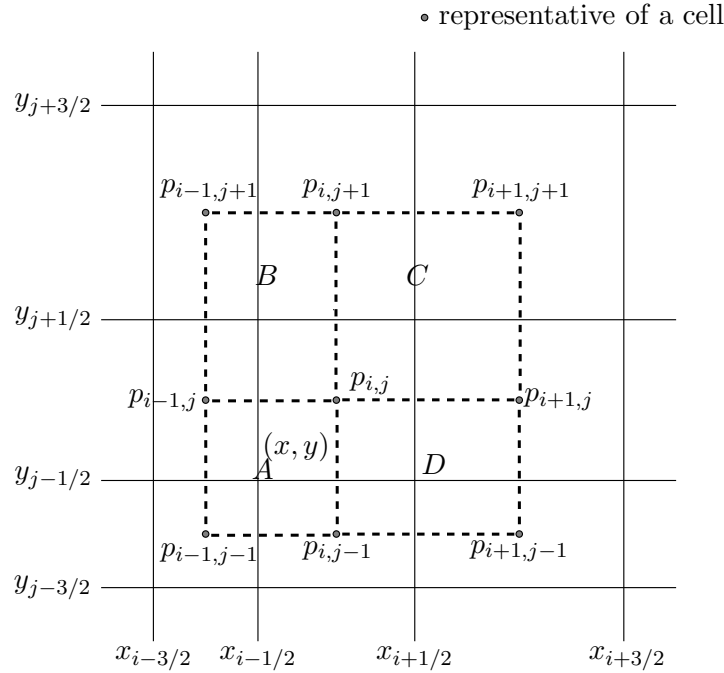


Figure 4.26: Sub-domains which produce particle birth at the node $P_{i,j}$.

is to demonstrate the difference between the extended cell average and fixed pivot techniques. We will consider two test cases in this section. The first test case presents the computation on a complete two-dimensional problem to check the ability of the schemes to estimate the complete particle property distribution and its moments. The second test case is an one-dimensional problem computed by the extended techniques to demonstrate the numerical diffusion.

Test case 1

First we considered a problem from Lushnikov [70]. He considered a discrete aggregation problem of two different types of particles. Analytical solutions for the number density and its moments for the constant kernels have been summarized in Appendix A.8. Two different types of mono-disperse particles with the same concentration have been taken as an initial condition, shown in Figure 4.27. The number of monomers of each type m and n are displayed on the x and y axes respectively. The z axis represents the number density of particles.

The computation is made at high degree of aggregation, $I_{agg} = 0.98$. The number of grids in each direction has been taken to be 20. First 10 grids are chosen linearly and the rest are taken geometrically by the rule $x_{i+1/2} = 2x_{i-1/2}$ in both the directions. A low order MATLAB ODE23 solver is used for integration. The ODE23 is based on an explicit Runge-Kutta (2,3) formula. A low order integrator had to be taken since higher order methods, like the explicit Runge-Kutta (4,5), produces negative values. A more sophisticated higher order method which preserve positivity must be used.

The complete particle size distribution at final time computed by the cell average technique is shown in Figure 4.28. The analytical and numerical particle property distributions computed by the fixed pivot technique match exactly with the Figure 4.28 and therefore we omitted to

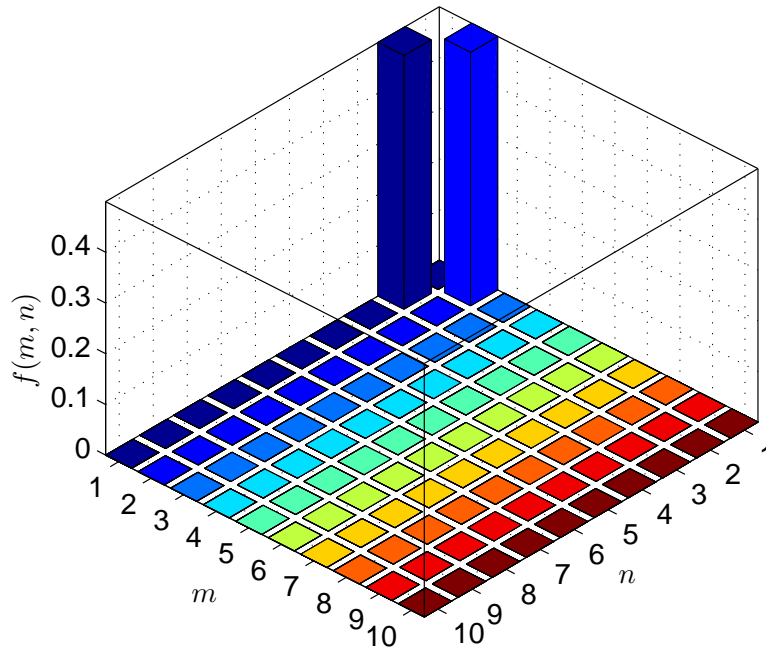


Figure 4.27: Initial condition for the test case 1.

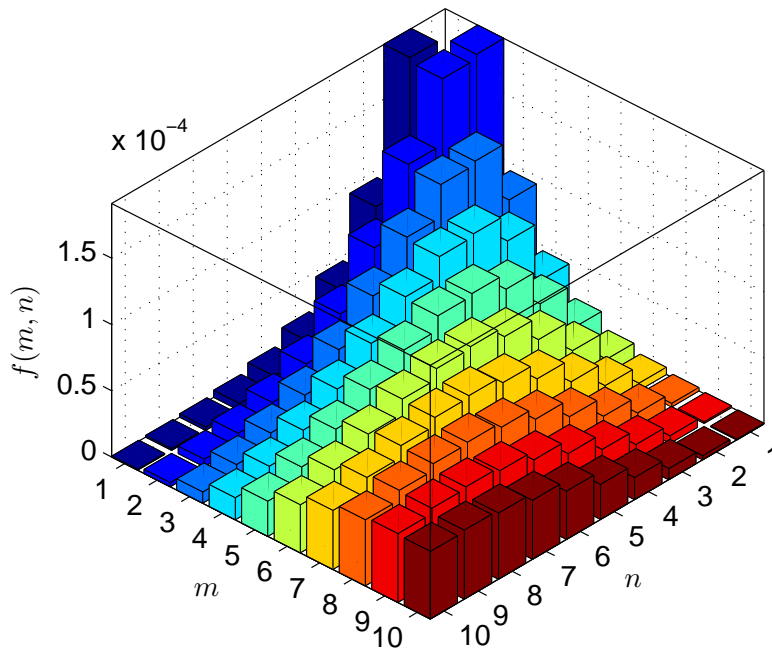


Figure 4.28: Complete particle property distribution, $I_{agg} = 0.98$.

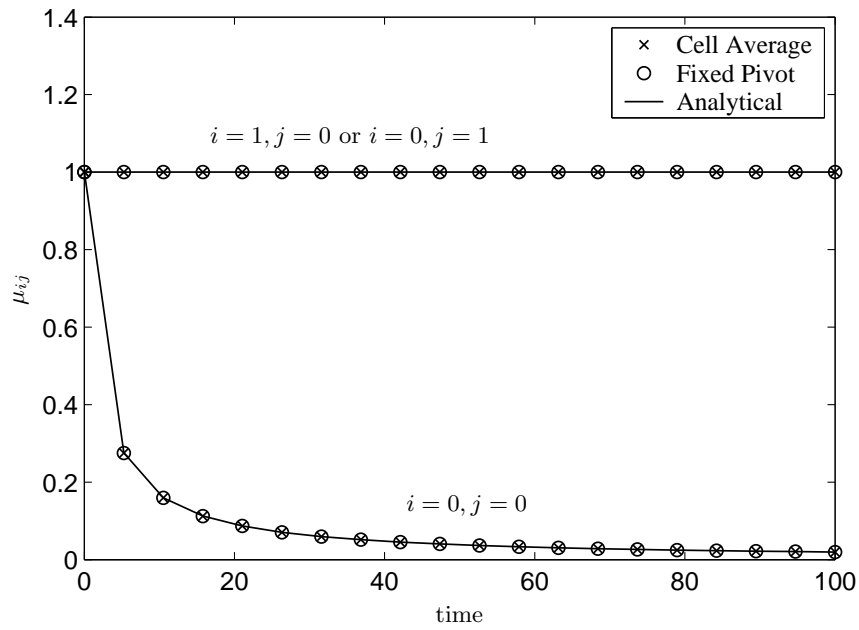


Figure 4.29: Temporal change of the first two moments, $I_{agg} = 0.98$.

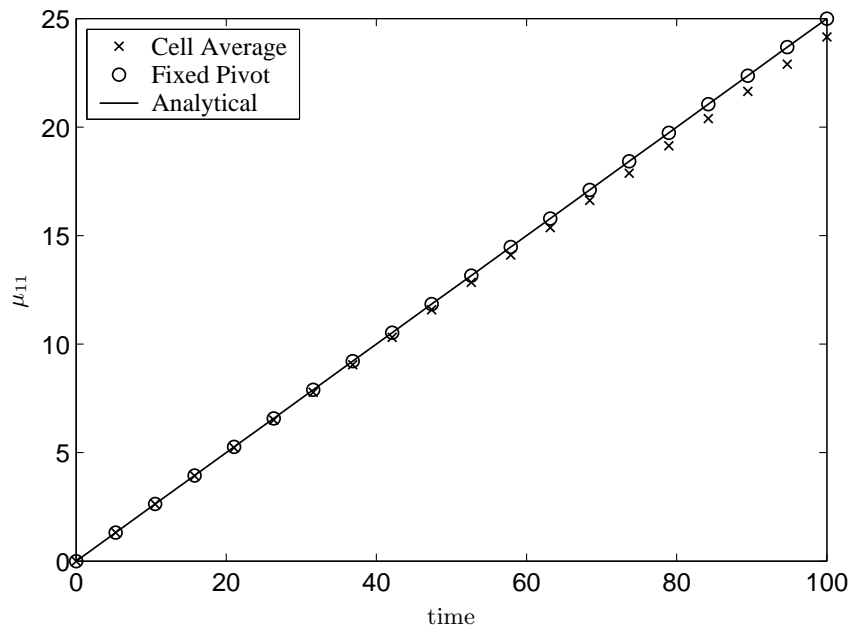


Figure 4.30: Temporal change of the first cross moment, $I_{agg} = 0.98$.

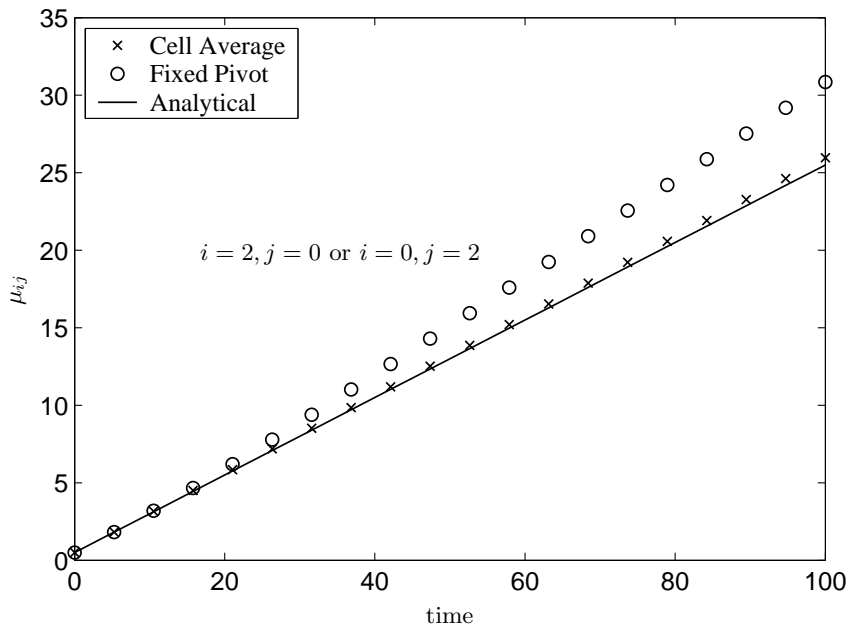


Figure 4.31: Temporal change the second moment, $I_{agg} = 0.98$.

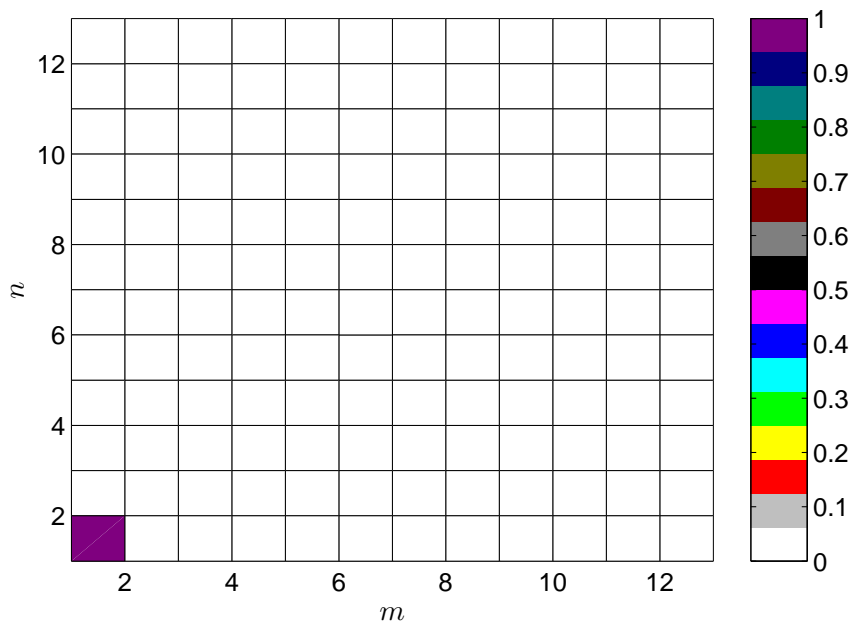
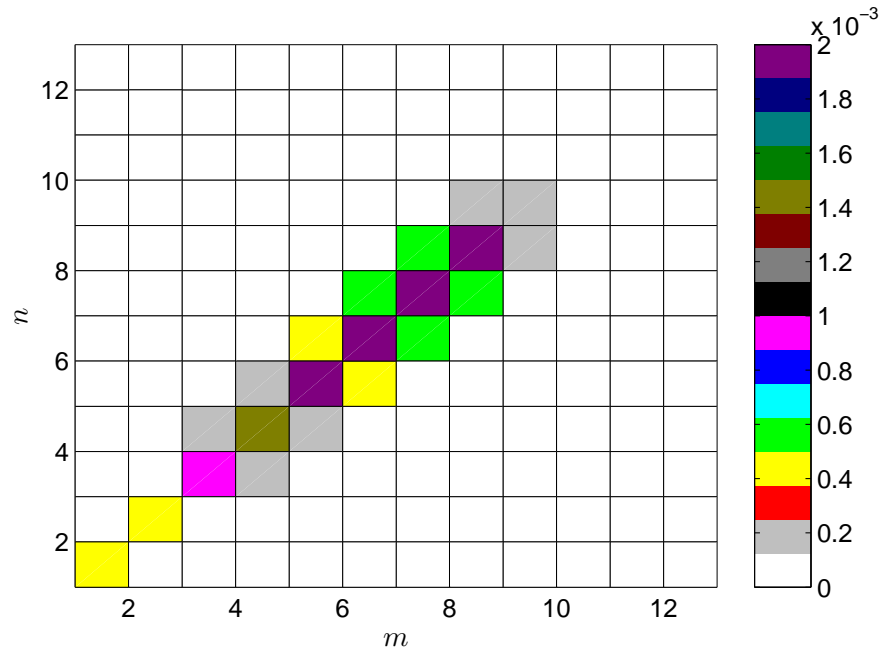
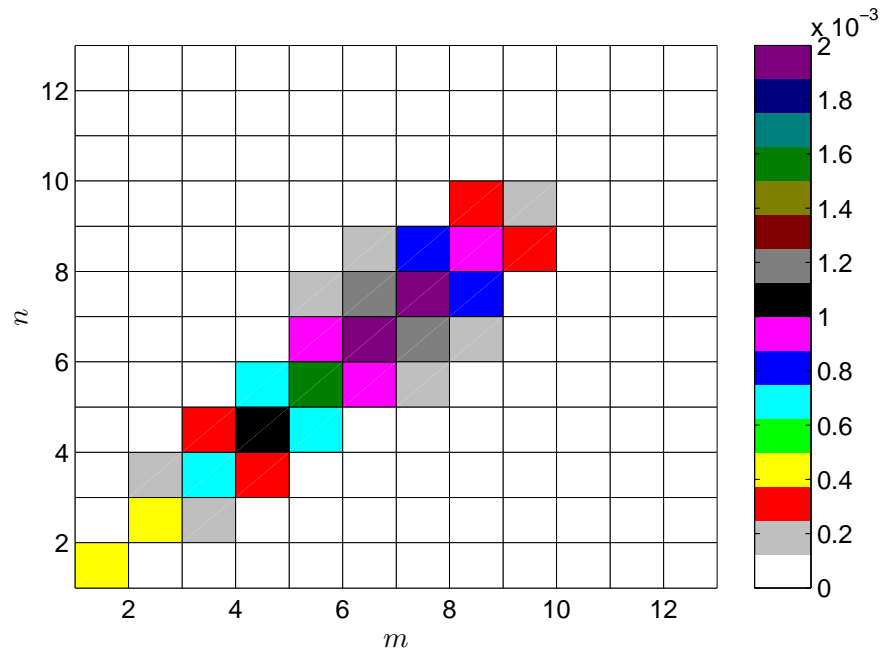


Figure 4.32: Initial condition for the test case 2.



(a) The cell average technique



(b) The fixed pivot technique

Figure 4.33: A comparison of the two technique showing numerical diffusion, $I_{agg} = 0.98$.

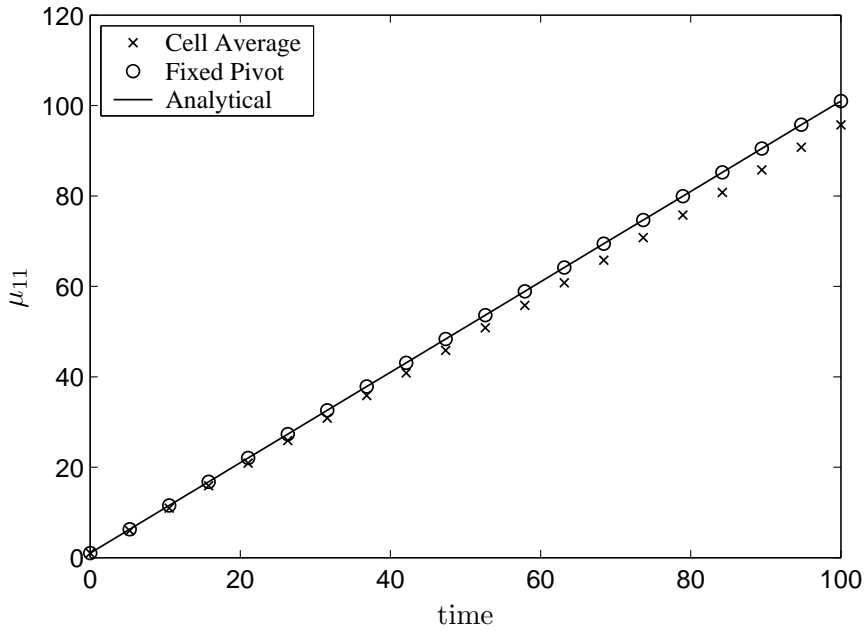


Figure 4.34: Temporal change of the first cross moment, $I_{\text{agg}} = 0.98$.

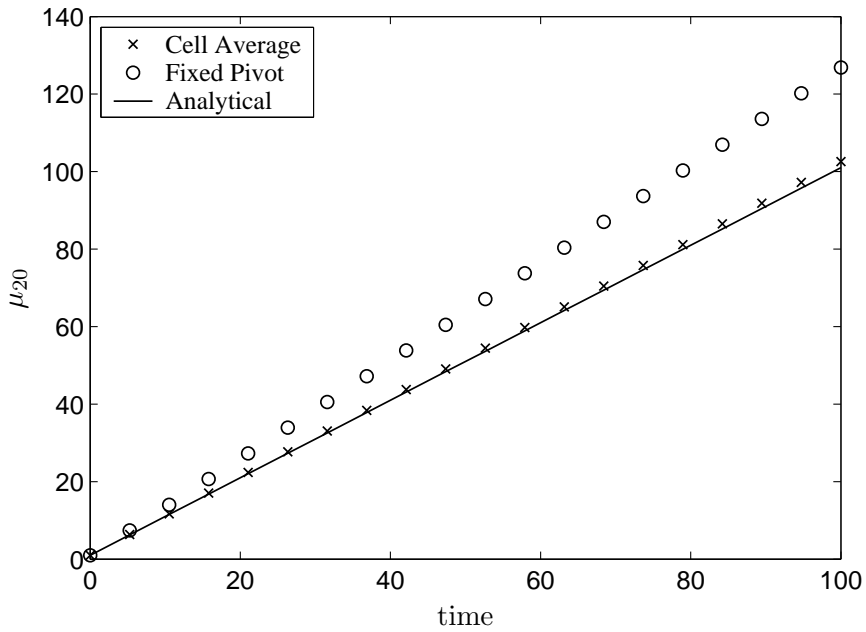


Figure 4.35: Temporal change of the second moment, $I_{\text{agg}} = 0.98$.

present them here. The numerical results are symmetrical since we have taken the same initial concentration of both types of particles. It is difficult to here to measure the efficiency of the schemes by direct comparison of the particle property distribution. Therefore we have compared the few important moments of the particle property distribution.

As expected, the prediction of the zeroth and first moment in Figure 4.29 is exactly matching with the analytical solutions and is the same by both the techniques. The first cross moments have been plotted in Figure 4.30. As we know that the cell average formulation is consistent only with the two moments μ_{00} and μ_{01} or μ_{10} , whereas besides these moments the fixed pivot technique is also consistent with μ_{11} . The same observations can be seen in the Figure 4.30. The prediction by the fixed pivot technique is exact while a slight under-prediction has been observed by the cell average technique. This is due to the fact that we lose during averaging process in the cell average technique.

Figure 4.31 presents the temporal evolution of the second moment. Completely different results are observed in this case. Though the cell average technique is consistent only with two moments, the prediction of the second moment is extremely accurate. On the other hand the fixed pivot technique which reproduces the first cross moment exactly, however, gives a very poor prediction of the second moment. A diverging behavior with time has been observed in the fixed pivot technique. The temporal change of the second moment clearly reflects the ability of the scheme of the cell average technique to predict higher moments with good accuracy.

We can not conclude from this test problem the choice of a better technique. The fixed pivot technique predicts three moments exactly but fails to predicts higher moments. On the other hand the cell average predicts higher moments with good accuracy. Nevertheless in the next case we will see that the cell average technique predicts not only higher moments accurately but also suffers from much less numerical diffusion.

Test case 2

Here we compute a one-dimensional problem with both extended techniques. We consider aggregation of mono-disperse 2-mer granules and each granule is composed of two different types of primary particles. Whenever two granules aggregate they will form a new granule with an equal number of primary particles of each type. In that way it is a one-dimensional problem. The initial condition is shown in Figure 4.32. The new granules will be formed along the diagonal only. The aim here is to calculate the PSD using both techniques and to see the numerical diffusion in each case. The computation is done with the constant aggregation kernel at $I_{agg} = 0.98$. The number of grid points in each direction is chosen to be 13 with the rule $x_{i+1/2} = 2x_{i-1/2}$. The grid point numbers have been shown on the x and y axis. Again the ODE23 MATLAB solver is used to solve the system of ODEs.

The distribution of granules has been presented in Figure 4.33. The grid points are displayed on x and y axes. The granules are supposed to be appear at the diagonal only. Due to the non-linear grids, granules do not appear exactly at the grid points and therefore a granule reassignment is done in both techniques which causes diffusion. The numerical diffusion can not be avoided completely. However, the Figure 4.33 clearly shows that the cell average technique is less diffusive than the fixed pivot technique.

CHAPTER 4. NEW NUMERICAL METHODS: MULTI-DIMENSIONAL

Furthermore, different moments of granule distribution have been compared with the analytical solutions. The first cross moment is plotted in Figure 4.34. Once again the same observations like in the previous test case have been obtained, i.e. a slight under-prediction by the cell average technique and exact prediction by the fixed pivot technique. A comparison of second moments has been shown in Figure 4.35. The prediction by the cell average technique is extremely accurate while a diverging behavior by the fixed pivot technique is obtained. Some of the results presented in this section can also be found in J. Kumar et al. [56].

Before concluding this chapter, some attention to the computational time must be given. The computations are made on a Pentium-4 PC with 1.5 GHz, and 512 RAM for both test cases. The computation times by both the techniques are approximately the same. The first test case takes a CPU time of about 60 seconds and the second takes only 20 seconds. In both the cases computational time is affordable by a desktop PC. Finally by taking all the factors into account we conclude that the extended cell average technique is superior to the extended fixed pivot technique and can be used for practical problems to compute higher moments as well as the complete particle property distribution.

Chapter 5

Conclusions

This work presents a new numerical scheme, the cell average technique, for solving population balance equations. The technique is based on the fixed pivot technique developed by Kumar and Ramkrishna [57]. The cell average technique follows a two step strategy, one to calculate average size of the newborn particles in a class and the other to assign them to neighboring nodes such that the properties of interest (moments) are exactly preserved. The main significance from the applicational point of view of the improved efficiency is that the cell average technique can be used as a tool for the calculation up to (or near to) the gelation point. On the other hand, it has been shown that the fixed pivot technique diverges before the gelation point due to the over-prediction of number density at large volumes. A comparison of the numerical results obtained by the fixed pivot and cell average techniques with the analytical results indicates that the cell average technique improves the under-prediction in the moderate size range and the over-prediction in the large size range. Furthermore, the cell average technique has been applied to physically relevant problems and the results have been compared with the fixed pivot and generalized approximation techniques. The numerical results for these problems are comparable to the generalized approximation method while the fixed pivot technique gives over-prediction in each case.

The cell average technique proposed in this work allows the convenience of using regular (linear, geometric- or equal-size) and irregular meshes. Furthermore, the cell average scheme is consistent with the zeroth and first moments, the same procedure can be used to provide consistency with any two or more than two moments. Consistency with more than two moments can be achieved by distributing particles to more grid points. Note that we are not computing moments but the complete distribution function. The numerical results have shown the ability of the cell average technique to predict very well the time evolution of the second moment as well as the complete particle size distribution.

An important attribute of a numerical scheme, the computational time, has been investigated for numerous problems. It has been found that the computation time taken by the cell average technique is comparable to that taken by the fixed pivot technique. Moreover, for several aggregation problems it was even less than the computation time taken by the fixed pivot technique. A complete stability and convergence analysis of the fixed pivot and cell average techniques for breakage problems has been performed. Mathematical analysis and also experimental evidence show that the fixed pivot technique is only a first order accurate for breakage problems. Whereas

CHAPTER 5. CONCLUSIONS

it has been proved that the cell average technique provides a second order accuracy for most of the breakage problems. It has also been confirmed by experimental order of convergence studies. For aggregation problems, it has been shown numerically that the cell average technique converges to the analytical solutions faster than the fixed pivot technique.

A new approach for solving growth population balance equations is presented. The growth process has been treated as aggregation of existing particles in the disperse phase with some imaginary nuclei appearing from the continuous phase. Thus, the growth population balance equation is converted to the aggregation population balance equation. The aggregation rate is expressed in terms of the growth rate. Consequently, it becomes a trivial task to apply the cell average technique to the transformed aggregation population balance equation. However, numerical results of the particle size distribution turn out to be very diffusive. Nonetheless, the cell average formulation predicts the first two moments extremely accurately without any computational difficulties.

Further, a new concept for the coupling of different processes has been introduced. All processes including growth and nucleation have been solved using the cell average technique by treating them uniformly. It has been demonstrated that the new approach of coupling is not only more accurate but also computationally less expensive. This is achieved by collecting all newborn particles in a cell independently of the events (aggregation, breakage, growth and nucleation processes) that make them appear in the cell. Then a similar treatment like the cell average technique provides to individual processes is given. A substantial success of this coupling is observed for combined processes where growth is present because the coupling of growth with other processes has been a challenging task. The new approach of coupling makes the numerical discretization very simple and more accurate.

In addition, the number density based breakage population balance equation has been transformed to the form of a mass conservation law. Then it has become easy to apply the well known finite volume schemes that have an important property of mass conservation. Although the number density distribution calculated by the finite volume scheme discussed in this work is more accurate than that obtained by the cell average technique, the finite volume scheme produces very poor results for the zeroth moment. In addition to the stability and convergence analysis some other properties of the numerical solution of the finite volume scheme have been studied rigorously. Then, the proposed finite volume scheme for breakage problems has been coupled with the existing finite volume scheme for aggregation. In order to assess the effectiveness of the finite volume and cell average schemes, the number density distributions computed by the two techniques for several coupled problems have been compared.

In this work the DTPBE of Hounslow et al. [33] has been modified since it was not consistent with the associated discretized population balance equation. The new version retains all the advantages of the original version. It has been tested for a simple aggregation problem in a batch system. Contrary to the original version, the new version predicts a constant ratio of tracer mass and granule mass during aggregation in a batch system. It has been shown that both versions predict the same results for total tracer mass, while the original version is more accurate for tracer-weighted mean particle volume. Moreover, the modified DTPBE has been extended for the geometric grid of the type $x_{i+1/2} = 2^{1/q}x_{i-1/2}$ while the original formulation

was valid for the grid of the type $x_{i+1/2} = 2x_{i-1/2}$. The new scheme, extended and modified formulation, has been validated by many problems where analytical solutions are available.

The cell average technique is then formulated for solving the tracer population balance equation. Contrary to the previously existing method of Hounslow et al., the new formulation can be applied to any type of grid. Moreover, we compared our new discretization with the modified DTPBE of Peglow et al. [86] for several problems. It has been found in each case that the new discretization predicts better results than the modified DTPBE. The new formulation is more efficient on coarse grids while both formulations produce similar results on fine grids. Additionally, a comparison of CPU time taken by both formulations concludes that the new formulation takes less computational time.

The cell average and fixed pivot techniques have also been extended for solving two-dimensional aggregation population balance equations. The schemes are based on the exact prediction of some selected moments. We have considered the exact prediction of the total number and total mass of each component of the population. In the cell average technique, this is done by collecting all of the particles in a cell and then distributing them to neighboring cells so that the scheme is consistent with the total number and mass. On the other hand, in the fixed pivot technique the newborn particles of different sizes in a cell have been distributed to neighboring nodes separately without collecting them first at a point in the cell. Moreover it has been observed that with this setting the prediction of one extra higher moment, the first cross moment of the distribution, is exact in the fixed pivot technique. Therefore the fixed pivot technique becomes consistent with three different moments. While the cell average technique remains consistent with the first two moments only. The accuracy of numerical results has been shown by comparing the particle size distribution and its moments for a test problem. Similar to the one-dimensional case, the numerical results, however, show that the cell average scheme has potential to predict the number density distribution as well as higher moments with better accuracy.

One of the main goals of this research was to develop a numerical scheme that retains all advantages of existing schemes as well as predicts more accurate results and can be applied to solve the different particulate processes simultaneously. A further objective was to extend the scheme for solving higher dimensional problems. These objectives have been successfully achieved. Nevertheless, based on the work carried out in this research, some future works are proposed below.

1. Though we have presented the cell average technique for two-dimensional aggregation problems in such a way that it could easily be extended for more than two-dimensional problems, but it will in that case become computationally very expensive. Therefore some other criteria to reduce the computational cost should be proposed.
2. A more sophisticated finite volume schemes must be developed which can at least predict the first two moments accurately.
3. Mathematical analysis for aggregation problems should be performed.
4. A dynamic grid refinement strategy may be accomplished with the cell average technique to make the technique more powerful.

Appendix A

Analytical Solutions

A.1 Pure breakage

Table A.1: Analytical solutions for pure breakage in batch systems, Ziff and McGrady [125]

<i>Case</i>	$S(x)$	$\beta(x, y)$	$n(0, x)$	Analytical solution, $n(t, x)$
1	x	$2/y$	$\delta(x - L)$	$\exp(-tx) \left(\delta(x - L) + [2t + t^2(L - x)] \theta(L - x) \right)$
2	x^2	$2/y$	$\delta(x - L)$	$\exp(-tx^2) [\delta(x - L) + 2tL\theta(L - x)]$
3	x	$2/y$	$\exp(-x)$	$\exp(-x(1 + t)) (1 + t)^2$
4	x^2	$2/y$	$\exp(-x)$	$\exp(-tx^2 - x) [1 + 2t(1 + x)]$

In this table the function θ is the step function defined as

$$\theta(x - L) = \begin{cases} 1, & x < L \\ 0, & \text{otherwise.} \end{cases} \quad (\text{A.1})$$

A.2 Pure aggregation

Analytical solution of the number density

Scott [102] provided a number of solutions for a variety of initial conditions and three types of coalescence kernel. A brief outline of the solutions is being presented here. They considered the following gaussian like initial condition

$$n(v, 0) = \frac{N_0 \check{a}^{\nu+1}}{v_2 \Gamma(\nu + 1)} \left(\frac{v}{v_2} \right)^\nu \exp(-\check{a}v/v_2), \quad (\text{A.2})$$

where ν , \check{a} and v_2 are constants which characterize the shape of the initial distribution. The mean volume is given by

$$v_0 = v_2(\nu + 1)/\check{a}. \quad (\text{A.3})$$

It is convenient to introduce the dimensionless volume unit x by

$$x = \frac{v}{v_0}, \quad (\text{A.4})$$

and the dimensionless density function ϕ ,

$$\phi(x, T_a) = \frac{v_0}{N_0} n(v, t), \quad (\text{A.5})$$

where T_a is a dimensionless time variable, defined in each case of the three different coalescence kernel. Initial distribution in terms of dimensionless variables is defined as

$$\phi(x, 0) = \frac{(\nu + 1)^{\nu+1} x^\nu \exp[-x(\nu + 1)]}{\Gamma(\nu + 1)}. \quad (\text{A.6})$$

Now three cases for different coalescence kernel are considered. In each cases, two different solutions are presented, one is valid for small values of x and the other one is asymptotic expression using saddle-point method valid for large values of x .

Constant coalescence kernel $\beta(\mathbf{u}, \mathbf{v}) = \beta_0$

The decay of total number can be obtained by integrating the equation (2.3) with respect to v from zero to infinity and solving the resulting ordinary differential equation. Thus

$$N(t) = \frac{2N_0}{2 + \beta_0 N_0 t}. \quad (\text{A.7})$$

Define the dimensionless time $T_a = \beta_0 N_0 t$. Using Laplace transforms and series expansions, exact solution for small values of x and T_a is given by

$$\phi(x, T_a) = \frac{4 \exp[-(\nu + 1)]}{x(T_a + 2)^2} \sum_{k=0}^{\infty} \frac{[x(\nu + 1)]^{(\nu+1)(k+1)}}{\Gamma[(\nu + 1)(k + 1)]} \left(\frac{T_a}{T_a + 2} \right)^k. \quad (\text{A.8})$$

An asymptotic expression valid for large values of x and T_a can be obtained by the saddle-point method. An approximate solution in this case is

$$\phi(x, T_a) \simeq \frac{4(\nu + 1) \exp[(y_s - 1)x(\nu + 1)]}{(T_a + 2)^2 y_s^\nu [2\pi(\nu + 1)(\nu + 1 - \nu/y_s x)]}, \quad (\text{A.9})$$

with the relation between T_a and y_s

$$\frac{T_a}{T_a + 2} = y_s^\nu (y_s - 1/x). \quad (\text{A.10})$$

Sum coalescence kernel $\beta(\mathbf{u}, \mathbf{v}) = \beta_0(\mathbf{u} + \mathbf{v})$

For this case

$$N(t) = N_0 \exp(-\beta_0 N_0 v_0 t) = N_0 \exp(-T_a) = N_0(1 - \tau), \quad (\text{A.11})$$

APPENDIX A. ANALYTICAL SOLUTIONS

where the dimensionless time T_a and parameter τ are defined as

$$\begin{aligned} T_a &= \beta_0 N_0 v_0 t, \\ \tau &= 1 - \exp(-T_a). \end{aligned}$$

A series solution is obtained by Laplace transforms and conformal transformation

$$\phi(x, T_a) = (1 - \tau) \exp[-(\tau + \nu + 1)x] \sum_{k=0}^{\infty} \frac{\tau^k x^{\nu+k(\nu+2)} (\nu+1)^{(\nu+1)(k+1)}}{(k+1)! \Gamma[(\nu+1)(k+1)]}. \quad (\text{A.12})$$

The saddle-point calculation leads to the following asymptotic expression

$$\phi(x, T_a) \simeq \frac{(1 - \tau) \exp[-(\tau + \nu + 1)x + (\nu + 2)x\tau^{1/(\nu+2)}]}{x^{3/2} \tau^{(2\nu+3)/(2\nu+4)} [2\pi(\nu+2)/(\nu+1)]^{1/2}} \left[1 - \frac{(2\nu+3)(\nu+3)}{24x\tau^{1/(\nu+2)}(\nu+1)(\nu+2)} \right]. \quad (\text{A.13})$$

Product coalescence kernel $\beta(\mathbf{u}, \mathbf{v}) = \beta_0 \mathbf{u}\mathbf{v}$

It can be easily shown that decay of total number in this case is given by

$$N(t) = N_0 - \frac{1}{2} \beta_0 N_0^2 v_0^2 t = N_0 \left(1 - \frac{1}{2} T_a \right), \quad (\text{A.14})$$

with dimensionless time T_a

$$T_a = \beta_0 N_0 v_0^2 t. \quad (\text{A.15})$$

Laplace transform and conformal transformation techniques yield a series solution

$$\phi(x, T_a) = \exp[-(T_a + \nu + 1)x] \sum_{k=0}^{\infty} \frac{T_a^k x^{\nu+k(\nu+3)} (\nu+1)^{(\nu+2)(k+1)}}{(k+1)! \Gamma[(\nu+2)(k+1)]}. \quad (\text{A.16})$$

An asymptotic expansion for this case is

$$\begin{aligned} \phi(x, T_a) &\simeq \frac{(\nu+2) \exp\{-x(T_a + \nu + 1) + x(\nu+3)T_a^{1/(\nu+3)} [(\nu+1)/(\nu+2)]^{(\nu+2)/(\nu+3)}\}}{x^{5/2} [T_a(\nu+2)/(\nu+1)]^{(2\nu+5)/(2\nu+6)} [2\pi(\nu+1)(\nu+3)]^{1/2}} \\ &\times \left\{ 1 - \left[\frac{(\nu+4)(2\nu+5)}{24xT_a^{1/(\nu+3)}(\nu+1)^{(\nu+2)/(\nu+3)}(\nu+2)^{1/(\nu+3)}(\nu+3)} \right] \right\}. \end{aligned} \quad (\text{A.17})$$

Particular cases

For the exponential initial distribution, the solution can be further simplified for the constant and sum kernel. So the initial condition is

$$n(v, 0) = \frac{N_0}{v_0} \exp(-v/v_0). \quad (\text{A.18})$$

For size independent kernel $\beta(u, v) = \beta_0$, the simplified form of analytical kernel is given by

$$n(v, t) = \frac{4N_0}{v_0(T_a + 2)^2} \exp\left(\frac{-2x}{(T_a + 2)}\right), \quad (\text{A.19})$$

where $T_a = N_0\beta_0 t$.

For the case where $\beta(u, v) = \beta_0(u + v)$, The analytical solution for the population density is

$$n(v, t) = \frac{N_0(1 - \tau)}{v_0 x \sqrt{\tau}} \exp(-(1 + \tau)x) I_1(2x\sqrt{\tau}), \quad (\text{A.20})$$

where τ and T_a are defined above for the sum kernel case and I_1 is the modified Bessel function of the first kind of order one. It is difficult to compute modified Bessel function for large arguments. Asymptotic expansions of modified Bessel function for the large arguments can be found in [1].

$$I_\nu(z) \sim \frac{\exp(z)}{\sqrt{2\pi z}} \left\{ 1 - \frac{\mu - 1}{8z} + \frac{(\mu - 1)(\mu - 9)}{2!(8z)^2} - \frac{(\mu - 1)(\mu - 9)(\mu - 25)}{3!(8z)^3} + \dots \right\},$$

where $\mu = 4\nu^2$ and $|\arg z| < \pi/2$.

Analytical solution of number density for mono-disperse initial condition with size unity

The analytical solution for this case can be found in Aldous [3]. For constant kernel $\beta(x, y) = 1$, the analytical number density is given by

$$n(t, x) = \left(1 + \frac{t}{2}\right)^{-2} \left(\frac{t}{2+t}\right)^{x-1}, \quad (\text{A.21})$$

where t may vary from 0 to ∞ . For the sum $\beta(x, y) = x + y$ and the product $\beta(x, y) = xy$ kernels, it is given by

$$n(t, x) = \exp(-t)B(1 - \exp(-t), x), \quad \text{with } 0 \leq t < \infty, \quad (\text{A.22})$$

and

$$n(t, x) = x^{-1}B(t, x), \quad \text{with } 0 \leq t < 1. \quad (\text{A.23})$$

Here the function B is defined as

$$B(\lambda, x) = (\lambda x)^{x-1} \exp(-\lambda x)/x!, \quad x = 1, 2, \dots; 0 \leq \lambda \leq 1. \quad (\text{A.24})$$

A.3 Pure growth

The rate of change of j th moment for pure growth can be obtained by multiplying the growth PBE by x^j and integrating over the complete size range as

$$\int_0^\infty x^j \frac{\partial n(t, x)}{\partial t} dx = - \int_0^\infty x^j \frac{\partial G(x)n(t, x)}{\partial x} dx. \quad (\text{A.25})$$

Using partial integration on the right hand side of the above equation gives

$$\frac{d\mu_j}{dt} = (x^j G(x)n) \Big|_0^\infty + \int_0^\infty jx^{j-1} G(x)n(t, x) dx. \quad (\text{A.26})$$

APPENDIX A. ANALYTICAL SOLUTIONS

The first term on the right hand side is zero since we have the following assumptions that $n(t, 0) = 0$ and $n(t, \infty) = 0$. Finally the rate of change of μ_j is given by

$$\frac{d\mu_j}{dt} = \int_0^\infty jx^{j-1}G(x)n(t, x) dx. \quad (\text{A.27})$$

Further simplifications is not possible without knowing the form of growth rate. We will consider two special forms of growth rate.

Constant growth rate

Moments: Substituting the growth rate $G(x) = G_0$ in the equation (A.27) we obtain

$$\frac{d\mu_j}{dt} = G_0 \int_0^\infty jx^{j-1}n(t, x) dx. \quad (\text{A.28})$$

The zeroth moment is calculated by

$$\frac{d\mu_0}{dt} = 0, \quad (\text{A.29})$$

which can be solved to give $\mu_0(t) = \mu_0(0)$. The rate of change of the first moment is given by

$$\begin{aligned} \frac{d\mu_1}{dt} &= G_0 \int_0^\infty n(t, x) dx \\ &= G_0 \mu_0(0). \end{aligned} \quad (\text{A.30})$$

It can be solved to give the temporal change of the first moment as

$$\mu_1(t) = \mu_1(0) + G_0 \mu_0(0)t. \quad (\text{A.31})$$

Number density: The growth rate is constant, so all points on the solution profile will move at the same speed $G(x) = G_0$. If $n_0(x)$ is the initial solution, then the time evolution of number density is given by

$$n(t, x) = n_0(x - G_0t). \quad (\text{A.32})$$

Linear growth rate

Moments: As we have seen that the rate of change of the zeroth moment is always zero independently of growth rate. Therefore the zeroth moment remains constant during the growth process i.e. $\mu_0(t) = \mu_0(0)$. The rate of change of the first moment in this case is calculated by

$$\begin{aligned} \frac{d\mu_1}{dt} &= G_0 \int_0^\infty xn(t, x) dx \\ &= G_0 \mu_1. \end{aligned} \quad (\text{A.33})$$

Finally, it gives

$$\mu_1(t) = \mu_1(0) \exp(G_0t). \quad (\text{A.34})$$

A.4. SIMULTANEOUS AGGREGATION AND BREAKAGE

Number density: For linear growth rate, $G(x) = G_0x$, Kumar and Ramkrishna [59] have provided the analytical solution for pure growth PBE

$$n(t, x) = n_0(x \exp(-G_0t)) \exp(-G_0t), \quad (\text{A.35})$$

where $n_0(x)$ is the initial particle size distribution.

A.4 Simultaneous aggregation and breakage

Patil et al. [81] provided an analytical solution for the PBE with simultaneous breakage and coalescence for a special case where the total number of particles is constant. They considered the following continuous PBE

$$\begin{aligned} \frac{\partial n(v, t)}{\partial t} = & \frac{1}{2} \int_0^v \beta(v-u, u) n(v-u, t) n(u, t) du - n(v, t) \int_0^\infty \beta(v, u) n(u, t) du \\ & + 2 \int_v^\infty S(u) n(u, t) b(v, u) du - S(v) n(v, t), \end{aligned} \quad (\text{A.36})$$

with the constraints

$$\begin{aligned} n(v, 0) & \geq 0, \\ 0 \leq \beta(u, v) & = \beta(v, u), \\ \int_0^w b(v, w) dv & = 1, \\ \int_0^w 2vb(v, w) dv & = w. \end{aligned}$$

Kernels are

$$\begin{aligned} \beta(u, v) & = \beta_0, \\ S(v) & = S_0v, \\ b(v, u) & = \frac{1}{u}. \end{aligned}$$

Analytical solutions are obtained for the following two initial conditions

$$n(v, 0) = N(0) \frac{N(0)}{\mu_1} \exp\left(-\frac{N(0)}{\mu_1}v\right), \quad (\text{A.37})$$

and

$$n(v, 0) = N(0) \left(2\frac{N(0)}{\mu_1}\right)^2 v \exp\left(-2\frac{N(0)}{\mu_1}v\right), \quad (\text{A.38})$$

where $N(t)$ is the total number of particles and $\mu_1 = \int_0^\infty vn(v, t)dv$ is the first moment of the distribution. It can also be proved that the total number is constant by choosing the values of the

APPENDIX A. ANALYTICAL SOLUTIONS

problem parameters to satisfy $\sqrt{2S_0\mu_1/\beta_0} = N(0)$. They introduced the following dimensionless variables

$$\Phi(T_s) = \frac{N(t)}{N(0)}, \quad \eta = \frac{vN(0)}{\mu_1}, \quad (\text{A.39})$$

$$T_s = N(0)\beta_0 t, \quad \text{and} \quad \phi(\eta, T_s) = \frac{n(v, t)\mu_1}{[N(0)]^2}. \quad (\text{A.40})$$

Now, equation (A.36) can be written in dimensionless form as

$$\begin{aligned} \frac{\partial \phi}{\partial T_s} = \frac{1}{2} \int_0^\eta \phi(\eta - x, T_s) \phi(x, T_s) dx - \phi(\eta, T_s) \Phi(T_s) + [\Phi(\infty)]^2 \int_\eta^\infty \phi(x, T_s) dx \\ - \frac{\eta}{2} [\Phi(\infty)]^2 \phi(\eta, T_s), \end{aligned} \quad (\text{A.41})$$

with the initial condition

$$\phi(\eta, 0) = \exp(-\eta) \quad \text{or} \quad \phi(\eta, 0) = 4\eta \exp(-2\eta), \quad (\text{A.42})$$

where $\Phi(\infty) = \sqrt{2S_0\mu_1/\beta_0}/N(0)$ and $\Phi(T_s) = \Phi(\infty) = 1$.

By the simple use of Laplace and inverse Laplace transform, they obtained the following equilibrium solution for the initial condition $\phi(\eta, 0) = \exp(-\eta)$,

$$\phi(\eta, T_s) = \exp(-\eta). \quad (\text{A.43})$$

If the initial condition is $\phi(\eta, 0) = 4\eta \exp(-2\eta)$, then the solution becomes

$$\begin{aligned} \phi(\eta, T_s) \approx \frac{1}{F(T_s) - E(T_s)} \left([E(T_s)]^2 [F(T_s) - 1] \exp[-E(T_s)\eta] \right. \\ \left. - [F(T_s)]^2 [E(T_s) - 1] \exp[-F(T_s)\eta] \right). \end{aligned} \quad (\text{A.44})$$

Here $F(T_s)$ and $E(T_s)$ are the real roots of the polynomial

$$L_1 + L_2 p + L_3 p^2 + L_4 p^3 + L_5 p^4, \quad (\text{A.45})$$

where

$$\begin{aligned} L_1 &= 1 \frac{3}{4} T_s^2 + \frac{1}{4} T_s^3 + \frac{1}{4} T_s^2 \exp(-T_s), \\ L_2 &= 7 T_s + 3 \frac{1}{4} T_s^2 + \frac{1}{4} T_s^3 + T \exp(-T_s) - \frac{1}{4} T_s^2 \exp(-T_s), \\ L_3 &= 7 + 10 T_s + 1 \frac{1}{2} T_s^2 + \exp(-T_s) - T \exp(-T_s), \\ L_4 &= 9 + 3 T_s - \exp(-T_s), \\ L_5 &= 2 p^4. \end{aligned}$$

Obtaining the root of the above polynomial is difficult, therefore the roots will be obtained numerically. They also mentioned that after enforcing constraints on the number and volume of

A.5. SIMULTANEOUS AGGREGATION AND NUCLEATION

the floc size distribution, there are only two significant real roots of the polynomial. Lage [61] made some simplifications, their final solution equivalent to the previous one is

$$\phi(\eta, T_s) = \sum_{i=1}^2 \frac{K_1(T_s) + p_i K_2(T_s)}{L_2(T_s) + 4p_i} \exp(p_i \eta), \quad \forall T_s > 0, \quad (\text{A.46})$$

where P_i 's are the roots of the polynomial $L_1(T_s) + L_2(T_s)p + 2p^2$, and the others parameters are

$$\begin{aligned} L_1(T_s) &= K_1(T_s) = 7 + T_s + \exp(-T_s), \\ K_2(T_s) &= 2 - 2 \exp(-T_s), \\ L_2(T_s) &= 9 + T_s - \exp(-T_s). \end{aligned} \quad (\text{A.47})$$

The roots of the polynomial can easily be obtained

$$p_1 = \frac{1}{4} [\exp(-T_s) - T_s - 9] + \frac{1}{4} \sqrt{d(T_s)}, \quad (\text{A.48})$$

and

$$p_2 = \frac{1}{4} [\exp(-T_s) - T_s - 9] - \frac{1}{4} \sqrt{d(T_s)}, \quad (\text{A.49})$$

where

$$d(T_s) = T_s^2 + [10 - 2 \exp(-T_s)] T_s + 25 - 26 \exp(-T_s) + \exp(-2T_s).$$

A.5 Simultaneous aggregation and nucleation

The continuous population balance equation in this case is given as

$$\frac{\partial n(v, t)}{\partial t} = \frac{1}{2} \int_0^v \beta(v-u, u) n(v-u, t) n(u, t) du - n(v, t) \int_0^\infty \beta(v, u) n(u, t) du + B_{\text{nuc}}(t, x). \quad (\text{A.50})$$

Analytical solutions are given for moments by considering the zero initial population with a constant aggregation kernel and a constant nucleation rate. In this case the analytical solutions for the first two moments are given by

$$\mu_0 = \check{b} \tanh(\check{b}\tau/2), \quad (\text{A.51})$$

and

$$\mu_1 = \sigma\tau, \quad (\text{A.52})$$

where

$$\begin{aligned} \sigma &= B_0 / (\beta_0 N_0^2), \\ \tau &= \beta_0 N_0 t, \end{aligned}$$

and

$$\check{b} = \sqrt{(2\sigma)}.$$

A.6 Simultaneous growth and aggregation

There are various combinations of growth rates and aggregation kernels where analytical solutions are available. These solutions can be found in Ramabhadran et al. [93]. So the PBE in this case is simplified as follows

$$\frac{\partial n(v, t)}{\partial t} + \frac{\partial [G(v)n(v, t)]}{\partial v} = \frac{1}{2} \int_0^v \beta(v-u, u)n(v-u, t)n(u, t) du - n(v, t) \int_0^\infty \beta(v, u)n(u, t) du. \quad (\text{A.53})$$

Exponential initial condition

Assuming that the initial condition follows an exponential dependence with respect to particle volume,

$$n(v, t = 0) = \frac{N_0}{v_0} \exp(-v/v_0), \quad (\text{A.54})$$

where N_0 and v_0 are the total number of particles and mean volume of particles at time $t = 0$, respectively. The dynamics of the PSD in particulate systems undergoing combined particle growth and aggregation will depend on the values of two characteristics time constants, namely, the dimensionless aggregation time, T_a , and the dimensionless growth time, T_g , as

$$T_a = \beta_0 N_0 t,$$

and

$$T_g = G(v_0)/tv_0.$$

Let us define some more dimensionless quantities

$$L_0 = 1 - 2\Lambda(1 - \tilde{\mu}_0)/\tilde{\mu}_0,$$

$$L_1 = 1 - 2\Lambda(1 - \tilde{\mu}_0)/\tilde{\mu}_1,$$

$$L_2 = (v/v_0)\tilde{\mu}_1 \sqrt{1 - \tilde{\mu}_0},$$

$$\tilde{\mu}_0(t) = \frac{N_{tot}(t)}{N_0} = \frac{1}{N_0} \int_0^\infty n(v, t) dv,$$

$$\tilde{\mu}_1(t) = \frac{V_{tot}(t)}{N_0 v_0} = \frac{1}{N_0 v_0} \int_0^\infty vn(v, t) dv,$$

and

$$\Lambda = T_g/T_a.$$

Now we will consider two particular cases.

A.7. SIMULTANEOUS GROWTH AND NUCLEATION

Constant aggregation and linear growth: For the case,

$$\beta = \beta_0 \quad \text{and} \quad G = G_0 v / v_0,$$

one can easily obtain the following analytical solution

$$n(v, t) = \frac{N_0 \tilde{\mu}_0^2}{v_0 \tilde{\mu}_1} \exp\left(-\frac{\tilde{\mu}_0}{\tilde{\mu}_1} v\right), \quad (\text{A.55})$$

where $\tilde{\mu}_0$ and $\tilde{\mu}_1$, are expressed as

$$\begin{aligned} \tilde{\mu}_0 &= 1/(1 + T_a/2), \\ \tilde{\mu}_1 &= \exp(T_g). \end{aligned}$$

Sum aggregation and linear growth: For the case that $\beta = \beta_0(u + v)$ and $G = G_0 v / v_0$, the analytical solution is the following

$$n(v, t) = \frac{N_0 \tilde{\mu}_0}{v_0 \tilde{\mu}_1} \frac{1}{L_2} \exp\left(-\frac{\tilde{\mu}_0}{\tilde{\mu}_1} \frac{v}{v_0} \left(\frac{2}{\tilde{\mu}_0} - 1\right)\right) I_1\left(\frac{2L_2 v}{v_0}\right), \quad (\text{A.56})$$

where I_1 is the modified Bessel function of the first kind of order one, and

$$\begin{aligned} \tilde{\mu}_0 &= \exp\left(\frac{1 - \exp(T_g)}{\Lambda}\right), \\ \tilde{\mu}_1 &= \exp(T_g). \end{aligned}$$

For large values of T_a and x , an asymptotic expression for modified bessel function can be used to calculate density function.

A.7 Simultaneous growth and nucleation

For this case, continuous population balance takes the following form

$$\frac{\partial n(v, t)}{\partial t} + \frac{\partial [G(v)n(v, t)]}{\partial v} = S(v), \quad (\text{A.57})$$

where S is the nucleation rate. Hounslow [32] solved this equation for constant growth rate ($G = G_0$) and mono-disperse nuclei $S(v) (= B_0 \delta(v - v_0))$ of zero size ($v_0 = 0$) with the initial condition $n(v, 0) = 0$. Using Laplace and inverse Laplace transform, he obtained the following solution

$$n(v, t) = \frac{B_0}{G_0} U\left(t - \frac{v}{G_0}\right), \quad (\text{A.58})$$

where U is the unit step function.

A.8 Analytical solutions of a two component PBE

Analytical solutions for constant kernel and initial condition $f(0, m, n) = c_1 \delta_{m,1} + c_2 \delta_{1,n}$ are the following.

APPENDIX A. ANALYTICAL SOLUTIONS

Number density:

$$f(t, m, n) = \binom{m}{n} \left(\frac{c_1}{c_0}\right)^m \left(\frac{c_2}{c_0}\right)^n f(t, m+n), \quad c_0 = c_1 + c_2, \quad (\text{A.59})$$

where $f(t, n+m)$ is the concentration of particles composed of $(m+n)$ monomers of either type. It is given by

$$f(t, i) = 4c_0 \frac{(T_z)^{i-1}}{(T_z + 2)^{i+1}}, \quad T_z = \beta_0 c_0 t. \quad (\text{A.60})$$

Moments:

$$\mu_{00} = \frac{2c_0}{T_z + 2}, \quad \mu_{10} = c_1, \quad \mu_{01} = c_2, \quad (\text{A.61})$$

$$\mu_{11} = c_0 \frac{c_2}{c_0} \frac{c_1}{c_0} T_z, \quad \mu_{20} = c_1 \left(1 + \frac{c_1}{c_0} T_z\right), \quad \mu_{02} = c_2 \left(1 + \frac{c_2}{c_0} T_z\right). \quad (\text{A.62})$$

A.9 Analytical solutions of tracer weighted mean particle volume

Table A.2: Tracer weighted mean particle volume

β	\bar{v}_T/v_0
β_0	$1 + \frac{t}{\tau} \frac{2I_{agg}}{(1 - I_{agg})^2}$
$(u + v)$	$\frac{1 - I_{agg}}{3I_{agg} - 1} + \frac{4I_{agg} - 2}{3I_{agg} - 1} \exp\left[\frac{t}{\tau} \frac{I_{agg}}{1 - I_{agg}}\right]$
$(u \cdot v)$	$\exp\left[\frac{t}{\tau} \frac{1 - \sqrt{1 - 8I_{agg}}}{2}\right]$

Appendix B

Mathematical Derivations

B.1 Birth and death rates for aggregation in the fixed pivot technique

Let us first summarize two important properties of Dirac-delta distribution:

- (i) $\delta(x - x_0) = 0, \quad x \neq x_0,$
- (ii) $\int_a^b f(x)\delta(x - x_0) dx = f(x_0),$ where $x_0 \in]a, b[$.

Birth rate

The birth rate in the i th cell according to the fixed pivot technique is given as

$$\begin{aligned} B_i^{\text{FP}} &= \frac{1}{2} \int_{x_i}^{x_{i+1}} a(x, x_i) \int_0^x \beta(t, x - \epsilon, \epsilon) n(t, x - \epsilon) n(t, \epsilon) d\epsilon dx \\ &\quad + \frac{1}{2} \int_{x_{i-1}}^{x_i} b(x, x_i) \int_0^x \beta(t, x - \epsilon, \epsilon) n(t, x - \epsilon) n(t, \epsilon) d\epsilon dx \\ &=: I_1 + I_2. \end{aligned}$$

First we consider the first term I_1 . The parameter t is not important here, we omit it in our derivation. Assuming $x_1 = \sigma$ with $\sigma < \min_j (x_{j+1} - x_j)$, this term can be rewritten as follows

$$\begin{aligned} I_1 &= \frac{1}{2} \int_{x_i}^{x_{i+1}} a(x, x_i) \sum_{j=1}^{i-1} \int_{x_j - \sigma}^{x_{j+1} - \sigma} \beta(x - \epsilon, \epsilon) n(x - \epsilon) n(\epsilon) d\epsilon dx \\ &\quad + \frac{1}{2} \int_{x_i}^{x_{i+1}} a(x, x_i) \int_{x_i - \sigma}^x \beta(x - \epsilon, \epsilon) n(x - \epsilon) n(\epsilon) d\epsilon dx. \end{aligned} \quad (\text{B.1})$$

Substituting $n(x) = \sum_{k=1}^I N_k \delta(x - x_k)$ in the equation (B.1), we obtain

$$\begin{aligned} I_1 &= \frac{1}{2} \int_{x_i}^{x_{i+1}} a(x, x_i) \sum_{j=1}^{i-1} \int_{x_j - \sigma}^{x_{j+1} - \sigma} \beta(x - \epsilon, \epsilon) \sum_{k=1}^I [N_k \delta(x - \epsilon - x_k)] \sum_{k=1}^I [N_k \delta(\epsilon - x_k)] d\epsilon dx \\ &\quad + \frac{1}{2} \int_{x_i}^{x_{i+1}} a(x, x_i) \int_{x_i - \sigma}^x \beta(x - \epsilon, \epsilon) \sum_{k=1}^I [N_k \delta(x - \epsilon - x_k)] \sum_{k=1}^I [N_k \delta(\epsilon - x_k)] d\epsilon dx. \end{aligned} \quad (\text{B.2})$$

APPENDIX B. MATHEMATICAL DERIVATIONS

Using the definition of Dirac-delta distribution, we get

$$\begin{aligned}
 I_1 &= \frac{1}{2} \int_{x_i}^{x_{i+1}} a(x, x_i) \sum_{j=1}^{i-1} \beta(x - x_j, x_j) \sum_{k=1}^I [N_k \delta(x - x_j - x_k)] N_j dx \\
 &\quad + \frac{1}{2} \int_{x_i}^{x_{i+1}} a(x, x_i) \beta(x - x_i, x_i) \sum_{k=1}^I [N_k \delta(x - x_i - x_k)] N_i dx.
 \end{aligned} \tag{B.3}$$

The foregoing equation can be further simplified to

$$\begin{aligned}
 I_1 &= \frac{1}{2} \sum_{j=1}^{i-1} N_j \int_{x_i}^{x_{i+1}} a(x, x_i) \beta(x - x_j, x_j) \sum_{k=1}^I [N_k \delta(x - x_j - x_k)] dx \\
 &\quad + \frac{1}{2} N_i \int_{x_i}^{x_{i+1}} a(x, x_i) \beta(x - x_i, x_i) \sum_{k=1}^I [N_k \delta(x - x_i - x_k)] dx.
 \end{aligned} \tag{B.4}$$

Again, applying the definition of Dirac-delta in both the terms, we get

$$\begin{aligned}
 I_1 &= \frac{1}{2} \sum_{j=1}^{i-1} N_j \sum_{x_i \leq (x_j + x_k) < x_{i+1}} a(x_j + x_k, x_i) \beta(x_k, x_j) N_k \\
 &\quad + \frac{1}{2} N_i \sum_{(x_i + x_k) < x_{i+1}} a(x_i + x_k, x_i) \beta(x_k, x_i) N_k.
 \end{aligned} \tag{B.5}$$

All terms in equation (B.5) which appear twice except for $j = k$ can be eliminated by rewriting the equation in the following way

$$I_1 = \sum_{\substack{j \geq k \\ x_i \leq (x_j + x_k) < x_{i+1}}} \left(1 - \frac{1}{2} \delta_{j,k} \right) a(x_j + x_k, x_i) \beta(x_j, x_k) N_j N_k. \tag{B.6}$$

Similarly the second term I_2 can be obtained as

$$I_2 = \sum_{\substack{j \geq k \\ x_{i-1} \leq (x_j + x_k) < x_i}} \left(1 - \frac{1}{2} \delta_{j,k} \right) b(x_j + x_k, x_i) \beta(x_j, x_k) N_j N_k. \tag{B.7}$$

Solving the equations (2.11) and (2.12) for the consistency of the first two moments, we get

$$a(x, x_i) = \frac{x_{i+1} - x}{x_{i+1} - x_i}, \quad b(x, x_{i+1}) = \frac{x - x_i}{x_{i+1} - x_i}. \tag{B.8}$$

Now the complete birth rate B_i^{FP} is given by

$$\begin{aligned}
 B_i^{\text{FP}} &= \sum_{\substack{j \geq k \\ x_i \leq x < x_{i+1}}} \left(1 - \frac{1}{2} \delta_{j,k} \right) \left(\frac{x_{i+1} - x}{x_{i+1} - x_i} \right) \beta(x_j, x_k) N_j N_k \\
 &\quad + \sum_{\substack{j \geq k \\ x_{i-1} \leq x < x_i}} \left(1 - \frac{1}{2} \delta_{j,k} \right) \left(\frac{x - x_{i-1}}{x_i - x_{i-1}} \right) \beta(x_j, x_k) N_j N_k,
 \end{aligned} \tag{B.9}$$

where $x = x_j + x_k$.

B.2. A DIFFERENT FORM OF THE FIXED PIVOT TECHNIQUE

Death rate

The derivation of the discrete death term can be derived in the similar way. The rate of death in i th cell is the following

$$D_i^{\text{FP}} = \int_{x_{i-1/2}}^{x_{i+1/2}} n(x) \int_0^\infty \beta(x, \epsilon) n(\epsilon) d\epsilon dx. \quad (\text{B.10})$$

Equation (B.10), truncated up to $x_{I+1/2}$, can be rewritten as follows

$$D_i^{\text{FP}} = \int_{x_{i-1/2}}^{x_{i+1/2}} n(x) \sum_{j=1}^I \int_{x_{j-1/2}}^{x_{j+1/2}} \beta(x, \epsilon) n(\epsilon) d\epsilon dx. \quad (\text{B.11})$$

Again using the Dirac-delta distribution, we obtain

$$\begin{aligned} D_i^{\text{FP}} &= \int_{x_{i-1/2}}^{x_{i+1/2}} \sum_{k=0}^I [N_k \delta(x - x_k)] \sum_{j=1}^I \int_{x_{j-1/2}}^{x_{j+1/2}} \beta(x, \epsilon) \sum_{k=0}^I [N_k \delta(\epsilon - x_k)] d\epsilon dx \\ &= \int_{x_{i-1/2}}^{x_{i+1/2}} \sum_{k=0}^I [N_k \delta(x - x_k)] \sum_{j=1}^I \beta(x, x_j) N_j dx \\ &= \sum_{j=1}^I N_j \int_{x_i}^{x_{i+1}} \sum_{k=0}^I [N_k \delta(x - x_k)] \beta(x, x_j) dx \\ &= \sum_{j=1}^I \beta(x_i, x_j) N_j N_i. \end{aligned} \quad (\text{B.12})$$

B.2 A different form of the fixed pivot technique

The formulation (2.18) can also be rewritten in the following simplified form as

$$\frac{dN_i}{dt} = \sum_{j=1}^{i-1} \sum_{k=j+1}^i \eta'(x) \beta_{j,k} N_j N_k + \frac{1}{2} \sum_{j=1}^i \eta'(x) \beta_{j,j} N_j^2 - N_i \sum_{k=1}^I \beta_{i,k} N_k, \quad (\text{B.13})$$

or,

$$\frac{dN_i}{dt} = \frac{1}{2} \sum_{j=1}^i \sum_{k=1}^i \eta'(x) \beta_{j,k} N_j N_k - N_i \sum_{k=1}^I \beta_{i,k} N_k, \quad (\text{B.14})$$

where

$$\eta'(x) = \begin{cases} \frac{x_{i+1} - x}{x_{i+1} - x_i}, & x_i \leq x < x_{i+1} \\ \frac{x - x_{i-1}}{x_i - x_{i-1}}, & x_{i-1} \leq x < x_i \\ 0, & \text{otherwise.} \end{cases} \quad (\text{B.15})$$

The formulation (B.14) looks very simple and easy to implement. But it should be noted that the formulation (B.14) will take more computational time than the formulation (2.18) due to several useless calculations.

B.3 Comparison of accuracy of local moments

Case 1, $\bar{v}_i \leq x_i$

The particle birth assigned at x_i by the cell average technique is given as

$$N_i^{\text{CA}} = \left(\frac{\bar{v}_i - x_{i-1}}{x_i - x_{i-1}} \right) \sum_{j=1}^{I_i} B_i^j, \quad \text{if } \bar{v}_i \leq x_i, \quad (\text{B.16})$$

where

$$\bar{v}_i = \frac{\sum_{j=1}^{I_i} y_i^j B_i^j}{\sum_{j=1}^{I_i} B_i^j}. \quad (\text{B.17})$$

We want to show that $N_i^{\text{CA}} \geq N_i^{\text{FP}}$. Thus, we consider the following expression

$$N_i^{\text{CA}} - N_i^{\text{FP}} = \left(\frac{\bar{v}_i - x_{i-1}}{x_i - x_{i-1}} \right) \sum_{j=1}^{I_i} B_i^j - \sum_{j=1}^k \left(\frac{y_i^j - x_{i-1}}{x_i - x_{i-1}} \right) B_i^j + \sum_{j=k+1}^{I_i} \left(\frac{x_{i+1} - y_i^j}{x_{i+1} - x_i} \right) B_i^j. \quad (\text{B.18})$$

We substitute \bar{v}_i into the above equation to get

$$\begin{aligned} N_i^{\text{CA}} - N_i^{\text{FP}} &= \left(\frac{\sum_{j=1}^{I_i} y_i^j B_i^j - \sum_{j=1}^{I_i} x_{i-1} B_i^j}{x_i - x_{i-1}} \right) - \sum_{j=1}^k \left(\frac{y_i^j - x_{i-1}}{x_i - x_{i-1}} \right) B_i^j - \sum_{j=k+1}^{I_i} \left(\frac{x_{i+1} - y_i^j}{x_{i+1} - x_i} \right) B_i^j \\ &= \sum_{j=1}^{I_i} \left(\frac{y_i^j - x_{i-1}}{x_i - x_{i-1}} \right) B_i^j - \sum_{j=1}^k \left(\frac{y_i^j - x_{i-1}}{x_i - x_{i-1}} \right) B_i^j - \sum_{j=k+1}^{I_i} \left(\frac{x_{i+1} - y_i^j}{x_{i+1} - x_i} \right) B_i^j \\ &= \sum_{j=k+1}^{I_i} \left(\frac{y_i^j - x_{i-1}}{x_i - x_{i-1}} \right) B_i^j - \sum_{j=k+1}^{I_i} \left(\frac{x_{i+1} - y_i^j}{x_{i+1} - x_i} \right) B_i^j \\ &= \sum_{j=k+1}^{I_i} \frac{(x_{i+1} - x_{i-1})(y_i^j - x_i)}{(x_i - x_{i-1})(x_{i+1} - x_i)} B_i^j \geq 0. \end{aligned} \quad (\text{B.19})$$

It gives $N_i^{\text{CA}} \geq N_i^{\text{FP}}$ and clearly if $B_i^j = 0$ for all $j \geq k + 1$ then equality holds.

Case 2, $\bar{v}_i \geq x_i$

A similar procedure as before can be followed in this case to obtain

$$\begin{aligned} N_i^{\text{CA}} - N_i^{\text{FP}} &= \left(\frac{\sum_{j=1}^{I_i} x_{i+1} B_i^j - \sum_{j=1}^{I_i} y_i^j B_i^j}{x_{i+1} - x_i} \right) - \sum_{j=1}^k \left(\frac{y_i^j - x_{i-1}}{x_i - x_{i-1}} \right) B_i^j - \sum_{j=k+1}^{I_i} \left(\frac{x_{i+1} - y_i^j}{x_{i+1} - x_i} \right) B_i^j \\ &= \sum_{j=1}^{I_i} \left(\frac{x_{i+1} - y_i^j}{x_{i+1} - x_i} \right) B_i^j - \sum_{j=1}^k \left(\frac{y_i^j - x_{i-1}}{x_i - x_{i-1}} \right) B_i^j - \sum_{j=k+1}^{I_i} \left(\frac{x_{i+1} - y_i^j}{x_{i+1} - x_i} \right) B_i^j \\ &= \sum_{j=1}^k \left(\frac{x_{i+1} - y_i^j}{x_{i+1} - x_i} \right) B_i^j - \sum_{j=1}^k \left(\frac{y_i^j - x_{i-1}}{x_i - x_{i-1}} \right) B_i^j \\ &= \sum_{j=1}^k \frac{(x_{i+1} - x_{i-1})(x_i - y_i^j)}{(x_{i+1} - x_i)(x_i - x_{i-1})} B_i^j. \end{aligned} \quad (\text{B.20})$$

B.4. DISCRETE BIRTH AND DEATH RATES FOR BREAKAGE

In this case we have proved that $N_i^{\text{CA}} \geq N_i^{\text{FP}}$ and equality holds if $B_i^j = 0$ for all $j \leq k$.

B.4 Discrete birth and death rates for breakage

Birth rate

The birth rate in the i th interval is given as

$$B_i = \int_{x_{i-1/2}}^{x_{i+1/2}} \int_x^\infty b(t, x, \epsilon) S(t, \epsilon) n(t, \epsilon) d\epsilon dx. \quad (\text{B.21})$$

Interchanging the order of integration the above term can be rewritten as

$$\begin{aligned} B_i &= \int_{x_{i-1/2}}^{x_{i+1/2}} \int_{x_{i-1/2}}^\epsilon b(t, x, \epsilon) S(t, \epsilon) n(t, \epsilon) dx d\epsilon + \int_{x_{i+1/2}}^\infty \int_{x_{i-1/2}}^{x_{i+1/2}} b(t, x, \epsilon) S(t, \epsilon) n(t, \epsilon) dx d\epsilon \\ &= \int_{x_{i-1/2}}^{x_{i+1/2}} \int_{x_{i-1/2}}^\epsilon b(t, x, \epsilon) S(t, \epsilon) n(t, \epsilon) dx d\epsilon \\ &\quad + \sum_{k=i+1}^I \int_{x_{k-1/2}}^{x_{k+1/2}} \int_{x_{i-1/2}}^{x_{i+1/2}} b(t, x, \epsilon) S(t, \epsilon) n(t, \epsilon) dx d\epsilon. \end{aligned} \quad (\text{B.22})$$

Substituting the number density $n(t, x) = \sum_{k=1}^I N_k(t) \delta(x - x_k)$, we obtain

$$B_i = N_i(t) \int_{x_{i-1/2}}^{x_i} b(t, x, x_i) S(t, x_i) dx + \sum_{k=i+1}^I N_k(t) \int_{x_{i-1/2}}^{x_{i+1/2}} b(t, x, x_k) S(t, x_k) dx. \quad (\text{B.23})$$

We can also combine the above two terms into one as follows

$$B_i = \sum_{k=i}^I N_k(t) S(t, x_k) \int_{x_{i-1/2}}^{p_k^i} b(t, x, x_k) dx, \quad (\text{B.24})$$

where $p_k^i = x_i$ for $k = i$ and $p_k^i = x_{i+1/2}$ elsewhere.

Death rate

Similarly, we substitute the number density $n(t, x) = \sum_{k=1}^I N_k(t) \delta(x - x_k)$ into the death rate to get

$$\begin{aligned} D_i &= \int_{x_{i-1/2}}^{x_{i+1/2}} S(t, x) \sum_{k=1}^I N_k(t) \delta(x - x_k) dx \\ &= S(t, x_i) N_i(t). \end{aligned} \quad (\text{B.25})$$

B.5 Second moment of the Gaussian-like distribution

We calculate the second moment for the Gaussian-like initial condition

$$n(v, 0) = \frac{N_0 a^{\nu+1}}{v_2 \Gamma(\nu + 1)} \left(\frac{v}{v_2} \right)^\nu \exp(-av/v_2). \quad (\text{B.26})$$

APPENDIX B. MATHEMATICAL DERIVATIONS

The second moment with respect to volume is given by

$$\mu_2(0) = \int_0^\infty v^2 \frac{N_0 a^{\nu+1}}{v_2 \Gamma(\nu+1)} \left(\frac{v}{v_2}\right)^\nu \exp(-av/v_2) dv. \quad (\text{B.27})$$

This can be simplified further as follows

$$\begin{aligned} \mu_2(0) &= \frac{N_0 a^{(\nu+1)}}{v_2^{\nu+1} \Gamma(\nu+1)} \int_0^\infty v^{\nu+2} \exp(-av/v_2) dv \\ &= \frac{N_0 a^{(\nu+1)}}{v_2^{\nu+1} \Gamma(\nu+1)} \int_0^\infty v^{\nu+2} \exp(-av/v_2) dv. \end{aligned} \quad (\text{B.28})$$

After the substitution, $av/v_2 = t$, we get

$$\mu_2(0) = \frac{N_0 a^{(\nu+1)}}{v_2^{\nu+1} \Gamma(\nu+1)} \left(\frac{v_2}{a}\right)^{\nu+3} \int_0^\infty t^{\nu+2} \exp(-t) dt. \quad (\text{B.29})$$

Using the definition of Gamma function

$$\begin{aligned} \mu_2(0) &= \frac{N_0 a^{(\nu+1)}}{v_2^{\nu+1} \Gamma(\nu+1)} \left(\frac{v_2}{a}\right)^{\nu+3} \Gamma(\nu+3) \\ &= N_0 \left(\frac{v_2}{a}\right)^2 (\nu+2)(\nu+1). \end{aligned} \quad (\text{B.30})$$

Equation (B.30) can be rewritten in the following form

$$\mu_2(0) = N_0 \left[\frac{v_2(\nu+1)}{a} \right]^2 \frac{(\nu+2)}{(\nu+1)}. \quad (\text{B.31})$$

The definition of initial mean volume, $v_0 = v_2(\nu+1)/a$, follows

$$\mu_2(0) = N_0 v_0^2 \frac{(\nu+2)}{(\nu+1)}. \quad (\text{B.32})$$

The particular case of exponential distribution, $\nu = 0$, gives

$$\mu_2(0) = 2N_0 v_0^2. \quad (\text{B.33})$$

B.6 Discrete birth rate for aggregation

Birth rate

The birth rate in the i th cell is given as

$$B_i = \frac{1}{2} \int_{x_{i-1/2}}^{x_{i+1/2}} \int_0^x \beta(t, x-u, u) n(t, x-u) n(t, u) du dx.$$

B.6. DISCRETE BIRTH RATE FOR AGGREGATION

The parameter t is not important here, we omit it in our derivation. Using $x_{1/2} = 0$, this term can be rewritten as follows

$$\begin{aligned}
 B_i &= \frac{1}{2} \int_{x_{i-1/2}}^{x_{i+1/2}} \sum_{j=1}^{i-1} \int_{x_{j-1/2}}^{x_{j+1/2}} \beta(x-u, u) n(x-u) n(u) du dx \\
 &\quad + \frac{1}{2} \int_{x_{i-1/2}}^{x_{i+1/2}} \int_{x_{i-1/2}}^x \beta(x-u, u) n(x-u) n(u) du dx.
 \end{aligned} \tag{B.34}$$

Substituting $n(x) = \sum_{k=1}^I N_k \delta(x - x_k)$ in equation (B.34), we obtain

$$\begin{aligned}
 B_i &= \frac{1}{2} \int_{x_{i-1/2}}^{x_{i+1/2}} \sum_{j=1}^{i-1} \int_{x_{j-1/2}}^{x_{j+1/2}} \beta(x-u, u) \sum_{k=1}^I [N_k \delta(x-u-x_k)] \sum_{k=1}^I [N_k \delta(u-x_k)] du dx \\
 &\quad + \frac{1}{2} \int_{x_{i-1/2}}^{x_{i+1/2}} \int_{x_{i-1/2}}^x \beta(x-u, u) \sum_{k=1}^I [N_k \delta(x-u-x_k)] \sum_{k=1}^I [N_k \delta(u-x_k)] du dx.
 \end{aligned} \tag{B.35}$$

Using the definition of Dirac-delta distribution in the first term and changing the order of integration in the second term, we get

$$\begin{aligned}
 B_i &= \frac{1}{2} \int_{x_{i-1/2}}^{x_{i+1/2}} \sum_{j=1}^{i-1} \beta(x-x_j, x_j) \sum_{k=1}^I [N_k \delta(x-x_j-x_k)] N_j dx \\
 &\quad + \frac{1}{2} \int_{x_{i-1/2}}^{x_{i+1/2}} \int_u^{x_{i+1/2}} \beta(x-u, u) \sum_{k=1}^I [N_k \delta(x-u-x_k)] \sum_{k=1}^I [N_k \delta(u-x_k)] dx du.
 \end{aligned} \tag{B.36}$$

The foregoing equation can be further simplified to

$$\begin{aligned}
 B_i &= \frac{1}{2} \sum_{j=1}^{i-1} N_j \int_{x_{i-1/2}}^{x_{i+1/2}} \beta(x-x_j, x_j) \sum_{k=1}^I [N_k \delta(x-x_j-x_k)] dx \\
 &\quad + \frac{1}{2} \int_{x_i}^{x_{i+1/2}} \beta(x-x_i, x_i) \sum_{k=1}^I [N_k \delta(x-x_i-x_k)] N_i dx.
 \end{aligned} \tag{B.37}$$

Again, applying the definition of Dirac-delta in both the terms, we get

$$B_i = \frac{1}{2} \sum_{j=1}^{i-1} N_j \sum_{x_{i-1/2} \leq (x_j+x_k) < x_{i+1/2}} \beta(x_k, x_j) N_k + \frac{1}{2} \sum_{(x_i+x_k) < x_{i+1/2}} \beta(x_k, x_i) N_k N_i. \tag{B.38}$$

All terms in equation (B.38) which appear twice except for $j = k$ can be eliminated by rewriting the equation in the following way

$$B_i = \sum_{x_{i-1/2} \leq (x_j+x_k) < x_{i+1/2}}^{j \geq k} \left(1 - \frac{1}{2} \delta_{j,k}\right) \beta(x_j, x_k) N_j N_k. \tag{B.39}$$

B.7 Stability condition for the combined problem

The finite volume scheme for simultaneous aggregation and breakage is given as

$$g_i^{m+1} = g_i^m - \frac{\Delta t}{\Delta x_i} \left(J_{i+1/2}^m - J_{i-1/2}^m \right). \quad (\text{B.40})$$

Here the numerical flux J is given by the algebraical sum of both individual fluxes as

$$J_{i+1/2}^m = J_{i+1/2,\text{agg}}^m + J_{i+1/2,\text{break}}^m. \quad (\text{B.41})$$

The fluxes $J_{i+1/2,\text{agg}}^m$ and $J_{i+1/2,\text{break}}^m$ are represented as

$$J_{i+1/2,\text{agg}}^m = \sum_{k=1}^i \Delta x_k g_k^m \left(\sum_{j=\alpha_{i,k}}^I \int_{\Lambda_j} \frac{\beta(u, x_k)}{u} du g_j^n + \int_{x_{i+1/2}-x_k}^{x_{\alpha_{i,k}-1/2}} \frac{a(u, x_k)}{u} du g_{\alpha_{i,k}-1}^m \right), \quad (\text{B.42})$$

and

$$J_{i+1/2,\text{break}}^m = - \sum_{k=i+1}^I g_k^m \int_{\Lambda_k} \frac{S(\epsilon)}{\epsilon} d\epsilon \int_0^{x_{i+1/2}} ub(x_k, u) du. \quad (\text{B.43})$$

We make use of the proof of Propositions 3.4.1 and 3.4.4 to get

$$\begin{aligned} J_{i+1/2}^m &\leq \Delta x_i g_i^m \int_{\delta}^R \frac{\beta(x_i, u)}{u} g(t^m, u) du + J_{i-1/2,\text{agg}}^m \\ &\quad + g_i^m \int_{\Lambda_i} \frac{S(\epsilon)}{\epsilon} d\epsilon \int_0^{x_{i+1/2}} ub(x_i, u) du + J_{i-1/2,\text{break}}^m. \end{aligned} \quad (\text{B.44})$$

where $\delta = \min(\Delta x_i/2; i = 1, 2, \dots, I)$. The above inequality can be rewritten as

$$J_{i+1/2}^m \leq \Delta x_i g_i^m \left(\int_{\delta}^R \frac{\beta(x_i, u)}{u} g(t^m, u) du + \frac{1}{\Delta x_i} \int_{\Lambda_i} \frac{S(\epsilon)}{\epsilon} d\epsilon \int_0^{x_{i+1/2}} ub(x_i, u) du \right) + J_{i-1/2}^m. \quad (\text{B.45})$$

Using the stability condition (3.272) we obtain

$$J_{i+1/2}^m - J_{i-1/2}^m \leq \frac{\Delta x_i}{\Delta t} g_i^m. \quad (\text{B.46})$$

Remaining steps are the same like in the proof of Proposition 3.4.1.

B.8 Mass conservation of modified DTPBE

Summing over all i the equation (4.42), we obtain

$$\begin{aligned}
 \sum_i \frac{dM_i}{dt} &= \sum_i \sum_{j=1}^{i-2} \frac{2^{j-i+2}}{2^{j-i+1} + 1} \beta_{i-1,j} (M_{i-1}N_j + N_{i-1}M_j) \\
 &\quad + \sum_i N_i \sum_{j=1}^{i-1} (1 - 2^{j-i}) \beta_{i,j} M_j \frac{1}{2^{j-i} + 1} + \sum_i \beta_{i-1,i-1} N_{i-1} M_{i-1} \\
 &\quad - \sum_i M_i \sum_{j=1}^{i-1} \frac{2^{j-i+1}}{2^{j-i} + 1} \beta_{i,j} N_j - \sum_i M_i \sum_{j=i} \beta_{i,j} N_j \\
 &= \sum_i M_{i-1} \sum_{j=1}^{i-2} \frac{2^{j-i+2}}{2^{j-i+1} + 1} \beta_{i-1,j} N_j + \sum_i N_{i-1} \sum_{j=1}^{i-2} \frac{2^{j-i+2}}{2^{j-i+1} + 1} \beta_{i-1,j} M_j \\
 &\quad + \sum_i N_i \sum_{j=1}^{i-1} \beta_{i,j} M_j \frac{1}{2^{j-i} + 1} + \sum_i N_i \sum_{j=1}^{i-i} \frac{2^{j-1}}{2^{j-i} + 1} \beta_{i,j} M_j \\
 &\quad + \sum_i \beta_{i-1,i-1} N_{i-1} M_{i-1} - \sum_i M_i \sum_{j=1}^{i-1} \frac{2^{j-i+1}}{2^{j-i} + 1} \beta_{i,j} N_j - \sum_i M_i \sum_{j=i} \beta_{i,j} N_j. \tag{B.47}
 \end{aligned}$$

Splitting the second term on the right hand side we get

$$\begin{aligned}
 \sum_i \frac{dM_i}{dt} &= \sum_i M_{i-1} \sum_{j=1}^{i-2} \frac{2^{j-i+2}}{2^{j-i+1} + 1} \beta_{i-1,j} N_j + \sum_i N_{i-1} \sum_{j=1}^{i-2} \frac{2^{j-i+1}}{2^{j-i+1} + 1} \beta_{i-1,j} M_j \\
 &\quad + \sum_i N_{i-1} \sum_{j=1}^{i-2} \frac{2^{j-i+1}}{2^{j-i+1} + 1} \beta_{i-1,j} M_j + \sum_i N_i \sum_{j=1}^{i-1} \beta_{i,j} M_j \frac{1}{2^{j-i} + 1} \\
 &\quad - \sum_i N_i \sum_{j=1}^{i-i} \frac{2^{j-1}}{2^{j-i} + 1} \beta_{i,j} M_j + \sum_i \beta_{i-1,i-1} N_{i-1} M_{i-1} \\
 &\quad - \sum_i M_i \sum_{j=1}^{i-1} \frac{2^{j-i+1}}{2^{j-i} + 1} \beta_{i,j} N_j - \sum_i M_i \sum_{j=i} \beta_{i,j} N_j. \tag{B.48}
 \end{aligned}$$

Rearranging the terms, the following equation is obtained

$$\begin{aligned}
 \sum_i \frac{dM_i}{dt} &= \sum_i M_{i-1} \sum_{j=1}^{i-2} \frac{2^{j-i+2}}{2^{j-i+1} + 1} \beta_{i-1,j} N_j - \sum_i M_i \sum_{j=1}^{i-1} \frac{2^{j-i+1}}{2^{j-i} + 1} \beta_{i,j} N_j \\
 &\quad + \sum_i N_{i-1} \sum_{j=1}^{i-2} \frac{2^{j-i+1}}{2^{j-i+1} + 1} \beta_{i-1,j} M_j - \sum_i N_i \sum_{j=1}^{i-i} \frac{2^{j-1}}{2^{j-i} + 1} \beta_{i,j} M_j \\
 &\quad + \sum_i N_{i-1} \sum_{j=1}^{i-2} \frac{2^{j-i+1}}{2^{j-i+1} + 1} \beta_{i-1,j} M_j + \sum_i N_i \sum_{j=1}^{i-1} \beta_{i,j} M_j \frac{1}{2^{j-i} + 1} \\
 &\quad + \sum_i \beta_{i-1,i-1} N_{i-1} M_{i-1} - \sum_i M_i \sum_{j=i} \beta_{i,j} N_j. \tag{B.49}
 \end{aligned}$$

APPENDIX B. MATHEMATICAL DERIVATIONS

The first term cancels with the second term and the third term cancels with the fourth. The fifth and sixth terms may be merged to one term to give

$$\begin{aligned}\sum_i \frac{dM_i}{dt} &= \sum_i N_i \sum_{j=1}^{i-1} \beta_{i,j} M_j + \sum_i \beta_{i-1,i-1} N_{i-1} M_{i-1} - \sum_i M_i \sum_{j=i} \beta_{i,j} N_j \\ &= \sum_i N_i \sum_{j=1}^i \beta_{i,j} M_j - \sum_i M_i \sum_{j=i} \beta_{i,j} N_j = 0.\end{aligned}\tag{B.50}$$

B.9 Discrete birth and death terms of TPBE

Birth rate

The birth rate in the i th interval is given as

$$B_{i,T} = \int_{v_i}^{v_{i+1}} \int_0^v \beta(t, v - \epsilon, \epsilon) M(t, v - \epsilon) n(t, \epsilon) d\epsilon dv.$$

The parameter t is not important here, we omit it in our derivation. Assuming $v_1 = 0$, this term can be rewritten as follows

$$\begin{aligned}B_{i,T} &= \int_{v_i}^{v_{i+1}} \sum_{j=1}^{i-1} \int_{v_j}^{v_{j+1}} \beta(v - \epsilon, \epsilon) M(v - \epsilon) n(\epsilon) d\epsilon dv \\ &\quad + \int_{v_i}^{v_{i+1}} \int_{v_i}^v \beta(v - \epsilon, \epsilon) M(v - \epsilon) n(\epsilon) d\epsilon dv.\end{aligned}\tag{B.51}$$

Substituting $n(v) = \sum_{k=1}^I N_k \delta(v - x_k)$ and $M(v) = \sum_{k=1}^I M_k \delta(v - x_k)$ in equation (B.51), we obtain

$$\begin{aligned}B_{i,T} &= \int_{v_i}^{v_{i+1}} \sum_{j=1}^{i-1} \int_{v_j}^{v_{j+1}} \beta(v - \epsilon, \epsilon) \sum_{k=1}^I [M_k \delta(v - \epsilon - x_k)] \sum_{k=1}^I [N_k \delta(\epsilon - x_k)] d\epsilon dv \\ &\quad + \int_{v_i}^{v_{i+1}} \int_{v_i}^v \beta(v - \epsilon, \epsilon) \sum_{k=1}^I [M_k \delta(v - \epsilon - x_k)] \sum_{k=1}^I [N_k \delta(\epsilon - x_k)] d\epsilon dv.\end{aligned}\tag{B.52}$$

Using the definition of Dirac-delta distribution in the first term and changing the order of integration in the second term, we get

$$\begin{aligned}B_{i,T} &= \int_{v_i}^{v_{i+1}} \sum_{j=1}^{i-1} \beta(v - x_j, x_j) \sum_{k=1}^I [M_k \delta(v - x_j - x_k)] N_j dv \\ &\quad + \int_{v_i}^{v_{i+1}} \int_{\epsilon}^{v_{i+1}} \beta(v - \epsilon, \epsilon) \sum_{k=1}^I [M_k \delta(v - \epsilon - x_k)] \sum_{k=1}^I [N_k \delta(\epsilon - x_k)] dv d\epsilon.\end{aligned}\tag{B.53}$$

The foregoing equation can be simplified further to

$$\begin{aligned}
 B_{i,T} &= \sum_{j=1}^{i-1} N_j \int_{v_i}^{v_{i+1}} \beta(v - x_j, x_j) \sum_{k=1}^I [M_k \delta(v - x_j - x_k)] dv \\
 &\quad + \int_{x_i}^{v_{i+1}} \beta(v - x_i, x_i) \sum_{k=1}^I [M_k \delta(v - x_i - x_k)] N_i dv.
 \end{aligned} \tag{B.54}$$

Again, applying the definition of the Dirac-delta distribution in both the terms, we get

$$B_{i,T} = \sum_{j=1}^{i-1} N_j \sum_{v_i \leq (x_j + x_k) < v_{i+1}} \beta(x_k, x_j) M_k + \sum_{(x_i + x_k) < v_{i+1}} \beta(x_k, x_i) M_k N_i. \tag{B.55}$$

Since each term $M_j N_k$ in equation (B.55) have a corresponding term $M_k N_j$ except for $j = k$, the equation (B.55) can be rewritten in the following way

$$B_{i,T} = \sum_{v_i \leq (x_j + x_k) < v_{i+1}}^{j \geq k} \left(1 - \frac{1}{2} \delta_{j,k} \right) \beta(x_j, x_k) (M_j N_k + M_k N_j). \tag{B.56}$$

Death rate

Tracer death in a cell is given by

$$D_{i,T} = \int_{v_i}^{v_{i+1}} M(v) \int_0^\infty \beta(v, \epsilon) N(\epsilon) d\epsilon dv. \tag{B.57}$$

Equation (B.57), truncated up to v_{I+1} , can be rewritten as follows

$$D_{i,T} = \int_{v_i}^{v_{i+1}} M(v) \sum_{j=1}^I \int_{v_j}^{v_{j+1}} \beta(v, \epsilon) N(\epsilon) d\epsilon dv. \tag{B.58}$$

Again using the Dirac-delta distribution, we obtain

$$\begin{aligned}
 D_{i,T} &= \int_{v_i}^{v_{i+1}} \sum_{k=0}^I [M_k \delta(v - x_k)] \sum_{j=1}^I \int_{v_j}^{v_{j+1}} \beta(v, \epsilon) \sum_{k=0}^I [N_k \delta(\epsilon - x_k)] d\epsilon dv \\
 &= \int_{v_i}^{v_{i+1}} \sum_{k=0}^I [M_k \delta(v - x_k)] \sum_{j=1}^I \beta(v, x_j) N_j dv \\
 &= \sum_{j=1}^I N_j \int_{v_i}^{v_{i+1}} \sum_{k=0}^I [M_k \delta(v - x_k)] \beta(v, x_j) dv \\
 &= \sum_{j=1}^I \beta(x_i, x_j) N_j M_i.
 \end{aligned} \tag{B.59}$$

B.10 Two-dimensional discrete PBE

Birth rate

The birth rate in a cell is given as

$$B_{ij} = \frac{1}{2} \int_{x_{i-}}^{x_{i+}} \int_{y_{j-}}^{y_{j+}} \int_0^x \int_0^y \beta(x - \epsilon, \epsilon, y - \gamma, \gamma) f(x - \epsilon, y - \gamma) f(\epsilon, \gamma) d\gamma d\epsilon dy dx. \quad (\text{B.60})$$

Assuming $x_1 = 0$ and $y_1 = 0$, it can be rewritten as

$$\begin{aligned} B_{ij} &= \frac{1}{2} \int_{x_{i-}}^{x_{i+}} \int_{y_{j-}}^{y_{j+}} \sum_{k=1}^{i-1} \int_{x_{k-}}^{x_{k+}} \sum_{m=1}^{j-1} \int_{y_{m-}}^{y_{m+}} \beta(x - \epsilon, \epsilon, y - \gamma, \gamma) f(x - \epsilon, y - \gamma) f(\epsilon, \gamma) d\gamma d\epsilon dy dx \\ &+ \frac{1}{2} \int_{x_{i-}}^{x_{i+}} \int_{y_{j-}}^{y_{j+}} \sum_{k=1}^{i-1} \int_{x_{k-}}^{x_{k+}} \int_{y_{j-}}^y \beta(x - \epsilon, \epsilon, y - \gamma, \gamma) f(x - \epsilon, y - \gamma) f(\epsilon, \gamma) d\gamma d\epsilon dy dx \\ &+ \frac{1}{2} \int_{x_{i-}}^{x_{i+}} \int_{y_{j-}}^{y_{j+}} \int_{x_{i-}}^x \sum_{m=1}^{j-1} \int_{y_{m-}}^{y_{m+}} \beta(x - \epsilon, \epsilon, y - \gamma, \gamma) f(x - \epsilon, y - \gamma) f(\epsilon, \gamma) d\gamma d\epsilon dy dx \\ &+ \frac{1}{2} \int_{x_{i-}}^{x_{i+}} \int_{y_{j-}}^{y_{j+}} \int_{x_{i-}}^x \int_{y_{j-}}^y \beta(x - \epsilon, \epsilon, y - \gamma, \gamma) f(x - \epsilon, y - \gamma) f(\epsilon, \gamma) d\gamma d\epsilon dy dx. \end{aligned} \quad (\text{B.61})$$

Substituting $f(t, x, y) = \sum_{i=1}^{I_x} \sum_{j=1}^{I_y} N_{ij} \delta(x - x_i) \delta(y - y_j)$ in preceding equation and making some simple transformations, we get

$$\begin{aligned} B_{ij} &= \frac{1}{2} \sum_{k=1}^{i-1} \sum_{x_{i-} \leq (x_k + x_l) < x_{i+}} \sum_{m=1}^{j-1} \sum_{y_{j-} \leq (y_m + y_n) < y_{j+}} \beta_{klmn} N_{km} N_{ln} \\ &+ \frac{1}{2} \sum_{k=1}^{i-1} \sum_{x_{i-} \leq (x_k + x_l) < x_{i+}} \sum_{(y_j + y_n) < y_{j+}} \beta_{kljn} N_{kj} N_{ln} \\ &+ \frac{1}{2} \sum_{(x_i + x_l) < x_{i+}} \sum_{m=1}^{j-1} \sum_{y_{j-} \leq (y_m + y_n) < y_{j+}} \beta_{ilmn} N_{im} N_{ln} \\ &+ \frac{1}{2} \sum_{(x_i + x_l) < x_{i+}} \sum_{(y_j + y_n) < y_{j+}} \beta_{iljn} N_{ij} N_{ln}. \end{aligned} \quad (\text{B.62})$$

It can be further simplified to the form

$$B_{ij} = \sum_{\substack{k \geq l \\ k, l \\ x_{i-} \leq (x_k + x_l) < x_{i+}}} \sum_{\substack{m \geq n \\ m, n \\ y_{j-} \leq (y_m + y_n) < y_{j+}}} \left(1 - \frac{1}{2} \delta_{k,l} \delta_{m,n} \right) \beta_{klmn} N_{km} N_{ln}. \quad (\text{B.63})$$

Death rate

Similar steps can be followed for discrete death rate as

$$D_{ij} = \int_{x_{i-}}^{x_{i+}} \int_{y_{j-}}^{y_{j+}} \int_0^\infty \int_0^\infty \beta(x, \epsilon, y, \gamma) f(x, y) f(\epsilon, \gamma) d\gamma d\epsilon dy dx. \quad (\text{B.64})$$

B.11. CONSISTENCY WITH THE FIRST CROSS MOMENT

For a finite domain, truncated up to x_{I_x+} and y_{I_y+} , the above birth term can be rewritten as

$$D_{ij} = \int_{x_{i-}}^{x_{i+}} \int_{y_{j-}}^{y_{j+}} f(x, y) \sum_{k=1}^{I_x} \int_{x_{k-}}^{x_{k+}} \sum_{m=1}^{I_y} \int_{y_{m-}}^{y_{m+}} \beta(x, \epsilon, y, \gamma) f(\epsilon, \gamma) d\gamma d\epsilon dy dx. \quad (\text{B.65})$$

Using the definition of Dirac-delta distribution, we obtain

$$D_{ij} = \int_{x_{i-}}^{x_{i+}} \int_{y_{j-}}^{y_{j+}} f(x, y) \sum_{k=1}^{I_x} \sum_{m=1}^{I_y} \beta(x, x_k, y, y_m) N_{km} dy dx. \quad (\text{B.66})$$

Again we make use of Dirac-delta distribution to give

$$D_{ij} = N_{ij} \sum_{k=1}^{I_x} \sum_{m=1}^{I_y} \beta_{ikjm} N_{km}. \quad (\text{B.67})$$

B.11 Consistency with the first cross moment

We want to prove the following equality

$$a_1 x_{i-1} y_{j-1} + a_2 x_i y_{j-1} + a_3 x_i y_j + a_4 x_{i-1} y_j = B_{ij} \bar{x}_i \bar{y}_j. \quad (\text{B.68})$$

We take the left hand side (L.H.S.) and substitute the values a_1 , a_2 , a_3 and a_4 from equations (4.80-4.83) to get

$$\begin{aligned} \text{L.H.S.} &= \frac{y_{j-1}(y_j - \bar{y}_j) B_{ij}}{(x_i - x_{i-1})(y_j - y_{j-1})} (x_i x_{i-1} - \bar{x}_i x_{i-1} + \bar{x}_i x_i - x_{i-1} x_i) \\ &\quad + \frac{y_j(\bar{y}_j - y_{j-1}) B_{ij}}{(x_i - x_{i-1})(y_j - y_{j-1})} (\bar{x}_i x_i - x_{i-1} x_i + x_i x_{i-1} - \bar{x}_i x_{i-1}) \\ &= \frac{y_{j-1}(y_j - \bar{y}_j) B_{ij}}{(x_i - x_{i-1})(y_j - y_{j-1})} (x_i - x_{i-1}) \bar{x}_i + \frac{y_j(\bar{y}_j - y_{j-1}) B_{ij}}{(x_i - x_{i-1})(y_j - y_{j-1})} (x_i - x_{i-1}) \bar{x}_i \\ &= \frac{\bar{x}_i B_{ij}}{(y_j - y_{j-1})} (y_{j-1} y_j - y_{j-1} \bar{y}_j + y_j \bar{y}_j - y_j y_{j-1}) \\ &= B_{ij} \bar{x}_i \bar{y}_j. \end{aligned} \quad (\text{B.69})$$

Bibliography

- [1] M. Abramowitz and I.A. Stegun. *Handbook of mathematical functions with formulas, graphs, and mathematical tables*. National Bureau of Standards Applied Mathematics Series 55. U.S. Department of Commerce, 10th edition, 1972.
- [2] A.A. Adetayo, J.D. Litster, S.E. Pratsinis, and B.J. Ennis. Population balance modelling of drum granulation of materials with wide size distribution. *Powder Technology*, 82:37–49, 1995.
- [3] D.J. Aldous. Deterministic and stochastic model for coalescence (aggregation and coagulation): A review of the mean-field theory for probabilists. *Bernoulli*, 5:3–48, 1999.
- [4] A.H. Alexopoulos and C.A. Kiparissides. Part II: Dynamic evolution of the particle size distribution in particulate processes undergoing simultaneous particle nucleation, growth and aggregation. *Chemical Engineering Science*, 60:4157–4169, 2005.
- [5] J.C. Barrett and J.S. Jheeta. Improving the accuracy of the moments method for solving the aerosol general dynamic equation. *Journal of Aerosol Science*, 27:1135–1142, 1996.
- [6] J.C. Barrett and N.A. Webb. A comparison of some approximate methods for solving the aerosol general dynamic equation. *Journal of Aerosol Science*, 29:31–39, 1998.
- [7] R.J. Batterham, J.S. Hall, and G. Barton. Pelletizing kinetics and simulation of full-scale balling circuits. Proceedings of the 3rd International Symposium on Agglomeration, Nürnberg, Germany, 1981. A136-A150.
- [8] M.K. Bennett and S. Rohani. Solution of population balance equations with a new combined Lax-Wendroff/Crank-Nicholson method. *Chemical Engineering Science*, 56:6623–6633, 2001.
- [9] R. Bleck. A fast, approximate method for integrating the stochastic coalescence equation. *Journal of Geophysics Research*, 75:5165–5171, 1970.
- [10] A.B. Boehm, C. Poor, and S.B. Grant. Particle coagulation and the memory of initial conditions. *Journal of physics A: Mathematical and General*, 31:9241–9254, 1998.
- [11] S. Bove, T. Solberg, and B.H. Hjertager. A novel algorithm for solving population balance equations: The parallel parent and daughter classes. Derivation, analysis and testing. *Chemical Engineering Science*, 60:1449–1464, 2005.

-
- [12] A.S. Bramley, M.J. Hounslow, and R.L. Ryall. Aggregation during precipitation from solution: A method for extracting rates from experimental data. *Journal of Colloid and Interface Science*, 183:155–165, 1996.
- [13] P.B. Bubovskii, V.A. Galkin, and I.W. Stewart. Exact solutions for the coagulation-fragmentation equations. *Journal of Physics A: Mathematical and General*, 25:4737–4744, 1992.
- [14] J. Burgschweiger and E. Tsotsas. Experimental investigation and modelling of continuous fluidized bed drying under steady-state and dynamic conditions. *Chemical Engineering Science*, 57:5021–5038, 2002.
- [15] S.C. Chang. The method of space-time conservation element and solution element-A new approach for solving the navier-stokes and euler equations. *Journal of Computational Physics*, 119:295–324, 1995.
- [16] A. Ding, C.A. Biggs, and M.J Hounslow. Population balance model selection for activated sludge flocculation modelling. Proceedings of the 2nd International Conference on Population Balance Modelling, Valencia, Spain, 2004.
- [17] A. Eibeck and W. Wagner. An efficient stochastic algorithm for studying coagulation dynamics and gelation phenomena. *SIAM Journal on Scientific Computing*, 22:802–821, 2000.
- [18] A. Eibeck and W. Wagner. Stochastic particle approximations for Smoluchowski’s coagulation equation. *The Annals of Applied Probability*, 11:1137–1165, 2001.
- [19] M.H. Ernst, R.M. Ziff, and E.M. Hendriks. Coagulation processes with a phase transition. *Journal of Colloid and Interface Science*, 97:266–277, 1984.
- [20] R.C. Everson, D. Eyre, and Q.P. Campbell. Spline method for solving continuous batch grinding and similarity equations. *Computers and Chemical Engineering*, 21:1433–1440, 1997.
- [21] F. Filbet and P. Laurençot. Numerical simulation of the Smoluchowski coagulation equation. *SIAM Journal on Scientific Computing*, 25:2004–2028, 2004.
- [22] Y. Fuke, M. Sekiguchi, and H. Matsuoka. Nature of stem bromelain treatments on the aggregation and gelation of soybean proteins. *Journal of Food Science*, 50:1283–1288, 1985.
- [23] F. Gelbard and J.H. Seinfeld. Modelling multicomponent aerosol particle growth by vapor consideration. *Aerosol Science and Technology*, 12:399–412, 1990.
- [24] F. Gelbard, Y. Tambour, and J.H. Seinfeld. Sectional representations for simulating aerosol dynamics. *Journal of Colloid and Interface Science*, 76:541–556, 1980.
- [25] A. Gerstlaur. *Herleitung und Reduction populationsdynamischer Modelle am Beispiel der Flüssig-Flüssig-Extraction*. Phd thesis, University of Stuttgart, Germany, 1999.
- [26] D.A. Gillette. A study of aging of lead aerosols-II: A numerical model simulating coagulation and sedimentation of a leaded aerosol in the presence of an unleaded background aerosol. *Atmospheric Environment*, 6:433–512, 1972.

BIBLIOGRAPHY

- [27] R. Gunawan, I. Fusman, and R.D. Braatz. High resolution algorithms for multidimensional population balance equations. *AIChE Journal*, 50:2738–2749, 2004.
- [28] G. Hämmerlin and K. Hoffmann. *Numerical Mathematics*. Springer-Verlag New York, USA, 1st edition, 1991.
- [29] S. Heinrich, M. Peglow, M. Ihlow, M. Henneberg, and L. Mörl. Analysis of the start-up process in continuous fluidized bed spray granulation by population balance modelling. *Chemical Engineering Science*, 22:73–92, 1995.
- [30] P.J. Hill and K.M. Ng. New discretization procedure for the breakage equation. *AIChE Journal*, 41:1204–1216, 1995.
- [31] M.J. Hounslow. A discretized population balance for continuous systems at steady state. *AIChE Journal*, 36:106–116, 1990.
- [32] M.J. Hounslow. *A discretized population balance for simultaneous nucleation, growth and aggregation*. Phd thesis, University of Adelaide, South Australia, 1990.
- [33] M.J. Hounslow, J.M.K. Pearson, and T. Instone. Tracer studies of high shear granulation: II. Population balance modelling. *AIChE Journal*, 47:1984–1999, 2001.
- [34] M.J. Hounslow, R.L. Ryall, and V.R. Marshall. A discretized population balance for nucleation, growth and aggregation. *AIChE Journal*, 38:1821–1832, 1988.
- [35] Q. Hu, S. Rohani, and A. Jutan. New numerical method for solving the dynamic population balance equations. *AIChE Journal*, 51:3000–3006, 2005.
- [36] H.M. Hulburt and S. Katz. Some problems in particle technology. A statistical mechanical formulation. *Chemical Engineering Science*, 19:555–578, 1964.
- [37] W. Hundsdorfer and J.G. Verwer. *Numerical solution of time-dependent advection-diffusion-reaction equations*. Springer-Verlag New York, USA, 1st edition, 2003.
- [38] D. Ilievski and M.J. Hounslow. Agglomeration during precipitations: II. Mechanism deduction from tracer data. *AIChE Journal*, 41:525–535, 1995.
- [39] C.D. Immanuel and F.J. Doyle. Solution technique for a multi-dimensional population balance model describing granulation processes. *Powder Technology*, 156:213–225, 2005.
- [40] S.M. Iveson. Limitations of one-dimensional population balance models of wet granulation processes. *Powder Technology*, 124:219–229, 2002.
- [41] S.M. Iveson, J.D. Litster, K. Hapgood, and B.J. Ennis. Nucleation growth and breakage phenomena in agitated wet granulation processes: A review. *Powder Technology*, 117:3–39, 2001.
- [42] M.Z. Jacobson. Development and application of a new air pollution modeling system-II. Aerosol structure and design. *Atmospheric Environment*, 31:131–144, 1997.

-
- [43] M.Z. Jacobson and R.P. Turco. Simulating condensational growth, evaporation and coagulation of aerosols using a combined moving and stationary size grid. *Aerosol Science and Technology*, 57:4369–4390, 2002.
- [44] C. Kettner, M. Peglow, T. Metzger, and E. Tsotsas. Distributed product quality in fluidized bed drying. Proceedings of the 15th International Drying Symposium, Budapest, Hungary, 2006.
- [45] Y.P. Kim and J.H. Seinfeld. Simulation of multicomponent aerosol condensation by the moving sectional method. *Journal of Colloid and Interface Science*, 135:185–199, 1990.
- [46] Y.P. Kim and J.H. Seinfeld. Simulation of multicomponent aerosol dynamics. *Journal of Colloid and Interface Science*, 149:425–449, 1992.
- [47] B. Koren. Kinetics of fluidized bed melt granulation IV. Selecting the breakage model. *A robust upwind discretization for advection, diffusion and source terms. In: Numerical Methods for Advection-Diffusion Problems. Eds. C.B. Vreugdenhil, B. Koren, Notes on Numerical Fluid Mechanics*, 45:117–138, 1993.
- [48] M. Kostoglou and A.J. Karabelas. Evaluation of zero order methods for simulating particle coagulation. *Journal of Colloid and Interface Science*, 163:420–431, 1994.
- [49] M. Kostoglou and A.J. Karabelas. Evaluation of numerical methods for simulating an evolving particle size distribution in growth processes. *Chemical Engineering Communications*, 136:177–199, 1995.
- [50] M. Kostoglou and A.J. Karabelas. An assessment of low-order methods for solving the breakage equation. *Powder Technology*, 127:116–127, 2002.
- [51] M. Kostoglou and A.J. Karabelas. Optimal low order methods of moments for solving the fragmentation equation. *Powder Technology*, 143-144:280–290, 2004.
- [52] F.E. Kruis, A. Maisels, and H. Fissan. Direct simulation Monte Carlo method for particle coagulation and aggregation. *AIChE Journal*, 46:1735–1742, 2000.
- [53] J. Kumar, M. Peglow, G. Warnecke, S. Heinrich, and L. Mörl. A two-dimensional population balance modelling for drying and agglomeration. Proceedings of the Asia Pacific Drying Conference, Kolkata, India, 2005.
- [54] J. Kumar, M. Peglow, G. Warnecke, S. Heinrich, and L. Mörl. A discretized model for tracer population balance equation: Improved accuracy and convergence. *Computers and Chemical Engineering*, 30:1278–1292, 2006.
- [55] J. Kumar, M. Peglow, G. Warnecke, S. Heinrich, and L. Mörl. Improved accuracy and convergence of discretized population balance for aggregation: The cell average technique. *Chemical Engineering Science*, 61:3327–3342, 2006.
- [56] J. Kumar, M. Peglow, G. Warnecke, S. Heinrich, E. Tsotsas, and L. Mörl. Numerical solution of a two-dimensional population balance equation for aggregation. Proceedings of the 5th World Congress on Particle Technology, Florida, USA, 2006.

BIBLIOGRAPHY

- [57] S. Kumar and D. Ramkrishna. On the solution of population balance equations by discretization - I. A fixed pivot technique. *Chemical Engineering Science*, 51:1311–1332, 1996.
- [58] S. Kumar and D. Ramkrishna. On the solution of population balance equations by discretization - II. A moving pivot technique. *Chemical Engineering Science*, 51:1333–1342, 1996.
- [59] S. Kumar and D. Ramkrishna. On the solution of population balance equations by discretization - III. Nucleation, growth and aggregation of particles. *Chemical Engineering Science*, 52:4659–4679, 1997.
- [60] A. Kurganov and E. Tadmor. New high-resolution central schemes for nonlinear conservation laws and convection-diffusion equations. *Journal of Computational Physics*, 160:141–182, 2000.
- [61] P.L.C. Lage. Comments on the "An analytical solution to the population balance equation with coalescence and breakage-the special case with constant number of particles" by D.P. Patil and J.R.G. Andrews. *Chemical Engineering Science*, 57:4253–4254, 2002.
- [62] I.J. Laurenzi, J.D. Bartels, and S.L. Diamond. A general algorithm for exact simulation of multicomponent aggregation processes. *Journal of Computational Physics*, 177:418–449, 2002.
- [63] K. Lee and T. Matsoukas. Simultaneous coagulation and breakage using constant-N Monte Carlo. *Powder Technology*, 110:82–89, 2000.
- [64] M.H. Lee. On the validity of the coagulation equation and the nature of runaway growth. *Icarus*, 143:74–86, 2000.
- [65] R.J. LeVeque. *Numerical methods for conservation laws. Lectures in Mathematics*. Birkhäuser-Verlag, Basel, ETH Zürich, Switzerland, 1st edition, 1990.
- [66] R.J. LeVeque. *Finite Volume Methods for Hyperbolic Problems*. Cambridge University Press, Cambridge, U.K., 1st edition, 2002.
- [67] Y. Lim, J.L. Lann, X.M. Meyer, X. Joulia, G. Lee, and E.S. Yoon. On the solution of population balance equations (PBE) with accurate front tracking methods in practical crystallization processes. *Chemical Engineering Science*, 2002:3715–3732, 2002.
- [68] Y. Lin, K. Lee, and T. Matsoukas. Solution of the population balance equation using constant-number Monte Carlo. *Chemical Engineering Science*, 57:2241–2252, 2002.
- [69] J.D. Litster, D.J. Smit, and M.J. Hounslow. Adjustable discretized population balance for growth and aggregation. *AIChE Journal*, 41:591–603, 1995.
- [70] A.A. Lushnikov. Evolution of coagulating systems. *Journal of Colloid and Interface Science*, 54:94–101, 1976.
- [71] G. Madras and B.J. McCoy. Reversible crystal growth-dissolution and aggregation-breakage: Numerical and moment solutions for population balance equations. *Powder Technology*, 143-144:297–307, 2004.

- [72] A.W. Mahoney and D. Ramkrishna. Efficient solution of population balance equations with discontinuities by finite elements. *Chemical Engineering Science*, 57:1107–1119, 2002.
- [73] J. Makino, T. Fukushige, Y. Funato, and E. Kokubo. On the mass distribution of planetesimals in the early runaway stage. *New Astronomy*, 3:411–417, 1998.
- [74] P. Marchal, R. David, J.P. Klein, and J. Villermaux. Crystallization and precipitation engineering-I. An efficient method for solving population balance in crystallization with agglomeration. *Chemical Engineering Science*, 43:59–67, 1988.
- [75] D.L. Marchisio and R.O. Fox. Solution of population balance equations using the direct quadrature method of moments. *Journal of Aerosol Science*, 36:43–73, 2005.
- [76] B.K. Mishra. Monte Carlo simulation of particle breakage process during grinding. *Powder Technology*, 110:246–252, 2000.
- [77] S. Motz, A. Mitrovic, and E. D. Gilles. Comparison of numerical methods for the simulation of dispersed phase systems. *Chemical Engineering Science*, 57:4329–4344, 2002.
- [78] M. Nicmanis and M.J. Hounslow. A finite element analysis of the steady state population balance equation for particulate systems: Aggregation and growth. *Computers and Chemical Engineering*, 20:S261–S266, 1996.
- [79] I. Nopens, D. Beheydt, and P.A. Vanrolleghem. Comparison and pitfalls of different discretised solution methods for population balance models: A simulation study. *Computers and Chemical Engineering*, 29:367–377, 2005.
- [80] S.H. Park and S.N. Rogak. A novel fixed-sectional model for the formation and growth of aerosol agglomerates. *Journal of Aerosol Science*, 35:1385–1404, 2004.
- [81] D.P. Patil and J.R.G. Andrews. An analytical solution to continuous population balance model describing floc coalescence and breakage - A special case. *Chemical Engineering Science*, 53:599–601, 1998.
- [82] M. Peglow. *Beitrag zur Modellbildung von eigenschaftsverteilten dispersen Systemen am Beispiel der Wirbelschicht-Sprühagglomeration*. Phd thesis, Otto-von-Guericke-University Magdeburg, Germany, 2005.
- [83] M. Peglow, J. Kumar, S. Heinrich, G. Warnecke, and L. Mörl. A new technique to determine rate constants for growth and agglomeration with size- and time-dependent nuclei formation. *Chemical Engineering Science*, 61:282–292, 2006.
- [84] M. Peglow, J. Kumar, S. Heinrich, G. Warnecke, E. Tsotsas, L. Mörl, and B. Wolf. A generic population balance model for simultaneous agglomeration and drying in fluidized beds. *Chemical Engineering Science*, accepted, 2006. Special Issue: Application of fluidization.
- [85] M. Peglow, J. Kumar, and L. Mörl. Investigation of coalescence kinetics of microcrystalline cellulose in fluidized bed spray agglomeration - experimental studies and modeling approach. *Brazilian Journal of Chemical Engineering*, 22:165–172, 2005.

BIBLIOGRAPHY

- [86] M. Peglow, J. Kumar, G. Warnecke, S. Heinrich, E. Tsotsas, L. Mörl, and M.J. Hounslow. An improved discretized tracer mass distribution of Hounslow et al. *AIChE Journal*, 52:1326–1332, 2006.
- [87] R.H. Perry and D.W. Green, editors. *Perry's Chemical Engineers' Handbook*. McGraw-Hill, New York, USA, 7th edition, 1997.
- [88] V.N. Piskunov and A.I. Golubev. The generalized approximation method for modeling coagulation kinetics-Part 1: Justification and implementation of the method. *Journal of Aerosol Science*, 33:51–63, 2002.
- [89] V.N. Piskunov, A.I. Golubev, J.C. Barrett, and N.A. Ismailova. The generalized approximation method for modeling coagulation kinetics-Part 2: Comparison with other methods. *Journal of Aerosol Science*, 33:65–75, 2002.
- [90] A Prakash, A.P. Bapat, and M.R. Zachariah. A simple numerical algorithm and software for solution of nucleation, surface growth and coagulation problem. *Aerosol Science and Technology*, 37:892–898, 2003.
- [91] W.H. Press, S.A. Teukolsky, W.T. Vetterling, and B.P. Flannery. *Numerical recipes in C++*. Cambridge University Press, The Edinburgh Building Cambridge, U.K., 2nd edition, 2002.
- [92] F. Puel, P. Marchal, and J. Klein. Habit transient analysis in industrial crystallization using two-dimensional crystal sizing technique. *Chemical Engineering Research and Design*, 75:193–205, 1997.
- [93] T.E. Ramabhadran, T.W. Peterson, and J.H. Seinfeld. Dynamics of aerosol coagulation and condensation. *AIChE Journal*, 22:840–851, 1976.
- [94] D. Ramkrishna. *Population balances. Theory and applications to particulate systems in engineering*. Academic Press, New York, USA, 1st edition, 2000.
- [95] A.D. Randolph and M.A. Larson. *The theory of particulate processes*. Academic Press, New York, USA, 1st edition, 1971.
- [96] A.D. Randolph and M.A. Larson. *Theory of particulate processes*. Academic Press, New York, USA, 2nd edition, 1988.
- [97] S. Rigopoulos and A.G. Jones. Finite-element scheme for solution of the dynamic population balance equation. *AIChE Journal*, 49:1127–1139, 2003.
- [98] M. Saleh, M. Steinmetz, and M. Hemati. Experimental study and modeling of fluidized bed coating an agglomeration. *Powder Technology*, 130:116–123, 2003.
- [99] K.V.S. Sastry and P. Gaschignard. Discretization procedure for the coalescence equation of particulate processes. *Industrial and Engineering Chemistry Fundamentals*, 8:355–361, 1981.
- [100] S. Schaafsma. *Down-scaling of a fluidised bed agglomeration process*. Phd thesis, University of Groningen, Netherlands, September 2000.

-
- [101] S.H. Schaafsma, P. Vonk, P. Segers, and N.W.F. Kossen. Description of agglomerate growth. *Powder Technology*, 97:183–190, 1998.
- [102] W.T. Scott. Analytic studies of cloud droplet coalescence. *Journal of the Atmospheric Sciences*, 25:54–65, 1968.
- [103] D.J. Smit, M.J. Hounslow, and W.R. Paterson. Aggregation and gelation-I. Analytical solutions for CST and batch operation. *Chemical Engineering Science*, 49:1025–1035, 1994.
- [104] M. Smith and T. Matsoukas. Constant-number Monte Carlo simulation of population balance. *Chemical Engineering Science*, 53:1777–1786, 1998.
- [105] L. Spanhel and M.A. Anderson. Semiconductor clusters in the sol-gel process-quatized aggregation, gelation and crystal growth in concentrated ZNO colloids. *Journal of American Chemical Society*, 113:2826–1833, 1991.
- [106] P.T. Spicer, O. Chaoul, S. Tsantilis, and S.E. Pratsinis. Titania formation by $TiCl_4$ gas phase oxidation, surface growth and coagulation. *Journal of Aerosol Science*, 33:17–34, 2002.
- [107] W.H. Stockmayer. Theory of molecular size distributions and gel formulation in polymerization. *Journal of Chemical Physics*, 11:45–55, 1943.
- [108] A.G. Sutugin and N.A. Fuchs. Formation of condensation aerosols under rapidly changing environmental conditions. Theory and method of calculation. *Journal of Aerosol Science*, 1:287–293, 1970.
- [109] H.S. Tan, A.D. Salman, and M.J. Hounslow. Kinetics of fluidised bed melt granulation IV. Selecting the breakage model. *Powder Technology*, 143-144:65–83, 2004.
- [110] H. Tanaka, S. Inaba, and K. Nakazawa. Steady-state size distribution for the self-similar collision cascade. *Icarus*, 12:450–455, 1996.
- [111] F. Tolfo. A simplified model of aerosol coagulation. *Journal of Aerosol Science*, 8:9–19, 1977.
- [112] T. Trautmann and C. Wanner. A fast and efficient modified sectional method for simulating multicomponent collisional kinetics. *Atmospheric Environment*, 33:1631–1640, 1999.
- [113] S. Tsantilis, H.K. Kammler, and S.E. Pratsinis. Population balance modeling of flame synthesis of titania nanoparticles. *Chemical Engineering Science*, 57:2139–2156, 2002.
- [114] S. Tsantilis and S.E. Pratsinis. Narrowing the size distribution of aerosol-made titania by surface growth and coagulation. *Journal of Aerosol Science*, 35:405–420, 2004.
- [115] M. Vanni. Discretization procedure for the breakage equation. *AIChE Journal*, 45:916–919, 1999.
- [116] M. Vanni. Approximate population balance equations for aggregation-breakage processes. *Journal of Colloid and Interface Science*, 221:143–160, 2002.

BIBLIOGRAPHY

- [117] D. Verkoeyen, G.A. Pouw, G.M.H. Meesters, and B. Scarlett. Population balances for particulate processes—a volume approach. *Chemical Engineering Science*, 57:2287–2303, 2002.
- [118] M. von Smoluchowski. Versuch einer mathematischen Theorie der Koagulationskinetik kolloider Lösungen. *Zeitschrift für Physikalische Chemie*, 92:129–168, 1917.
- [119] S. Watano, T. Fukushima, and K. Miyanami. Heat transfer and rate of granule growth in fluidized bed granulation. *Chemical and Pharmaceutical Bulletin*, 44:572–576, 1996.
- [120] E. Wynn. Improved accuracy and convergence of discretized population balance of Lister et al. *AIChE Journal*, 42:2084–2086, 1996.
- [121] E. Wynn. Simulating aggregation and reaction: New Hounslow DPB and four-parameter summary. *AIChE Journal*, 50:578–588, 2004.
- [122] Y. Xiong and S.E. Pratsinis. Formation of irregular particles by coagulation and sintering—a two-dimensional solution of the population balance equation. *Journal Aerosol Science*, 22:S199–S202, 1991.
- [123] Y. Xiong and S.E. Pratsinis. Formation of agglomerate particles by coagulation and sintering—Part I. A two-dimensional solution of the population balance equation. *Journal Aerosol Science*, 24:283–300, 1993.
- [124] R.M. Ziff. New solution to the fragmentation equation. *Journal of Physics A: Mathematical and General*, 24:2821–2828, 1991.
- [125] R.M. Ziff and E.D. McGrady. The kinetics of cluster fragmentation and depolymerization. *Journal of Physics A: Mathematical and General*, 18:3027–3037, 1985.

Curriculum Vitae

Personal Information

Name	Jitendra Kumar
Date of birth	01.04.1978
Place of birth	Bijnor, India

Education and Employment

1983 - 1995	Schooling, Bijnor, India
1995 - 1998	Bachelor of Science (B.Sc.) in Mathematics, Vardhman College Bijnor, M.J.P. Rohilkhand University, Bareilly, India
1999 - 2001	Master of Science (M.Sc.) in Industrial Mathematics and Informatics, Indian Institute of Technology (IIT) Roorkee, India
2001 - 2003	Master of Science (M.Sc.) in Industrial Mathematics: Modelling and Scientific Computing, Technical University of Kaiserslautern, Germany
2001 - 2003	Scientific Assistant, Department of Flow in Complex Structure, Fraunhofer Institute of Techno- und Wirtschaftsmathematik, Kaiserslautern, Germany
2003 - 2006	PhD Graduation (DFG Scholarship) within the Graduiertenkolleg 828, Faculty of Mathematics, OvG University, Magdeburg, Germany
2006 -	Research Associate, Institute for Analysis and Numerics, Faculty of Mathematics, OvG University, Magdeburg, Germany

Academic Honors

- Full Freeship (Merit Based) in M.Sc.-IIT Roorkee (1999-2001)
- University Medal for standing first in M.Sc.-IIT Roorkee (2001)
- Qualified CSIR-UGC National Eligibility Test (NET-2001)
- Scholarship awarded by University of Kaiserslautern, Germany (2001-2003)
- German Research Foundation (DFG) Graduiertenkolleg Scholarship (2003-2006)